BEST AVAILABLE IMAGES

Defective images within this document are accurate representations of the original documents submitted by the applicant.

Defects in the images may include (but are not limited to):

- BLACK BORDERS
- TEXT CUT OFF AT TOP, BOTTOM OR SIDES
- FADED TEXT
- ILLEGIBLE TEXT
- SKEWED/SLANTED IMAGES
- COLORED PHOTOS
- BLACK OR VERY BLACK AND WHITE DARK PHOTOS
- GRAY SCALE DOCUMENTS

IMAGES ARE BEST AVAILABLE COPY.

As rescanning documents *will not* correct images, please do not report the images to the Image Problem Mailbox.

A003US

IN THE UNITED STATES PATENT AND TRADEMARK OFFICE

PATENT APPLICATION

Examiner	:	Richard A. Schnizer
Group	:	1635
Applicants	:	Jeffrey Browning and Yves Chicheportiche
Application No.	:	09/245,198
Confirmation No.	:	4642
Filing Date	:	February 5, 1999
For	:	A TUMOR NECROSIS FACTOR RELATED LIGAND

Hon. Commissioner for Patents
P.O. Box 1450
Alexandria, Virginia 22313-1450

DECLARATION OF JEFFREY BROWNING, Ph.D.
UNDER 37 C.F.R. § 1.132

I, Jeffrey Browning, Ph.D., hereby declare and state as follows:

1. I am one of the named co-inventors of the above-identified patent application. I currently hold the

position of Distinguished Investigator at Biogen, Inc., now Biogen Idec MA Inc. ("Biogen"), the assignee of the above-identified patent application. I have been employed at Biogen, in Cambridge, Massachusetts, since 1984. During that time, I have served as Project Leader for the following projects: New TNF Members, BAFF and TWEAK; Development of Agonist LTβR mAb for Solid Tumors; Surface Lymphotoxin: Structure and Function and Studies on the Role of Exo-PLA2 in disease. I have also conducted investigations and evaluations of the anti-inflammatory properties of interferons and annexin-1, and have studied novel cytokines and the active domains of interleukin-2. From 1982 to 1984, I held the position of Senior Scientist at Angenics, Inc. in Cambridge, Massachusetts. My research there involved the development of anti-β-lactam monoclonal antibodies. From 1981 to 1982, I was a Postdoctoral Fellow in the laboratory of Dr. Louis Reichardt, Departments of Physiology and Biochemistry, University of California at San Francisco, working on applications of hybridoma technology to the study of intermediate filaments at neuromuscular junctions. From 1976 to 1981, I was a Postdoctoral Fellow in the laboratory

of Dr. Joachin Seeling, Department of Biophysical Chemistry, University of Basel, Switzerland. There, my work related to studies on phospholipids in membranes using solid state nuclear magnetic resonance methods.

2. I received a Ph.D. degree in Biochemistry from the University of Wisconsin in 1976. I received a B.S. degree cum laude in Biochemistry from Michigan State University in 1972. As illustrated by the bibliography in my curriculum vitae, which is attached as Exhibit A, I have been an active researcher in the fields of Biochemistry, Molecular Biology and Immunology. Further details of my education and research career are set forth in Exhibit A.

3. I have read and considered the above-identified application, as well as the July 22, 2003 Office Action ("the Office Action") in the application. I am informed and believe that the application claims an effective filing date of August 7, 1996.

4. I have read and considered claims 1-4, 6-8, 10, 28, 30, 31, and 39-47 of the above-identified application, which I am informed and believe were pending at the time of the Office Action. I understand that those claims stand rejected under 35 U.S.C. § 112, first

paragraph. Specifically, I understand that, in the Examiner's view, the claims are not supported by a description in the specification that enables a person of skill in the art to make and/or use the claimed invention without carrying out undue experimentation.

5. I make this declaration to demonstrate that a person of skill in the art, following the teachings of the above-identified application, would appreciate the biological function of Tumor Necrosis Factor Related Ligand ("TRELL"). Given that appreciation, a person of skill in the art would recognize the utility of and be able to use nucleic acids encoding TRELL polypeptides, as well as the TRELL polypeptides themselves, in the development of therapeutics, diagnostics or drug targets, as described in the application.

6. For the purpose of this declaration, "a person of skill in the art" as of August 7, 1996 would have a Ph.D. degree at the time and several years of relevant clinical and/or research experience involving Immunology.

7. In my opinion, a person of skill in the art would appreciate the biological function of nucleic acids encoding TRELL polypeptides and the TRELL polypeptides

themselves, as described in the above-identified application. In light of such appreciation, that person would be enabled to use those nucleic acids and the polypeptides they encode, in the development of therapeutics, diagnostics or drug targets, without resort to undue experimentation. My opinion is based on information and data presented in the application, as well as the confirmatory studies discussed below.

8. The above-identified application described TRELL (a then-new member of the tumor necrosis factor family of cytokines), the amino acid sequences of human and murine TRELL polypeptides, as well as the DNA sequences encoding those polypeptides. The application teaches that human TRELL is expressed in many tissues and organs of the immune system, such as the spleen, peripheral blood lymphocytes, lymph nodes, appendix, thymus, fetal liver and bone marrow (see, e.g., page 31, lines 4-11 and Figure 4). In addition, the application teaches that human TRELL is also expressed in organs of the secondary immune system, such as the ovary, prostate, small intestine, colon, heart, brain, placenta, lung, liver, skeletal muscle, kidney and pancreas (see, e.g., page 31, lines 12-14 and Figure 4). Such expression

indicates an immunological function for TRELL (see, e.g., page 11, lines 33-34; page 13, lines 13-14 and 19-22 of the application). Based on such teaching, a person of skill in the art would appreciate a likely role of TRELL in the immune system, as well as immune-related disorders, such as cancer.

9. As discussed in the "Background of the Invention" section of the above-identified application, TNF family members function by binding to a receptor. A person of skill in the art would appreciate that, as is true for other TNF family members, a function of TRELL would involve its interaction of TRELL with a receptor. As taught at page 15, lines 16-19 of the above-identified application, TRELL polypeptides specifically interact with a receptor.

10. Pages 35-37 of the above-identified application teach that soluble human TRELL polypeptide can bind to a number of tumor cell lines, including K562 promyelocytic cells, THP-1 monocytic leukemic cells, 293 embryonic kidney cells, Cos kidney fibroblast cells and HT29 colon adenocarcinoma cells (see Table II on page 37 of the application). A person of skill in the art would appreciate that observed binding to denote: (1) the presence of TRELL

receptors on those tumor cells and (2) a potential role of TRELL in cancer pathology. That person would also appreciate that cancer therapy could be based on an agonistic or blocking interaction between TRELL and its receptor on tumor cells.

11. Further elucidating the role of TRELL in immune-related disorders, such as cancer, the application also describes the ability of human TRELL polypeptide to induce cytotoxicity in HT29 human adenocarcinoma cells (see page 8, lines 3-6; page 36, lines 1-10 and Table II of the application). A person of skill in the art would recognize, based on the binding properties of TRELL, coupled with its cytotoxic activity on tumor cells, that TRELL may be useful as an agonist in cancer therapy to promote tumor killing.

12. In the Office Action, the Examiner discounts the HT29-14 cytotoxicity assay, on the basis that the structure of the TRELL polypeptide used in the assay was not disclosed. That is not the case. The HT29-14 cytotoxicity assay is detailed at page 36, line 1 to page 37, line 28 of the above-identified application. As stated on page 36, lines 1-4, the HT29-14 cytotoxicity assay was carried out using human TRELL. In my view, it is apparent from the

application that the soluble human TRELL polypeptide produced in the Example on page 34, line 24 to page 35, line 9, was the TRELL polypeptide used in the HT29-14 cytotoxicity assay, as that Example immediately precedes the Example relating to the assay.

13. Citing Dermer, Biotechnology, 12: 320 (1994), the Examiner also discounts the relevance of the HT29-14 cell line to disease, based on the view that *in vitro* cell lines are a poor representation of malignancy, with characteristics profoundly different from human disease. In my opinion, that view would not be shared by a person of skill in the art.

14. For several reasons, a person of skill in the art would recognize the utility of the HT29-14 cell line for assessing a potential anti-tumor agent. The HT29-14 cell line represents a subclone (number 14) of conventional HT29 cells, that is routinely used to avoid culture drift. The properties of that cell line are identical to those observed in the parental HT29 tumor cell line maintained at the American Type Tissue Culture. The HT29 cell line resembles an early epithelial progenitor cell capable of differentiating into a number of specialized epithelial cell

types (Neutra et al.[1]). As such, it is similar to many primary human colorectal tumors. Based on additional work carried out at Biogen using gene chip analyses, gene profiling has shown that the HT29 cell line may resemble as much as 30% of the spectrum of primary colorectal tumors. In fact, during the period from 1976-1986, the National Cancer Institute adopted HT29 cells (called "CX-1") as its primary tumor screen for assessing efficacy of potential therapeutics for colon cancer (Plowman et al.[2]). Furthermore, development of other therapies has also relied substantially on the HT29 cell line, *e.g.*, the original work on the TNF family member lymphotoxin-α/β, which led to the development of an agonist anti-LT-β-R monoclonal antibody to mimic ligand binding (Browning et al.[3]). Thus, a person of skill in the art would appreciate the cell death inducing activity of human TRELL polypeptide on the HT29-14 tumor

---

[1] Functional Epithelial Cells in Culture LIss: 363-398 (1989), a copy of which is provided at Exhibit B hereto.

[2] In Anticancer Drug Development Guide: Preclinical screening, clinical trials and approval. B. Teicher, ed. Humana Press Inc., Totown, 101-125 (1997), a copy of which is provided at Exhibit C hereto.

[3] J. Exp. Med. 183:867-878 (1996), a copy of which is provided at Exhibit D hereto.

cell line, as demonstrated in the above-identified application, to be indicative of the biological function of TRELL in cancer pathology.

15. On information and belief, I understand that additional work carried out at Biogen demonstrates the ability of soluble human TRELL polypeptide to induce cytotoxic activity in a number of tumor cell lines, other than in the HT29-14 cell line, either in the presence or absence of IFN-γ. Those additional cell lines include: WiDr colon adenocarcinoma cells, Geo colon carcinoma cells, MDA-MB-231 breast carcinoma cells, MX-1 breast carcinoma cells and the NCI-ADR breast carcinoma cells (data not shown). These additional cell lines have been routinely used in tumor screening panels. The colonic adenocarcinoma cell lines, HT29 and WiDr, were established originally from the same human patient, yet these tumor cell lines behave very differently in terms of their responsiveness to chemotherapy. The Geo colon tumor cell line has been included routinely in the National Cancer Institute's *in vitro* tumor screening panel for testing the efficacy of anti-cancer therapeutics for colon cancer. Similarly, the MX-1 breast carcinoma cell line has been used by the

National Cancer Institute in both its *in vivo* and later, *in vitro* tumor screens for assessing the efficacy of potential therapeutics for breast cancer. The MDA-MB-231 breast carcinoma cell line has also been included as part of the *in vitro* screening panel for therapeutics designed for the treatment of breast cancer. Based on the teachings in the above-identified application and the additional confirmatory studies discussed above, a person of skill in the art would appreciate that *in vitro* cell lines of different tissue origins are of use for assessing potential anti-tumor agents, such as TRELL.

16. In my opinion, for all of the reasons detailed above, it is simply not the case that *in vitro* cell lines, such as HT29-14, have little relevance to the *in vivo* disease state. Indeed, several anti-tumor therapeutics have been identified and evaluated based on activity in *in vitro* cell cultures. One such example is the highly successful anti-cancer drug Herceptin®, a humanized antibody approved for the treatment of HER2 positive metastatic breast cancer, which was developed following demonstration of strong efficacy *in vitro* against a limited number of tumor cell

lines (Shepard et al.[4]). Specifically, Shepard et al. discusses clinical application of anti-HER2 monoclonal antibodies for the treatment of breast cancer based on moderate to strong anti-proliferative activity against two *in vitro* tumor breast cell lines overexpressing the HER2 protoncogene ($p185^{HER2}$).

17. The biological activity of TRELL polypeptides taught in the above-identified application, and confirmed by the additional *in vitro* assays discussed above, is further confirmed by additional studies carried out at Biogen. On information and belief, I understand those studies to confirm the ability of antibodies directed to TRELL polypeptides to detect the expression of TRELL polypeptides in various diseases and conditions, as taught at page 16, line 17 to page 18, line 15 of the application.

18. Following the teachings of the application, additional studies at Biogen have led to a sensitive ELISA using anti-TRELL monoclonal antibodies to detect the level of TRELL polypeptide in the sera of patients suffering from diseases, such as lupus. The ELISA assay was based on a

---

[4] J. Clin. Immunol. 11:117-127 (1991), a copy of which is provided at Exhibit E hereto.

hamster anti-human TRELL monoclonal antibody ("the BEB3 antibody") coupled with a biotinylated mouse anti-TRELL antibody ("the P5G9 antibody"). As illustrated in Figure 1 (Exhibit F hereto), the anti-TRELL antibodies detected significantly higher systemic levels of TRELL polypeptide in the sera of lupus patients (n=183), as compared with sera of control patients (n=42), $p<2.85E-06$. This sensitive ELISA provides not only a diagnostic tool for numerous diseases and conditions associated with TRELL but confirms the above-identified application's teaching of the role of TRELL in diseases related to the immune system. The ELISA is also useful in assays to detect TRELL polypeptide levels, for screening drug candidates which are either agonists or antagonists of the normal cellular function of TRELL or its receptor.

19. On information and belief, I understand that additional studies carried out at Biogen confirm a biological role of TRELL in the development of a number of other diseases *in vivo*, based on the ability of anti-TRELL antibodies to alleviate disease severity in conventional *in*

vivo models for arthritis (Bendele et al.[5]) and stroke (Martin-Vellalba et al.[6]) (data not shown).

20. The art has also confirmed that TRELL induces a range of proinflammatory mediators that may have anti-tumor activity. In general, induction of a pro-inflammatory program within a tumor environment can be beneficial, as it draws leukocytes into the tumor and provokes an immunological response. Generally, leukocytes, especially monocytes, do not penetrate effectively into the tumor environment. As is true for other TNF family receptors, activation of the TRELL receptor can trigger pro-inflammatory-like responses in various cells. In the case of TRELL, IL-8 release has been demonstrated (Chicheportiche et al.[7]), along with release of IP-10 and Mig, two chemokines that bind to the CXCR3 receptor (based on additional work carried out at Biogen). While the actual effects of releasing a spectrum of pro-inflammatory

---

[5] Arthritis Rheum. 43:2648-2659 (2000), a copy of which is provided at Exhibit G hereto.

[6] Cell Death Differ. 8:679-686 (2001), a copy of which is provided at Exhibit H hereto.

[7] J. Biol. Chem. 272:32401-32410 (1997), a copy of which is provided at Exhibit I.

chemokines is difficult to predict, a person of skill in the art would appreciate that expression of some of these chemokines can lead to anti-tumor activity (Dias et al.[8]). For example, the CXCR3 binding chemokines have been reported to be both anti-tumor growth and anti-angiogenic (Tannenbaum et al.[9]). For these reasons, TRELL therapy may have clinical benefit by involving the immune system in addition to directing an anti-tumor effect.

21. The above-identified application describes on page 15, lines 16-19, that TRELL polypeptides specifically interact with an unidentified receptor. The application further teaches use of the disclosed peptides and methods to identify that receptor (page 31, line 17-page 32, line 12 of the application). A person of skill in the art, having TRELL polypeptide in hand, would be able to identify the receptor for TRELL polypeptide, as methods for identifying receptors for identified ligands were conventional at the time. For example, using soluble recombinant TRELL, Wiley

---

[8] Cancer Invest. 19:732-738(2001), a copy of which is provided at Exhibit J hereto.

[9] J. Immunol. 161:927-932 (1998), a copy of which is provided at Exhibit K hereto.

et al.[10] identified the fibroblast growth factor-inducible 14 (Fn14) as a TRELL receptor which was responsible for TWEAK-induced proliferation of endothelial cells and angiogenesis.

22. In my opinion, the above-identified application, read in light of the state of the art at the time, teaches a person of skill in the art the biological function of TRELL. In view of such teaching, the application provides a nexus between TRELL and its biological function in the development and progression of a number of immune-associated diseases and enables a person of skill in the art to use nucleic acids encoding TRELL polypeptides, and the TRELL polypeptides which they encode, in therapies and diagnostics directed to such diseases. Further, the application enables such uses without resort to undue experimentation.

23. I declare further that all statements made herein of my own knowledge are true and that all statements made herein on information and belief are believed to be true; and further, that these statements were made with the

---

[10] Immunity 15:837-846 (2001), a copy of which is provided at Exhibit L hereto.

knowledge that willful false statements and the like so made are punishable by fine or imprisonment, or both, under Section 1001, Title 18, United States Code, and that such willful false statements may jeopardize the validity of this application and any patent issuing thereon.

Jeffrey Browning, Ph.D.

Signed at Cambridge, Massachusetts,
this 6 day of Feb, 2004

EXHIBIT A

CURRICULUM VITAE

JEFFREY L. BROWNING

Biogen
12 Cambridge Center
Cambridge, Massachusetts 02142

Home
32 Milton Rd.
Brookline, MA 02146

(617) 679-3312 FAX: (617) 679-2304
e-mail jeff_browning@biogen.com

Birthplace: Pontiac, Michigan
Birthdate: December 1, 1951

EDUCATION

1976 — University of Wisconsin, Madison, Wisconsin.
Ph.D., Department of Biochemistry

1972 — Michigan State University, East Lansing, Michigan.
B.S. (cum laude), Biochemistry.

RESEARCH EXPERIENCE - OVERVIEW

March 1984-Present — Currently: Distinguished Investigator, Biogen Research
-New TNF Family Members, BAFF and TWEAK (Project Leader)
-Development of agonist LTBR mAb for Solid tumors (Project Leader)
-Surface Lymphotoxin:Structure and function (Project Leader)
- Studies on the role of exo-PLA2 in disease (Project Leader)
-Investigation of the anti-inflammatory properties of interferons.
-Exploration of the anti-inflammatory properties of annexin-I
-Evaluation of novel cytotoxins.
-Investigation of the active domains of Interleuken-2.

September, 1982 to March, 1984 — Angenics, Inc. Cambridge, Massachusetts.
Senior Scientist.
- Development of anti-β-lactam monoclonals

1981 - 1982 — University of California, San Francisco, California.
Departments of Physiology and Biochemistry.
Post-doctoral work with Dr. Louis Reichardt.
- Application of hybridoma technology to the study of intermediate filaments at neuromuscular junctions

1976 - 1981 — University of Basel, Basel, Switzerland. Biocenter,
Department of Biophysical Chemistry.
Post-doctoral work with Dr. Joachin Seelig.

- Studies on phospholipids in membranes using solid state nuclear magnetic resonance methods

1973 - 1976 University of Wisconsin, Madison, Wisconsin.
Department of Biochemistry.
Graduate studies with Dr. David Nelson.
- Biochemical approaches to ion gating in nerve-like systems.

FELLOWSHIPS

1981 - 1982	Muscular Dystrophy Post-Doctoral Fellowship.
1978	NIH Post-Doctoral Fellowship (did not accept)
1978	Muscular Dystrophy Post-Doctoral Fellowship (did not accept)
1977	American-Swiss Foundation for Scientific Exchange Fellow.
1976	NATO Post-Doctoral Fellowship (did not accept)
1976 - 1978	Cystic Fibrosis Post-Doctoral Fellowship.
1975 - 1976	Proctor & Gamble Pre-Doctoral Fellowship.

PUBLICATIONS

1). **Browning, J**. and Nelson, D. (1976) "Biochemical Studies on the Excitable Membrane of Paramecium I. Ca^{++} Fluxes Across the Resting and Excited Membrane", Biochim. Biophys. Acta, 448:338-351.

2). **Browning, J.** and Nelson, D. (1976) "Membrane Excitability in Paramecium Evidence for a Role for the Bilayer Couple", Proc. Natl. Acad. Sci. USA, 73:452-456.

3). **Browning, J.**, Nelson, D. and Hansma, H. (1976) "Ca^{++} Influx Across the Excitable Membrane of Behavioural Mutants of Paramecium", Nature, 259:491-494.

4). Seelig, J. and **Browning, J.** (1978) "General Features of Phospholipid Conformation in Membranes", FEBS Letters, 92:41-44.

5). **Browning, J**. and Nelson, D. (1979) "Fluorescent Probes for Asymmetric Lipid Bilayers; Synthesis and Properties in Phosphatidylcholine Liposomes and Erythrocyte Membranes", J. Membrane Biology, 49:75-103.

6). **Browning, J.** and Seelig, J. (1979) "Synthesis of Specifically Deuterated Saturated and Unsaturated Phosphatidylserine", Chem. Phys. Lipids, 24:103-118.

7). **Browning, J.** and Seelig, J. (1980) "Bilayers of Phosphatidylserine: A Deuterium and Phosphorus Magnetic Resonance Study", Biochemistry, 19:1262-1270.

8). **Browning, J.** (1981) "The Motions and Interactions of Phospholipid Headgroups I. Simple Alkyl Headgroups", Biochemistry, 20:7123-7133.

9). **Browning, J.** (1981) "The Motions and Interactions of Phospholipid Headgroups II. Headgroups with Hydroxy Groups", Biochemistry, 20:7133-7143.

10). **Browning, J.** (1981) "The Motions and Interactions of Phospholipid Headgroups III. Dynamic Properties of Amine Containing Headgroups", Biochemistry, 20:7144-7151.

11). **Browning, J.** and Akutsu, H. (1981) "Local Anesthetics and Divalent Cations Have the Same Effect on the Phosphocholine and Phosphoethanolamine Headgroups" Biochim.Biophys. Acta, 648:172-178.

12). Pepinsky, R.B., Sinclair, L., **Browning, J.**, Mattaliano, R., Smart, J., Chow, P.-C., Falbel, T., Ribolini, A., Garwin, J., and Wallner, B. (1986) "Purification and Partial Sequence Analysis of a 37-kDa Protein That inhibits Phospholipase A2 Activity from Rat peritoneal Exudates", J. Biol. Chem. 261: 4239-4246.

13). **Browning, J.**, Mattaliano, R., Chow, P.-C., Liang, S.-M., Allet, B., Rosa, J., and Smart, J. (1986) "Disulfide Scrambling of Interleukin-2: HPLC Resolution of the Three Possible Isomers", Anal. Biochem., 155:123-128.

14). Huang, K.-S., Wallner, B., Mattaliano, R., Tizard, R., Burne, C., Frey, A., Hession, C., McGray, P., Sinclair, L., Chow, P.-C., **Browning, J.**, Ramachandran, K.,Tang, J., Smart, J., and Pepinsky, R. B. (1986) "Isolation, Characterization and Primary Structure of Two Human 35-kD Phospholipase A_2 Inhibitory Proteins and Their Relationships to Substrates of $pp60^{v\text{-}src}$ and of the Epidermal Growth Factor Receptor/ Kinase", Cell, 46:191-199.

15). Wallner, B.P., Mattaliano, R.J., Hession, C., Cate, R.L., Tizard, R., Sinclair, L.K., Foeller, C., Chow, E.P., **Browning, J.L.**, Ramachandran, K.L., Pepinsky, R.B. (1986) "Cloning and Expression of Human Lipocortin, a Phospholipase A_2 Inhibitor with Potential Anti-inflammatory Activity", Nature, 320:77-81.

16). Cirino, G., Flower, R., **Browning, J.**, Sinclair, L., Pepinsky, R. (1987) "Recombinant Human Lipocortin 1 Inhibits Thromboxane Release from Guinea-pig Isolated Perfused Lung", Nature, 328:270-272.

17). **Browning, J.** (1987) "Interferons and Rheumatoid Arthritis: Insight into Interferon Biology?", Immunology Today, 8:372-374.

18). **Browning, J.**, and Ribolini, A. (1987) "Interferon Blocks Interleukin-1 Induction of Prostaglandin E_2 from Human Peripheral Monocytes", J. Immunol., 138: 2857-2863 .

19). Pepinsky, R., Tizard, R., Mattaliano, R. Sinclair, L., Miller, G., **Browning, J.**, Pinchang Chow, E., Burne, C., Huang, K-S., Pratt, D., Wachter, L., Hession, C., Frey, A., Wallner, B. (1988) "Five Distinct Calcium and Phospholipid Binding Proteins Share Homology with Lipocortin I", J. Biol. Chem., 263:10799-10811.

20). **Browning, J.** and Ribolini, A. (1989) "Studies on the Differing Effects of Tumor Necrosis Factor and Lymohotoxin on the Growth of Several Human Tumor Lines" J. Immunol. 143:1859-1867.

21). Cirino, G., Peers, S., Flower, R., **Browning, J.** and Pepinsky, B. (1989) "Human Recombinant Lipocortin-1 has Acute Local Antiinflammatory Properties in the Rat Paw Edema Test" Proc. Natl. Acad. Sci. 86:3428-3432.

22). Violette, S., King, I., **Browning, J.**, Pepinsky, B., Wallner, B. and Sartorelli, A. (1990) "Role of Lipocortin-1 in the Glucocorticoid Induction of the Terminal Differentiation of a Human Squamous Carcincoma" J. Cell. Physiol. 142:70-77.

23). Pepinsky, B., Sinclair, L. Dougas, I., Liang, C-M., Lawton, P. and **Browning, J.** (1990) "Monoclonal Antibodies to Lipocortin-1 as Probes for Biological Function" FEBS Letters 261:247-252.

24). Goulding, N., Podgorski, M., Hall, N., FLower, R., **Browning, J.**, Pepinsky, B., and Maddison, P. (1990) "Autoantibodies to Recombinant Lipocortin-1 in Rheumatoid Arthritis and Systemic Lupus Erythematosus" Ann. Rheum. Dis. 48:843-850.

25). Bomalaski, J., P. Lawton and **J. Browning**. (1991). "Recombinant Human Extracellular Phospholipase A2 induces an inflammatory response in rabbit joints" J. Immunol. 146: 3904-3910.

26). **Browning, J. L.**, Androlewicz, M. J. and C. F. Ware. (1991). "Lymphotoxin and an associated 33 kDa glycoprotein are expressed on the surface of an activated human T cell hybridoma" J. Immunol. 147: 1230-1237.

27). Scott, D.L., White, S.P., **Browning, J.L.**, Rosa, J.J., Gelb, M.H. and Sigler, P.B. (1991) "Structures of free and inhibited human secretory phospholipase A2 from inflammatory exudate" Science 254: 1007-1010.

28). Androlewicz, M.J., **Browning, J.L.** and Ware, C.F. (1992) "Lymphotoxin is expressed as a heteromeric complex with a distinct 33 kDa glycoprotein on the surface of an activated human T cell hybridoma" J. Biol. Chem. 267: 2542-2547 .

29). Ware, C.F., Crowe, P. D., Grayson, M.H., Androlewicz, M.J. and **Browning, J.L.** (1992) "Expression of surface lymphotoxin and tumor necrosis factor on activated T, B and Natural Killer Cells" J. Immunol. 149:3881-3888.

30). Pruzanski, W., Wilmore, D.W., Suffedini, A., Martich, G.D., Hoffman, G.D., **Browning, J.L.**, Stefanski, E., Sternby, B. and P. Vadas (1992) "Hyperphospholipasemia A2 in human volunteers challenged with intravenous endotoxin" Inflammation 16:561-570.

31). Bayburt, T., Yu, B-Z., Lin, H-K., **Browning, J.L**, Jain, M.K., and Gelb, M.H. (1993). "Human nonpancreatic secreted phospholipase A2: Interfacial parameters substrate specificites and competitive inhibitors" Biochemistry 32:573-582.

32). **Browning, J.L.**, Ngam-ek, A., Lawton, P., DeMarinis, J., Tizard, R., Chow, E.P., Hession, C., O-Brine-Greco, B., Foley, S., and Ware, C.F. (1993) "Lymphotoxin-ß: A novel member of the TNF family that forms a heteromeric complex with lymphotoxin on the cell surface" Cell 72:847-856.

33). Santos, A., Scheltinga, M., Lynch, E., Brown, E., Lawton, P., Chambers, E., **Browning, J.L.**, Dinarello, C., Wolff, S. and Wilmore, D. (1993) "Elaboration of interleukin-1 receptor antagonist is not attenuated by glucocorticoids following endotoxemia" Arch Surgery 128:138-144.

34). Cirino, G., Cicala, C., Sorrentino, L. and **Browning, J. L.**, (1993) "Human recombinant platelet phospholipase A2 has anticoagulant activity in vitro on human plasma" Thrombosis Res. 70:337-342.

35). Cirino, G., Cicala, C., Sorrentino, L., **Browning, J.L.** and Page, C.P. (1994). "Human recombinant phospholipase A2 inhibits platelet aggregation in vitro and in vivo in rat and guinea pig" Eur. J. Pharmacol. 252:147-154.

36). Cirino, G., Cicala, C., Sorrentino, L., Maiello, F.M. and **Browning, J.L.** (1994). "Human extracellular recombinant phospholipase A2 induces a synovitis-like inflammation in rat air pouch" J. Rheumatol. 21:824-9.

37). Pruzanski, W., Vadas, P. and **Browning, J. L.** (1993) "Secretory non-pancreatic PLA2 phospholipase A2: Role in physiologic and inflammatory processes" J. Lipid Mediators 8:161-167.

38). Santos, A.A., **Browning, J.L.**,Scheltinga, M.R., Lynch, E.A., Brown, E.F., Lawton, P., Chambers, E., Dougas, I., Benjamin, C., Dinarello, C.A., Wolff, S.M., Jacobs, D.O. and Wilmore, D.W.(1994). "Does circulating PLA2 cause sepsis-related events following endotoxemia?" Arch Surgery 219: 183-192.

39). Crowe, P. D., VanArsdale, T. L., Walter, B. N., Ware, C. F., Hession, C., Ehrenfels, B., **Browning, J. L.**, Din, W., Goodwin, R. G. and C. A. Smith (1994) "A novel receptor specific for lymphotoxin-β" Science 264:707-710.

40). **Browning, J. L.,** Dougas, I., Ngam-ek, A., Bourdon, P., Ehrenfels, B., Miatkowski, K., , Zafari, M., Yampaglia, A., Lawton, P., Benjamin, C., Meier, W. and C. Hession. (1995) "Characterization of surface lymphotoxin forms: use of specific monoclonal antibodies and soluble receptors" J. Immunol. 154: 33-46.

41). Lawton, P., Nelson, J., Tizard, R. and **J. L. Browning.** (1995). "Characterization of the mouse lymphotoxin-beta gene" J. Immunol. 154: 239-246.

42). Force, W.R., Walter, B.N., Hession, C., Tizard, R., Kozak, C.A., **Browning, J.L.** and Ware, C.F. (1995) "Mouse lymphotoxin-β receptor: Molecular genetics, ligand binding and expression" J. Immunol. 155:5280-5288.

43). **Browning, J. L.,** Miatkowski, K., Sizing, I., Griffiths, D. A., Zafari, M., Benjamin, C. D., Meier, W. and MacKay, F. (1996). "Signaling through the lymphotoxin-β receptor induces the death of some adenocarcinoma tumor lines" J. Exp. Med. 183: 867-878

44). **Browning, J. L.,** Miatkowski, D., Griffiths, D. A., Bourdon, P., Hession, D., Ambrose, C. M. and W. Meier (1996). "Characterization of soluble recombinant forms of lymphotoxin-α/β complexes" J. Biol. Chem. 271: 8618-8626

45). MacKay, F., Majeau, G. R., Hochman, P. S. and **J. L. Browning** (1996). "Lymphotoxin-β receptor triggering induces activation of the NF-κB transcription factor in various cell types" (1996) J. Biol. Chem. 271:24934-24938

46). Rennert, P. D., **Browning, J. L.,** Mebius, R., Mackay, F. and Hochman, P. S. (1996) "Surface lymphotoxin alpha/beta complex is required for the development of peripheral lymph nodes" J. Exp. Med. 184:1999-2006

47). Hochman, P. S., Majeau, G. R., Mackay, F. and **Browning, J. L.** (1996) "Proinflammatory responses are efficiently induced by homotrimeric but not heterotrimeric lymphotoxin ligands" J. Inflammation 46:220-234

48). Ettinger, R., **Browning, J. L.,** Mitchie, S. A., van Ewijk, W. and McDevitt, H. O. (1996) "Disrupted splenic architecture, but normal lymph node development in mice expressing a soluble lymphotoxin- receptor-IgG1 Fc chimeric fusion protein" Proc. Natl. Acad. Sci. USA 93:13102-13107

49). Bodmer, J-L., Burns, K., Schneider, P., Hofmann, K., Steiner, V., Thome, M., Bornand, T., Hahne, M., Schroeter, M., Becker, K., Wilson, A., French, L. E., **Browning, J.L.,** MacDonald, H.R. and J. Tschopp (1997) "TRAMP, a novel apoptosis-mediating receptor with sequence homology to tumor necrosis factor receptor 1 and Fas (apo-1/CD95)" Immunity 6: 79-88.

50). P. D. Rennert, **J. L. Browning** and P.S. Hochman (1997) "Lymphotoxin ligands selectively function to generate and organize secondary lymphoid tissues" Intlernational Immunity 9, 1627-1639

51). Mackay, F., Majeau, G. R., Lawton, P., Hochman, P.S. and **J. L. Browning** (1997) "Inhibition of the LT and TNF pathways in normal adult mice reveals immunological roles separate from developmental effects" Eur. J. Immunol. 27:2033-2042

52). Koni, P. A., A. K., Sacca, R., Lawton, P., **Browning, J. L.,** Ruddle, N.H. and R.A. Flavell (1997) "Distinct roles in lymphoid organogenesis for lymphotoxins alpha and beta revealed in lymphotoxin-beta deficient mice" Immunity 6:491-500

53). **Browning, J.L.,** Sizing, I. D., Lawton, P., Bourdon, P., Rennert, P. D., Majeau, G. R., Ambrose, C.A., Hession, C., Miatkowski, K., Griffiths, D.A., Ngam-ek, A., Meier, W., Benjamin, C.A. and Hochman, P.S. (1997) "Characterization of lymphotoxin-alpha/beta complexes on the surface of mouse lymphocytes" J. Immunol. 159:3288-3298

54). Mackay, F., Bourdon, P., Griffiths, D.A., Lawton, P., Zafari, M., Sizing, I.D., Miatkowski, K., Ngam-ek, A., Benjamin, C.D., Hession, C., Ambrose, C.M., Meier, W. and **J.L. Browning** (1997) "Cytotoxic activities of recombinant soluble murine lymphotoxin-alpha and lymphotoxin-alpha/beta complexes" J. Immunol. 159:3299-3310

55). Canella, B., Dougas-Sizing, I., Benjamin, C. D., **Browning, J.L.**, Raine, C.S. (1997) "Antibodies to lymphotoxin alpha and LT beta recognize different glial cell types in the central nervous system" J. Neuroimmunology 78:172-179

56). Gonzalez, M, Mackay, F., **Browning, J. L.**, Kosco-Vilbois, M. H. and R. J. Noelle (1998) "The sequential role of lymphotoxin and B cells in the development of splenic follicles" J. Exp. Med. 187, 997-1007.

57). Chicheportiche, Y., Bourdon, P. R., Xu, H., Hsu, Y-M., Scott, H., Hession, C., Garcia, I. and **Browning, J.L.** (1997) "TWEAK, a new secreted ligand in the tumor necrosis factor family that weakly induces apoptosis" J. Biol. Chem. 272:32401-32410

58). Mackay, F., **Browning, J. L.**, Lawton, P., Shah, S. A., Comiskey, M., Bhan, A. K., Mizoguchi, E., Terhorst, C. and Simpson, S. (1998) "Both the lymphotoxin and TNF pathways are involved in experimental colitits" Gastroenterology 115: 1464-1475

59). Ettinger, R., Mebius, R., **Browning, J.L.**, Michie, S. A., Tuijl, S. V., Kraal, G., Ewijk, W.V. and McDevitt, H. O. (1998) International Immunol. 10, 727-741.

60). Mackay, F. and **Browning, J. L.** (1998) "Turning off folicular dendritic cells" Nature 395, 26-27

61). Rennert, P. D., James, D., Mackay, F., **Browning, J.L.** and Hochman, P. S. (1998) "Lymph node genesis is induced by signaling through the lymphotoxin-beta receptor" Immunity 9, 71-79.

62). Ngo, V. N., Korner, H., Peschon, J. J., Gunn, M. D., Schmidt, K. N., Cooper, M. D., **Browning, J. L.**, Sedgwick, J. D. and Cyster, J. G. (1998) "Tumor necrosis factor-alpha and lymphotoxin-alpha/beta direct expression of lymphoid tissue chemokines needed for lymphocyte compartmentalization in the spleen" J. Exp. Med. 189: 403-412

63). Lucas, R., Tacchini-Cottier, F., Guler, R., Vesin, S., Jemelin, S., Marchal, G., Vassalli, P., **Browning, J.** and I. Garcia (1998) "A protective role for lymphotoxin in host defense against mycobasterial infection" Eur. J. Immunol. 29, 4002

64). Murphy, M., Walter, B. N., Pike-Noble, L., Fanger, N. A., Guyre, P. M., **Browning, J. L.**, Ware, C. F. and Epstein, L. (1998) "Expression of the lymphotoxin-beta receptor on follicular dendritic stromal cells in human lymphoid tissues" Cell Death and Diff. 5, 497-505

65). Schneider, P., Mackay, F., Steiner, V., Ambrose, C., Lawton, P., Hofmann, K., Acha-Ochea, H., Bodmer, J-L., Holler, N., Valmori, D., Romero, P., Werner-Favre, C., Zubler, R. H., **Browning, J. L.** and Tschopp, J. (1999) "BAFF, a novel ligand of the tumor necrosis factor family, stimulates B-cell growth" J. Exp. Med. 189, 1747-1756

66). Marshall, W. L., Brinkman, B., Ambrose, C. M., Pesavento, P. A., Uglialoro, A. M., Teng, E., Finberg, R. W., **Browning, J. L.**, and Goldfeld, A. E. (1999) "Signaling through the lymphotoxin-beta receptor stimualtes HIV-1 replication alone and in combination with soluble or membrane bound TNF" J. Immunol. 162, 6016-6023

67). Mackay, F., Woodcock, S. A, Lawton, P., Ambrose, C., Baetscher, M., Schneider, P., Tschopp, J. and **J. L. Browning** (1999) Mice transgenic for BAFF develop lymphocytic disorders along with autoimmune manifestations" J. Exp. Med. 190, 1697-1710

68). Wu, Q., Wang, Y., Wang, J., Hedgeman, E., **Browning, J. L.**, and Y-X. Fu (1999) "The requirement for membrane lymphotoxin for the presence of dendritic cells in lymphoid tissues" J. Exp. Med. 190, 629-638

69). Puglielli, M., **Browning, J.L.**, Brewer, A.W., Schreiber, R., Sheih, W-J., Altman, J., Oldstone, M., Zaki, S. and R. Ahmed (1999) "Reversal of virus-induced systemic shock and respiratory failure by blockade of the lymphotoxin pathway" Nature Medicine 5, 1370-1374

70). Ansel, K.M., Ngo, V.N., Hyman, P. L., Luther, S.A., Forster, R., Sedgewick, J.D., **Browning,J.L.**, Lipp, M. and Cyster, J.G. (2000) "A chemokine-driven positive feedback loop organizes lymphoid follicles" Nature 406, 309-314

71). Husson, H., Lugli, S. M., Ghia, P., Cardoso, A., Roth, A., Brohmi, K., Carideo, E.G., Choi, Y.S., **Browning J.L.** and Freedman, A.S. (2000) "Functional effects of TNF and lymphotoxin a.b on FDC-like cells" Cell. Immunol. 203, 134-143

72). Batten, M, Groom, J, Cachero, T.G., Xian, F., Schneider, P., Tschopp,J., **Browning, J. L.** and Mackay, F. (2000) "BAFF mediates survival of peripheral immature B-lymphocytes" J. Exp. Med. 192, 1453

73). Debard, N., Sierro, F., **Browning J** and J-P Kraehenbuhl (2001) "The role of mature lymphocytes and lymphotoxin on the development of follicle-associated epithelium and M cells in mouse Peyer's Patches" Gastroenterology 120, 1173

74). Thompson, J. S., Schneider, P., Kalled, S. L., Wang, L., Lefevre, E. A., Cachero, T. G., MacKay, F., Bixler, S. A., Zafari, M., Liu, Z. Y., Woodcock, S. A., Qian, F., Batten, M., Madry, C., Richard, Y., Benjamin, C. D., **Browning, J. L.**, Tsapis, A, Tschopp, J.. and Ambrose, C. (2000) "BAFF binds to the tumor necrosis factor receptor-like molecule B cell maturation antigen and is important for maintaining the peripheral B cell population" J. Exp. Med. 192, 129

75). Rennert, P., Schneider, P., Cachero, T.G, Thompson, J., Trabach, L., Hertig, S., Holler, N., Qian, F., Mullen, C., Strauch, K., **Browning, J.L.**, Ambrose, C. and J. Tschopp (2000) "A soluble form of B cell maturation antigen, a receptor for the tumor necrosis factor family member APRIL, inhibits tumor cell growth" J. Exp. Med. 192, 1677.

76). Rennert, P., Hochman, P.S., Flavell, RA, Chaplin, DD., Jayaraman, S., **Browning, JL.**, and YX Fu (2001) "Essential role for lymph nodes in contact hypersensitivity revealed in lymphotoxin-alpha deficient mice" J. Exp. Med. 193, 1227.

77). Dohi, T., Rennert, P., Fujihashi, K., Kiyono, H., Shirai, Y., Kawamura, YI., **Browning, JL.**, and JR. McGhee (2001) "Elimination of colonic patches with lymphotoxin-beta receptor prevents Th2 -type colitis" J. Immunol. 167, 2781.

78). Thompson, JS., Bixler, SA., Qian, F., Vora, K., Scott, ML., Cachero, TG., Hession, C., Schneider, P., Sizing, I., Mullen, K., Zafari, M., Benjamin, CD, Tschopp, J., **Browning, JL.**, and C. Ambrose (2001) "BAFF-R, a novel TNF receptor that specifically interacts with BAFF" Science 293, 2108

79). **Browning J. L.** and French, L. (2002) "Visualization of developing peripheral lymph nodes in the mouse embryo and a comparison of embryonic lymphotoxin-beta and lymphotoxin-beta receptor expression" J. Immunol. 168, 5079-5087

80). Wilson, C. A. and **J. L. Browning** (2002) "Caspase-dependent and -independent apoptosis induced by signalling through TNF family receptors" Cell Death Diff. 9, 1321

81). Gommerman, J. L., Mackay, F., Chutkowski, C., Donskoy, E., Meier, W., Martin, P. and **J.L. Browning** (2002) "Manipulation of lymphoid microenvironments in non-human primates by an inhibitor of the lymphotoxin pathway" J. Clin. Invest. 110, 1359

82) Fava, R. A., Notidis, E., Hunt, J., Szanya, V., Ratcliffe, N., Ngam-ek, A., de fougerolles, A., Sprague, A. and **J. L. Browning** (2003) "Critical role for the lymphotoxin pathway in the induction and progression of collagen arthritis" J. Immunol. 171: 115-126

83). Gommerman, J., Giza, K, Perper, S., Sizing, I., Ngam-ek, A., Nickerson-Nutter, C., and **J. L. Browning** (2003) J. Clin. Invest. 112: 755-767

REVIEWS

Browning, J.L. (1981) "NMR Studies of the Structural and Motional Properties of Phospholipids in Membranes", a chapter in Liposomes: from Physical Structure to Therapeutic Applications, (C. G. Knight, ed.) Elsevier/North Holland Biomedical Press.

Browning, J.L., Ward, M., Wallner, B. and Pepinsky, B. (1990) "Studies on the Structural Properties of Lipocortin-1 and the Regulation of its Synthesis by Steroids" in Cytokines and Lipocortins in Inflammation and Differentiation. eds. Melli, M. and Parente, L. Wiley-Liss New York, N.Y.

Vadas, P., **Browning, J.L.**, Edelson, J. and Pruzanski, W. (1993). Extracellular phospholipase A2 expression and inflammation: The relationship with associated disease states. J. Lipid Mediators 8:1-30.

Ware, C.F, VanArsdale, T., Crowe, P. and **J.L. Browning.** (1995) The ligands and receptors of the lymphotoxin system. in Pathways for Cytolysis, pp 175-218, eds. Griffiths and Tschopp, Springer-Verlag

MacKay, F and **J. L. Browning** (2002) "BAFF, a fundamental survival factor for B cells" Nature Immunol. Rev. 2, 465-476

Mackay, F., Schneider, P, Rennert, P. and **J. L. Browning** (2003) "BAFF and APRIL: a tutorial on B cell survival" Ann. Rev. Immunol 20 (2003) *(invited review)*

Gommerman, J. and **J. L. Browning** (2002) " Lymphotoxin, microenvironments and autoimmune disease" Nature Immunol Rev. 3: 642-655 *(invited review)*

Manuscripts in preparation

Lukashev, M., Garber, E., Xu, X., Wilson, C., Ngam-ek, A., Zeng, W., Griffith, L., Bailly, V. and **J.L. Browning** "Lymphotoxin-beta receptor regulates the expression of the CXCR3 ligands IP-10, Mig and I-TAC" in preparation

Gommerman, J., Sizing, I., Groom, J., Woodcock, S., Kalled, S., Mackay, F., **Browning, J.L.** "Two different type of lupus models are revealed by use of LT and CD40 pathway inhibitors" in preparation

Lukashev, M., Lepage, D., Wilson, C., Bailly, V., **Browning, J.L.** "Use of gene profling to define colorectal tumors that respond to activation of the LTBR" in preparation

EXHIBIT B

Functional Epithelial Cells in Culture: 363–398

Differentiation of Intestinal Cells In Vitro

Marian Neutra and Daniel Louvard

Department of Anatomy and Cellular Biology, and Digestive Diseases Center, Harvard Medical School, Boston, Massachusetts 02115 (M.N.); Membrane Biology Unit, Department of Molecular Biology, The Pasteur Institute, Paris, 75724, France (D.L.)

I. INTESTINAL EPITHELIUM: A MODEL SYSTEM FOR STUDY OF CELL DIFFERENTIATION AND POLARIZED CELL FUNCTIONS

The intestinal epithelium is a valuable tissue for study of *cell differentiation* in that it is spatially organized around its proliferative units, the crypts. Each crypt consists of a clone of cells [Ponder et al. 1985] produced by a group of undifferentiated, proliferative cells whose progeny express at least four dramatically different phenotypes [Leblond and Cheng, 1976]. The determinants of phenotype commitment and expression in this tissue are unknown. The temporal sequence of differentiative changes occurring in each cell type can be readily defined, however, since the orderly upward migration of cells from crypt to villus arranges the cells along this axis in order of age [Madara and Trier, 1987]. A major unfulfilled goal of intestinal culture systems is the controlled recreation of the crypt-villus axis of epithelial differentiation in the absence of the complex connective tissue lamina propria.

Like all simple epithelia, the intestine provides a valuable model for study of *cell polarity*. Fully differentiated intestinal cells are more strictly polarized than many other epithelial cell types, perhaps because they are designed to face the threats of the intestinal lumen, a situation in which mis-sorting of membrane components could compromise the epithelial barrier. Also unique to this epithelium is the dramatic conversion that occurs during fetal development from a nonpolarized, stratified cell layer to a simple columnar epithelium [Trier and Moxey, 1979; Colony and Neutra, 1983]. This process provides the opportunity to follow normal, in vivo assembly of tight junctions and de novo formation of apical membrane domains [Madara et al., 1981].

The specialized apical domain of intestinal absorptive cells provides a valuable system for study of the *synthesis and processing of membrane glycoproteins*. The microvillus membrane is rich in intramembrane transporters, membrane-anchored hydrolases, and other glycoproteins, many with characteristic patterns of intracellular and cell surface processing [Hauri, 1983; Semenza, 1986]. Indeed, expression of specific microvillar hydrolases is currently the most reliable indicator of intestinal cell differentiation in vitro. Errors in processing and transport have been identified and associated with clinical malabsorption in humans, and differentiated cell culture systems have recently been used for accurate analysis of these molecular processes [Hauri et al., 1985].

The apical brush border of intestinal absorptive cells, designed to expand the membrane surface area available for hydrolysis and transport, provides a unique model for study of *cytoskeleton assembly* and *cytoskeleton–membrane* interactions. The molecular architecture of this structure has been defined in considerable detail using normal intestinal cells [Mooseker, 1985] but synchronously differentiating in vitro systems provide an opportunity to define

SYSTEM FOR STUDY RIZED CELL

r study of *cell differentiation* ative units, the crypts. Each 85] produced by a group of express at least four drama- 1976]. The determinants of are unknown. The temporal ach cell type can be readily ation of cells from crypt to of age [Madara and Trier, re systems is the controlled fferentiation in the absence

a valuable model for study s are more strictly polarized cause they are designed to on in which mis-sorting of ithelial barrier. Also unique urs during fetal development columnar epithelium [Trier This process provides the tight junctions and de novo t al., 1981].

tive cells provides a valuable *f membrane glycoproteins*. ne transporters, membrane- y with characteristic patterns ri, 1983; Semenza, 1986]. es is currently the most reli- vitro. Errors in processing with clinical malabsorption have recently been used for uri et al., 1985].

e cells, designed to expand is and transport, provides a nd *cytoskeleton–membrane* ructure has been defined in [Mooseker, 1985] but syn- le an opportunity to define

the factors that control assembly and maintenance of this unique polarized structure.

The intestinal epithelium conducts both absorption and secretion of ions and water. Because it is an extensive and accessible epithelial surface, its *ion transport and permeability* characteristics have been defined in considerable detail [Powell, 1987]. Extracellular and intracellular mechanisms that control ion movements across this monolayer are complex, however, and vary with both cell type and stage of differentiation [Marcial and Madara, 1984]. Such variations have been partially defined using intact mucosal tissue, but the availability of well defined monolayer cultures opens the way for rapid advances in understanding transport phenomena.

Intestinal absorptive cells also provide unique models for study of *endocytosis and transepithelial transport*. In suckling rodents, sorting of IgG–receptor complexes from soluble proteins, and selective transepithelial transport, occurs in jejunal absorptive cells [Rodewald and Abrahamson, 1982]. Ileal cells in sucklings contain a highly polarized system of endosomal compartments that have been isolated and found to contain a membrane antigen that serves as a useful marker for ileal cell endosomal tubules [Wilson et al., 1987a]. In adults, intestinal absorptive cells conduct receptor-mediated transport of polymeric immunoglobulins from basolateral to apical surfaces and express for this purpose a membrane receptor with a unique itinerary (Golgi—> basolateral—>apical) that is cleaved and released into the lumen along with its ligand [Mostov et al., 1980; Mostov and Blobel 1983]. In addition, unique epithelial "M" cells in lymphoid follicle-associated epithelium are models for study of transepithelial transport in that they are highly endocytic but seem to lack a lysosome-directed pathway, instead directing all endocytic vesicles to a specialized basolateral surface [Neutra et al., 1987].

Finally, the mucin-secreting goblet cells of the intestinal epithelium are valuable models in which to study the process of *regulated secretion*. Their large, clearly polarized Golgi complex has facilitated localization of enzymes involved in O-linked glycosylation [Roth, 1987]. The relatively slow, highly polarized movement of mucin secretory granules in goblet cells and the dramatic structural events that accompany stimulated secretion make them a potentially valuable model for study of polarized secretory cell function [Neutra and Forstner, 1987]. They have not been fully exploited for this purpose, however, because normal goblet cells are a minority in the complex and heterogeneous intestinal mucosa and have not been available for study in isolation.

The goal in establishing intestinal cell culture systems is to obtain cells and tissues that mimic as closely as possible their counterparts in vivo. Ideally, epithelial cell cultures should allow the process of normal cell differentiation and function or neoplastic transformation to be recapitulated, manipulated, and observed under controlled conditions. This has proved particularly diffi-

cult to achieve for the intestinal epithelium, where the normal in vivo state is a complex, dynamic one, with continuous cell proliferation and cell loss, in which individual cells survive only for a few days. It is thus useful to review the salient features of intestinal differentiation in vivo as a reference point for assessing available in vitro systems.

II. INTESTINAL EPITHELIAL CELL DIFFERENTIATION IN VIVO

A. Adult: The Crypt-Villus Axis

The intestinal epithelium is a vast sheet of cells composed of millions of tiny differentiating units. Stem cells located near the bottom of each crypt give rise to proliferative cells whose progeny differentiate along one of several paths and migrate slowly up the crypt wall, with the exception of Paneth cells that remain at the crypt base [Leblond and Cheng, 1976]. The three major migratory cell types, columnar cells (enterocytes), goblet cells, and enteroendocrine cells, acquire differentiated features and perform important physiologic functions while still in the crypts. For example, crypt enterocytes actively secrete chloride ions [Welsh et al., 1982] and conduct receptor-mediated transepithelial transport of secretory immunoglobulins from the lamina propria into the lumen [Mostov and Blobel, 1982]; crypt goblet cells conduct acetycholine-regulated mucin secretion [Specian and Neutra, 1980; Neutra and Forstner 1987]; and crypt endocrine cells release regulatory peptides and amines in response to neural, endocrine, and luminal signals [Walsh, 1987]. As these cells migrate out of the crypts and onto the villi (in the small intestine) or onto the flat mucosal surface (in the colon, appendix, and rectum), they rapidly undergo a second phase of differentiation. At the crypt mouth, columnar cells assemble highly organized apical microvillous borders [Madara and Trier, 1987] and express membrane-associated enzymes for terminal digestion and absorption of nutrients [Moog 1979; Simon et al., 1979]. At the same transition point, goblet cells lose cholinergic sensitivity [Specian and Neutra, 1980; Phillips et al., 1984]. Because of continuous cell production, movement of new cells up the crypt wall and cell loss from the villus tip, this entire sequence of differentiative events is displayed along each crypt-villus axis at any moment in time (Table I). This has permitted relatively precise definition not only of morphologic and enzymatic changes but also of the appearance and disappearance of antigenic markers during intestinal cell differentiation in vivo [Quaroni, 1984; Quaroni and Isselbacher, 1985].

B. Rat Fetal and Neonatal Development

Prior to the establishment of the adult steady-state system, the epithelium as a whole passes through major differentiative stages. These stages have been documented most thoroughly in rats and mice, in which rapid differentiation

re the normal in vivo state is
roliferation and cell loss, in
s. It is thus useful to review
vivo as a reference point for

ERENTIATION IN VIVO

lls composed of millions of
ar the bottom of each crypt
erentiate along one of several
the exception of Paneth cells
ng, 1976]. The three major
s), goblet cells, and entero-
id perform important physio-
le, crypt enterocytes actively
conduct receptor-mediated
bulins from the lamina pro-
; crypt goblet cells conduct
nd Neutra, 1980; Neutra and
gulatory peptides and amines
nals [Walsh, 1987]. As these
n the small intestine) or onto
, and rectum), they rapidly
crypt mouth, columnar cells
ders [Madara and Trier, 1987]
rminal digestion and absorp-
79]. At the same transition
ecian and Neutra, 1980; Phil-
oduction, movement of new
is tip, this entire sequence of
pt-villus axis at any moment
recise definition not only of
f the appearance and disap-
cell differentiation in vivo

state system, the epithelium
ages. These stages have been
n which rapid differentiation

TABLE I. Landmarks of Epithelial Differentiation in Adult Small Intestine: The Crypt-Villus Axis*

	Crypt	Transition	Villus	
Cell position	Base	Mouth	Base	Tip
Morphologic features of enterocytes	Short microvilli free ribosomes	Brush border assembly	Long microvilli terminal web	Cell sloughing
	Occluding junctions simple		Occluding junction complex	
Physiologic parameters	^{3}H-thymidine uptake, mitosis mRNA synthesis			
	Goblet cells: cholinergic sensitivity		Goblet cells: insensitive to cholinergics	
	Secretagogue-induced chloride secretion		Ion-water absorption Na-dependent nutrient transport	
Enzyme activities	Thymidine kinase		Three disaccharidases Four peptidases } Apical	
		Basolateral Na, K-ATPase Apical Alkaline phosphatase		
Other antigens and biochemical markers		28–34 kD antigen	Fucose-rich apical glycoproteins	

*For references, see section IIA in text.

occurs late in fetal life, establishing a highly differentiated epithelial system specialized for the suckling period, the first three weeks of life (Table II). In humans, a similar stage occurs much earlier, during the first trimester of pregnancy, but is maintained only until the midpoint of gestation and is no longer present during the suckling period.

1. Predifferentiated fetal epithelium. The intestinal epithelium of fetal rats 1 week before birth (and of fetal humans at 8–9 weeks gestation) is a multilayer of undifferentiated cells [Trier and Moxey, 1979]. In rats, cells of the upper layer are joined by tight junctions that prevent paracellular passage of macromolecules, and luminal membranes have short, sparse microvilli [Trier and Moxey, 1979; Colony and Neutra, 1985]. Deeper cells show no polarity and mitoses occur throughout the epithelium [Hermos et al., 1971]. At this

TABLE II. Markers of Epithelial Differentiation During Normal Rat Intestinal Development*

Developmental stage	Age of onset	Morphologic indicators	Biochemical and immunological markers
Fetal			
Pre differentiation	Up to 15 days of gestation	Simple columnar epithelium Apical tight junctions	Villin: diffuse cytoplasmic
Proliferation	15–16 days of gestation	Stratified epithelium (mammals)	"Fetal antigens" throughout eptihelium
Epithelial conversion	17–19 days of gestation	Secondary lumens Apical cell loss Simple columnar epithelium reestablished	Alkaline phosphatase pI 7–8 (apical) Na,K-ATPase (basolateral)
Cytodifferentiation Stage I	19–21 days of gestation	Assembly of brush borders Villus formation	Villin localized in brush borders 110 kD protein localized in brush borders TW 260/240 localized in brush borders
		Assembly of apical endocytic complexes	IgG Fc receptors (proximal) Endosomal gp55–61 (distal)
			Brush border enzymes appear: Alkaline phosphatase (pI 5–6)

conversion		Apical cell loss Simple columnar epithelium reestablished	(apical) Na,K-ATPase (basolateral)
Cytodifferentiation Stage I	19–21 days of gestation	Assembly of brush borders Villus formation	Villin localized in brush borders 110 kD protein localized in brush borders TW 260/240 localized in brush borders
		Assembly of apical endocytic complexes	IgG Fc receptors (proximal) Endosomal gp55–61 (distal)
			Brush border enzymes appear: Alkaline phosphatase (pI 5–6)
			Lactase Aminopeptidase Maltase (low level) Other antigens
		Other cell types appear: Enteroendocrine cells Paneth cells Goblet cells	Enteric peptide hormones Lysozyme Mucin
Establishment of proliferative units	1–5 days after birth	Crypt formation: mitosis confined to crypts	"Fetal antigens" confined to crypts
Cytodifferentiation Stage II	18–25 days after birth	Adult-type absorptive cells (no apical endocytic complexes)	Disappearance of IgG receptors Disappearance of gp55–61 Decrease in lactase
		Villi in proximal colon with small intestinal morphology and enzymes	Brush border enzymes increase: Aminopeptidase Maltase Sucrase-isomaltase appears
		Crypt goblet cells respond to acetylcholine	Other brush border enzymes and antigens appear

*For references, see text.

stage, "fetal antigens" representing carbohydrate epitopes are present throughout the epithelium [Quaroni, 1986a]. These antigens are limited to cells of the crypts and lower villi in suckling rats and to crypt cells alone in adults. Between 17 and 20 days gestation in rats (9–10 weeks in humans), the stratified epithelium is converted to simple columnar by a complex process involving formation of new tight junctions and secondary lumens and sloughing of apical cells into the lumen [Trier and Moxey, 1979; Madara et al., 1981]. During this process, in rats, polarized apical and basolateral "marker" phosphatases (alkaline phosphatase and Na, K-ATPase) first became detectable, already sorted to the proper domain [Colony and Neutra, 1983; Amerongen et al., 1987]. At 18 days in rat small intestine and at 19 days in colon, differentiated goblet and endocrine cells begin to appear, identified by their characteristic storage granules. In general, differentiative changes appear first in proximal intestine and 1–2 days later in distal regions.

2. Cytodifferentiation stage I. About 1 day after the conversion of the epithelium to a monolayer in rat small intestine (19 days) and colon (20 days), a dramatic burst of cytodifferentiation occurs, and a variety of polarized, differentiated features suddenly appear (Table II). For example, the microvilli of absorptive cells elongate and dramatically increase in number while assembly of the complex brush border cytoskeletal morphology is completed. In chickens, in which the epithelium is a simple monolayer throughout development, assembly of the brush border cytoskeleton from previously synthesized proteins is completed just before hatching [Shibayama et al., 1987]. In rats, integral membrane enzymes such as lactase and aminopeptidase are synthesized and inserted into apical microvillus membranes at 17–19 days, and maltase appears about 2 days later [Koldovsky, 1969; Quaroni, 1985a]. At the same time, specialized endocytic membrane systems assemble at the apical poles of absorptive cells, as if in anticipation of birth and the onset of suckling [Trier and Moxey, 1979; Wilson et al., 1987b]. At this stage, regional differences in absorptive cells appear: In proximal small intestine, the membrane systems designed for Fc receptor-mediated uptake of maternal IgG appear, including polarized apical endosomal compartments [Colony and Neutra, 1985]; in distal small intestine and proximal colon, specialized intermicrovillus membrane invaginations and apical endosomal tubules develop bearing nonintegral luminal arrays; this endosomal membrane system contains an integral 55–61 kD glycoprotein that serves as a marker for these membranes throughout the suckling period [Wilson et al., 1987a]. In the 2 days before birth, endosomal vesicles and multivesicular bodies are assembled in the apical cytoplasm of ileal absorptive cells, while dense vesicles, presumably primary lysosomes, accumulate near the Golgi complex [Wilson et al., 1987b]. Luminal macromolecules, in part derived from swallowed amniotic fluid, are endocytosed by both proximal and distal absorptive cells in late fetal life, and

both transepithelial transport and lysosomal digestion occur [Colony and Neutra, 1985].

Relatively few dramatic changes occur at birth in rats. With the first milk meal, multivesicular bodies and lysosomes in ileal absorptive cells rapidly fuse to form the giant lysosomal vacuole in which milk components are digested [Wilson et al., 1987b]. Transepithelial transport of maternal IgG [Rodewald and Abrahamson, 1982] and growth factors present in milk [Siminoski et al., 1986; Gonnella et al., 1987] occurs in proximal and distal absorptive cells, respectively. Mitotic activity, widespread in the fetal epithelium, becomes limited to intervillus regions and then to the crypts that develop during the first few days after birth, establishing the crypt-villus axis of differentiation [Hermos et al., 1971; Quaroni, 1985b]. Three new apical antigens of unknown function appear after birth and disappear at weaning [Quaroni, 1985a]. In general, however, the brush border protein profile, in which identified enzymes account for a minority of membrane proteins [Hauri et al., 1985], is stable from before birth to the end of the suckling period in rats [Quaroni, 1985a]. The relative paucity of brush border hydrolases during the suckling period is related to the importance of intracellular lysosomal digestion of nutrients during this stage.

3. Cytodifferentiation stage II. At weaning (18–25 days postnatally in rats), the final phase of differentiation is accomplished by production of new, adult-type cells from proliferative precursors in the crypts and progressive displacement of suckling-type cells toward the villus tips [Koldovsky, 1969; Moog, 1979]. Thus individual absorptive cells do not change phenotype, but the epithelium as a whole shows dramatic changes from cell replacement (Table II). Brush border membranes of adult villus cells are rich in hydrolytic enzymes; some of those that were present on suckling cells shift to more acidic forms, and new enzymes appear [Quaroni, 1985a]. Endocytic activity declines, and the cells with elaborate apical endocytic systems with their marker antigens, along with IgG receptors in jejunum and gp 55-61 in ileum, disappear. Crypt goblet cells produced during and after weaning are responsive to cholinergic secretagogues, in contrast to goblet cells of fetal and suckling intestine in which cholinergic agents have no effect [Neutra et al., 1984]. After weaning, a stable sequence of cell differentiation along the crypt-villus axis is present and persists through adult life, as described above (Table I).

C. Human Fetal Development

Much less information is available about human fetal intestinal differentiation, but morphologic and tracer studies have established that the human intestine is relatively mature at birth [Grand et al., 1976]. The same general sequence of differentiative changes observed in rats occurs early during human fetal life [Trier and Moxey, 1979]. At 8–9 weeks of gestation, the human epithelium is stratified. Goblet cells appear in the stratified epithelium as early as 9–10 weeks

and endocrine and Paneth cells soon thereafter. Formation of secondary lumens, conversion to simple columnar epithelium, and formation of villi occurs by 10–11 weeks in the duodenum; both villi and crypts are well developed by 12 weeks.

Stage I cytodifferentiation in humans occurs at 10–12 weeks of gestation. Between 10 and 20 weeks, absorptive cells that line villi throughout the human fetal intestine bear morphologic resemblance to cells of suckling rat ileum, with abundant apical tubules bearing luminal arrays and multiple large lysosome-like vesicles [Trier and Moxey, 1979]. Electron-dense tracers injected into amniotic fluid of a fetal monkey in vivo or injected into the intestinal lumen in an aborted human fetus were endocytosed at this stage but not transported transepithelially [Lev and Orlic, 1973; Moxey and Trier, 1979]. It is not known whether human fetal cells that are actively endocytic express IgG receptors or other components found in suckling rat endocytic pathways or whether they conduct selective transepithelial transport of antibodies, hormones, or other proteins from swallowed amniotic fluid.

Stage II cytodifferentiation in humans occurs at the midpoint of gestation. By 22 weeks, endocytic cells have disappeared in proximal intestine; the exact time of their disappearance from distal regions is unknown [Trier and Moxey, 1979]. Thus an adult-like epithelium is established in the small intestine by the midpoint of human pregnancy, and no dramatic changes occur at birth or at weaning. The human fetal colon at 3–5 months of gestation resembles small intestine in that rudimentary villi are present, and brush border hydrolases; including sucrase-isomaltase and aminopeptidase, are expressed [Koldovsky, 1969; Grand et al., 1976]. These enzymes are absent from colonic epithelial cells at birth and thereafter but reappear in certain well differentiated lines of colon carcinoma cells (see below).

III. INTESTINAL EPITHELIAL CULTURE SYSTEMS

In attempts to reproduce these complex stages of epithelial differentiation, investigators have used three general strategies: 1) separation and culture of normal epithelial cells, 2) maintenance of intestinal explants in organ culture, and 3) culture of neoplastic epithelial cells derived from intestinal adenocarcinomas.

A. Culture of Normal Intestinal Cells

Attempts at establishing primary, differentiated cell cultures or short-term differentiated monolayers from adult intestine have been uniformly unsuccessful. Dispersed epithelial cells are readily obtained from intestinal mucosa of adult rodents, rabbits, chickens, and humans, but they remain viable in culture for only a few hours at most. Such cells have been useful for short-term physiologic experiments that do not require maintenance of polarity, but they

do not proliferate or reestablish monolayers [Moyer, 1983]. This presumably is due to the fact that most such cells are derived from villi and even in vivo would be nonproliferative and short-lived.

As one alternative, intact sheets of epithelium in which tight junctions and crypt-villus architecture are preserved have been obtained from rodents by brief intravascular EDTA perfusion [Bjerknes and Cheng, 1981]. Protein and glycoprotein synthesis continues, apical-basolateral polarity is maintained, and exocytosis can be induced for up to 1 hour in such floating epithelia [Phillips et al., 1984], but basolateral surfaces rapidly lose their normal organization. For example, Na, K-ATPase, normally concentrated in the lateral domain in intact epithelium, moves into the basal domain and is endocytosed shortly after epithelial isolation [Amerongen et al., 1987]. Thus such preparations are of limited usefulness for studies of transport physiology or membrane polarity. It is possible that viability of epithelial sheets could be extended somewhat by culture in or upon media containing appropriate extracellular matrix (ECM) components [Sugrue and Hay, 1982], but it is unlikely that the complex crypt-villus system can be maintained for many hours in this way.

Successful long-term primary culture of undifferentiated intestinal epithelial cells was achieved using benign human tumor cells [Friedman et al., 1981], rat fetal epithelial cells [Negrel et al., 1983], and collagenase-dissociated cells from suckling rat small intestine [Quaroni et al., 1979; Quaroni and May, 1980]. Selected epithelial colonies from the latter cultures were serially passaged, providing nonneoplastic, proliferative lines of intestinal epithelial cells (IEC). These lines, now maintained for nearly a decade, can form monolayers of cuboidal, polarized cells but consistently fail to differentiate in monolayer culture or to express brush border enzymes. Since IEC cells retain proliferative capacity, they presumably are analagous to crypt cells [Quaroni and May, 1980]. Recently, Kedinger and collaborators [1986a, b] succeeded in inducing IEC and fetal cell differentiation by seeding them onto denuded 14 day rat fetal mesenchyme and grafting the recombinant tissue under the kidney capsule of adult rats. Within 10 days, implants that survived developed typical intestinal mucosal structures, with all four epithelial cell types including absorptive cells that expressed typical brush border enzymes. This work established the pluripotent nature of IEC cells and also underscored the importance of mesenchymal cells and their products in intestinal morphogenesis and cytodifferentiation [Kedinger et al., 1981, 1986a, 1987; Haffen et al., 1987]. The recombination grafting technique results in a complex tissue, however, in which individual cell types are as inaccessible as in normal intestine.

B. Culture of Intestinal Explants

Small (2–4 mm^2) samples of intact intestinal mucosa, obtained from humans by biopsy and from experimental animals by surgery, have been maintained in

vitro for up to 24 hours [Trier, 1976; Neutra, 1980; Shields et al., 1979; Arsenault and Menard, 1984]. These preparations have been useful for short-term physiologic studies but are too short-lived for experimental manipulation of cell differentiation. Rodent and chick fetal explants consisting of short tubular segments of intestine, however, can survive for long periods immersed in culture medium and can proceed to differentiate as in vivo [DeRitis et al., 1975; Black and Moog, 1978; Ishizuya-Oka, 1983; Truding et al., 1981; Kondo et al., 1984]. Differentiation of fetal segments also has been demonstrated after subcutaneous implantation into adult rats [Leapman et al., 1974; Montgomery et al., 1981]. In all these cases, survival and differentiation in culture could be initiated only with predifferentiated intestinal segments (17–18 days gestation in the rat) when the epithelium is stratified and cytodifferentiation has not yet begun.

Several attempts have been made to obtain cultured epithelial monolayers derived from undifferentiated fetal intestinal cells. Montgomery and coworkers [1983] cultured mixed populations of trypsin-dissociated intestinal cells from 18 day fetal rats. After initial growth in vitro, cells were injected subcutaneously or intraperitoneally into adult rats, and a differentiated intestinal mucosa was assembled in these sites [Montgomery et al., 1983]. To obtain a more accessible system, mixed fetal epithelial and mesenchymal cells were seeded on collagen substrates or within a collagen "sandwich," with or without added Matrigel, producing villus-like structures on the flat substrates and tubular structures in the sandwich [Montgomery, 1986]. The resulting cultures in all cases consisted of mesenchymal cells underlying a cuboidal or columnar, well-polarized epithelial monolayer with goblet cells, showing proliferative activity. Apical alkaline phosphatase was expressed, but terminal differentiation analagous to villus cells in vivo was not observed [Montgomery, 1986].

Terminal differentiation did occur in epithelial-mesenchymal structures produced by Quaroni [1985c] as outgrowths from 18 day fetal segments in organ culture. Epithelial cells in these outgrowths were tall columnar and highly polarized with multiple cell types, well developed apical brush borders, and expression of many of the plasma membrane antigens present on normal villus cells. In addition, the endocytic complex typical of suckling rat ileal absorptive cells appeared in cells of the cultured outgrowths. Pure epithelial cell cultures isolated from these outgrowths, however, failed to differentiate in culture and resembled the IEC cells derived from suckling rat intestinal crypts described above [Quaroni, 1985c]. Thus, in all systems tested so far, cells derived from normal intestinal epithelium seem to require the presence and presumably the products of intestinal mesenchymal cells in order to differentiate [Haffen et al., 1987; Kedinger et al., 1987]. Standard basal lamina components are present under the normal intestinal epithelium [Laurie et al., 1982] but their exact roles in epithelial differentiation have not been defined. Faced

with this limitation of normal intestinal cell culture, many investigators have turned to immortal cell lines derived from human colonic tumors.

C. Intestinal Adenocarcinoma Cell Lines

Dozens of human adenocarcinoma cell lines are available because adenocarcinoma of the colon is a common human malignancy [Fogh and Trempe, 1975]. The growth properties of many lines in culture and in transplants have been described and reviewed [Fogh et al., 1977]. An antibody that specifically recognized a component present only on normal rat fetal and neonatal intestinal cells also recognized its antigen on 11 of 12 malignant human cell lines [Quaroni, 1986b], confirming the general similarity of neoplastic colonic cells and fetal epithelial cells [Zweibaum et al., 1983, 1984]. Such a relationship had been initially suggested 25 years ago with the discovery of carcinoembryonic antigen [Gold and Freedman, 1965]. Colon carcinomas vary widely in their degree of differentiation in situ and in their differentiative capacity when grown as tumors in nude mice [Fogh et al., 1977]. Differentiation was observed when colon carcinoma cells were cultured on fetal rat mesenchyme [Fukamachi et al., 1986]. (For a detailed review of the metabolic and physiologic properties of established adenocarcinoma cell lines in culture, see Zweibaum et al. [1988] and Chantret et al. [1988].) Under standard cell culture conditions, most cell lines do not differentiate.

1. Caco-2. One important exception is the Caco-2 cell line. Caco-2 cells were derived from a relatively well differentiated tumor and grow slowly in nude mice. When seeded either on permeable filters or impermeable substrates (plastic or glass) at high density, they consistently form well polarized monolayers joined by tight junctions, with well developed apical microvilli [Pinto et al., 1983]. Such monolayers survive for up to 30 days in culture before spontaneously detaching from the substrate. Although derived from adult human colon, where microvillar hydrolases are not expressed, Caco-2 cells express two disaccharidases and two peptidases typical of normal small intestinal villus cells; they also transport ions and water toward the basolateral surface, forming domes on impermeable substrates [Pinto et al., 1983]. Despite this superficial resemblance to normal small intestinal absorptive enterocytes, Caco-2 cells are more closely analagous to enterocytes of the normal 15-week human fetal colon, in which microvillar hydrolases are transiently expressed [Koldovsky, 1969; Grand et al., 1976]. Indeed, Caco-2 membrane hydrolases were shown to occur in molecular forms typical of fetal tissues [Hauri et al., 1985]. In their electrical parameters, ion conductance, and permeability properties, Caco-2 monolayers resemble colonic crypt cells [Grasset et al., 1984]. Whereas crypts contain multiple cell types, however, Caco-2 monolayers are remarkably homogeneous, suggesting that these cells represent the neoplastic equivalent of crypt

enterocytes committed to the absorptive cell line but arrested in differentiation at the crypt/fetal stage.

2. T84. The T84 cell line, originally derived from a lung metastasis of a human colon carcinoma, resembles Caco-2 in its ability to form spontaneously well polarized monolayers of high electrical resistance [Dharmsathaphorn et al., 1984, 1985]. Unlike Caco-2 cells, T84 cells do not form well developed brush borders and fail to express microvillar membrane hydrolases. In their morphology, electrical parameters, and ion transport activities, T84 monolayers resemble adult colonic crypt cells [Madara and Dharmsathaphorn, 1985]. Like Caco-2 cells, T84 cell monolayers are homogeneous and appear to represent a line derived from committed crypt cells (see elsewhere in this volume). In both Caco-2 and T84 cells, monolayer formation and differentiation are accelerated on substrates such as collagen that enhance cell attachment, and differentiation is preceded by synthesis and polarized secretion of basal lamina components [Madara et al., 1987].

3. HT29. The HT29 cell line, in contrast, does not show polarity or other differentiated characteristics of intestinal cells under standard conditions (in media containing glucose and normal serum), and until recently these cells were useful only for studies of general cell features, such as ubiquitous receptors and carbohydrate metabolism [Rousset et al., 1981; Rousset, 1986]. When grown in the absence of glucose, however, HT29 cells exhibit a high degree of differentiation [Pinto et al., 1982], surpassing in some respects all other neoplastic lines developed to date [Rousset, 1986]. Phenotypes resembling terminally differentiated goblet and absorptive cells appeared in highly polarized, confluent HT29 cell monolayers when galactose, inosine, or uridine were substituted for glucose as carbon sources [Pinto et al., 1982; Wice et al., 1985] or even in the total absence of these additives [Zweibaum et al., 1985]. Conditions permissive for differentiation also include the presence of supplemental human transferrin and nonessential amino acids and seeding at high density so that confluence is reached within a few days after plating. Differentiated HT29 cells express four brush border enzymes: alkaline phosphatase, sucrase-isomaltase, aminopeptidase N and dipeptidylpeptidase IV [Pinto et al., 1982; Zweibaum et al., 1983, 1984, 1985], all of which are typical of normal fetal colon. HT29 cells grown in the absense of glucose form highly polarized, differentiated monolayers either on permeable filters or uncoated, impermeable glass. Although they do not secrete a basal lamina visible by electron microscopy, both undifferentiated and differentiated HT29 cells do secrete immunoreactive laminin. Since differentiation can be manipulated in culture, HT29 monolayers offer unique opportunities to reproduce and dissect the process of intestinal cell differentiation and to identify factors that govern the physiologic functions of terminally differentiated intestinal cells.

The value of the HT29 cell line has been further extended by isolation of

clones and subclones. A clone designated HT29-18 was shown to be multipotent, giving rise to both goblet and absorptive cells when grown in the absence of glucose, and a fraction of these cells retained partially differentiated characteristics, such as the ability to form monolayers when returned to glucose-containing medium [Huet et al., 1987]. Subcloning of differentiated HT29-18 cells by limiting dilution and replating in medium containing glucose produced colonies that expressed a single phenotype, either goblet cell or absorptive cell (Fig. 1) [Huet et al., 1987]. Further studies have established that fully differentiated HT29 subclones, like the HT29 parent and cloned lines, show many characteristics typical of terminally differentiated surface epithelial cells in the human fetal colon. These features are described in more detail below.

IV. USE OF IN VITRO SYSTEMS FOR STUDY OF INTESTINAL CELL BIOLOGY

A. Cell Differentiation

IEC cells consistently fail to differentiate in monolayer culture [Quaroni and May, 1980], and so far this requirement has not been fulfilled by coating culture surfaces with ECM components reconstituted from tissue extracts. IEC cells did differentiate when seeded onto denuded native fetal mesenchyme and implanted in vivo (as did fetal endodermal cells); differentiation was induced in these recombinant tissues regardless of the source of the mesenchyme—either intestine or skin [Kedinger et al., 1986b, 1987; Haffen et al., 1987]. Similarly, differentiation of epithelial cells from dissociated fetal tissue [Montgomery, 1986] and in outgrowths of fetal intestinal explants [Quaroni, 1985c] has been obtained only in the presence of mesenchymal cells, although the overall shape of the resulting tissue can be influenced by the contour of the substrate provided [Montgomery, 1986]. Direct epithelial cell interactions with mesenchymal cells occurs during normal fetal development [Mathan et al., 1972; Burgess, 1976] and in vitro this poorly defined interrelationship is a prerequisite for the epithelial differentiative response to glucocorticoids [Kedinger et al., 1987]. Seeding of IEC or fetal endoderm cells onto preformed, cell-free adult intestinal basal lamina or other native matrix has not yet been reported. It is clear, however, that the crypt-villus axis of differentiation is not readily reproduced using normal intestinal cells on the artificial basal lamina preparations now available. In vivo, adult intestinal cells are accompanied during crypt-villus migration by a distinct population of subepithelial fibroblasts that migrates in parallel [Marsh and Trier, 1974; Parker et al., 1974], and these may supply chemical signals that influence expression of fully differentiated epithelial features [Haffen et al., 1987].

The neoplastic cells described above are apparently released from this con-

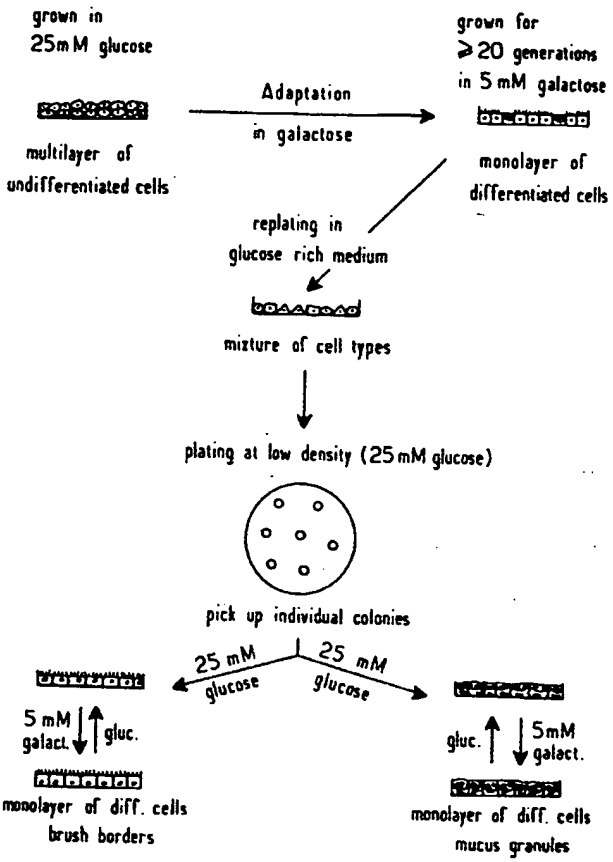

Fig. 1. Schematic diagram showing the method of isolation of HT29 clones and subclones. Clone HT29-18 was isolated after three successive clonings of the parent HT29 cell line. HT29-18 cells adapted to glucose-free medium differentiated into both absorptive and goblet cells. Further cloning of HT29-18 cells yielded subclones that were selected for their ability to differentiate into homogeneous monolayers of either absorptive cells (HT29-18/Cl) or goblet cells (HT29-18/N2). (Reproduced from the Journal of Cell Biology, 1987, 105:349, by copyright permission of the Rockefeller University Press.)

straint and proceed to differentiate without strict substrate requirements. T84 cells in conventional media and HT29 cells in media lacking glucose proliferate and form mixed monolayers/multilayers soon after seeding. Subsequent homogeneous monolayer formation is accompanied by appearance of intracellular and intraepithelial lumens containing apical membrane markers and microvilli [Madara et al., 1987; LeBivic et al., 1988b; Phillips et al., 1988] reminiscent of the secondary lumens that appear in normal fetal intestine during epithelial conversion from stratified to simple columnar [Madara et al., 1981; Colony and Neutra 1983]. This phenomenon may be useful in understanding establishment of membrane polarity, as described below.

Soon after polarized monolayers are established, all three cell lines resemble undifferentiated crypt cells morphologically, but they are not identical. Caco-2 cells seem committed to a single hybrid phenotype, expressing the ion transport properties of colonic crypt cells [Grasset et al., 1984] and some (but not all) of the apical membrane enzymes of fetal colonic villus cells [Hauri et al., 1985]. T84 cells are also committed to the enterocyte phenotype but differentiate only to the level of normal crypt epithelium [Madara and Dharmsathaphorn, 1985; Madara et al., 1987], conducting electrogenic chloride secretion that is induced by secretagogues [Dharmsathaphorn et al., 1984, 1985]. Whether T84 cells grown under other culture conditions could proceed to become analagous to colonic surface absorptive cells is unknown.

HT29 cells mimic more closely the normal crypt-villus system [Zweibaum et al., 1988]. Whereas both the parent line and clone HT29-18 are multipotent, like crypt stem cells, the subclones derived from HT29-18 when immature (shortly after confluence) are analogous to crypt cells committed to a single phenotype, either absorptive cell (HT29-18C1) or goblet cell (HT29-18N2) [Huet et al., 1987]. Other HT29 clones have also been identified as single-phenotype [Augeron and Laboisse, 1984]. Commitment of the parent cells was apparently induced either by forcing an alteration in carbohydrate metabolism [Zweibaum et al., 1985] or by long-term treatment with sodium butyrate [Augeron and Laboisse, 1984]. Evidence from both Caco-2 and HT29 cells indicates that important changes in glucose metabolism accompany differentiation: Glucose consumption and lactic acid production, as well as available UDP-N-acetylhexosamines, decline as glycoprotein synthesis increases. Availability of committed homogeneous clones and subclones has opened the way for study of the differentiation process of single cell types on the crypt-villus axis. Specific studies of HT29 absorptive cells [Dudouet et al., 1987] and goblet cells [Phillips et al., 1988] are described below.

B. Membrane Polarity

Various types of epithelial cells seem to differ in their degree of membrane polarity and their ability to sort apical and basolateral proteins. Some of these

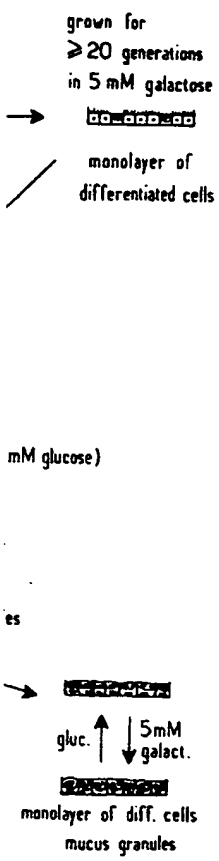

tion of HT29 clones and subclones.
of the parent HT29 cell line. HT29-18
oth absorptive and goblet cells. Fur-
selected for their ability to differenti-
cells (HT29-18/Cl) or goblet cells
ology, 1987, 105:349, by copyright

differences reflect the greater polarity achieved by normal cells in vivo as compared to cultured monolayers, and others may be attributed to the specific properties in vitro of the various cell lines used as models. Polarized delivery of viral glycoproteins in infected MDCK cells requires cell–substrate or cell–cell contact [Rodriguez-Boulan 1983a, 1983b]. Correct insertion of MDCK cell apical membrane components requires lateral cell-cell contact [Vegas-Salas et al., 1987], and maintenance of polarity depends on the tight junctional barrier [Gumbiner and Simons, 1986]. Cells of polarized, tight MDCK monolayers sort endogenous membrane proteins intracellularly in the trans-Golgi compartment [Matlin and Simons, 1984; Fuller et al., 1985]. A transfected membrane protein, the IgA receptor, was also properly sorted by MDCK monolayers [Mostov and Deitcher, 1986]. On the other hand, transfected MDCK cells expressing exogenous secretory proteins released them by "default" onto both surfaces [Gottlieb et al., 1986; Kondor Koch et al., 1985]. Some exogenous secretory proteins expressed in transfected endocrine cells were sorted properly in the trans-Golgi, entering regulated secretory granules [Moore and Kelly, 1985). In part, this may reflect the absence of a regulated secretory pathway in MDCK cells. It is not yet established whether the inability of some transfected cells to sort certain exogenous proteins properly is due to lack of the specialized recognition machinery that correctly sorts these molecules in the cells that normally express them. Terminally differentiated intestinal cells, unlike MDCK cells, show extreme structural polarity and elaborately-organized apical domains [Reggio et al., 1988]. Most of the specialized apical membrane components of enterocytes are not even synthesized until well after a high degree of polarity is established. The site of sorting in intestinal cells, however, is not clearly established. Indeed, the exact itinerary of apical and basolateral membrane proteins from the trans-Golgi cisternae to the plasma membrane in various specialized, differentiated cell types is still controversial, as discussed below.

Cultured monolayers derived from normal rat intestinal cells such as IEC lines have been of limited use in membrane polarity studies, because in monolayer culture they fail to achieve high polarity and do not express polarized membrane markers. Neoplastic intestinal cell lines, in contrast, can achieve high polarity in monolayer culture and express multiple, specific endogenous markers for both apical and basolateral domains (Figs. 2 and 3). Endogenous intestinal cell basolateral membrane components are synthesized and correctly delivered to the basolateral domain in polarized HT29 cell monolayers, including NA, K-ATPase, transferrin receptor, polymeric immunoglobulin (IgA) receptor, and histocompatibility antigen (HLA-1). An antigen of unknown function defined by monoclonal antibodies is also localized in the basolateral membrane of HT29 cells [LeBivic et al., 1988b]. In nonpolarized, undifferentiated

Fig. 2. Confluent HT29-18/Cl cells grown in medium containing glucose. This absorptive cell subclone forms polarized monolayers with tight junctions and expresses some brush border hydrolases in the presence of glucose. Bar = 1 μm.

HT29 cells grown in glucose-containing medium, these proteins are expressed over the entire surface, but, after formation of apical domains in polarized monolayers grown without glucose, they are strictly confined to the basolateral side [Godefroy et al., 1988]. This phenomenon resembles that observed during cell polarization in normal fetal rat intestine: Na, K-ATPase is distributed uniformly on surfaces of unpolarized cells in the stratified fetal epithelium but is consistently excluded from newly formed apical domains as tight junctions assemble and polarization develops [Colony and Neutra, 1983; Amerongen et al., 1987].

Fig. 3. Confluent HT29-18/Cl cells grown in medium lacking glucose but containing 5 mM galactose. In the absence of glucose, well developed brush borders are formed and the apical membrane contains sucrase-isomaltase (visualized by immunoperoxidase labeling), a marker for terminal differentiation. Bar = 1 μm.

In Caco-2 cell monolayers grown on permeable filters, secretion of the endogenous enterocyte product apolipoprotein (which in adults in vivo would be released into the circulation) and α-fetoprotein (a product of fetal endodermal tissues) occurred only toward the basolateral side as expected [Rindler and Traber, 1988]. Treatment of MDCK cell monolayers with weak bases was shown to disrupt polarized basolateral secretion of laminin, the endogenous product [Caplan et al., 1987], but in Caco-2 cells [Rindler and Traber, 1988] and HT29 cells correct basolateral delivery of endogenous products was not affected by such treatment. Furthermore, secretion of exogenous proteins (human growth hormone introduced by gene transfection and a lysosomal enzyme deficient in glycosylation) was exclusively basolateral in Caco-2 cells [Rindler and Traber, 1988]. Together, these findings indicate that basolateral delivery of membrane proteins and secretory products in intestinal cells could occur partly or entirely by default and may not require sorting signals. In addition, they underscore the danger in extrapolating data obtained using MDCK cells to specialized, highly polarized epithelial cells such as intestinal enterocytes.

Delivery of newly synthesized membrane glycoproteins to the apical domain, in contrast, seems to require the presence of tight junctions [LeBivic et al., 1988b] and functional microtubules [Blok et al., 1981a; Bennett et al., 1984] and probably depends on specific molecular sorting signals. The earliest-detected apical protein expressed in the stratified epithelium of fetal rat colon, alkaline

icking glucose but containing 5 mM
h borders are formed and the apical
nunoperoxidase labeling), a marker

filters, secretion of the endog-
h in adults in vivo would be
(a product of fetal endoder-
ral side as expected [Rindler
nolayers with weak bases was
of laminin, the endogenous
lls [Rindler and Traber, 1988]
endogenous products was not
of exogenous proteins (human
and a lysosomal enzyme defi-
eral in Caco-2 cells [Rindler
icate that basolateral delivery
n intestinal cells could occur
sorting signals. In addition,
obtained using MDCK cells
uch as intestinal enterocytes.
proteins to the apical domain,
ght junctions [LeBivic et al.,
, 1981a; Bennett et al., 1984]
g signals. The earliest-detected
um of fetal rat colon, alkaline

phosphatase, appears only after tight junctions have assembled and have defined the apical membrane domains of the mucosal surface and intra epithelial lumens [Colony and Neutra, 1983; Amerongen et al., 1987]. Cells in the fetus that lack apical domains do not express apical antigens. A 170 kD antigen normally confined to human colonic cell apical membranes is expressed in neoplastic HT29 cells even before monolayer formation, but in unpolarized HT29 cells this antigen is weakly expressed and is confined to intracellular vacuoles [LeBivic et al., 1988b]. Undifferentiated HT29 cells grown in glucose have no immunologically detectable sucrase-isomaltase, but metabolic labeling studies revealed that high-mannose and complex forms of the enzyme are synthesized and rapidly degraded. This contrasts with differentiated cells where the enzyme is processed, delivered to the cell surface, and remains stable for at least 48 hours [Trugnan et al., 1987]. Further studies demonstrated that N-glycan processing is severely altered in undifferentiated, neoplastic enterocytes [Ogier-Denis et al., 1988].

Formation of monolayers by T84 cells, as well as HT29 cells grown without glucose, is often accompanied by appearance of intraepithelial lumens defined by junctional complexes and lined by microvilli [LeBivic et al., 1988b; Madara et al., 1987; Phillips et al., 1988]. During monolayer formation in HT29 cells, the apical 170 kD antigen appeared on these small lumens as well as on the apical side of the epithelium once tight junctions were present [LeBivic et al., 1988b]. Formation of aberrant lumens between or within differentiating HT29 or T84 cells is thus reminiscent of normal fetal events. Although it must be recalled that these are neoplastic cells, the mechanisms that direct apical membrane insertion in normal cells are presumably operative in neoplastic cells as well. Thus these culture systems permit de novo formation of apical membrane to be followed (and in HT29 cells to be manipulated with culture conditions) so that factors controlling expression and sorting of apical membrane glycoproteins can be defined more clearly.

There is evidence that sorting of apical glycoproteins in intestinal cells, as in MDCK cells, occurs in the trans-Golgi compartment based on the distribution of these proteins in subcellular fractions after metabolic labeling [Danielson and Cowell, 1985] and on immunolocalization of intestinal apical proteins [Fransen et al., 1985]. There is also evidence, however, for initial targeting of apical glycoproteins to the lateral membrane, followed by rapid sorting and selective transepithelial transport to the apical side [Louvard, 1980; Massey et al., 1987]. Recent evidence from metabolic labeling studies in hepatocytes has revealed a similar pattern: Glycoproteins concentrated in the bile canalicular (apical) membrane at steady state appear transiently in the sinusoidal (basolateral) membrane soon after synthesis [Bartles and Hubbard, 1988]. Intestinal cells share with hepatocytes an endodermal origin, constitutive basolateral secretion of certain serum proteins, a basolateral-to-apical transport pathway

for IgA, and a highly specialized apical domain. It is thus conceivable that all intestinal apical membrane glycoproteins could first be inserted basolaterally, along with the IgA receptor, and then rapidly sorted for delivery to the apical domain [Bartles and Hubbard, 1988]. On the other hand, intestinal cells synthesize much larger amounts of apical membrane constituents than do hepatocytes: At least half of newly synthesized, [^{3}H]fucose-labeled membrane macromolecules appeared in apical membrane soon after synthesis, and predominantly basolateral delivery was observed only after disruption of microtubules with drugs [Blok et al., 1981a; Bennett et al., 1984]. Further studies using cultured monolayers of well differentiated intestinal cells should finally resolve this issue.

C. Synthesis and Processing of Apical Membrane Glycoproteins

Glycoproteins of the microvillus membranes show diverse and unique features that have been extensively investigated and reviewed [Hauri, 1983; Semenza, 1986]. Sucrase-isomaltase, for example, is synthesized in mammalian enterocytes as a large precursor that is processed in the rough endoplasmic reticulum (RER) and Golgi, and cleaved into two subunits—the larger intramembrane isomaltase and smaller sucrase—after insertion in the apical membrane by cell-surface proteases derived from pancreatic secretions [Hauri et al., 1982]. In the fetus, where pancreatic protease secretion is negligable, final processing does not occur, and the high-molecular-weight form persists in the apical membrane [Hauri, 1983]. Caco-2 cells express two of the three disaccharidases (sucrase-isomaltase and lactase) identified in microvillar membranes of normal intestine. Metabolic labeling and immunochemical studies of Caco-2 hydrolases revealed that the 217 kD single-chain precursor form of sucrase-isomaltase persists in Caco-2, as in human fetal intestine, and also confirmed that lactase is synthesized as a large precursor that is proteolytically cleaved, perhaps intracellularly, without the participation of pancreatic enzymes [Hauri et al., 1985]. Caco-2 cells also express aminopeptidase N and dipeptidylpeptidase IV in normal fetal forms, slightly smaller than the normal adult human enzymes. Pulse-labeling studies using the Caco-2 monolayer system further revealed that microvillar proteases are transported from RER to Golgi more rapidly than are disaccharidases [Hauri et al., 1985]. Detailed understanding of the synthetic and processing steps involved in normal enzyme production in enterocytes, derived in part from monolayer culture systems, is important for eventually elucidating the molecular and genetic defects underlying human clinical malabsorption syndromes such as lactase and sucrase-isomaltase deficiency [Naim et al., 1988].

D. Development of a Polarized Cytoskeleton

The molecular architecture of the enterocyte brush border has been extensively studied as a model system for membrane-cytoskeleton interactions and assembly of actin filaments and filament bundles [for review, see Mooseker,

1985]. The apical microvilli of enterocytes contain cell-specific actin-associated components, including villin, a 95 kD protein that controls polymerization of actin [Bretscher and Weber, 1980; Mooseker, 1985] and a 110 kD protein–calmodulin complex that contains actin-activated Mg-ATPase activity and forms periodic actin-membrane cross bridges along the microvillus [Collins and Borysenko, 1984; Conzelman and Mooseker, 1987], in association with a 140/200 kD membrane glycoprotein [Coudrier et al., 1983]. Microvillus actin core rootlets also interact with an enterocyte brush border-specific form of spectrin [Glenney and Glenney, 1983; Pearl et al., 1984].

Immunocytochemical studies in developing chick embryos showed that key elements of the brush border cytoskeleton are present in diffuse form early in development, but their assembly in the brush border occurs in stages and is completed just before hatching when typical brush border ultrastructure is established. Three actin-associated proteins of the microvillar core moved into place at the apical pole at different times: villin at 8 days, fimbrin at 10 days, and 110 kD protein only at 21–22 days [Shibayama et al., 1987].

Villin in mammalian enterocytes is also diffusely distributed in undifferentiated cells of adult crypts and fetal intestine but concentrates in the apical brush border as cells undergo terminal differentiation [Robine et al., 1985]. Because villin is present in enterocytes at all differentiative stages, including primitive fetal endoderm, and in tumors derived from intestinal epithelium regardless of their state of differentiation, it provides a diagnostically valuable antigenic marker for identification of adenocarcinomas of intestinal origin [Robine et al., 1985].

Terminal differentiation of HT29 cells, the multipotent clone HT29-18, and the enterocyte subclone HT29-18C1 is accompanied by assembly of well developed brush borders (Fig. 3). The presence and distribution of villin, like other markers of differentiation, was dramatically altered by shifting cells from glucose-containing to glucose-free media. Enzyme-linked immunosorbant assay (ELISA) and immunoflourescence using specific antivillin monoclonal antibodies revealed that villin in well differentiated HT29-18 cells is as abundant as in normal human enterocytes and is concentrated in microvillar cores, whereas villin in undifferentiated HT29-18 cells is diffusely distributed and present at low levels [Dudouet et al., 1987]. HT29-18 cells dramatically increase rates of villin synthesis during differentiation, attributable either to an increase in transcription or to stabilization of villin mRNA [Pringault et al., 1986]. The HT29 cell system, in which brush border assembly can be controlled by manipulating culture conditions, opens the way for clearer understanding of brush border assembly using molecular biological approaches.

E. Vectoral Ion Transport

Net ion and water movements across the normal intestinal epithelium represent the sum of movements across distinct microareas: ion secretion from

crypts and ion absorption from villi [Welsh et al., 1981; Powell, 1987]. Furthermore, fluxes within each area may represent the sum of paracellular permeability differences among various cell types [Marcial et al., 1984]. The homogenous monolayer culture systems T84 and Caco-2 have been proved valuable alternatives to the complex normal situation even though they are derived from neoplastic cells that may differ in some respects from normal enterocytes. Transport and permeability studies using the T84 cell system are described in detail elsewhere in this volume.

Caco-2 cells grown under standard culture conditions show ion transport properties analagous to normal colonic crypt cells and not to cells on the mucosal surface [Grasset et al., 1985]. Differentiation of Caco-2 cells was accompanied by a tenfold increase in receptors for vasoactive intestinal peptide (VIP), a secretagogue that induces vectoral transport of fluid and electrolytes in normal intestinal crypts [Laburthe et al., 1987]. Caco-2 cell monolayers are sensitive to physiological secretagogues such as VIP and other agents that elevate intracellular cyclic AMP concentrations, and respond with an apically directed secretion of chloride ions [Grasset et al., 1985], but they do not exhibit electrogenic, amiloride-sensitive sodium absorption [Grasset et al., 1984]. Caco-2 cells grown on impermeable substrates in the absense of secretagogues form domes, however, indicating their ability to transport ions in an apical to basolateral direction [Pinto et al., 1983]. Caco-2 cell monolayers develop tight junctions that prevent passage of macromolecules [Hidalgo et al., 1988], as do cells of normal crypts [Phillips et al., 1987], and provide electrical resistance of about 150 ohms/cm^2 [Grasset et al., 1984]. This value is somewhat lower than that of normal colonic mucosa in vivo, where both leaky crypt and tighter surface junctions are present [Powell, 1987].

F. Endocytosis and Transport of Macromolecules

Nonselective endocytosis and transepithelial transport of luminal macromolecules occur in the rat fetal intestinal epithelium at all stages [Colony and Neutra, 1985]. In rats, specific receptor-mediated endocytosis and transepithelial transport of milk macromolecules, including maternal IgG [Rodewald and Abrahamson, 1982] and growth factors [Siminoski et al., 1986; Gonnella et al., 1987], is confined to the absorptive cells of the suckling period and involves highly polarized apical endosomal compartments [Wilson et al., 1987a]. The IEC monolayer culture system derived from normal rat intestinal crypts does not produce suckling-type endocytic cells even when fully differentiated on mesenchymal substrates [Kedinger et al., 1986b]. Cultures derived from rat fetal explants including fetal mesenchyme did produce epithelial cells with the apical tubules and lysosomal vacuoles characteristic of the suckling rat ileum, but pure epithelial monolayers isolated from these explants failed to develop such features [Quaroni, 1985].

al., 1981; Powell, 1987]. Fur-
it the sum of paracellular per-
s [Marcial et al., 1984]. The
nd Caco-2 have been proved
ituation even though they are
n some respects from normal
using the T84 cell system are

conditions show ion transport
s and not to cells on the muco-
n of Caco-2 cells was accom-
active intestinal peptide (VIP),
f fluid and electrolytes in nor-
co-2 cell monolayers are sen-
P and other agents that elevate
pond with an apically directed
, but they do not exhibit elec-
[Grasset et al., 1984]. Caco-2
bsense of secretagogues form
ansport ions in an apical to
cell monolayers develop tight
les [Hidalgo et al., 1988], as
, and provide electrical resis-
984]. This value is somewhat
o, where both leaky crypt and
37].

cules

transport of luminal macro-
ium at all stages [Colony and
endocytosis and transepithelial
naternal IgG [Rodewald and
oski et al., 1986; Gonnella et
e suckling period and involves
s [Wilson et al., 1987a]. The
mal rat intestinal crypts does
when fully differentiated on
b]. Cultures derived from rat
produce epithelial cells with
acteristic of the suckling rat
from these explants failed to

Adult rat and human absorptive cells nonselectively endocytose small amounts of luminal protein but generally direct them to apical lysosomes [Blok et al., 1981a]. Absorptive cells with apical endocytic systems morphologically comparable to those seen in suckling rat ileum are present in human fetal enterocytes between 10 and 20 weeks of gestation [Trier and Colony, 1979], but such cells have not been observed to date in cultured human adenocarcinoma cell lines. Differentiation of HT29 cells in glucose-free medium, for example, seems to recapitulate the crypt-villus axis of development in fetal colon at a later gestational stage, after the disappearance of endocytic cells. Caco-2 cells are also comparable to fetal colonic cells at a stage that lacks endocytic complexes. Like normal adult rat and human enterocytes, they endocytose fluid-phase tracers from both apical and basolateral surfaces and direct the tracers to apical lysosomes [Hidalgo et al., 1988]. Thus there is presently no monolayer system in which the elaborate, polarized endocytic systems of fetal/neonatal enterocytes are reproduced in monolayer culture.

Adult intestinal cells in the ileum conduct receptor-mediated endocytosis of intrinsic factor (IF)–cobalamin (vitamin B_{12}) complexes from apical coated pits between microvilli [Levine et al., 1986], but the intracellular fates of IF and its receptor are unclear. Recently, Caco-2 cell monolayers were shown to bind and internalize both IF–cobalamin and cobalamin alone, and the receptor was identified as a 90 kD glycoprotein, contrasting with the 180 kD species identified as a cobalamin receptor in normal human ileum [Muthiah and Seetharam, 1987].

The basolateral membrane of adult enterocytes contains receptors for transferrin and polymeric IgA, both of which mediate uptake of their respective ligands into basolateral endosomes [Slot and Geuze, 1984; Banerjee et al., 1986]. In HT29-18C1 cells, as in other polarized cells [Klausner et al., 1983], ferrotransferrin uptake into acidic compartments delivers iron to the cell, and apotransferrin–receptor complexes are recycled to the basolateral plasma membrane [Godefroy et al., 1988]. IgA–receptor complexes, in contrast, do not recycle but are delivered to the apical surface, where the receptor is cleaved, releasing secretory IgA into the lumen [Mostov and Blobel, 1982]. Separation of flourescently labeled IgA and tranferrin after basolateral endocytosis in enterocytes has been reported, but detailed studies on receptor movements in the endocytic membrane systems at the basolateral cell surface are lacking.

The HT29 cell system provides an excellent enterocyte-like model in which basolateral receptors can be followed morphologically and biochemically. In addition to receptors for transferrin, Ia antigen (MHC II) is present on basolateral membranes of normal crypt enterocytes [Gorvel et al., 1984; Mayrhofer, 1984]. Both transferrin receptors and histocompatibility antigen are basolateral on well polarized HT29 cells. These two membrane proteins are uniformly dis-

tributed on nonpolarized HT29 cells but acquire polarized distribution during differentiation, being excluded from the newly formed apical membrane domain [Godefroy et al., 1988]. Study of transferrin receptor, IgA receptor, and other molecular traffic in HT29 cells will serve to extend the information already gained from other polarized cell systems such as hepatocytes. Further study of the synthesis, trafficking, and function of intestinal epithelial histocompatibility complexes in HT29 cells may reveal their exact function in normal intestine, which is presently unknown; this may help to clarify the interactions of crypt enterocytes with luminal antigens and with cells of the mucosal immune system [Mayrhofer, 1984].

G. Regulated Secretion

Much of the information currently available regarding the mechanisms of sorting of secretory proteins into constitutively secreted vesicles or regulated storage granules has been derived from endocrine cells [for review see Kelly, 1985]. Polarized epithelial monolayer culture systems that reproduce the regulated, polarized secretion of exocrine cells have not generally been available. The AR42J rat pancreatic cell line, proposed for this purpose, synthesizes amylase and releases it in response to cholecystokinin when grown in monolayer culture [Logsdon et al., 1984] but these cells do not store secretory granules to the same degree as do normal pancreatic cells.

The HT29-18N2 subclone now provides a valuable alternative. When grown in the absense of glucose, these cells form highly polarized, homogeneous monolayers showing the morphological features of fully differentiated intestinal goblet cells [Huet et al., 1987], a cell type highly specialized for exocrine secretion of mucin [Neutra and Forstner, 1987]. The sequence of morphologic changes in HT29-18N2 cells during cytodifferentiation in confluent monolayers resembles that seen during goblet cell differentiation in normal crypts in vivo [Phillips et al., 1988] (Fig. 4). Immunocytochemical analysis, using a panel of monoclonal antibodies directed against defined oligosaccharide and peptide epitopes of normal human colonic mucin, revealed that HT29-18N2 cells synthesize human colonic mucin but show more heterogeneity in oligosaccharide epitopes than do normal human goblet cells (Fig. 5). Constitutive secretion of glycoproteins was detected prior to differentiation, but immunoreactive mucin appeared only after formation of stored secretory granules. Terminally differentiated HT29-18N2 goblet cells respond to cholinergic secretagogues, analagous to intestinal crypt goblet cells [Phillips et al., 1988].

These cells can be grown on both permeable and impermeable substrates, allowing application of secretagogues to basolateral membranes. In addition, differentiation can be modulated by changing culture conditions so that some degree of synchrony can be obtained, a situation impossible to obtain in vivo. HT29-18N2 goblet cells store secretory granules to the same extent as their

polarized distribution during
med apical membrane domain
ptor, IgA receptor, and other
tend the information already
is hepatocytes. Further study
stinal epithelial histocompat-
xact function in normal intes-
to clarify the interactions of
cells of the mucosal immune

egarding the mechanisms of
ecreted vesicles or regulated
e cells [for review see Kelly,
stems that reproduce the reg-
ve not generally been avail-
l for this purpose, synthesizes
kinin when grown in mono-
s do not store secretory gran-
ells.
able alternative. When grown
ly polarized, homogeneous
f fully differentiated intesti-
ghly specialized for exocrine
. The sequence of morpho-
rentiation in confluent mono-
ferentiation in normal crypts
tochemical analysis, using a
defined oligosaccharide and
n, revealed that HT29-18N2
more heterogeneity in oligo-
t cells (Fig. 5). Constitutive
differentiation, but immuno-
f stored secretory granules.
respond to cholinergic secre-
s [Phillips et al., 1988].
nd impermeable substrates,
ral membranes. In addition,
ture conditions so that some
impossible to obtain in vivo.
to the same extent as their

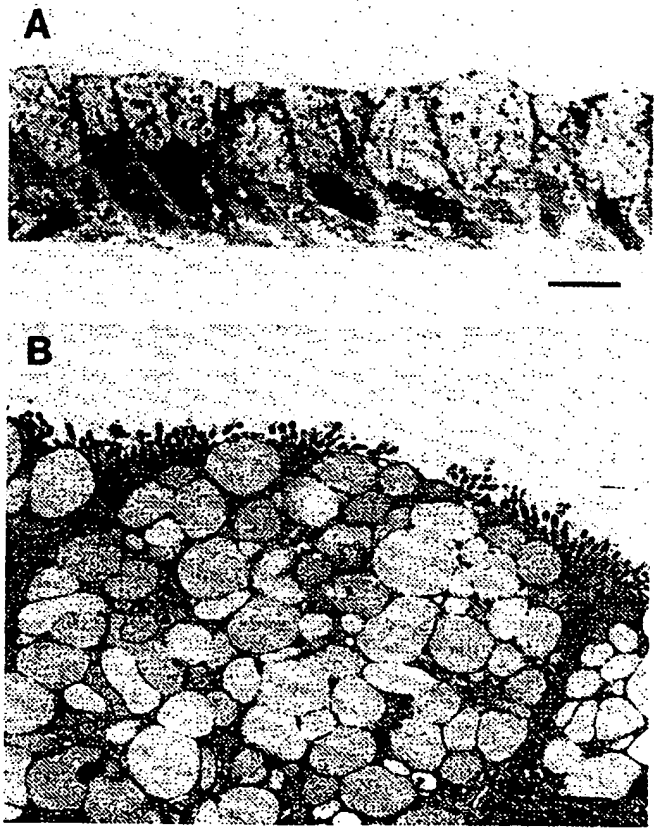

Fig. 4. Confluent HT29-18/N2 cells grown in medium lacking glucose but containing 5 mM galactose. **A:** By light microscopy, this subclone forms a homogeneous monolayer of goblet cells when fully differentiated. Bar = 10 μm. **B:** By electron microscopy, the apical poles of diffentiated cells are filled with large granules typical of mucin-secreting cells. Bar = 1 μm.

counterparts in vivo [Neutra and Forstner, 1987]. This subclone can now be exploited to gain a clearer understanding of some of the key functions common to regulated exocrine cells, including mechanisms of sorting of secretory proteins into regulated granules, assembly of storage granules and their unique membrane components, and mechanisms governing compound exocytosis during stimulated secretion.

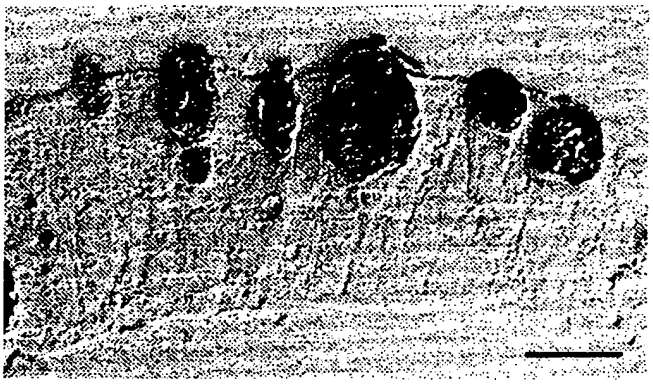

Fig. 5. Nomarski image of confluent HT29-18/N2 cells grown as for Figure 4, but not yet fully differentiated. Differentiation of monolayers is not synchronous: Some cells have many secretory granules containing immunoreactive mucin (visualized by imunoperoxidase labeling); others have not yet begun mucin synthesis or storage. Bar - 10 μm.

V. REFERENCES

Amerongen HM, Mack JA, Wilson JM, Bilbo PR, Neutra MR (1987) A lateral membrane protein in intestinal epithelial cells. J Cell Biol 105:146a.

Arsenault P, Menard D (1984) Insulin influences the maturation and proliferation of suckling mouse mucosa in serum-free organ culture. Biol Neonate 46:229–236.

Augeron C, Laboisse CL (1984) Emergence of permanently differentiated cell clones in a human colonic cancer cell line in culture after treatment with sodium butyrate. Cancer Res 44:3961–3969.

Banerjee D, Flanagan PR, Cluett J, Valberg LS (1986) Transferrin receptors in the human gastrointestinal tract. Relationship to body iron stores. Gastroenterology 91:861–869.

Bartles JR, Feracci HM, Steiger B, Hubbard AL (1987) Biogenesis of the rat hepatocyte plasma membrane in vivo: Comparison of the pathways taken by apical and basolateral proteins using subcellular fractionation. J Cell Biol 105:1241–1252.

Bartles JR, Hubbard AL (1988) Plasma membrane protein sorting in epithelial cells: Do secretory pathways hold the key? Trends Biochem Sci 13:181–184.

Bennett G, Carlet E, Wild G, Parsons S (1984) Influence of colchicine and vinblastine on the intracellular migration of secretory and membrane glycoproteins: III. Inhibition of intracellular migration of membrane glycoproteins in rat intestinal columnar cells and hepatocytes as visualized by light and electron-microscope radioautography after ^{3}H-fucose injection. Am J Anat 170:545–566.

Bjerknes M, Cheng H (1981) Methods for the isolation of intact epithelium from the mouse intestine. Anat Rec 199:565–574.

Black BL, Moog F (1978) Alkaline phosphatase and maltase activity in the embryonic chick intestine in culture. Dev Biol 66:232–249.

Blok J, Ginsel LA, Mulder-Stapel AA, Onderwater JJM, Daems WT (1981a) The effect of col-

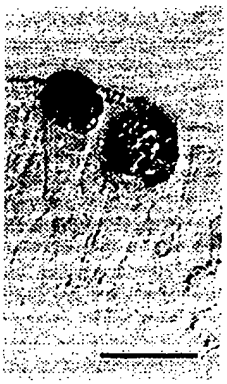

own as for Figure 4, but not yet fully
onous: Some cells have many secre-
ed by immunoperoxidase labeling);
10 μm.

MR (1987) A lateral membrane pro-
1.
uration and proliferation of suckling
nate 46:229–236.
differentiated cell clones in a human
with sodium butyrate. Cancer Res

nsferrin receptors in the human gas-
Jastroenterology 91:861–869.
genesis of the rat hepatocyte plasma
n by apical and basolateral proteins
–1252.
sorting in epithelial cells: Do secre-
181–184.
of colchicine and vinblastine on the
lycoproteins: III. Inhibition of intra-
ntestinal columnar cells and hepato-
pe radioautography after ^{3}H-fucose

f intact epithelium from the mouse

ase activity in the embryonic chick

aems WT (1981a) The effect of col-

chicine on the intracellular transport of ^{3}H-fucose-labelled glycoproteins in the absorptive cells of cultured human small-intestinal tissue. Exp Cell Res 215:1–12.

Blok J, Mulder-Stapel AA, Ginsel LA, Daems WT (1981b) Endocytosis in absorptive cells of cultured human small intestinal tissue: Horseradish peroxidase, lactoperoxidase, and ferritin as markers. Cell Tissue Res 216:1–13.

Bretscher A and Weber K (1980) Villin is a major protein of the microvillus cytoskeleton which binds both G and F actin in a calcium-dependent manner. Cell 20:839–847.

Burgess DR (1976) Structure of the epithelial mesenchymal interface during early morphogenesis of the chick duodenum. Tissue Cell 8:147–158.

Caplan MJ, Stow JL, Newman AP, Madri JA, Anderson HC, Farguhar MG, Palade GE, Jamieson JD (1987) Dependence on pH of polarized sorting of secreted proteins. Nature 329:632–635.

Chantret I, Barbat A, Dussaulx E, Brattain M, Zweibaum A (1988) Epithelial polarity, villin expression, and enterocytic differentiation of cultured human colon carcinoma cells: a survey of twenty cell lines. Cancer Res 48:1936–1942.

Chastre E, Emami S, Rosselin G, Gespach C (1985) Vasoactive intestinal peptide receptor activity and specificity during enterocyte-like differentiation and retrodifferentiation of the human colonic cancerous subclone HT29-18. FEBS Lett 188:197–204.

Collins JH, Borysenko CW (1984) The 110,000-dalton actin- and calmodulin-binding protein from intestinal brush border is a myosin-like ATPase. J Biol Chem 259:14128–14135.

Colony PC, Neutra MR (1983) Epithelial differentiation in the fetal rat colon: plasma membrane phosphatase activities. Dev Biol 97:349–363.

Colony PC, Neutra MR (1985) Macronolecular transport in the fetal rat intestine. Gastroenterology 89:294–306.

Conzelman KA, and Mooseker MS (1987) The 110-kD protein-clamodulin complex of the intestinal microvillus is an actin-activated MgATPase. J Cell Biol 105:313–324.

Coudrier E, Reggio H, Louvard D. (1983) Characterization of an integral membrane glycoprotein associated with microfilaments of pig intestinal microvilli. EMBO J 2:469–475.

Danielsen EM, and Cowell GM (1985) Biosynthesis of intestinal microvillar proteins: Evidence for an intracellular sorting taking place in, or shortly after, exit from the Golgi complex. Eur J Biochem 152:493–499.

DeRitis G, Falchuk ZM, Trier JS (1975) Differentiation and maturation of cultured fetal rat jejunum. Dev Biol 45:304–317.

Dharmsathaphorn K, Mandel KG, Masui H, McRoberts JA. (1985) VIP-induced chloride secretion by a colonic epithelial cell line: Direct participation of a basolaterally localized Na+, K+, Cl^- cotransport system. J Clin Invest 75:462–471.

Dharmsathaphorn K, Mandel KG, McRoberts JA, Tisdale LD, Masui H (1984) A human colonic tumor cell line that maintains vectorial electrolyte transport. Am J Physiol 246:G204–G208.

Dudouet B, Robine S, Huet C, Sahuquillo-Merino C, Blair L, Coudrier E, Louvard D (1987) Changes in villin synthesis and subcellular distribution during intestinal differentiation of HT29–18 cells. J Cell Biol 105:359–369.

Fogh J, Fogh JM, Orfeo T (1977) One hundred and twenty seven cultured human tumor cell lines producing tumors in nude mice. J Natl Cancer Inst 59:221–226.

Fogh J, Trempe G (1975) New human tumor cell lines. In Fogh J (ed): Human Tumor Cells in vitro. New York: Plenum Publishing Corp., pp 115–141.

Fransen JAM, Ginsel L, Hauri HP, Sterchi E, Blok J (1985). Immuno-electronmicroscopical localization of a microvillus membrane disaccharidase in the human small-intestinal epithelium with monoclonal antibodies. Eur J Cell Biol 38:6–15.

Friedman EA, Higgins PJ, Lipkin M, Shinya H, Gelb AM (1981) Tissue culture of human epithelial cells from benign colonic tumors. In Vitro 17:632–644.

Fukamachi H, Mizuno T, Kim YS (1986) Morphogenesis of human colon cancer cells with fetal rat mesenchymes in organ culture. Experientia 42:312–315.

Fuller SD, Bravo R, Simons K (1985) An enzymatic assay reveals that proteins destined for the apical and basolateral domains of an epithelial cell line share the same late Golgi compartments. EMBO J 4:297–307.

Glenney JR, Glenney P (1983) Spectrin, fodrin, and TW260/240: A family of related proteins lining the plasma membrane. Cell Motil 3:671–682.

Godefroy O, Huet C, Blair LAC, Sahuquillo-Merino C, Louvard D (1988) Differentiation properties of a clone isolated from the HT29 cell line (a human colon carcinoma): Polarized differentiation of histocompatibility antigens (HLA) and of transferrin receptors. Biol Cell 63:41–56.

Gold P, Freedman SO (1965) Specific carcinoembryonic antigens of the human digestive system. J Exp Med 122:467–481.

Gonnella PA, Siminoski K, Murphy RA, Neutra MR (1987) Transepithelial transport of epidermal growth factor by absorptive cells of suckling rat ileum. J Clin Invest 80:22–32.

Gottlieb TA, Beaudry G, Rizzolo L, Colman A, Rindler M, Adesnik M, Sabatini DD (1986) Secretion of endogenous and exogenous proteins from polarized MDCK cell monolayers. Proc Natl Acad Sci USA 83:2100–2104.

Grand RJ, Watkins JB, Torti EM (1976) Development of the human gastrointestinal tract: A review. Gastroenterology 70:790–810.

Grasset E, Bernabeu J, Pinto M (1985) Epithelial properties of human colon carcinoma cell line Caco-2: Effect of secretagogues. Am J Physiol 248:C410–C418.

Grasset E, Pinto M, Dussaulx E, Zweibaum A, Desjeux JF (1984) Epithelial properties of human colonic carcinoma cell line Caco-2: Electrical parameters. Am J Physiol 247:C260–C267.

Gumbiner B, Simons K (1986) A functional assay for proteins involved in establishing an epithelial occluding barrier: Identification of a uvomorulin-like polypeptide. J Cell Biol 102:457–468.

Haffen K, Kedinger M, Simon-Assmann P (1987) Mesenchyme-dependent differentiation of epithelial progenitor cells in the gut. J Pediatr Gastroenterol Nutr 6:14–23.

Hauri HP (1983) Biosynthesis and transport of plasma membrane glycoproteins in the rat intestinal epithelial cell: studies with sucrase-isolmaltase. In Porter R, Collins GM (eds) Brush Border Membrane (Ciba Foundation Symposium 95): London; Pitman, pp 132–149.

Hauri HP, Sterchi EE, Bienz D, Fransen JAM, Marxer A (1985) Expression and intracellular transport of microvillus membrane hydrolases in human intestinal epithelial cells. J Cell Biol 101:838–851.

Hauri HP, Wacker H, Rickli EE, Bigler-Meier B, Quaroni A, Semenza G (1982) Biosynthesis of sucrase-isomaltase: Purification and NH_2-terminal sequence of the rat sucrase-isomaltase precursor from fetal intestinal transplants. J Biol Chem 257:4522–4528.

Hermos JA, Mathan M, Trier JS (1971) DNA synthesis and proliferation by villous epithelial cells in fetal rats. J Cell Biol 50:255–258.

Hidalgo IJ, Raub TJ, Borchardt RT (1988) Permeability properties of an intestinal epithelial model system (Caco-2 cell). FASEB J 2:A733.

Huet C, Sahuquillo-Merino C, Coudrier E, Louvard D (1987) Absorptive and mucus-secreting subclones isolated from a multipotent intestinal cell line (HT29) provide new models for cell polarity and terminal differentiation. J Cell Biol 105:345–358.

Ingber DE, Madri JA, Jamieson JD (1986) Basement membrane as a spatial organizer of polarized epithelia. Am J Pathol 122:129–139.

Ishizuya-Oka A (1983) Electron microscopical study of self-differentiation potency in the chick embryonic endoderm cultured in vitro. Whilhelm Roux Arch Dev Biol 192:171–178.
Kedinger M, Simon-Assmann PM, Alexander E, Haffen K (1987) Importance of a fibroblastic support for in vitro differentiation of intestinal endodermal cells and for their response to glucacorticoids. Cell Differ 20:171–182.
Kedinger M, Simon-Assmann PM, Haffen K (1986a) Control mechanisms in the ontogenesis of villus cells. In Desnuelle, Noren 0, Sjostrom H (eds): Molecular and Cellular Biology of Digestion. Amsterdam/New York: Elsevier/North-Holland Biomedical Press, pp 315–326.
Kedinger M, Simon-Assmann PM, Lacroix B, Marxer A, Hauri HP, Haffen K (1986b) Fetal gut mesenchyme induces differentiation of cultured intestinal endodermal and crypt cells. Dev Biol 113:474–483.
Kedinger M, Simon PM, Grenier JF, Haffen K (1981) Role of epithelial-mesenchymal interactions in the ontogenesis of intestinal brush border enzymes. Dev Biol 86:339–347.
Kelly RB (1985) Pathways of protein secretion in eukaryotes. Science 230: 25–32.
Klausner RD, Ashwell G, Van Renswoude J, Harford JB, Bridges KR (1983): Binding of apotransferrin to K562 cells: Explanation of the transferrin cycle. Proc Natl Acad Sci USA 80:2263.
Koldovsky O (1969) Development of the Functions of the Small Intestine in Mammals and Man. Basel: S. Karger AG.
Kondo Y, Rose I, Young GP, Whitehead RH (1984) Growth and differentiation of fetal rat small intestinal epithelium in tissue culture. Exp Cell Res 153:121–134.
Kondor Koch C, Bravo R, Fuller SD, Cutler D, Garoff H (1985) Exocytotic pathways exist to both the apical and basolateral cell surfaces of the polarized epithelial cell MDCK. Cell 43:297–306.
Laburthe M, Rousset M, Rouyer-Fessard C, Couvineau A, Chantret I, Chevalier G, Zweibaum A (1987) Development of vasoactive intestinal peptide-responsive adenylate cyclase during enterocytic differentiation of Caco-2 cells in culture. Evidence for an increased receptor level. J Biol Chem 262:10180–10184.
Laurie GW, Leblond CP, Martin GR (1982) Localization of type IV collagen, laminin, heparan sulfate proteoglycan, and fibronectin to the basal lamina of basement membranes. J Cell Biol 95:340–344.
Leapman SB, Deutsch AA, Grand RJ, Folkman J (1974) Transplantation of fetal intestine: Survival and function in a subcutaneous location in adult animals. Ann Surg 179:109–114.
LeBivic A, Bosc-Biern I, Reggio H (1988a) Characterization of a glycoprotein expressed on the basolateral membrane of human intestinal epithelial cells and cultured colonic cell lines. Eur J Cell Biol 46:113–120.
LeBivic A, Hirn M, Reggio H (1988b) HT-29 cells are an in vitro model for the generation of cell polarity in epithelia during embryonic differentiation. Proc Natl Acad Sci USA 85:136–140.
Leblond CP, Cheng H (1976) Identification of stem cells in the small intestine of the mouse. In Cairnie AB, Lala RK, Osmond DG (eds): Stem Cells of Renewing Cell Populations. New York: Academic Press, pp 7–31.
Lev R, Orlic D (1973) Uptake of protein in swallowed amniotic fluid by monkey fetal intestine in utero. Gastroenterology 65:60–68.
Levine JS, Nakane PK, Allen RH (1982) Immunocytochemical localization of intrinsic factor-cobalamin bound to guinea pig ileum in vivo. Gastroenterology 82:284–290.
Logsdon C, Moessner J, Williams JA, Goldfine ID (1984) Glucocorticoids increase amylase mRNA levels, secretory organelles, and secretion in pancreatic acinar AR42J cells. J Cell Biol 100:1200–1208.

Lorenzsonn V, Korsmo H, Olsen WA (1987) Localization of sucrase-isomaltase in the rat enterocyte. Gastroenterology 92:98–105.

Louvard D (1980) Apical membrane aminopeptidase appears at site of cell-cell contact in cultured kidney epithelial cells. Proc Natl Acad Sci USA 77:4132–4136.

Madara JL, Dharmsathaphorn K (1985) Occluding junction structure-function relationships in a cultured epithelial monolayer. J Cell Biol 101:2124–2133.

Madara JL, Neutra MR, Trier JS (1981) Junctional complexes in fetal rat small intestine during morphogenesis. Dev Biol 86:170–178.

Madara JL, Stafford J, Dharmsathaphorn K, Carlson S (1987) Structural analysis of a human intestinal epithelial cell line. Gastroenterology 92:1133–1145.

Madara J, Trier JS (1987) Functional morphology of the mucosa of the small intestine. In Johnson L (ed): Physiology of the Gastrointestinal Tract, vol 2. New York: Raven Press, pp 1209–1250.

Marcial MA, Carlson SL, Madara JL (1984) Partitioning of paracellular conductance along the crypt-villus axis: A hypothesis based on structural analysis with detailed consideration of tight junction structure-function relationships. J Membrane Biol 80:59–70.

Marsh MN, Trier JS (1974) Morphology and cell proliferation of subepithelial fibroblasts in adult mouse jejunum. Gastroenterology 67:622–635.

Massey D, Feracci H, Gorvel JP, Rigal A, Soulie JM, Maroux S (1987) Evidence for the transit of aminopeptidase N through the basolateral membrane before it reaches the brush border of enterocytes. J Membrane Biol 96:19–25.

Mathan M, Hermos JA and Trier JS (1972) Structural features of the epithelial-mesenchymal interface of rat duodenal mucosa during development. J Cell Biol 52:577–588.

Matlin KS, Simons K (1984) Sorting of an apical plasma membrane glycoprotein occurs before it reaches the cell surface in cultured epithelial cells. J Cell Biol 99:2131–2139.

Montgomery RK (1986) Morphogenesis in vitro of dissociated fetal rat small intestinal cells upon an open surface and subsequent to collagen gel overlay. Dev Biol 117:64–70.

Montgomery RK, Sybicki MA, Grand RJ (1981) Autonomous biochemical and morphological differentiation in fetal rat intestine transplanted at 17 and 20 days of gestation. Dev Biol 87:76–84.

Montgomery RK, Zinman HM, Smith BT (1983) Organotypic differentiation of trypsin-dissociated fetal rat intestine. Dev Biol 100:181–189.

Moog F (1979) The differentiation and redifferentiation of the intestinal epithelium and its brush border membrane. In Elliott K, Whelan J (eds): Development of Mammalian Absorptive Processes (Ciba Foundation Symposium 70). Amsterdam: Exerpta Medica, pp 31–44.

Moore HPH, Kelly RB (1985) Secretory protein targeting in a pituitary cell line: Differential transport of foreign secretory proteins to distinct secretory pathways. J Cell Biol 101: 1773–1781.

Mooseker MS (1985) Organization, chemistry and assembly of the cytoskeletal apparatus of the intestinal brush border. Annu Rev Cell Biol 1:209–241.

Mostov K, Blobel G (1983) Biosynthesis, processing and function of secretory component. Methods Enzymol 98:458–466.

Mostov, KE, Deitcher DL (1986) Polymeric inumunoglobulin receptor expressed in MDCK cells transcytoses IgA. Cell 46:613–621.

Mostov K, Kraehenbuhl JP, Blobel G (1980). Receptor-mediated transcellular transport of immunoglobulins: Synthesis of secretory component as multiple or larger transmembrane forms. Proc Natl Acad Sci USA 177:7257–7272.

Moxey PC, Trier JS (1979) Specialized cell types in the human fetal small intestine. Anat Rec 191:269–286.

Moyer MP (1983) Culture of human gastrointestinal epithelial cells. Proc Soc Exp Biol Med 174:11–5.

Muthiah R, Seetharam B (1987) ^{57}Colcyanocobalamin uptake by human colon adenocarcinoma cell line (Caco-2). J Cell Biol 105:235a.

Naim HY, Roth J, Sterchi EE, Lentze M, Milla P, Schmitz J, Hauri HP (1988) Sucrase-isomaltase deficiency in humans. Different mutations disrupt intracellular transport, processing and function of an intestinal brush border enzyme. J Clin Invest 82:667–679.

Negrel R, Rampal R, Nano JL, Cavenel C, Ailhaud G (1983) Establishment and characterization of an epithelial intestinal cell line from rat fetus. Exp Cell Res 143:427–437.

Neutra MR (1980) The use of human intestinal mucosa in organ culture for the study of birth defects. In Danes BS: In Vitro Epithelia and Birth Defects. New York: Alan R. Liss, Inc., pp 261–273.

Neutra MR, Forstner JF (1987) Gastrointestinal mucus: synthesis, secretion and function. In Johnson LR (ed): Physiology of the Gastrointestinal Tract, vol 2. New York: Raven Press, pp 975–1009.

Neutra MR, Phillips TL, Mayer EL, Fishkind DJ (1987) Transport of membrane-bound macromolecules by M cells of follicle-associated epithelium of rabbit Peyer's patch. Cell Tissue Res 247:537–546.

Neutra MR, Phillips TH, Phillips TE (1984) Regulation of intestinal goblet cells in situ, in mucosal explants and in the isolated epithelium. In Nugent J, O'Connor M (eds) Mucus and Mucosa (Ciba Foundation Symposium 109), London: Pitman, pp 20–29.

Ogier-Denis E, Codogno P, Chantret I, Trugnan G (1988) The processing of asparagine-linked oligosaccharides in HT-29 cells is a function of their state of enterocytic differentiation. J Biol Chem 263:6031–6037.

Parker FG, Barnes EN, Kaye GI (1974) The pericryptal fibroblast sheath. Gastroenterology 67:607–621.

Pearl M, Fishkind D, Mooseker S, Keene D, Keller TCS (1984) Studies on the spectrin-like protein from the intestinal brush border, TW 260/240, and characterization of its interaction with cytoskeleton and actin. J Cell Biol 98:66–78.

Phillips TE, Huet C, Bilbo PR, Podolsky DK, Louvard D, Neutra MR (1988) Human intestinal goblet cells in monolayer culture: Characterization of a mucus-secreting subclone derived from the HT29 colon adenocarcinoma cell line. Gastroenterology 94: 1390–1403.

Phillips TE, Phillips TL, Neutra MR (1984) Regulation of intestinal goblet cell secretion. III. Isolated intestinal epithelium. Am J Physiol 247:6674–6681.

Phillips TE, Phillips TL, Neutra MR (1987) Macromolecules can pass through occluding junctions of rat ileal epithelium during cholinergic stimulation. Cell Tissue Res 247: 547–554.

Pinto M, Appay MD, Simon-Assmann P, Chevalier G, Dracopoli N, Fogh J, Zweibaum A (1982) Enterocytic differentiation of cultured human cancer cells by replacement of glucose by galactose in the medium. Biol Cell 44:193–196.

Pinto M, Robine-Leon S, Appay MD, Kedinger M, Triadou N, Dussaulx E, Lacroix B, Simon-Assmann P, Haffen K, Fogh J, Zweibaum A (1983) Enterocyte-like differentiation and polarization of the human colon carcinoma cell line CaCo-2 in culture. Biol Cell 47:323–330.

Ponder BAJ, Schmidt CH, Wilkinson MM, Wood MJ, Monk M, Reid A (1985) Derivation of mouse intestinal crypts from single progenitor cells. Nature 313:689–691.

Powell DW (1987) Intestinal water and electrolyte transport. In Johnson LR (ed): Physiology of the Gastrointestinal Tract, vol 2 New York: Raven Press, pp 1267–1306.

Pringault E, Arpin M, Garcia A, Finidori J, Louvard D (1986) A human villin cDNA clone to

investigate the differentiation of intestinal and kidney cells in vivo and in culture. EMBO J 5:3119–3124.

Quaroni A (1984) Identification and biogenesis of intestinal cell surface components. In Wolman SR, Mastromarino AJ (eds): Markers of Colonic Cell Differentiation. (Progress in Cancer Research and Therapy, Vol 29). New York: Raven Press, pp 267–293.

Quaroni A (1985a) Pre-and postnatal development of differentiated functions in rat intestinal epithelial cells. Dev Biol 111:280–292.

Quaroni A (1985b) Crypt cell development in newborn rat small intestine. J Cell Biol 100: 1601–1610.

Quaroni A (1985c) Development of fetal rat intestine in organ and monolayer culture. J Cell Biol 100:1601–1610.

Quaroni A (1986a) Fetal characteristics of small intestinal crypt cells. Proc Natl Acad Sci USA 83:1723–1727.

Quaroni A (1986b) Crypt cell antigen expression in human colon tumor cell lines: Analysis with a panel of monoclonal antibodies to CaCo-2 luminal membrane components. J Natl Cancer Inst 76:571–585.

Quaroni A, Isselbacher KJ (1985) Study of intestinal cell differentiation with monoclonal antibodies to intestinal cell surface components. Dev Biol 111:267–279.

Quaroni A, May RJ (1980) Establishment and characterization of intestinal epithelial cell cultures. In Harris GC, Trump BF, Stoner GD (eds): Methods in Cell Biology, Vol 21B. New York: Academic Press, Inc., pp 403–427.

Quaroni A, Wands J, Trelstad RL, Isselbacher KJ (1979) Epithelial cell cultures from rat small intestine. Characterization by morphologic and immunologic criteria. J Cell Biol 80: 248–265.

Quaroni A, Weiser MM, Lee S, Amodeo D (1986) Expression of developmentally regulated crypt cell antigens in human and rat intestinal tumors. J Natl Cancer Inst 77:405–415.

Reggio H, Webster P, Louvard D (1983) Use of immunocytochemical techniques in studying the biogenesis of cell surfaces in polarized epithelia. Methods Enzymol 98:379–395.

Rindler MJ, Ivanov IE, Plesken H, Rodriguez-Boulan EJ, Sabatini DD (1984) Viral glycoproteins destined for the apical or basolateral plasma membrane domains traverse the same Golgi apparatus during their intracellular transport in Madin-Darby canine kidney cells. J Cell Biol 98:1304–1319.

Rindler MJ, Traber MG (1988) A specific sorting signal is not required for the polarized secretion of newly-synthesized proteins from cultured intestinal epithelial cells. J Cell Biol 107:471–479.

Robine S, Huet C, Moll R, Sahuquillo-Merino C, Coudrier E, Zweibaum A, Louvard D (1985) Can villin be used to identify malignant and undifferentiated normal digestive epithelial cells? Proc Natl Acad Sci USA 82:8488–8492.

Rodewald R, Abrahamson DR (1982) Receptor-mediated transport of IgG across the intestinal epithelium of the neonatal rat. In Evered D, Collins GM (eds) Membrane Recycling (Ciba Foundation Symposium 92). London: Pitman, pp 209–225.

Rodriguez-Boulan E (1983) Polarized assembly of enveloped viruses from cultured epithelial cells. Methods Enzymol 98:486–501.

Rodriguez-Boulan E, Paskiet KT, Sabatini DD (1983) Assembly of enveloped viruses in Madin-Darby canine kidney cells: Polarized budding from single attached cells and from clusters of cells in suspension. J Cell Biol 96:866–874.

Roth J (1987) Subcellular organization of glycosylation in mammalian cells. Biochim Biophys Acta 906:405–436.

Rousset M (1986) The human colon carcinoma cell lines HT-29 and Caco-2: Two in vitro models for the study of intestinal differentiation. Biochimie 68:1035–1040.

Rousset M, Laburthe M, Chevalier G, Boissard C, Rosselin G, Zweibaum A (1981) Vasoactive intestinal peptide (VIP) control of glycogenolysis in the human colon carcinoma cell line HT-29 in culture. FEBS Lett 126:38–40.

Semenza G (1986) Anchoring and biosynthesis of stalked brush border membrane glycoproteins. Annu Rev Cell Biol 2:255–314.

Shibayama T, Carboni JM, Mooseker MS (1987) Assembly of the intestinal brush border: Appearance and redistribution of microvillar core proteins in developing chick enterocytes. J Cell Biol 105:335–344.

Shields HM, Yedlin ST, Bair FA, Goodwin CL, Alpers DH (1979) Successful maintenance of suckling rat ileum in organ culture. Am J Anat 155:375–390.

Siminoski K, Gonnella P, Bernanke J, Owen L, Neutra M, Murphy RA (1986) Uptake and transepithelial transport of nerve growth factor in suckling rat ileum. J Cell Biol 103: 1979–1990.

Simon PM, Kedinger M, Raul F, Grenier JF, Haffen K (1979) Developmental pattern of rat intestinal brush-border enzymic proteins along the crypt-villus axis. Biochem J 178: 407–413.

Slot JW, Geuze HJ (1984) Transcytosis of IgA in duodenal epithelial cells observed by immunocytochemistry. J Cell Biol 99:7a.

Specian RD, Neutra MR (1980) Mechanism of rapid mucus secretion in goblet cells stimulated by acetylcholine. J Cell Biol 85:626–640.

Sugrue SP, Hay ED (1982) Interaction of embryonic corneal epithelium with exogenous collagen, laminin, and fibronectin: Role of endogenous protein synthesis. Dev Biol 92:97–106.

Trier JS (1976) Organ-culture methods in the study of gastrointestinal-mucosal function and development. N Engl J Med 295:150–155.

Trier JS, Moxey PC (1979) Morphogenesis of the small intestine during fetal development. In Harries JT Development of Mammalian Absorptive Processes (Ciba Foundation Symposium 70). Amsterdam: Excerpta Medica, pp 3–29.

Truding RA, Quaroni A, Walker A (1981) The use of fetal intestinal explants to study differentiation of the gut. Gastroenterology 80:1305.

Trugnan G, Rousset M, Chantret I, Barbat A, Zweibaum A (1987) The posttranslational processing of sucrase-isomaltase in HT-29 cells is a function of their state of enterocytic differentiation. J Cell Biol 104:1199–1205.

Vegas-Salas DE, Salas PJI, Rodriguez-Boulan E (1987) Modulation of the expression of an apical plasma membrane protein of Madin-Darby canine kidney epithelial cells: Cell-cell interactions control the appearance of a novel intracellular storage compartment. J Cell Biol 104:1249–1259.

Walsh JH (1987) Gastrointestinal hormones. In Johnson LR (ed): Physiology of the Gastrointestinal Tract. New York: Raven Press, pp 181–254.

Welsh MJ, Smith PL, Fromm M, Frizzell RA (1982) Crypts are the site of intestinal fluid and electrolyte secretion. Science 218:1219–1221.

Wice BML, Trugnan G, Pinto M, Rousset M, Chevalier G, Sussaulx E, Lacroix B, Zweibaum A (1985) The intracellular accumulation of UDP-N-acetylhexosamines is concomitant with the inability of human colon cancer cells to differentiate. J Biol Chem 260:139–146.

Wilson JM, Whitney JA, Neutra MR (1987a) Identification of an endosomal antigen specific to absorptive cells of suckling rat ileum. J Cell Biol 105:691–703.

Wilson JM, Whitney JA, Neutra MR (1987b) Assembly of the endosome-lysosome system during fetal development of rat ileal absorptive cells. J Cell Biol 105:248a.

Zweibaum A, Hauri HP, Sterchi E, Chantret I, Haffen K, Bamat J, Sordat B (1984) Immunohistological evidence obtained with monoclonal antibodies of small intestinal brush border hydrolases in human colon cancers and foetal colons. Int J Cancer 34:591–598.

Zweibaum A, Laburthe M, Grasset E, Louvard D (1988) In: Handbook of Physiology. The Gastrointestinal System, IV. In press.

Zweibaum A, Pinto M, Chevalier G, Dussaulx E, Triadou N, Lacroix B, Haffen K, Brun JL, Rousset M (1985) Enterocytic differentiation of a subpopulation of the human colon tumor cell line HT29 selected for growth in sugar-free medium and its inhibition by glucose. J Cell Physiol 122:21–29.

Zweibaum A, Triadou N, Kedinger M, Augeron C, Robine-Leon S, Pinto M, Rousset M, Haffen K (1983) Sucrase-isomaltase: A marker of foetal and malignant epithelial cells of the human colon. Int J Cancer 32:407–412.

EXHIBIT C

ANTICANCER DRUG DEVELOPMENT GUIDE

PRECLINICAL SCREENING, CLINICAL TRIALS, AND APPROVAL

Edited by

BEVERLY A. TEICHER

Dana-Farber Cancer Institute, Boston, MA

HUMANA PRESS
TOTOWA, NEW JERSEY

For the beautiful ones
Emily and Joseph

999 Riverview Drive, Suite 208
Totowa, New Jersey 07512

For additional copies, pricing for bulk purchases, and/or information about other Humana titles, contact Humana at the above address or at any of the following numbers: Tel.: 201-256-1699; Fax: 201-256-8341; E-mail: humana@mindspring.com; or visit Humana on the Internet at: http://humanapress.com

This publication is printed on acid-free paper. ∞
ANSI Z39.48-1984 (American Standards Institute) Permanence of Paper for Printed Library Materials.

Cover illustration: From Fig. 1 in Chapter 14, "Discovery of TNP-470 and Other Angiogenesis Inhibitors," by Donald E. Ingber, in *Cancer Therapeutics: Experimental and Clinical Agents*, Edited by Beverly A. Teicher, Humana Press, 1997.

Cover design by Patricia F. Cleary.

Printed in the United States of America. 10 9 8 7 6 5 4 3 2 1

Library of Congress Cataloging-in-Publication Data

Anticancer drug development guide: preclinical screening, clinical trials, and approval / edited by
Beverly A. Teicher.
p. cm. – (Cancer drug discovery and development)
Includes index.
ISBN 0-89603-461-5 (alk. paper)
1. Antineoplastic agents–Testing. I. Teicher, Beverly A., 1952– .
II. Series.
[DNLM: 1. Antineoplastic Agents–standards. 2. Drug Approval. 3. Drug Screening. QV 269 A62953 1997]
RC271.C5A6722 1997
616.99'4061–dc21
DNLM/DLC
for Library of Congress 96-38113
CIP

CONTENTS

6 Human Tumor Xenograft Models in NCI Drug Development

Jacqueline Plowman, PhD,
Donald J. Dykes, BS,
Melinda Hollingshead, PhD,
Linda Simpson-Herren, BS,
and Michael C. Alley, PhD

CONTENTS

1. INTRODUCTION

The preclinical discovery and development of anticancer drugs by the NCI consist of a series of test procedures, data review, and decision steps that have been summarized recently (*1*). Test procedures are designed to provide comparative quantitative data, which in turn, permit selection of the best candidate agents from a given chemical or biological class. Periodic, comprehensive reviews by various NCI committees serve not only to identify and expedite the development of active lead compounds that may provide more efficacious treatments for human malignancy, but also to eliminate agents that are inactive and/or highly toxic from further consideration.

Various components in NCI's drug discovery and development process have evolved in response to a combination of factors—scientific, clinical, technological, and fiscal. A series of review articles have charted the evolution of the drug screening program and have described specific elements of the process, e.g., acquisition, screening, analog development and testing, pharmacology, and toxicology (*2–12*). The present chapter provides: a brief history of the in vivo screens used by NCI; a description of the human tumor xenograft systems, which are currently employed in preclinical drug development; a discussion of how these xenograft models are employed for both initial efficacy testing as well as detailed drug evaluations; and a description of a new model that may facilitate preclinical drug development.

From: *Anticancer Drug Development Guide: Preclinical Screening, Clinical Trials, and Approval*
Edited by: B. Teicher Humana Press Inc., Totowa, NJ

2. HISTORICAL DEVELOPMENT OF NCI SCREENS

Analyses of various screening methods available prior to 1955 indicated that (1) nontumor systems were incapable of replacing tumor systems as screens, and (2) no single tumor system was capable of detecting all active antitumor compounds (*13*). Since that time, the preclinical discovery and development of potentially useful anticancer agents by the NCI have utilized a variety of animal and human tumor models not only for initial screening, but also for subsequent studies designed to optimize antitumor activity of a lead compound or class of compounds. Although the various preclinical data review steps and criteria have remained essentially the same throughout the years, the modes and rationale of in vivo testing employed by NCI have evolved significantly.

2.1. Murine Tumor Screens, 1955–1975

In 1955, NCI initiated a large-scale in vivo anticancer drug screening program utilizing three murine tumor models: sarcoma 180, L1210 leukemia, and carcinoma 755. By 1960, in vivo drug screening was performed in L1210 and in two additional rodent models selected from a battery of 21 possible models. In 1965, screening was limited to the use of two rodent systems, L1210 and Walker 256 carcinosarcoma. In 1968, synthetic agents were screened in L1210 alone, whereas natural product testing was conducted in both L1210 and P388 leukemias. A special testing step was added to the screen in 1972 to evaluate active compounds against B16 melanoma and Lewis lung carcinoma. It is noteworthy that this first 20 years of in vivo screening relied heavily on testing conducted in the L1210 model.

2.2. Prescreen and Tumor Panel, 1976–1986

In late 1975, NCI initiated a new approach to drug discovery that involved prescreening of compounds in the ip-implanted murine P388 leukemia model, followed by evaluation of selected compounds in a panel of transplantable tumors (*14*). The tumors in the panel were chosen as representative of the major histologic types of cancer in the US and, for the first time in NCI history, included human solid tumors. The latter was made possible through the development of immunodeficient athymic (nu/nu) mice and transplantable human tumor xenografts in the early 1970s (*15,16*). Beginning in 1976, the tumor panel consisted of paired murine and human tumors of breast ($CD8F_1$ and MX-1), colon (colon 38 and CX-1 [the same as HT29]) and lung (Lewis and LX-1), together with the B16 melanoma and L1210 leukemia used in previous screens.

The majority of the early NCI testing conducted with the human tumors used small fragments growing under the renal capsule of athymic mice. The subrenal capsule (src) technique and assay were developed by Bogden and associates (*17*). Although labor-intensive, the src assay provided a rapid means of evaluating new agents against human tumor xenografts at a time when the testing of large numbers of compounds against sc xenografts seemed untenable. As experience was gained with the husbandry of athymic mice, longer-duration sc assays became manageable.

A detailed evaluation of the sensitivities of individual tumor systems employed from 1976–1982 revealed a wide range in sensitivity profiles as well as "yield" of active compounds (*14*). The data clearly indicated that rodent models may not be capable of detecting all compounds with potential activity against human malignan-

cies, and indicated that the best strategy for testing is to employ a combination of tumor systems to minimize loss of potentially useful compounds. These findings prompted the NCI in 1982 to develop a strategy for testing compounds that involved a sequential process of "progressive selection": NCI continued to use the P388 leukemia as a prescreen, but subsequent evaluation of selected agents was conducted in a modified tumor panel composed of "high-yield" models from the original panel (i.e., src-implanted MX-1 mammary carcinoma, and ip-implanted B16 melanoma and L1210 leukemia) and a new model, the ip-implanted M5076 sarcoma. Thereafter, evaluation of selected compounds would be "compound-oriented" and use protocols and models, selected on the basis of prior testing results and known properties of each compound, that would present the compound with increased biological and pharmacological challenge.

Alternate approaches to in vivo drug evaluation have been prompted by investigations on the metastatic heterogeneity of tumor cell populations. During the 1980s, several investigators associated with NCI conducted studies to assess the metastatic potential of selected murine and human tumor cell lines (B16, A-375, LOX-IMVI melanomas, and PC-3 prostate adenocarcinoma) and their suitability for experimental drug evaluation (e.g., *18–21*). A series of investigations by Fidler and associates demonstrated that metastasis is not random, but selective and that metastasis consists of a progression of sequential steps, the pattern of which is dependent on injection site (*22,23*). Such findings support the importance of establishing in vivo models derived from the implantation of tumor material in host tissues that are anatomically correct—"seed" and "soil" compatibility. Such "orthotopic" models also have been developed and utilized to study lung cancer (e.g., *24*), breast cancer (e.g., *25*), and prostate cancer (*26*). Although it may not be possible for NCI to employ these models in the initial steps of in vivo drug evaluations, such models may be well suited for subsequent, more detailed evaluation of compounds that exhibit activity against specific tumor types. Metastases and orthotopic models are discussed in greater detail in Chapters 7 and 8 of this volume.

2.3. Human Tumor Colony Formation Assay, 1981–1985

Based on initial reports by Salmon and colleagues (*27,28*), various clinical investigators working with fresh human tumor samples from patients and/or with early passage human tumor xenograft materials utilized various culture techniques to identify chemotherapeutic agents active against human malignancies (e.g., *29,30*). The NCI sponsored a pilot drug screening project utilizing a human tumor colony-forming assay (HTCFA) at multiple clinical cancer centers. Although it was possible to identify unique antitumor drug "leads" using such a technique, the HTCFA could be employed only for a limited number of tumor types and was not found suitable for large-scale drug screening (*31*).

2.4. Human Tumor Cell Line Screen, 1985–Present

In 1985, the NCI initiated a new project to assess the feasibility of employing human tumor cell lines for large-scale drug screening (*12; also see* Chapter 2 of this volume). Cell lines derived from seven cancer types (brain, colon, leukemia, lung, melanoma, ovarian, and renal) were acquired from a wide range of sources, cryopreserved, and subjected to a battery of in vitro and in vivo characterizations, including

testing in drug sensitivity assays. The approach was deemed suitable for large-scale drug screening in 1990 (*1*). With the implementation of a 60-member cell line in vitro screen, in vivo testing procedures were substantially altered as discussed below.

3. HUMAN TUMOR XENOGRAFT MODELS IN CURRENT USE

The new in vitro human tumor cell line screen shifted the NCI screening strategy from "compound-oriented" to "disease-oriented" drug discovery (*12*). Compounds of interest identified by the screen (e.g., those demonstrating disease-specific differential cytotoxicity) were to be considered "leads," requiring further preclinical evaluation to determine their therapeutic potential. As part of this followup testing, the antitumor efficacy of the compounds was to be evaluated in in vivo tumor models derived from the in vitro tumor lines used in the screen. Although only a subset of cell lines, selected on the basis of in vitro sensitivity, would be used for each agent, it was anticipated that for any selected compound, any cell line might be required as a xenograft model. In order to accomplish such an objective, a concerted developmental effort was required to establish a battery of human tumor xenograft models. As discussed below and elsewhere (*32*), tumorigenicity was demonstrated for the majority of the tumor lines utilized in the in vitro screen that became fully operational in April 1990 (*1*). Then, in 1993, composition of the cell line screen was modified: cell lines with variable growth characteristics and those providing redundant information were replaced by groups of prostate and breast tumor lines. As a consequence, additional xenograft model development was initiated for prostate and breast cancers.

3.1. Development of Human Tumor Xenografts

Efforts focused on the establishment of sc xenografts from human tumor cell-culture lines obtained from the NCI tumor repository at Frederick, MD. The approach is outlined in Fig. 1. The cryopreserved cell lines were thawed, cultured in RPMI 1640 medium supplemented with 10% heat-inactivated fetal bovine serum (HyClone), and expanded until the population was sufficient to yield $\geq 10^8$ cells. Cells were harvested and then implanted sc into the axillary region of 10 athymic NCr nu/nu mice (1.0×10^7 cells/0.5 mL/mouse) obtained from the NCI animal program, Frederick, MD. Mice were housed in sterile, polycarbonate, filter-capped Microisolator™ cages (Lab. Products, Inc.), maintained in a barrier facility on 12-h light/dark cycles, and provided with sterilized food and water ad libitum. The implanted animals were observed twice weekly for tumor appearance. Growth of the solid tumors was monitored using *in situ* caliper measurements to determine tumor mass. Weights (mg) were calculated from measurements (mm) of two perpendicular dimensions (length and width) using the formula for a prolate ellipsoid and assuming a specific gravity of 1.0 g/cm^3– (*33*). Fragments of these tumors were subjected to histological, cytochemical, and ultrastructural examination to monitor the characteristics of the in vivo material and to compare them with those of the in vitro lines and, where possible, with those reported for initial patient tumors (*34*). Both in vitro and in vivo tumor materials exhibited characteristics consistent with tissue type and tumor of origin. However, not unexpectedly, differences in the degree of differentiation were noted between some of the cultured cell lines and corresponding xenograft materials.

The initial solid tumors established in mice were maintained by serial passage of 30–40 mg tumor fragments implanted sc near the axilla. There was an apparent cell

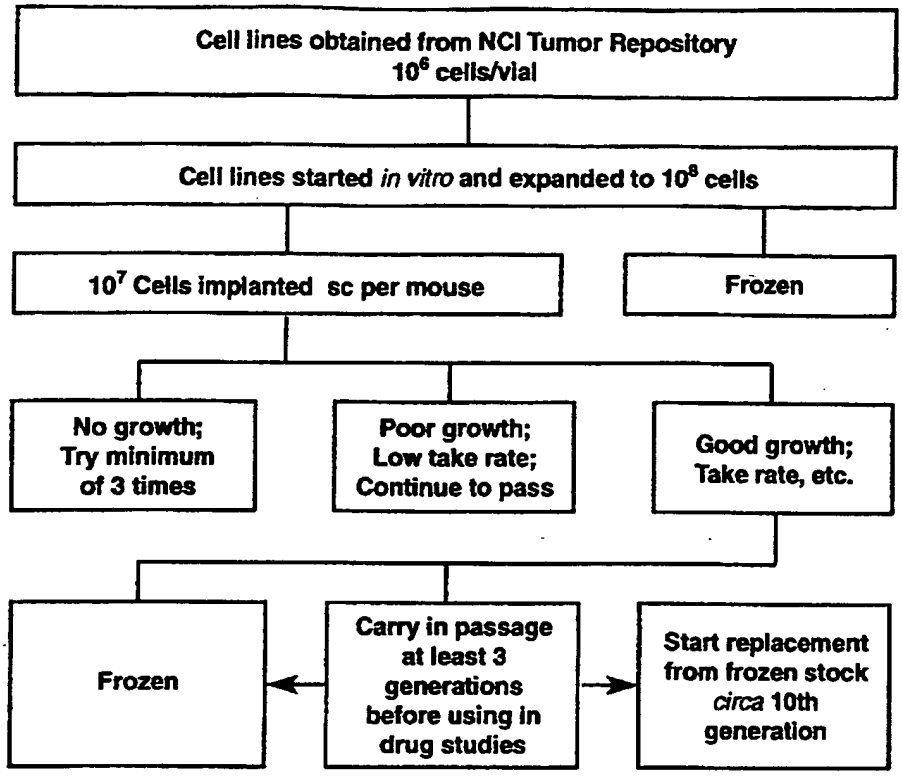

Fig. 1. Schematic of the development of in vivo models for drug evaluation.

population selection occurring in some of the tumors as they adapted to growth in animals during early in vivo passage, with growth rates increasing appreciably in sequential passages (*32*). Thus, xenografts were not utilized for drug evaluation until the volume-doubling time stabilized, usually around the fourth or fifth passage. The doubling time of xenografts derived from tumor cell lines constituting both the initial (1990) and the modified (1993) human tumor cell line screens, plus three additional breast tumors, are presented in Table 1. Also provided in the table is information on the take-rate of the tumors, and the experience of the NCI in the use of the tumors as early stage sc models. The doubling times were determined from vehicle-treated control mice used in drug evaluation experiments (only data for passage numbers 4–20 have been included). For each experiment, the doubling time is the median of the time interval for individual tumors to increase in size from 200–400 mg (usually a period of exponential growth). Both ranges and mean values are provided to demonstrate the inherent variability of growth for some of the xenograft materials even after a period of stabilization. Mean doubling times range from < 2 d for five tumors (SF-295 glioblastoma, MOLT 4 leukemia, DMS 273 small-cell lung tumor, and LOX-IMVI and SK-MEL-28 melanomas) to > 10 d for the MALME-3M and M19-MEL melanomas.

Difficulty was experienced in establishing and/or using some of the sc models. For example, even though HOP-62 nonsmall-cell lung tumors exhibited good growth rates, poor take-rates of 70, 50, 64, and 30% attained in the second through fifth passages, respectively, precluded their use for experimental drug testing. Although serial passage of OVCAR-3 ovarian tumors from sc-implanted fragments was difficult,

Table 1
Growth Characteristics of sc-Implanted Human Tumor Xenografts

Tumor Origin	Line	*In vitro* panel status 1990	*In vitro* panel status 1993	Mean volume doubling time (range) in days[a]	Take Rate[b]	Opinion for use as early-stage sc model
Colon	SW-620	Yes	Yes	2.4(1.7-3.9)	Good	Good
	KM12	Yes	Yes	2.4(1.9-3.3)	Good	Good
	HCT-116	Yes	Yes	2.6(1.8-3.4)	Good	Good
	HCT-15	Yes	Yes	3.4(1.8-5.0)	Good	Good
	HCC-2998	Yes	Yes	3.5(2.4-7.7)	Good	Acceptable
	DLD-1	Yes	No	3.8(3.1-5.5)	Good	Acceptable
	KM20L2	Yes	No	3.9(2.5-5.4)	Good	Acceptable
	COLO 205	Yes	Yes	4.3(2.4-8.9)	Good	Acceptable
	HT29	Yes	Yes	5.1(2.4-7.6)	Good	Acceptable
CNS	SF-295	Yes	Yes	1.4(1.0-2.0)	Good	Good
	SNB-75	Yes	Yes	3.1(2.0-4.6)	Good	Good
	U251	Yes	Yes	4.3(2.4-8.9)	Good	Good
	XF 498	Yes	No	4.4(2.6-8.3)	60-70%	Not Acceptable
	SNB-19	Yes	Yes	6.9(3.1-4.4)	60-70%	Not Acceptable
	SF-539	Yes	Yes	8.4(one only)	70%	Not Acceptable
	SF-268	Yes	Yes	NA[c]	Minimal growth	NA
	SNB-78	Yes	No	NA	No Growth	NA
Leukemia	MOLT-4	Yes	Yes	1.2(2.0-5.6)	80-100%	Acceptable
	HL-60(TB)[d]	Yes	Yes	3.3(2.1-4.9,ip)	85-100%(ip)	Good(ip)
	CCRF-CEM	Yes	Yes	4.6(4.3-4.6)	60-80%	Acceptable
	SR	Yes	Yes	5.1(one only)	80%	Not Acceptable
	RPMI-8226	Yes	Yes	NA	Minimal growth	NA
	K-562	Yes	Yes	NA	Minimal growth	NA
Lung: non-small cell	NCI-H460	Yes	Yes	2.1(1.3-3.0)	Good	Good
	NCI-H522	Yes	Yes	2.3(1.0-3.4)	Good	Good
	HOP-62	Yes	Yes	3.6(3.3-3.8)	30-65%	Not Acceptable
	NCI-H23	Yes	Yes	3.7(2.0-6.4)	Good	Good
	NCI-H322M	Yes	Yes	4.0(2.7-5.9)	Good	Acceptable
	EKVX	Yes	Yes	5.5(3.5-7.9)	Good	Acceptable
	HOP-92	Yes	Yes	6.0(5.1-8.4)	Good	Accepable
	A549/ATCC	Yes	Yes	8.4(5.8-10.9)	70-80%	Not Acceptable
	HOP-18	Yes	No	NA	Minimal growth	NA
	NCI-H266	Yes	Yes	NA	Minimal growth	NA

tumors grew more readily from sc implants of brei derived from ip-passaged material. The HL-60 (TB) promyelocytic leukemia did not grow well sc, but an ascitic ip line with a good take-rate was established successfully (Table 1). Growth characteristics of sc-implanted RXF 393 renal tumors are perhaps better suited for evaluation of a survival end point than for measurements of tumor size. Although demonstrating

Table 1 (Continued)

Tumor Origin	Line	*In vitro* panel status 1990	*In vitro* panel status 1993	Mean volume doubling time (range) in days[a]	Take Rate[b]	Opinion for use as early-stage sc model
Lung: small cell	DMS273	Yes	No	1.7(1.6-2.1)	Good	Good
	DMS114	Yes	No	4.8(2.8-7.5)	75-90%	Acceptable
Mammary	ZR-75-1	No	No	1.8(1.5-1.9)	Good	Good
	MX-1	No	No	2.7(2.2-3.0)	Good	Good
	UISO-BCA-1	No	No	4.1(2.8-4.8)	Good	Acceptable
	MDA MB-231/ATCC	No	Yes	4.4(2.7-7.7)	Good	Acceptable
	MCF7[e]	No	Yes	4.5(2.2-8.0)	Good	Acceptable
	MCF7/ADR-RES	No	Yes	6.1(4.2-7.9)	Good	Acceptable
	MDA-MB-435	No	Yes	6.6(2.8-13.6)	Good	Acceptable
	MDA-N	No	Yes	7.9(4.5-10.2)	Good	Acceptable
	HS578T	No	Yes	NA	Minimal growth	NA
	BT-549	No	Yes	NA	No growth	NA
	T-47D	No	Yes	NA	No growth	NA
Melanoma	LOX-IMVI	Yes	Yes	1.5(1.1-2.1)	Good	Good
	SK-MEL-28	Yes	Yes	1.9(1.1-2.5)	Good	Good
	UACC-62	Yes	Yes	2.8(1.8-4.2)	70-80%	Not Acceptable
	UACC-257	Yes	Yes	5.4(3.8-7.7)	Good	Acceptable
	SK-MEL-2	Yes	Yes	5.7(4.8-6.6)	80-90%	Not Acceptable
	M14	Yes	Yes	6.7(2.8-12.7)	Good	Acceptable
	SK-MEL-5	Yes	Yes	7.3(5.1-8.2)	Good	Acceptable
	MALME-3M	Yes	Yes	11.2(7.1-16.9)	80-90%	Not Acceptable
	M19-MEL	Yes	No	12.3(8.7-16.8)	60-90%	Not Acceptable
Ovarian	OVCAR-5	Yes	Yes	3.3(2.2-4.3)	Good	Good
	SK-OV-3	Yes	Yes	3.4(2.6-4.9)	Good	Good
	OVCAR-3[f]	Yes	Yes	5.5(5.0-5.9)	Good	Acceptable
	OVCAR-4	Yes	Yes	6.2(one only)	70-100%	Acceptable
	IGROV1	Yes	Yes	6.4(5.3-8.6)	Good	Acceptable
	OVCAR-8	Yes	Yes	12.2(11.2-13.0)	70%	Not Acceptable

(*continued*)

good initial growth, the RXF 393 tumors cause death in mice with low tumor burden, probably owing to paraneoplastic mechanisms. Other cell lines failed to become functional in vivo tumors, including two CNS, two nonsmall-cell lung, three breast, three renal tumor lines, and two leukemias, although minimal in vivo growth was observed with 9 of these 12 cultured lines (Table 1). With more extensive studies, it might be possible to attain improved tumor take-rates and growth by implanting tumors in

Table 1 (Continued)

Tumor Origin	Line	*In vitro* panel status 1990	*In vitro* panel status 1993	Mean volume doubling time (range) in days[a]	Take Rate[b]	Opinion for use as early-stage sc model
Prostate	PC-3	No	Yes	2.4(1.5-3.9)	Good	Good
	DU-145	No	Yes	4.4(2.0-7.9)	Good	Acceptable
Renal	CAKI-1	Yes	Yes	2.1(1.3-2.5)	Good	Good
	RXF 631	Yes	No	3.3(1.5-6.8)	Good	Acceptable
	A498	Yes	Yes	3.4(2.2-4.3)	Good	Acceptable
	RXF 393	Yes	Yes	3.4(2.3-5.7)	Good	Good
	SN12C	Yes	Yes	5.6(3.2-11.4)	Good	Acceptable
	786-0	Yes	Yes	6.7(one only)	80%	Not Acceptable
	ACHN	Yes	Yes	NA	Minimal growth	NA
	UO-31	Yes	Yes	NA	Minimal growth	NA
	TK-10	Yes	Yes	NA	No growth	NA

[a] Time for tumors to increase in size from 200–400 mg. Data are compiled from experiments using passage numbers 4–20. Tumors are listed in order of increasing mean doubling time/histologic type.
[b] Good: reproducible take-rate of ≥ 90%.
[c] NA: not applicable.
[d] Based on ip implant of 1.0×10^7 cells.
[e] MCF7 growth in athymic NCr nu/nu mice requires 17β-estradiol supplementation.
[f] Limited sc data obtained from implant of 0.5 mL 25% brei derived from ip-passaged tumor: poor growth is attained with serial passage of fragments from sc tumors.

severe combined immunodeficient (SCID) mice (scid/scid) (*35*). As discussed below, tumor take for some human lymphoma lines was markedly superior in SCID mice compared to athymic (nu/nu) (*36*) or triple-deficient BNX (bg/nu/xid) mice (*37*).

Establishment of breast tumor xenografts in vivo raised issues concerning hormonal requirements for growth of these tumors. For example, the importance of hormones in the growth of MCF7 breast carcinoma cells as solid tumors in athymic mice has been described (*38*). Our experience with this tumor also has shown the importance of 17 β-estradiol supplementation for the growth of the sc-implanted MCF7; 60-d release, 17 β-estradiol pellets (Innovative Research of America) are implanted sc in athymic mice 24 h prior to implanting MCF7 fragments in all NCI studies with this tumor. Growth of the remaining breast tumor xenografts appeared to be independent of estradiol supplements. For example, growth curves of individual early passage ZR-75-1 tumors implanted into athymic mice receiving either estradiol or no estradiol supplements completely overlapped (Fig. 2A), even though in this early passaged material, there was a large variation in the time postimplant for growth of individual tumors to be observed. The independence of ZR-75-1 tumor growth from estradiol supplements is further illustrated in Fig. 2B. Early stage vehicle-treated control tumors in mice receiving no estradiol supplementation demonstrate rapid growth (median doubling time 1.9 d) soon after implantation. The estrogen receptor (ER) status of the in vivo passaged ZR-75-1 tumors has not been determined, but the

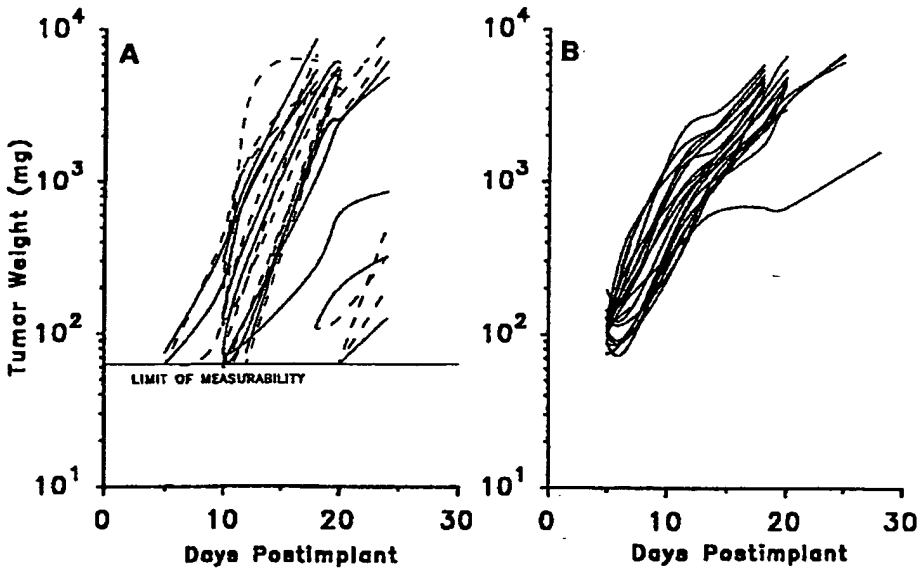

Fig. 2 Growth comparison of individual ZR-75-1 human breast tumor xenografts with and without estradiol supplementation. **A.** Passage number 5, -- with 1.7 mg sc 17β-estradiol pellet implants; —without estradiol supplementation. **B.** Passage number 14, without estradiol supplementation.

growth characteristics of the tumors suggest an ER− status even though early evaluations of the in vitro cell line indicated an ER+ status (*39*).

The in vivo growth characteristics of the xenografts determine their suitability for use in the evaluation of test agent antitumor activity, particularly when the xenografts are utilized as early stage sc models. For the purposes of the current discussion, the latter model is defined as one in which tumors are staged to 63–200 mg prior to the initiation of treatment. Our experience with the suitability of the xenografts as early stage models is listed in Table 1. Growth characteristics considered in rating tumors include take-rate, time to reach 200 mg, doubling time, and susceptibility to spontaneous regression. As can be noted, the faster-growing tumors tend to receive the higher ratings.

Since non-Hodgkin's lymphoma is one of the two principal malignancies occurring in the growing population of HIV-infected persons (*40*), the Developmental Therapeutics Program (DTP) has also established a group of human lymphoma xenografts for evaluating potential chemotherapeutic agents (*41*). This includes AS283, an Epstein-Barr virus (EBV)-positive, HIV-negative Burkitt's lymphoma derived from an AIDS patient (*42*); KD488, an EBV-negative, pediatric Burkitt's lymphoma (*43–46*); and RL, a diffuse, small noncleaved B-cell lymphoma (*47*). These lines grow sc with take-rates in excess of 90% in SCID mice, whereas much lower take-rates occur in athymic or triple-deficient BNX mice. Our finding of greater take-rates for the human leukemias/lymphomas in SCID mice compared to athymic mice is consistent with the known capacity of SCID mice to support xenografts of normal human hematopoietic cells (*48*).

3.2. Advanced-Stage sc Xenograft Models

Advanced-stage sc-implanted tumor xenograft models were established originally for use in evaluating the antitumor activity of test agents, so that clinically relevant

parameters of activity could be determined, i.e., partial and complete regressions, durations of remission (*49–51*). Tumor growth is monitored, and test agent treatment is initiated when tumors reach a weight range of 100–400 mg (staging day, median weights approx 200 mg), although depending on the xenograft, tumors may be staged at larger sizes. Tumor size and body weights are obtained approximately 2 times/wk and entered into DTP's DEC 10,000 Model 720 AXP computer. Through software programs developed by staff of the Information Technology Branch of DTP, in particular by David Segal and Penny Svetlik, data are stored, various parameters of effect are calculated, and data are presented in both graphic and tabular formats. Parameters of toxicity and antitumor activity are defined as follows:

1. Parameters of toxicity: Both drug-related deaths (DRDs) and maximum percent relative mean net body weight losses are determined. A treated animal's death is presumed to be treatment-related if the animal dies within 15 d of the last treatment, and either its tumor weight is less than the lethal burden in the control mice, or its net body weight loss at death is 20% greater than the mean net weight change of the controls at death or sacrifice. A DRD also may be designated by the investigator. The mean net body weight of each group of mice on each observation day is compared to the mean net body weight on staging day. Any weight loss that occurs is calculated as a percent of the staging day weight. These calculations also are made for the control mice, since tumor growth of some xenografts has an adverse effect on the weight of the mice.
2. Optimal % T/C: Changes in tumor weight (Δ weights) for each treated (T) and control (C) group are calculated for each day tumors are measured by subtracting the median tumor weight on the day of first treatment (staging day) from the median tumor weight on the specified observation day. These values are used to calculate a percent T/C as follows:

$$\%\ T/C = (\Delta T / \Delta C) \times 100 \text{ where } \Delta T > 0 \text{ or}$$
$$= (\Delta T / T_I) X\ 100 \text{ where } \Delta T < 0 \quad (1)$$

   and T_I is the median tumor weight at the start of treatment. The optimum (minimum) value obtained after the end of the first course of treatment is used to quantitate antitumor activity.
3. Tumor growth delay: This is expressed as a percentage by which the treated group weight is delayed in attaining a specified number of doublings (from its staging day weight) compared to controls using the formula:

$$[(T - C) / C] \times 100 \quad (2)$$

   where T and C are the median times in days for treated and control groups, respectively, to attain the specified size (excluding tumor-free mice and DRDs). The growth delay is expressed as percentage of control to take into account the growth rate of the tumor since a growth delay based on T − C alone varies in significance with differences in tumor growth rates.
4. Net log cell kill: An estimate of the number of $\log_{10}$ units of cells killed at the end of treatment is calculated as:

$$\{[(T - C) - \text{duration of treatment}] \times 0.301 / \text{median doubling time}\} \quad (3)$$

   where the doubling time is the time required for tumors to increase in size from 200–400 mg, 0.301 is the $\log_{10}$ of 2, and T and C are the median times in days for treated and control tumors to achieve the specified number of doublings. If the duration of treat-

ment is 0, then it can be seen from the formulae for net log cell kill and percent growth delay that log cell kill is proportional to percent growth delay. A log cell kill of 0 indicates that the cell population at the end of treatment is the same as it was at the start of treatment. A log cell kill +6 indicates a 99.9999% reduction in the cell population.

5. Tumor regression: The importance of tumor regression in animal models as an end point of clinical relevance has been propounded by several investigators (*49–51*). Regressions are defined as partial if the tumor weight decreases to 50% or less of the tumor weight at the start of treatment without dropping below 63 mg (5 *X* 5 mm tumor). Both complete regressions (CRs) and tumor-free survivors are defined by instances in which the tumor burden falls below measurable limits (< 63 mg) during the experimental period. The two parameters differ by the observation of either tumor regrowth (CR) or no regrowth (tumor-free) prior to the final observation day. Although one can measure smaller tumors, the accuracy of measuring a sc tumor smaller than 4 × 4 or 5 × 5 mm (32 and 63 mg, respectively) is questionable. Also, once a relatively large tumor has regressed to 63 mg, the composition of the remaining mass may be only fibrous material/scar tissue. Measurement of tumor regrowth following cessation of treatment provides a more reliable indication of whether or not tumor cells survived treatment.

Most xenografts that grow sc are amenable to use as an advanced-stage model, although for some tumors, the duration of the study may be limited by tumor necrosis. As mentioned previously, this model enables the investigator to measure clinically relevant parameters of antitumor activity and provides a wealth of data on the effects of the test agent on tumor growth. Also, by staging day, the investigator is ensured that angiogenesis has occurred in the area of the tumor, and staging enables no-takes to be eliminated from the experiment. However, the model can be costly in terms of time and mice. For the slower-growing tumors, the passage time required before sufficient mice can be implanted with tumors may be at least 3–4 wk, and an additional 2–3 wk may be required before the tumors can be staged. In order to stage tumors, more mice than needed for actual drug testing must be implanted, often 50%, and sometimes 100% more.

3.3. Early Treatment and Early Stage sc Xenograft Models

Early treatment and early stage sc models are similar to the advanced-stage model, but because treatment is initiated earlier in the development of the tumor, the models are not suitable for tumors that have less than a 90% take-rate or have a > 10% spontaneous regression rate. We define the early treatment model as one in which treatment is initiated before tumors are measurable, i.e., < 63 mg, and the early stage model as one in which treatment is initiated when tumor size ranges from 63–200 mg. The 63-mg size is used as an indication that the original implant of approx 30 mg has demonstrated some growth. Parameters of toxicity are the same as those for the advanced-stage model; parameters of antitumor activity are similar. Percent T/C values are calculated directly from the median tumor weights on each observation day instead of as changes (Δ) in tumor weights, and growth delays are based on the time in days after implant for the tumors to reach a specified size, e.g., 500 or 1000 mg. Tumor-free mice are recorded, but may be designated no-takes or spontaneous regressions if the vehicle-treated control group contains more than 10% mice with similar growth characteristics. A no-take is a tumor that fails to become established and grow progressively. A spontaneous regression (graft failure) is a tumor that, after

a period of growth, decreases to 50% or less of its maximum size. Tumor regressions are not normally recorded, since they are not always a good indicator of antineoplastic effects in the early stage model. For those experiments in which treatment is initiated when tumors are 100 mg or less, only a minimal reduction in tumor size may bring the tumor below the measurable limit, and for some small tumors early in their growth, reductions in tumor size may reflect erractic growth rather than a true reflection of a cell killing effect. The big advantage of the early treatment model is the ability to use all implanted mice. The latter is the reason for requiring a good tumor take-rate, and in practice, the tumors most suitable for this model tend to be the faster-growing ones.

3.4. Challenge Survival Models

Although not utilized to a significant degree in the current NCI program, a few studies are conducted that depend on determining the effect of human tumor growth on the life-span of the host. Three tumors have been used as ip-implanted models: the HL-60 (TB) promyelocytic leukemia, the LOX-IMVI melanoma, and the OVCAR-3 ovarian carcinoma. Also, the SF-295 and U251 glioblastomas have been implanted intracerebrally. All mice dying or sacrificed owing to a moribund state or extensive ascites prior to the final observation day are used to calculate median days of death for treated (T) and control (C) groups. These values are then used to calculate a percent increase in life-span as follows:

$$\% \text{ ILS} = [(T - C)/C] \times 100 \quad (4)$$

Wherever possible, titration groups are included to establish a tumor doubling time for use in $\log_{10}$ cell kill calculations. Laboratory personnel may designate a death (or sacrifice) as drug-related based on visual observations and/or the results of necropsy. Otherwise, treated animal deaths are designated as treatment-related if the day of death precedes the mean day of death of the controls minus 2 SD or if the animal dies without evidence of tumor within 15 d of the last treatment.

3.5. Response of Xenograft Models to Standard Agents

The drug sensitivity profiles for the advanced-stage sc xenograft models in our program have been established using 12 clinical antitumor drugs (Table 2). Each of these agents, obtained from the Drug Synthesis and Chemistry Branch, DTP, were evaluated following ip administration at multiple dose levels. The activity ratings are based on the optimal effects attained with the maximally tolerated dose ($< LD_{20}$) of each drug for the treatment schedule shown. The latter were selected on the basis of the doubling time of a given tumor, with longer intervals between treatments for slower-growing tumors. Apparent inconsistencies between the doubling times shown in Table 1 and selected schedules in Table 2 are the result of increased tumor growth rates for some tumors in the later studies depicted in Table 1. In later chemotherapeutic trials with breast tumors, paclitaxel was included in the group of clinical drugs evaluated, and drug characteristics were considered to some extent in the selection of treatment regimens (Table 3).

With the caveat that no attempts were made to optimize drug administration in each model, it can be seen that at least minimal antitumor effects ($\%T/C \leq 40$) were

Table 2
Response of Staged sc-Implanted Human Tumor Xenografts to 12 Clinical Anticancer Drugs[b]

Tumor	IP Treatment Schedule	Alkylating Agents						DNA Binders			Antimetabolites		Mitotic Inhibitor
		L-PAM	CYT	DTIC	BCNU	MMC	DDPt	Act D	ADR	BLEO	MTX	5FU	VBL
Colon:													
SW-620	q7dx3	1	0	4	3	4	1	0	0	1	0	0	0
KM12	q4dx3	NA	NA	0	1	NA	0	0	NA	1	0	0	0
HCT-116	q4dx3	NA	0	0	0	1	0	1	NA	1	0	0	0
HCT-15	q7dx3	1	0	0	0	1	0	1	0	0	0	0	0
HCC-2998	q4dx3	0	0	0	0	4	0	0	0	1	0	0	0
KM20L2	q4dx3	0	1	0	0	1	1	0	0	0	0	1	0
COLO 320DM	q4dx3	0	0	3	0	0	NA	0	0	0	0	1	0
COLO 205	q4dx3	1	0	0	0	3	1	1	0	0	0	1	1
HT29	q4dx3	0	0	0	0	2	2	0	0	1	0	0	0
CNS:													
SF-295	q4dx3	0	1	0	1	0	1	0	0	0	0	0	4
U251	q4dx3	0	2	4	4	3	3	1	0	0	0	0	1
XF 498	q7dx3	0	0	4	3	1	1	0	1	0	0	0	0
SNB-19	q4dx3	1	2	3	NA	3	NA	0	NA	NA	0	0	1
Leukemia:													
MOLT-4	q4dx3	4	1	0	0	1	1	0	1	1	1	0	0
Lung, non-small cell:													
NCI-H460	q4dx3	NA	0	NA	NA	4	NA	0	0	1	NA	0	0
NCI-H522	q4dx3	1	0	0	NA	≥2	1	NA	1	NA	NA	0	NA
HOP-62	q4dx3	2	NA	NA	NA	1	1	0	0	1	0	0	1
Lung, non-small cell:													
NCI-H23	q4dx3	3	1	0	0	4	4	1	1	1	1	1	0
NCI-H322M	q7dx3	0	0	0	0	4	1	0	0	0	0	1	0
EKVX	q4dx3	1	1	1	0	1	0	0	0	1	0	0	1
HOP-92	q4dx3	1	0	4	2	0	1	0	1	0	0	0	1
Lung, small cell:													
DMS 273	qdx4	1	1	0	0	1	0	1	0	1	1	1	2
DMS 114	q4dx3	0	1	0	1	1	0	0	0	0	0	0	1
NCI-H69	q4dx3	4	1	3	4	2	NA	0	NA	0	0	1	0
Melanoma:													
LOX-IMVI	qdx5	1	2	2	2	2	1	0	NA	0	NA	0	2
SK-MEL-28	q4dx3	0	1	0	0	1	0	0	0	0	0	0	0
UACC-62	q7dx3	0	0	1	1	1	1	1	1	1	0	0	1
SK-MEL-31	q4dx3	0	0	0	NA	1	1	1	0	NA	0	0	NA
UACC-257	q7dx3	0	0	4	1	2	1	1	1	0	0	1	0
SK-MEL-2	q7dx3	1	0	0	0	1	1	1	0	1	0	1	2
M14	q4dx3	0	0	0	0	0	0	0	1	1	0	1	0
MALME-3M	q4dx3	1	0	4	1	1	1	1	0	1	0	0	0
Ovarian:													
SK-OV-3	q7dx3	0	0	NA	NA	1	0	0	0	1	0	0	0
IGROV1	q4dx3	1	0	0	0	1	1	1	0	1	1	1	0
OVCAR-8	q7dx3	0	0	0	0	1	1	0	1	0	0	0	0

(continued)

produced in each tumor model by at least 2, and as many as 10, clinical drugs (Table 4). The number of responses appeared to be independent of doubling time and histological type with a range in the number of responses observed for tumors in each subpanel. When the responses are considered in terms of the more clinically relevant end points of partial or complete tumor regression, it can be seen that the tumor models were quite refractory to standard drug therapy with 30 of 48 (62.5%) not responding

Table 2 (Continued)

Tumor	IP Treatment Schedule	Alkylating Agents						DNA Binders			Antimetabolites		Mitotic Inhibitor
		L-PAM	CYT	DTIC	BCNU	MMC	DDPt	Act D	ADR	BLEO	MTX	5FU	VBL
Prostate:													
PC-3	qdx4	1	0	1	0	0	0	0	0	1	1	0	0
DU-145	q4dx3	NA	1	NA	NA	NA	1	0	NA	NA	1	0	0
Renal:													
CAKI-1	q7dx3	1	1	0	0	1	1	1	1	0	0	1	0
SN12K1	q7dx3	0	0	0	0	4	0	0	0	0	0	0	1
A498	q7dx3	0	0	1	1	1	1	0	1	1	0	0	0
RXF 393	q4dx3	1	1	1	1	2	1	0	1	1	0	0	1
SN12C	q7dx3	0	0	0	1	0	0	0	0	1	0	0	0
786-0	q7dx3	0	NA	NA	NA	1	1	0	NA	NA	0	NA	NA

[a] Standard agents are melphalan (L-PAM), cytoxan (CYT), dacarbazine (DTIC), 1, 3-bis (2-chloroethyl)-1-nitrosourea (BCNU), mitomycin C (MMC), cisplatin (DDPt), actinomycin D (act D), doxorubicin (ADR), bleomycin (BLEO), methotrexate (MTX), 5-fluorouracil (5FU), vinblastine (VBL).

[b] Activity rating based on optimal %Δ T/Δ C attained after treatment had ended:
0 = Inactive, %T/C > 40.
1 = Tumor inhibition, %T/C range 1–40.
2 = Tumor stasis, %T/C range 0 to −49.
3 = Tumor regression, %T/C range −50 to −100.
4 = %T/C range −50 to −100 and >30% tumor-free mice at experiment end.

Table 3
Response of Staged sc-Implanted Breast Tumor Xenografts to 13 Clinical Anticancer Drugs[a]

Tumor[b]	Alkylating Agents						DNA Binders			Antimetabolites		Mitotic Inhibitor	
	L-PAM	CYT	DTIC	BCNU	MMC	DDPt	Act D	ADR	BLEO	MTX	5-FU	VBL	PAC
ZR-75-1	1[b]	1	4	1	1	1	1	3	1	0	0	1	NA
MX-1	4	4	0	1	4	4	0	2	1	1	0	0	4
UISO-BCA-1	0	0	1	0	NA	0	0	0	0	NA	0	0	3
MCF7	1	0	1	1	1	0	0	0	1	0	NA	0	0
MDA-MB-435	1	0	4	3	NA	0	NA	0	1	NA	0	1	4
MDA-N	0	0	4	0	0	0	1	1	0	0	NA	0	3

[a] Clinical drugs include those listed in Table 2, plus paclitaxel (PAC). Treatment regimens were ip qd x 5 for MTX and 5FU, ip q4d x 3 for L-PAM, CYT, DTIC, BCNU, MMC, DDPt, Act D, BLEO, and VBL, iv q4d x 3 for ADR, and iv qd x 5 for PAC.

[b] Activity rating: *see* legend to Table 2.

to any of the drugs tested (Table 4). As tested, the clinical drugs producing the highest response rates (number of tumors responding [%T/C ≤ −50%]/ total tumors evaluated) were DTIC (11/44) and mitomycin C (9/45) (Tables 2 and 3). Paclitaxel was not evaluated in the majority of tumors, but demonstrated excellent activity in four of five breast tumor models (Table 3).

Table 4
Response of Staged sc Human Tumor Xenografts to Clinical Anticancer Drugs

Panel	Tumor	Number of drugs active[a]: Minimal activity[b]	Tumor regression[c]
Colon	SW-620	6	3
	KM12	2/8	0/8
	HCT-116	3/10	0/10
	HCT-15	3	0
	HCC-2998	2	1
	KM20L2	4	0
	COLO 320DM	2/11	0/11
	COLO 205	6	1
	HT29	3	0
CNS	SF-295	4	1
	U251	7	4
	XF 498	5	2
	SNB-19	5/8	2/8
Lung, non-small cell	NCI-H460	2/7	1/7
	NCI-H522	4/7	0/7
	HOP-62	5/9	0/9
	NCI-H23	9	3
	NCI-H322M	3	1
	EKVX	6	0
	HOP-92	6	1
Lung, small cell	DMS 273	8	0
	DMS 114	4	0
	NCI-H69	6/10	3/10
Mammary	ZR-75-1	10/12	2/12
	MX-1	9	5
	UISO-BCA-1	2/11	1/11
	MCF7	5/12	0/12
	MDA-MB-435	6/10	3/10
	MDA-N	4/12	2/12

(*continued*)

3.6. Strategy for Initial Compound Evaluation In Vivo

The in vitro primary screen provides the basis for selection of the most appropriate lines to use for the initial followup in vivo testing, with each compound tested only against xenografts derived from cell lines demonstrating the greatest sensitivity to the

Table 4 (Continued)

Panel	Tumor	Number of drugs active[a]	
		Minimal activity[b]	Tumor regression[c]
Melanoma	LOX-IMVI	7/10	0
	SK-MEL-28	2	0
	UACC-62	8	0
	SK-MEL-31	3/9	0/9
	UACC-257	7	0
	SK-MEL-2	7	0
	M14	3	0
	MALME-3M	7	1
Ovarian	SK-OV-3	2/10	0/10
	IGROV1	7	0
	OVCAR-8	3	0
Prostate	PC-3	4	0
	DU-145	3/6	0/6
Renal	CAKI-1	7	0
	SN12K1	2	0
	A498	6	0
	RXF 393	9	0
	SN12C	2	0
	786-0	2/5	0/5

[a]Except where noted, the number of clinical drugs evaluated was 12 for the tumors listed in Table 2, and 13 for the breast tumors listed in Table 3.
[b]% T/C ≤ 40, ratings 1–4 in Tables 2 and 3.
[c]% T/C ≤ −50, ratings 3 and 4 in Tables 2 and 3.

agent in vitro. Our early strategy for in vivo testing emphasized the treatment of animals bearing advanced-stage tumors. Examples of the in vivo data obtained with one such agent are summarized in Table 5. The quinocarmycin derivative DX-52-1, identified as a melanoma-specific agent in vitro, demonstrated statistically significant antitumor activity against five of seven melanoma xenografts following ip administration on intermittent schedules (*52*). The best in vivo activity was observed against the rapidly dividing LOX-IMVI melanoma.

The strategy for in vivo testing has undergone some modifications as experience has been gained with the screen and the xenograft models. Currently, dose range finding studies in nontumored mice are conducted for new compounds identified by the in vitro screen. Unless information is available to guide dose selection, single mice are treated with single ip bolus doses of 400, 200, and 100 mg/kg and observed for 14 d. Sequential three-dose studies are conducted as necessary, until a nonlethal dose range is established, after which the compound is evaluated in the ip-implanted murine P388 leukemia model on an ip multidose treatment regimen. The latter provides dos-

Table 5
Response of Advanced-Staged sc Human Melanoma Xenografts to the Quinocarmycin Derivative, DX-52-1[a]

Melanoma	Treatment days	Dose (ip, mg/kg/day)[b]	Optimal %T/C (Day)[c]	Growth delay: %(T-C)/C[d]	Regressions Complete	Regressions Partial
LOX-IMVI	5, 9, 13	90	-54	181	2/10	3/10
	5, 9, 13, 17 21, 25	60	-100°	389	4/6	0/6
SK-MEL-2	14, 21, 28	90	10(32)	118	2/6	0/6
SK-MEL-5	15, 19, 23	40	49(33)	27	0/6	0/6
UACC-62	16, 23, 30	90	18(34)	185	0/7	0/7
UACC-257	16, 20, 24	90	12(27)	35	0/6	0/6
M14	12, 16, 20	90	19(26)	56	0/6	0/6
MALME-3M	27, 31, 35	90	64(72)	4	0/6	0/6

[a]Adapted from ref. *52*.
[b]Maximally tolerated dose, $\leq LD_{10}$ and $< 20\%$ net body wt loss.
[c]*See* Section 3.2., Step 2 for calculation of % T/C. The number in parenthesis is the day on which the optimal (minimum) T/C was attained.
[d]*See* Section 3.2., Step 3 for calculation of growth delay. Based on an end point of two doublings (four for LOX-IMVI).

ing information for the more costly xenograft models and data for retrospective comparison with previous NCI screening. The test agent is then evaluated in three sc xenograft models using tumors that were among the most sensitive to the test agent in vitro and that are suitable for use as early staged models (Table 1). The compounds are administered ip, often as suspensions, on schedules based, with some exceptions, on the mass doubling time of the tumor. For doubling times of 1.3–2.5, 2.6–5.9, and 6–10 d, the schedules are daily for five treatments (qd × 5), every fourth day for three treatments (q4d × 3), and every seventh day for three treatments (q7d × 3). For most tumors, the interval between individual treatments approximates the doubling time of the tumors, and the treatment period allows a 0.5–1.0 $\log_{10}$ unit of control tumor growth. For tumors staged at 100–200 mg, the tumor sizes of the controls at the end of treatment range from 500–2000 mg, which allows sufficient time after treatment to evaluate the effects of the test agent before it becomes necessary to sacrifice mice owing to tumor size.

Table 6
Effect of Route of Administration on the Activity of Paclitaxel Against Staged sc-Implanted MX-1 Mammary Carcinoma Xenografts

Treatment		Complete	Tumor-	Minimum	Growth	Net Log
Route, Schedule	Opt. Dose (mg/kg/day)[a]	Regressions /Total	Free on Day 40	%T/C[b] (Day)	Delay: %(T-C)/C[c]	Cell Kill
iv, D8-12	22.5	1/9	8	-100(15)[d]	449	2.9
ip, D8-12	15.0	2/9	1	28(19)	29	-0.2
iv, D8,12,16	22.5	6/9	2	-100(15)	357	2.1
ip, D8,12,16	30	0/9	0	20(22)	70	-0.3

[a]Paclitaxel was administered as a solution in 12.5% ethanol: 12.5% cremophor: 75% normal saline at multiple dose levels. Data from doses ($\leq LD_{10}$) producing the optimal effects are shown.
[b]*See* Section 3.2. for an explanation of the parameters of antitumor effects.
[c]Based on an end point of two doublings, C = 7.1 d. Tumor-free mice and mice dying of apparent drug-related effects were excluded from the calculations.
[d]Number in parentheses indicates the observation day on which data were obtained.

3.7. Detailed Drug Studies

Once a compound has been identified that demonstrates some in vivo efficacy in initial evaluations, more detailed studies can be designed and conducted in human tumor xenograft models to explore further the compound's therapeutic potential. By varying the concentration and exposure time of the tumor cells and the host to the drug, it is possible to devise and recommend treatment strategies designed to optimize antitumor activity. As many of the initial in vivo studies deliver suspensions of the compound into the peritoneal cavity, it is unlikely that the sc tumors receive optimal concentrations of, and exposure to, test agents. The early preclinical antitumor evaluation of paclitaxel illustrates this problem. In NCI studies, prior to its clinical evaluation, paclitaxel had demonstrated its best effects against ip-implanted tumors, and no activity was observed in sc models following ip administration as a suspension (*53*, *54*). Later investigations demonstrated that sc-implanted MX-1 mammary carcinoma xenografts were highly responsive to treatment with iv solutions of paclitaxel (*55*), although they had failed to respond to treatment with ip suspensions (*54*). As illustrated in Table 6, iv solutions of paclitaxel administered on either a daily or intermittent schedule produced complete tumor regressions in the majority of the treated mice. Some of these mice remained tumor-free 24–28 d after the last treatment, and tumor growth delays in the remaining mice were excellent. In contrast, only modest antitumor effects were observed following the ip administration of paclitaxel solutions. Pharmacokinetic data obtained in mice indicated only 10% bioavailability of paclitaxel from ip administration (*56*).

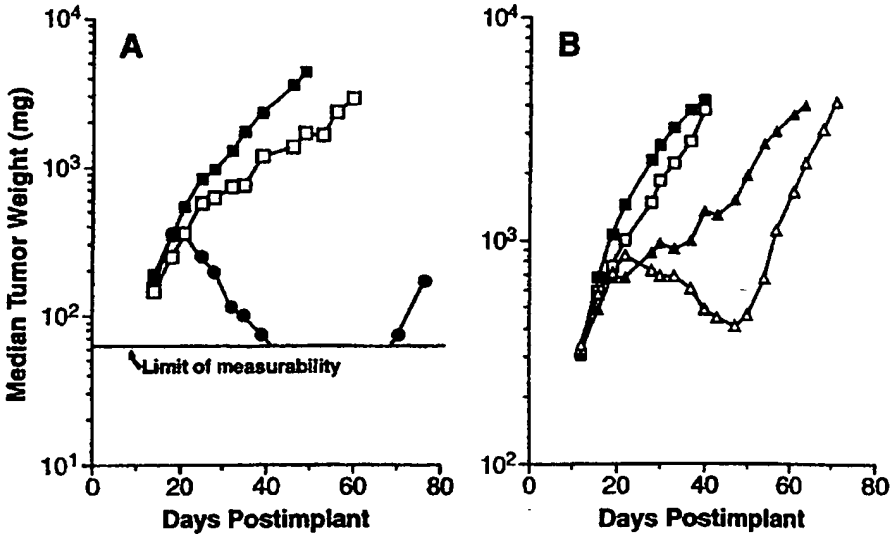

Fig. 3 Response of advanced-stage sc human HT29 colon tumor xenografts to 9-amino-20(*S*)-camptothecin (9-AC). **A.** ■—■, Vehicle-treated (saline:tween 80) controls; ●—●, 4 mg/kg/d administered as an sc bolus suspension in saline:tween 80; □—□, 4 mg/kg/d administered as an sc bolus solution in propylene glycol (PG):polyethylene glycol 400 (PEG 400): DMSO (95% of an 80% PG: 20% PEG mixture + 5% DMSO). Treatments were administered on a q4d x 8 schedule starting 14 d postimplant. **B.** ■—■, Vehicle-treated (saline:tween 80) controls; □—□, 4 mg/kg/d sc q4d x 8; ▲—▲, 3 mg/kg/d, sc q2d x 16; Δ—Δ, 1 mg/kg/d, sc qd x 32. All 9-AC treatments were given as solutions in the PG:PEG:DMSO vehicle starting on day 12.

The importance of "concentration x time" on the antitumor effects of test agents is well illustrated by data obtained with 9-amino-20(*S*)-camptothecin (9-AC). Although an sc bolus injection of a 9-AC suspension caused complete tumor regression of advanced-stage sc-implanted human HT29 colon tumor xenografts, only a marginal growth-inhibitory effect was observed when 9-AC was administered as a solution (Fig. 3A). Augmented activity with the solution was obtained by increasing the frequency of administration (Fig. 3B). Characterization of the plasma pharmacokinetics in mice, conducted in conjunction with the efficacy studies, indicated that absorption of 9-AC from sc-injected solutions was rapid and efficient, but elimination also was fast (*57*). The plasma profile afforded from the suspension differed profoundly: peak plasma levels were lower and the rate of elimination much slower (*57*). The studies indicated that maintaining the 9-AC lactone plasma concentration above a threshold level for a prolonged period of time was required for optimal therapeutic effects.

4. HOLLOW-FIBER ASSAYS: A NEW APPROACH TO IN VIVO DRUG TESTING

DTP is evaluating the suitability of a model that would be integrated into the present drug development scheme between the in vitro 60 cell line screen and the in vivo sc xenograft assays. This model, based on human tumor cell lines growing in hollow fibers, is being developed as a prioritization tool through which lead compounds

identified in the in vitro screen would pass (*58*). The goal is to direct the most promising compounds into in vivo testing as rapidly as possible after their selection for testing from the in vitro screening data. Presently, 10,000 compounds are screened in vitro each year and 8–10% of these are referred for in vivo testing. Current resources provide testing for approx 300–350 compounds in the xenograft models annually. Thus, the in vivo evaluation of compounds for activity is limited by the availability of testing resources. A method for prioritizing compounds for testing in the xenograft models, and for identifying the most sensitive cell lines to use in the models, would increase the prospect of rapidly identifying those compounds with the greatest potential for having in vivo efficacy. The hollow-fiber assay is intended to serve this purpose. In brief, tumor cells are inoculated into hollow fibers (1-mm internal diameter), and the fibers are heat-sealed and cut at 2-cm intervals. These samples are cultivated for 24–48 h in vitro and then implanted into athymic (nu/nu) mice. At the time of implantation, a representative set of fibers is assayed for viable cell mass by the "stable-end point" MTT dye conversion technique (*59*) in order to determine the time zero cell mass for each cell line. The mice are treated with experimental therapeutics on a daily treatment schedule, and the fibers are collected 6–8 d postimplantation. At collection, the quantity of viable cells contained in the fibers is measured. The antitumor effects of the test agent are determined from the changes in viable cell mass in the fibers collected from compound-treated and diluent-treated mice. Using this technique, three different tumor cell lines can be grown conveniently in each of two physiologic sites (ip and sc) within each experimental mouse (*58*). Thus, this model provides a method whereby a test agent can be administered ip to evaluate its effect against tumor cells growing in both the ip cavity and the sc compartment. With this simultaneous assessment of multiple tumor cell lines grown in two physiologic compartments, it is possible to identify lead compounds rapidly with the greatest promise of in vivo activity.

A graphic representation of typical data generated with this assay is shown in Fig. 4. The experimental mice received an ip and an sc hollow fiber of each of three human cell lines (COLO 205 colon, U251 CNS, and OVCAR-5 ovarian tumors) being evaluated. The mice were treated ip with the test agent on days 1–4, and the hollow fibers were removed on day 6. The viable cell mass was determined for the fiber samples, and the percent net growth of each cell line was calculated with reference to the time zero viable cell mass present in the hollow fibers on the day of implantation into mice. The net growth of each cell line in the ip and sc fibers is shown in Fig. 4A and B, respectively. The test agent was effective in suppressing growth of all three cell lines with the greater activity measured against ip implants. Of the cell lines tested, COLO 205 was the most sensitive, a finding that was confirmed by the results of the sc xenograft evaluations conducted following the hollow-fiber assay.

Experimentation to date indicates that this in vivo/in vitro hollow-fiber system may be well suited for the prioritization of compounds for more advanced stages of in vivo drug evaluation. In a practical sense, this hollow-fiber system is viewed as a means to facilitate traditional chemotherapeutic testing, since it is rapid, appears to be sensitive, and is broadly applicable to a variety of human tumor cell types. Additionally, it requires only a limited quantity of test compound, a small number of animals, and very limited animal housing space.

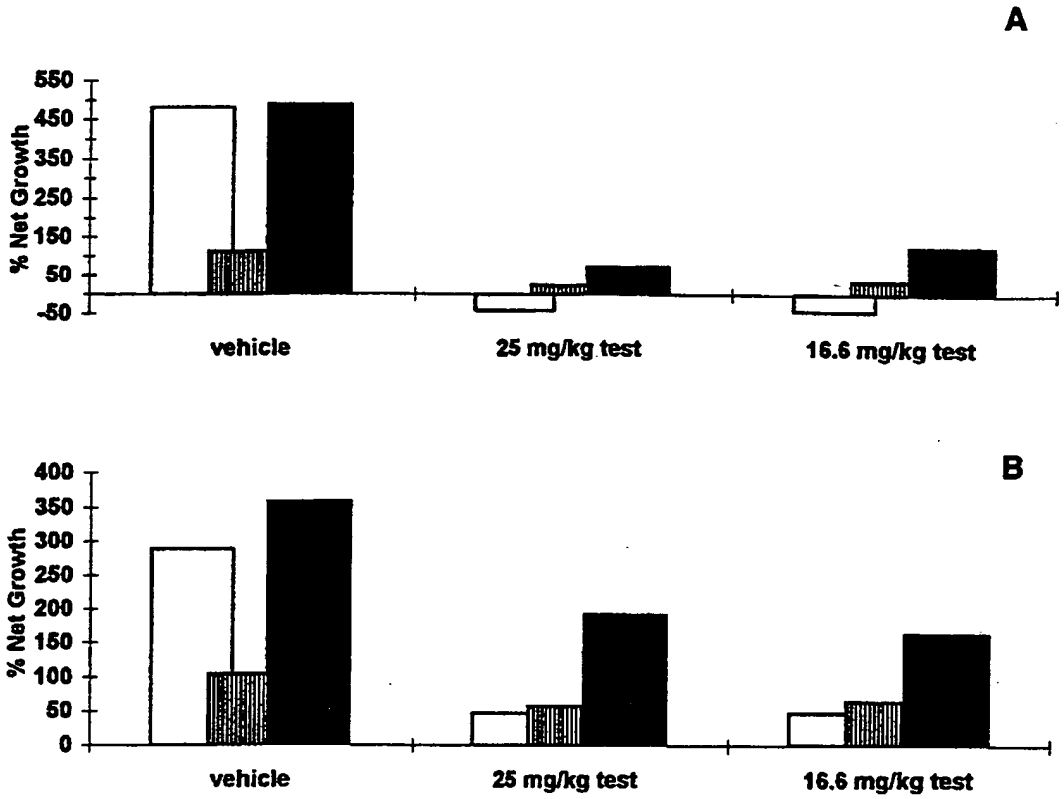

Fig. 4 In vivo effects of test agents on growth of human tumor cells in hollow fibers. Cell lines are COLO 205 colon, open bars; U251 glioblastoma, striped bars; and OVCAR-5 ovarian; solid bars. **A.** ip Implants. **B.** sc Implants. Test agents was administered ip on days 1–4, and fiber contents were assayed on day 6.

5. SUMMARY

The discovery and development of potential anticancer drugs by NCI are based on a series of sequential screening and detailed testing steps to identify new, efficacious lead compounds and to eliminate inactive and/or highly toxic materials from further consideration. Past experience in large-scale screening with a wide variety of animal and human tumor systems and the management of disease-free athymic mouse facilities has proven to be highly valuable for the recent characterization, calibration, and utilization of newly acquired human tumor xenograft models. Furthermore, DTP's experience with computer programming has enabled the development and implementation of specialized analytical software, which permits acquisition, storage, and presentation of data in readily accessible tabular and graphic formats. Many of the human tumor xenografts have been employed to test a variety of distinct chemical compound classes over the past five years. Thus, the in vivo drug sensitivity profiles of these human tumor xenografts are well suited to serve as "benchmarks" for the testing of newly synthesized agents as well as agents isolated from natural product sources that are currently under investigation.

In addition to standard models of in vivo testing, NCI has also utilized human tumor materials to explore the suitability of alternate model systems, e.g., "metastasis" and "orthotopic" models. At present, our program is investigating the utility of a capillary hollow-fiber implantation model as a means to prioritize compounds active in the in vitro screen for subsequent in vivo evaluations. It is hoped that further refinement and application of the procedures described in this chapter will facilitate the identification and preclinical development of more efficacious treatments for human malignancy.

ACKNOWLEDGMENTS

The authors thank Jacquelyn Tubbs, Bonnie Beall, Katherine Gill, and Rebecca Brown for their invaluable assistance in assembling data and typing.

REFERENCES

1. Grever MR, Schepartz SA, Chabner BA. The National Cancer Institute: Cancer drug discovery and development program. *Semin Oncol* 1992; 19:622–638.
2. Zubrod CG, Schepartz S, Leiter J, Endicott KM, Carrese LM, Baker CG. The chemotherapy program of the National Cancer Institute: History, analysis and plans. *Cancer Chemother Rep* 1966; 50:349–540.
3. Goldin A, Schepartz SA, Venditti JM, DeVita VT Jr. Historical development and current strategy of the National Cancer Institute Drug Development Program. In: DeVita VT Jr, Busch H, eds. *Methods in Cancer Research*, vol. XVI. New York: Academic. 1979:165–245.
4. DeVita VT Jr, Goldin A, Oliverio VT, Rubin D, Muggia FM, Henney J, Wiernik PW, Schepartz S, Ziegler J. The drug development and clinical trials programs of the Division of Cancer Treatment, National Cancer Institute. *Cancer Clin Trials* 1979; 2:195–216.
5. Goldin A, Venditti JM. The new NCI screen and its implications for clinical evaluation. In: Carter SK, Sakurai Y, eds. *Recent Results in Cancer Research*, vol. 70 Berlin, Heidelberg: Springer-Verlag. 1980:5–20.
6. Venditti JM. Preclinical drug development: Rationale and methods. *Semin Oncol* 1981; 8: 349–361.
7. Frei E. The national chemotherapy program. *Science (Wash DC)* 1982; 217:600–606.
8. Venditti JM. The National Cancer Institute antitumor drug discovery program current and future perspectives: A commentary. *Cancer Treatment Rep* 1983; 67:767–772.
9. Driscoll J. The preclinical new drug research program of the National Cancer Institute. *Cancer Treatment Rep* 1984; 68:63–76.
10. Goldin A. Screening at the National Cancer Institute: Basic concepts. In: Hellman K, Carter SK, eds. *Fundamentals of Cancer Chemotherapy*. New York: McGraw-Hill. 1987:141–149.
11. Suffness M, Newman DJ, Snader K. Discovery and development of antineoplastic agents from natural sources. In: Scheuer P, ed. *Bioorganic Marine Chemistry*, vol. 3. Berlin: Springer-Verlag. 1989:131–168.
12. Boyd MR. Status of the NCI preclinical antitumor drug discovery screen. In: DeVita VT Jr, Hellman S, Rosenberg SA, eds. *Cancer: Principles and Practice of Oncology, Updates*, vol. 3. Philadelphia: Lippincott. 1989:1–12.
13. Gellhorn A, Hirschberg E. Investigation of diverse systems for cancer chemotherapy screening. *Cancer Res* 1955; 15 (suppl 3):1–125.
14. Venditti JM, Wesley RA, Plowman J. Current NCI preclinical antitumor screening in vivo: Results of tumor panel screening, 1976–1982, and future directions. In: Garrattini S, Goldin A, Hawking F, eds. *Advances in Pharmacology and Chemotherapy*, vol 20. Orlando, FL: Academic. 1984:1–20.
15. Rygaard J, Povlsen CO. Heterotransplantation of a human malignant tumor to "nude" mice. *Acta Pathol Microbiol Scand* 1969; 77:758–760.

16. Giovanella BC, Stehlin JS. Heterotransplantation of human malignant tumors in "nude" thymusless mice. I. Breeding and maintenance of "nude" mice. *J. Natl Cancer Inst* 1973; 51: 615–619.
17. Bogden A, Kelton D, Cobb W, Esber H. A rapid screening method for testing chemotherapeutic agents against human tumor xenografts. In: Houchens D, Ovejera A, eds. *Proceedings of the Symposium on the Use of Athymic (Nude) Mice in Cancer Research*. New York, Stuttgart: Gustav Fischer. 1978:231–250.
18. Fidler IJ, Kripke ML. Metastasis results from preexisting variant cells within a malignant tumor. *Science* 1977; 197:893–895.
19. Kozlowski JM, Fidler IJ, Campbell D, Xu Z, Kaighn ME, Hart IR. Metastatic behavior of human tumor cell lines grown in the nude mouse. *Cancer Res* 1984; 44:3522–3529.
20. Dykes DJ, Shoemaker RH, Harrison SD, Laster WR, Griswold DP, Mayo JG, Abbott BJ, Fine DL, Fodstad O, Boyd MR. Development and therapeutic response of a spontaneous metastasis model of a human melanoma (LOX) in athymic mice. *Proc Am Assoc Cancer Res* 1987; 28:431.
21. Shoemaker RH, Dykes DJ, Plowman J, Harrison SD Jr, Griswold DP Jr, Abbott BJ, Mayo JG, Fodstad O, Boyd MR. Practical spontaneous metastasis model for in vivo therapeutic studies using a human melanoma. *Cancer Res* 1991; 51:2837–2841.
22. Fidler IJ. Rationale and methods for the use of nude mice to study the biology and therapy of human cancer metastasis. *Cancer and Metastasis Rev* 1986; 5:29–49.
23. Fidler IJ, Wilmanns C, Staroselsky A, Radinsky R, Dong Z, Fan D. Modulation of tumor cell response to chemotherapy by the organ environment. *Cancer and Metastasis Rev* 1994; 13: 209–222.
24. McLemore TL, Liu MC, Blacker PC, Gregg M, Alley MC, Abbott BJ, Shoemaker RH, Bohlman ME, Litterst CC, Hubbard WC, Brennan RH, McMahon JB, Fine DL, Eggleston JC, Mayo JG, Boyd MR. A novel intrapulmonary model for the orthotopic propagation of human lung cancers in athymic nude mice. *Cancer Res* 1987; 47:5132–5140.
25. Leone A, Flatow U, VanHoutte K, Steeg PS. Transfection of human nm23-H1 into the human MDA-MB-435 breast carcinoma cell line: Effects on tumor metastatic potential, colonization and enzymatic activity. *Oncogene* 1993; 8:2325–2333.
26. Carter CA, Dykes DJ. Characterization of tumor growth and drug sensitivity for human prostate tumors implanted orthotopically. *Proc Am Assoc Cancer Res* 1994; 35:280.
27. Hamburger AW, Salmon SE. Primary bioassay of human tumor stem cells. *Science (Wash DC)* 1977; 197:461–463.
28. Salmon SE, Hamburger AW, Soehnlen B, Durie BGM, Alberts DS, Moon TE. Quantitation of differential sensitivity of human tumor stem cells to anticancer drugs. *N Engl J Med* 1978; 298: 1321–1327.
29. Taetle R, Koessler AK, Howell SB. In vitro growth and drug sensitivity of tumor colony-forming units from human tumor xenografts. *Cancer Res* 1981; 41:1856–1860.
30. Salmon SE, Trent J, eds. *Human Tumor Cloning*. New York: Grune and Stratton, 1984.
31. Shoemaker RH, Wolpert-DeFilippes MK, Kern DH, Lieber MM, Makuch RW, Melnick NR, Miller WT, Salmon SE, Simon RM, Venditti JM, Von Hoff DD. Application of a human tumor colony forming assay to new drug screening. *Cancer Res* 1985; 45:2145–2153.
32. Dykes DJ, Abbott BJ, Mayo JG, Harrison SD Jr, Laster WR Jr, Simpson-Herren L, Griswold DP Jr. Development of human tumor xenograft models for in vivo evaluation of new antitumor drugs. In: Huber H, Queißer W, eds. *Contributions to Oncology*, vol. 42. Basel: Karger. 1992: 1–12.
33. Geran RI, Greenberg NH, Macdonald MM, Schumacher AM, Abbott BJ. Protocols for screening chemical agents and natural products against animal tumors and other biological systems. *Cancer Chemother Rep* 1972; 3, Part 3:51.
34. Stinson SF, Alley MC, Koop WC, Fiebig HH, Mullendore LA, Pittman AF, Kenney S, Keller J, Boyd MR. Morphological and immunocytochemical characteristics of human tumor cell lines for use in a disease-oriented anticancer drug screen. *Anticancer Res* 1992; 12:1035–1054.
35. Boxma GC, Custer RP, Bosma MJ. A severe combined immunodeficiency mutation in the mouse. *Nature* 1983; 301:527–530.
36. Fogh J, Fogh JM, Orfeo, T. One hundred and twenty-seven cultured human tumor cell lines producing tumors in nude mice. *J Natl Cancer Inst* 1977; 59:221–225.

37. Andriole GL, Mule JJ, Hansen DT, Linehan WM, Rosenberg SA. Evidence that lymphokine-activated killer cells and natural killer cells are distinct based on an analysis of congenitally immunodeficient mice. *J Immunol* 1985; 135:2911–2913.
38. Shafle SM, Grantham FH. Role of hormones in the growth and regression of human breast cancer cells (MCF-7) transplanted into athymic nude mice. *J Natl Cancer Inst* 1981; 67:51–56.
39. Engel LW, Young NA, Tralka TS, Lippman ME, O'Brien SJ, Joyce MJ. Establishment and characterization of three new continuous cell lines derived from human breast carcinomas. *Cancer Res* 1978; 38:3352–3364.
40. Boyle MJ, Sewell WA, Milliken ST, Cooper DA, Penny R. HIV and malignancy. *J Acquired Immune Defic Syndrome* 1993; suppl 1:S5–9.
41. Grever MR, Giavazzi R, Anver M, Hollingshead MG, Mayo JG, Malspeis L. An in vivo AIDS-related lymphoma model for assessing chemotherapeutic agents. *Proc Am Assoc Cancer Res* 1994; 35:369.
42. Personal communication: Ian Magrath, Pediatrics Branch, Division of Cancer Treatment, NCI.
43. Magrath IT, Pizzo RA, Whang-Peng J, Douglass EC, Alabaster O, Gerber P, Freeman CB, Novikovs L. Characterization of lymphoma-derived cell lines: Comparison of cell lines positive and negative for Epstein-Barr virus nuclear antigen. I. Physical cytogenetic, and growth characteristics. *J Natl Cancer Inst* 1980; 64:465–476.
44. Magrath IT, Freeman CB, Pizzo P, Gadek J, Jaffe E, Santaella M, Hammer C, Frank M, Reaman G, Novikovs L. Characterization of lymphoma-derived cell lines: Comparison of cell lines positive and negative for Epstein-Barr virus nuclear antigen. II. Surface markers. *J. Natl Cancer Inst* 1980; 64:477–483.
45. Magrath I, Freeman C, Santaella M, Gadek J, Frank M, Spiegel R, Novikovs L. Induction of complement receptor expression in cell lines derived from human undifferentiated lymphomas. II. Characterization of the induced complement receptors and demonstration of the simultaneous induction EBV receptor. *J Immunol* 1981; 127:1039–1043.
46. Benjamin D, Magrath IT, Maguire R, Janus C, Todd HD, Parson RG. Immunoglobulin secretion by cell lines derived from African and American undifferentiated lymphomas of Burkitt's and non-Burkitt's type. *J Immunol* 1982; 129:1336–1342.
47. Beckwith M, Urba WJ, Ferris DK, Freter CE, Kuhns DB, Moratz CM, Longo DL. Anti-IgM-mediated growth inhibition of a human B lymphoma cell line is independent of phosphatidylinositol turnover and protein kinase C activation and involves tyrosine phosphorylation. *J Immunol* 1991; 147 (7):2411–2418.
48. Mosier DE, Gulizia RJ, Baird SM, Wilson DB. Transfer of a functional human immune system to mice with severe combined immunodeficiency. *Nature* 1988; 335:256–259.
49. Martin DS, Stolfi RL, Sawyer RC. Commentary on "clinical predictivity of transplantable tumor systems in the selection of new drugs for solid tumors: rationale for a three-stage strategy." *Cancer Treat Rep* 1984; 68:1317–1318.
50. Martin DS, Balis ME, Fisher B, Frei E, Freireich EJ, Heppner G, Holland JF, Houghton JA, Houghton PJ, Johnson RK, Mittelman A, Rustum Y, Sawyer RC, Schmid FA, Stolfi RL, Young CW. Role of murine tumor models in cancer treatment research. *Cancer Res* 1986; 46: 2189–2192.
51. Stolfi RL, Stolfi LM, Sawyer RC, Martin DS. Chemotherapeutic evaluation using clinical criteria in spontaneous, autochthonous murine breast tumors. *J Natl Cancer Inst* 1988; 80:52–55.
52. Plowman J, Dykes DJ, Narayanan VL, Abbott BJ, Saito H, Hirata T, Grever MR. Efficacy of the quinocarmycins KW2152 and DX-52-1 against human melanoma lines growing in culture and in mice. *Cancer Res* 1995; 55:862–867.
53. Suffness M, Cordell G. Antitumor alkaloids. In: Brossi A, ed. *The Alkaloids*, vol. XXV. New York: Academic. 1985:1–355.
54. Rose WC. Taxol: a review of its preclinical in vivo antitumor activity. *Anticancer Drugs* 1992; 3:311–321.
55. Plowman J, Dykes DJ, Waud WR, Harrison SD Jr., Griswold DP Jr. Response of murine tumors and human tumor xenografts to taxol (NSC 125973) in mice. *Proc Am Assoc Cancer Res* 1992; 33:514.
56. Eiseman JL, Eddington N, Leslie J, MacAuley C, Sentz D, Kujawa J, Zuhowski M, Haidir S, Young D, Egorin MJ. Pharmacokinetics and development of a physiologic model of taxol in CD2F1 mice. *Proc Am Assoc Cancer Res* 1993; 34:396.

57. Supko JG, Plowman J, Dykes DJ, Zaharko DS. Relationship between schedule dependence of 9-amino-20(*S*)-camptothecin (AC; NSC 603071) antitumor activity in mice and its plasma pharmacokinetics. *Proc Am Assoc Cancer Res* 1992; 33:432.
58. Hollingshead M, Alley M, Abbott B, Mayo J, Grever M. Short-term in vivo cultivation of human tumor cell lines for assessing potential chemotherapeutic agents. *Proc Am Assoc Cancer Res* 1993; 34:429.
59. Alley MC, Pacula-Cox CM, Hursey ML, Rubinstein LR, Boyd MR. Morphometric and colorimetric analyses of human tumor cell line growth and drug sensitivity in soft agar culture. *Cancer Res* 1991; 51:1247–1256.

EXHIBIT D

Signaling through the Lymphotoxin β Receptor Induces the Death of Some Adenocarcinoma Tumor Lines

By Jeffrey L. Browning, Konrad Miatkowski, Irene Sizing, David Griffiths, Mohammad Zafari, Christopher D. Benjamin, Werner Meier, and Fabienne Mackay

From the Departments of Immunology and Inflammation and Protein Engineering, Biogen, Cambridge, Massachusetts 02142

Summary

Surface lymphotoxin (LT) is a heteromeric complex of LT-α and LT-β chains that binds to the LT-β receptor (LT-β-R), a member of the tumor necrosis factor (TNF) family of receptors. The biological function of this receptor-ligand system is poorly characterized. Since signaling through other members of this receptor family can induce cell death, e.g., the TNF and Fas receptors, it is important to determine if similar signaling events can be communicated via the LT-β-R. A soluble form of the surface complex was produced by coexpression of LT-α and a converted form of LT-β wherein the normally type II LT-β membrane protein was changed to a type I secreted form. Recombinant LT-α_1/β_2 was cytotoxic to the human adenocarcinoma cell lines HT-29, WiDr, MDA-MB-468, and HT-3 when added with the synergizing agent interferon (IFN) γ. When immobilized on a plastic surface, anti–LT-β-R monoclonal antibodies (mAbs) induced the death of these cells, demonstrating direct signaling via the LT-β-R. Anti–LT-β-R mAbs were also identified that inhibited ligand-induced cell death, whereas others were found to potentiate the activity of the ligand when added in solution. The human WiDr adenocarcinoma line forms solid tumors in immunocompromised mice, and treatment with an anti–LT-β-R antibody combined with human IFN-γ arrested tumor growth. The delineation of a biological signaling event mediated by the LT-β-R opens a window for further studies on its immunological role, and furthermore, activation of the LT-β-R may have an application in tumor therapy.

The TNF family of ligands and receptors is a set of regulatory elements in the immune system (1). TNF was discovered as a cytolytic agent circulating in the blood of endotoxin-stimulated animals (2–4). Originally cloned in the expectation that TNF would be a novel antitumor agent, it was later shown that its primary physiologic function lies in initiating the inflammatory cascade underlying the host's immediate defensive response to infection or stress. More complex immunological functions have been described (5, 6). Lymphotoxin (LT)[1] α (also called TNF-β) is a similar cytokine secreted by activated lymphocytes (7) and was originally characterized as having the same functions as TNF. Later, activated T and B cells were found to display LT-α on their surfaces in an unusual form complexed with another member of the TNF family called LT-β in an LT-α_1/β_2 stoichiometry (8–13). A complex with an apparent LT-α_2/β_1 stoichiometry is also present, but only in minor amounts on human lymphocytes. The major LT-α_1/β_2 form does not bind to the known TNF receptors, referred to here as TNF-R55 and TNF-R75, but rather interacts with another receptor in the TNF family called the LT-β receptor (LT-β-R) (9, 14).

Currently, the function of the LT system is poorly characterized, however, there are suggestions that LT signaling is involved in the development of the peripheral lymphoid organs. Genetic disruption of the LT-α gene in mice led to an unusual phenotype. The mice lacked lymph nodes and lost the organization of T and B cells in the follicles in the spleen (15, 16). A similar loss of lymph nodes occurs in *aly*, mice although this mouse, unlike the LT-α knockout mouse, is severely immunocompromised (17). Signaling through the two known TNF receptors has not been shown to mediate the development of the lymph nodes since knockout of either receptor does not lead to the loss of lymph nodes (18, 19). Thus, it has been postulated that signaling through the LT-β-R constitutes a regulatory pathway that is distinct from TNF-related events and may

[1] *Abbreviations used in this paper:* LT, lymphotoxin; LT-β-R, LT-β receptor; MTT, 3-(4,5-dimethylthiazol-2-yl) 2,5 diphenyltetrazolium bromide; TUNEL, terminal deoxynucleotidyl transferase UTP nick-end labeling; VCAM, vascular cell adhesion molecule.

J. Exp. Med. © The Rockefeller University Press • 0022-1007/96/03/867/12 $2.00
Volume 183 March 1996 867–878

account for the unique phenotype of the LT-α knockout mouse (12, 15, 16).

Activation of several members of the TNF family of receptors can have cytotoxic or growth-inhibitory consequences (1). For example Fas receptor activation results in apoptosis of many cell types, including both transformed and nontransformed cells (20, 21), and this process is likely to play a role in the deletion of autoreactive lymphocytes in the periphery (22). TNF and LT-α also can kill some transformed cells, and it is likely that tumor cells respond abnormally by either necrosing or apoptosing to what is normally a differentiation-like signal. More recently, TNF signaling has been proposed to induce the death of nontransformed lymphoblasts in a slow fashion (23, 24), and this process appears to require TNF-R75. The physiological significance of this event remains to be explored. The Fas receptor and the TNF-R55 both possess a unique cytoplasmic domain, called the death domain, that is required to initiate cell death (25). CD30 and CD40 signaling can inhibit growth and may also induce apoptosis, yet these receptors as well as the TNF-R75 and the LT-β-R lack obvious death domains (12, 26, 27). We have investigated whether LT-β-R signaling could induce cell death both because of its possible immunological relevance and to provide a practical starting point for studying the role of the LT system. Using either recombinant ligands or antireceptor mAbs with agonist activity, the ability of LT-β-R activation to induce cell death in various transformed lines was examined. In this report, we show that LT-β-R signaling can induce cell death in a limited group of adenocarcinoma tumor lines.

Materials and Methods

Cells. All cells were obtained from American Type Culture Collection (ATCC) (Rockville, MD) except for WEHI 164 clone 13, which was obtained from Dr. Eric Kawashima (Glaxo Institute for Molecular Biology, Geneva, Switzerland). WEHI 164 cells were cultured in RPMI 1640 with 10% fetal bovine serum (FBS). HT-29 and WiDr cells were maintained in MEM with Earle's salts, 10% FCS with glutamine, penicillin/streptomycin, nonessential amino acids, and sodium pyruvate. These two cell lines are thought to be derived from the same patient (28). In our assays, the original ATCC HT-29 line was heterogenous in its response to LT-α_1/β_2, and not all of the cells died in a parallel manner. Subclones from the line were isolated by limiting dilution, and the HT-29-14 line was one subclone that behaved homogenously in these assays. All of the results can be reproduced qualitatively with the parental line.

Materials. The anti-Fas mAb CH11 was obtained from Kamiya Biomedical Co. (Thousand Oaks, CA), the control IgG1 mouse mAb MOPC 21 from Organon Technica (Durham, NC) and the anti-CD40 mAb BB20 from R&D Systems (Minneapolis, MN). The anti-human LFA-3 mAb 1E6 has been described (29) and the anti-LFA-3 mAb TS2/9 was provided by Barbara Wallner. The anti-TNF mAb 104c has been described (30). The HT-29/26 hybridoma that produces a mAb that recognizes an abundant antigen on the HT-29 surface was obtained from ATCC, cells were grown, and the mAb purified by protein A–Sepharose chromatography. The LT-β-R–hIgG1 and TNF-R55–hIgG1 Fc fusion proteins have been described (9).

Recombinant Cytokines. Human TNF and IFN-γ were produced at Biogen (30). Recombinant human LT-α was prepared by expression in insect cells as described (31) and was similar to material expressed in CHO cells (30). The recombinant LT-α/β heteromeric forms were prepared by coinfection of insect cells with two baculoviruses encoding the human LT-α and human LT-β proteins (Browning, J.L., K. Miatkowski, D.A. Griffiths, P.R. Bourdon, C. Hession, C.M. Ambrose, and W. Meier, manuscript in preparation). The transmembrane region of the LT-β gene was replaced with a vascular cell adhesion molecule (VCAM) leader sequence to enable secretion of mixed LT-α/β forms. The trimers LT-α_1/β_2, LT-α_2/β_1, and LT-α_3 were purified using combinations of p55 TNF-R and LT-β-R affinity columns. The resultant preparations have been well characterized, contain only LT forms, are trimeric, and are >95% pure with respect to LT forms based on ion exchange chromatographic resolution of the three stoichiometrically different trimers. The LT-α_1/β_2 preparation contained <1 part in 5,000 of LT-α_3–like activity as assessed using the WEHI 164 indicator line and by comparison of various LT trimers prepared with a LT-α D50N mutation that eliminates TNF-R binding (Browning J.L., K. Miatkowski, D.A. Griffiths, P.R. Bourdon, C. Hession, C.M. Ambrose, and W. Meier, manuscript in preparation).

Cytotoxicity Assays. In the cytotoxicity assays, serial dilutions of the cytokines or antibodies were prepared in 50 μl in 96-well plates, and 5,000 HT-29-14 cells were added in 50 μl of media with or without IFN-γ. After 3–4 d, 10 μl of 5 mg/ml MTT [3-(4,5-dimethylthiazol-2-yl) 2,5 diphenyltetrazolium bromide] was added, and after 3 h the formazan was dissolved by adding 100 μl of 10% SDS in 10 mM HCl. After a further 24-h incubation at 37°C, the OD was quantitated at 550 nm. In some experiments, soluble receptor forms or pure human IgG were added in 10 μl before the addition of the cells. To immobilize mAbs on the plastic surface, 96-well tissue culture plates were first coated with 50 μl of 10 μg/ml affinity-purified goat anti-mouse Fc polyclonal antibody (Jackson ImmunoResearch Laboratories, Inc., West Grove, PA), washed with 5% FBS in PBS, and then coated with varying amounts of the various mAbs diluted into tissue culture media with FBS. The plates were washed with media before use. Cells were added and growth assessed as indicated above. To survey the panel of cells shown in Table 4, cells were plated in the presence of 50 U/ml IFN-γ with various dilutions of TNF, anti-Fas, LT-α_1/β_2, or into wells coated with various anti–LT-β-R mAbs as described above. Growth was assessed with the MTT readout, and wells were also visually inspected for morphology changes. Dramatic growth inhibition was scored as two pluses (++), partial growth inhibition at reasonable concentrations was noted as one plus (+), and partial effects requiring high concentrations of ligand was marked as plus/minus (+/−).

Mouse Anti–LT-β-R mAbs. Mouse hybridomas producing mAbs to the human LT-β-R were prepared by immunization of RBF mice with the LT-β-R–Fc chimera essentially as described previously (9). All mAbs were IgG1 isotypes.

FACS® Binding Assays. To monitor receptor binding to surface ligand, 200 ng/ml soluble LT-β-R–Fc were added to PMA-activated II-23 T cell hybridoma cells, and binding was detected using a PE-labeled donkey anti–human Ig essentially as described (9). To assess the blocking ability of the mAbs, mAbs were preincubated with the soluble receptor for 20 min before addition of the receptor–mAb mixture to the II-23 cells. In other experiments, receptor expression on adherent tumor lines was determined by FACS® analysis of cells removed with PBS with 5 mM EDTA and stained using anti–LT-β-R mAbs and a PE-labeled

donkey anti–mouse IgG reagent (Jackson ImmunoResearch Laboratories).

Epitope Mapping by BIAcore™ Analysis. Affinity-purified goat anti–human Fc (Jackson ImmunoResearch Laboratories) was immobilized onto an *N*-hydroxysuccinimide–activated sensor chip, and LT-β-R-Fc was captured onto the anti–human-Fc–coated chip. The various pairs of anti–LT-β-R mAbs were then bound sequentially, and the ability of the second mAb to bind in the presence of the first mAb was measured using a BIAcore™ 2000 (Pharmacia Biosensor, Uppsala, Sweden). The entire array of 49 mAb combinations were assessed for cross-blocking in this manner and analyzed essentially as described (32).

Analysis of Apoptosis. Terminal deoxynucleotidyl transferase UTP nick-end labeling (TUNEL) of free DNA ends, i.e., TUNEL staining, was carried out using the ApopTag™ kit (Oncor Inc., Gaithersburg, MD) according to the manufacturer's specifications.

Tumor Growth in SCID Mice. BALB/c SCID female mice at 6–8 wk old (The Jackson Laboratory, Bar Harbor, ME) were injected with 10^6 trypsinized and washed WiDr cells in a volume of 0.2 ml of PBS subcutaneously onto the back of the animal. Mice were treated with or without antibody either with or without 10^6 antiviral U/mouse of human IFN-γ by intraperitoneal injection in 0.2 ml on days 0 and 1 or as indicated. The amounts of IFN-γ and antibody have not been optimized. Tumor volume was calculated from the radius as determined by caliper measurements in two dimensions. The results shown in Fig. 6 *B* were determined in a blinded format.

Results

LT-α_1/β_2 Is Cytotoxic to HT-29 Cells. Recombinant LT-α_1/β_2 and LT-α_2/β_1 trimers were tested for their ability to inhibit the growth of a number of tumor lines. IFN-γ was included in the screening as it had been shown to enhance the cytolytic properties of TNF (33). Recombinant soluble LT-α_1/β_2 inhibited the growth of human HT-29 cells only in the presence of IFN-γ (Fig. 1) and, as shown previously, this cell line was also sensitive to the anti-Fas receptor mAb CH11, TNF, and LT-α (30, 34, 35). IFN-α and -β were 100-fold less effective when compared on the basis of antiviral units (data not shown). Soluble LT-α_2/β_1 was much less active in this assay.

The specificity of the LT-α_1/β_2 cytotoxicity was examined in several ways. Soluble TNF-R55 and LT-β-R immunoglobulin chimeras (TNF-R55–Fc and LT-β-R–Fc) were tested for their ability to block the various activities (9). These receptors can bind to the appropriate cleft between two subunits in the trimeric ligand structures and interfere with the ability of receptor on the membrane to bind ligand. As expected and shown previously (36, 37), TNF-R55-Fc completely blocked TNF-induced growth inhibition by binding to TNF and preventing its interaction with surface receptor (Table 1). Soluble TNF-R had no effect on LT-α_1/β_2–mediated antiproliferative effects. In contrast, LT-β-R–Fc blocked LT-α_1/β_2 effects, but not those of TNF or LT-α. Moreover, anti–LT-α–neutralizing mAbs (9) did not affect the LT-α_1/β_2 cytotoxicity (data not shown), confirming that soluble trace LT-α contaminants were not involved in the activity of LT-α_1/β_2 on HT-29 cells. Additionally, a mutated form of LT-α (D50N) that lacks the ability to signal through the TNF-R was examined (38). LT-α_1/β_2 prepared with the mutant LT-α retained essentially full activity on HT-29 and WiDr cells (see below), further eliminating TNF-R55 binding as a possible mechanism for the cytotoxic effects of LT-α_1/β_2 (Ambrose, C., unpublished data). An anti-TNF neutralizing mAb 104c, also had no effect on LT-α_1/β_2 activity, precluding the induction of TNF synthesis as a mechanism for the LT-α_1/β_2 effects. These assays indicate that LT-α_1/β_2 can trigger cytotoxic events via non–TNF-R–mediated mechanisms.

Mechanism of Growth Inhibition. The growth inhibition assay alone does not discriminate between death and stasis; however, direct observation of the treated HT-29 cells showed that Fas receptor activation led to rapid cell death, i.e., within 12–24 h, whereas TNF effects were slower and required ~24 h. LT-α_1/β_2–treated cells underwent a much slower death, with dead cells not being visible until 1.5–2 d. The morphology of the dying cells was identical in all three cases. Some cells have the appearance of apoptotic bodies with condensed nuclei, whereas in others the nucleus appears to condense and the cytoplasm balloons out and becomes clear (Fig. 2). Substantial cell lysis does not occur even after 3–4 d. The TNF-, anti-Fas receptor mAb– or LT-α_1/β_2–treated populations had more cells that stained brightly with HOECHST dye staining (data not shown), which can be indicative of chromatin condensation accompanying apoptotic events. Internucleosomal DNA fragmen-

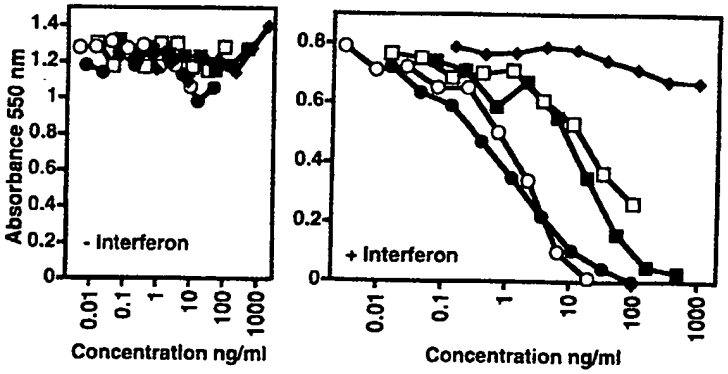

Figure 1. The cytotoxic effects of LT-α_1/β_2 on the human adenocarcinoma HT-29 cells. Comparison of the cytotoxic activity of anti-Fas receptor mAb CH-11 (●), TNF (○), LT-α (□), LT-α_1/β_2 (■), and LT-α_2/β_1 (◆) in the presence and absence of 80 U/ml IFN-γ.

Table 1. *Ability of LT-β-R and TNF-R55 Immunoglobulin Fusion Proteins to Block the Inhibitory Effects of Various TNF and LT Ligands on HT-29 Growth*

	Concentration of cytotoxic agent resulting in 50% growth inhibition		
	Presence of*		
Cytotoxic agent	hu-IgG control	TNF-R55–Fc	LT-β-R–Fc
	ng/ml	*ng/ml*	*ng/ml*
TNF	0.08	>10‡	0.08
LT-α	3.0	>1000	3.0
LT-α_1/β_2	5.0	5.0	>200.0
Anti-Fas mAb	2.0	2.0	2.0

*Each cytotoxic agent was premixed with the Ig fusion proteins for 10 min before addition to the cells. The final concentration of fusion protein was 5 μg/ml.
‡Higher concentrations were not tested.

tation or laddering was not observed after LT-α_1/β_2, TNF, or anti-Fas treatment of HT-29 or WiDr cells, although a prominent large DNA band was visible (data not shown) after all three treatments. This large fragment is reminiscent of the large 50–200-kb cleavage products previously described in dying epithelial tumor cells (39, 40). Some DNA fragmentation was observed using TUNEL staining of 3′ hydroxyl ends of DNA, which is more sensitive than DNA laddering (Fig. 3). Therefore, the death induced by TNF-R, Fas, or LT-β-R signaling may be basically apoptotic even though all of the classic features of apoptosis have not been observed in epithelial tumors (39, 41).

Properties of Anti–LT-β-R mAbs. Antibodies to receptors in the TNF family can have either antagonistic or agonistic effects, and as tools they have been very useful in delineating the consequences of receptor activation. To determine if LT-β-R cross-linking could induce cell death, we prepared and characterized similar LT-β-R–specific mAbs. Mice were immunized with the LT-β-R–Fc fusion protein, and a panel of mouse anti–LT-β-R mAbs were isolated. These mAbs were grouped into four subsets based on their performance in the following assays: (*a*) the ability to cross-block each other in a mAb/antigen-binding experiment using plasmon resonance detection (i.e., a BIAcore™ epitope mapping experiment); (*b*) the ability to block soluble LT-β-R–Fc binding to surface ligand on PMA-activated II-23 cells; and (*c*) the ability to affect LT-α_1/β_2–induced cell death. The results of this analysis are summarized in Table 2.

Epitope mapping using the BIAcore™ instrument defined four separate epitopes recognized by this panel of mAbs and formed the basis of the grouping shown in Table 2. Within each group, the mAbs effectively blocked each other. The group I mAbs did not cross-block any other mAbs. The group II epitope partially overlapped the group III epitope. We identified only one mAb, CBE11, with group IV properties, and its epitope slightly overlapped the BCG6 and BKA11 sites. To directly assess the ability of the mAbs to inhibit receptor–ligand binding, a FACS® binding assay was used. Antibodies were premixed with soluble receptor, and the ability of the receptor to bind to ligand on the surface of II-23 cells was quantitated. This assay has the advantage that any agonistic activity of the antireceptor mAbs would not be apparent. mAbs from groups I, II, and IV were effective inhibitors, suggesting that they bind close to the ligand binding region of the receptor (Table 2).

In the HT-29 cytoxicity assay, all mAbs in these groups either weakly inhibited growth or lacked activity when simply added to the culture in the absence of ligand (Fig. 4 *A*). There was considerable variability in this assay possibly reflecting differing receptor densities at the start of the experiment; e.g., compare Fig. 4 *A* and Table 3. In dramatic contrast, when the mAbs were immobilized on the plastic, all mAbs were found to have potent cytotoxic activity (Fig. 4 *B*), and this activity was again completely dependent on the presence of IFN-γ. This result demonstrates that LT-β-R cross-linking is sufficient to induce cell death. Moreover, we reasoned that mAbs to two different epitopes should be able to cross-link receptors more effectively, and indeed Table 3 shows that certain pairs of mAbs were cytotoxic in solution. In general, mAbs from two different groups had to be paired to get cytotoxic activity.

In addition to the direct agonistic effects of the mAbs described above, we investigated the effects of the mAbs on ligand induced cell death. Each of the four groups of mAbs had differing effects reinforcing the grouping based on BIAcore™ epitope mapping. Group I mAbs primarily blocked LT-α_1/β_2 activity with a small amount of direct growth inhibition occurring in the absence of ligand (Fig. 4 *C*). In some experiments (data not shown), a Fab fragment of BDA8 was used, and the small growth inhibitory activity disappeared and only direct inhibition was observed. Such complex mixed agonist/antagonist effects have been observed with anti-CD40 mAbs (42). The group II mAbs had complex effects that suggested mixed agonistic and antagonistic behavior (data not shown). Group III mAbs potentiated LT-α_1/β_2 activity presumably by creating local regions of high receptor density that would enhance ligand mediated cross-linking (Fig. 4 *D*), and there was no evidence of antagonistic effects. The cytotoxic effects of TNF were also slightly potentiated by these mAbs, suggesting that certain signal transduction elements were facilitating or priming the cells for TNF signaling. The group IV mAb, CBE11, did not affect ligand-mediated cytotoxicity. Because the LT-β-R–specific mAbs can directly effect death, one can conclude that the LT-β-R is able to signal cell death, and this event accounts for the cytotoxic activity of LT-α_1/β_2.

Survey of Sensitive Cell Lines. A series of human tumor lines have been screened for sensitivity to cytotoxic or growth-inhibitory effects of either the LT-α_1/β_2 ligand or plastic immobilized anti–LT-β-R mAbs in the presence of IFN-γ (summarized in Table 4). The WiDr line (43) was found to be sensitive to LT-α_1/β_2 in a very similar manner as the HT-29 line, and it is likely that this line is actually a

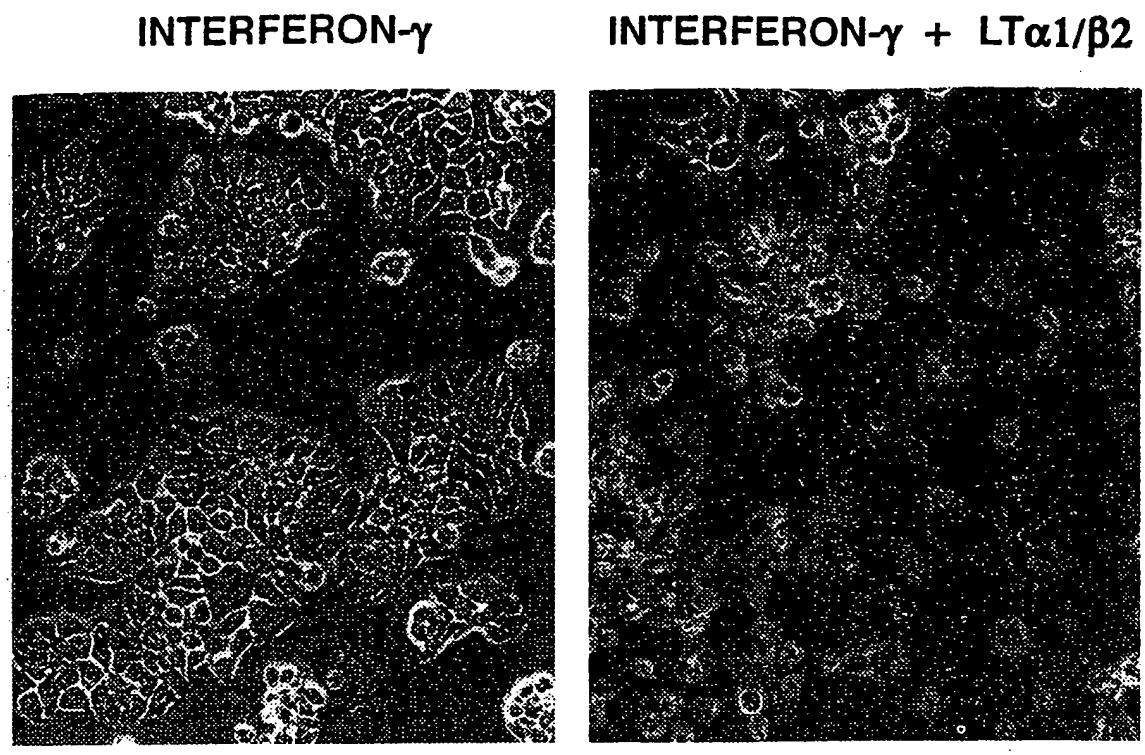

Figure 2. Photograph of HT-29 cells treated with IFN-γ (80 U/ml) alone or IFN-γ plus 50 ng/ml LT-α_1/β_2 for 3 d ×200.

derivative of HT-29 (28). The breast adenocarcinoma MDA-MB-468 and cervical carcinoma HT-3 lines were growth inhibited, and whether cell death occurred was not rigorously determined. In general, however, the majority of tumor lines are not sensitive under these relatively fixed conditions. This survey was complicated by the fact that the sensitivity of the cells to IFN-γ varied dramatically, and the lines are often heterogenous, with mixtures of responsive and nonresponsive cells obfuscating a simple MTT-based test.

Cell surface levels of LT-β-R were examined to determine whether LT-β-R presence is the determining factor for sensitivity to the LT ligand. Fig. 5 shows a comparison of LT-β-R and CD40 receptor levels on four different tumor lines. The CD40 staining is included since its surface levels are very abundant on some epithelial tumor lines, as is the LT-β-R. All four cell lines are LT-β-R positive, and these results are typical of most nonlymphoid cells (Mackay, F., and J.L. Browning, unpublished results). Despite the presence of LT-β-R on all four cell types, only HT-29 cells are appreciably sensitive to LT-α_1/β_2, indicating that sensitivity does not correlate simply with receptor presence. In the TNF, Fas, and CD40 signaling systems, no correlation has ever been observed between the level of surface receptor and whether a cell type responds biologically. Relative to Fas, TNF-R55, and TNF-R75, LT-β-R is very abundant on cells. Experiments on the HT-29 and WiDr lines indicated that IFN-γ treatment did not upregulate the LT-β-R, whereas in the same experiments the Fas receptor was dramatically upregulated as described previously (35).

There was no evidence that LT-β-R signaling was cytostatic to normal human fibroblasts, endothelial cells, or primary lymphocytes, which was expected since lymphocytes do not express the receptor (Hochman, P., J.L. Browning, and C. Ware, unpublished observations). The growth of the human diploid fibroblastoid line WI-38 was stimulated by LT-β-R signaling (data not shown). The adenocarcinoma lines SW620 and SW1417 both displayed altered morphology in response to LT-β-R signaling without growth arrest.

Anti–LT-β-R mAb Inhibits the Growth of WiDr in SCID Mice. We have explored the ability of an anti–LT-β-R mAb, CBE11, to block the growth of the WiDr line in immunodeficient mice. When the mice were treated intraperitoneally with the CBE11 mAb at the same time as the WiDr cells were inoculated subcutaneously, tumor outgrowth was dramatically blocked (Fig. 6 *A*). The antitumor action was enhanced by IFN-γ; however, the mAb was effective even without exogenous IFN-γ. In the CBE11 + IFN-γ group, 7 of 16 animals completely lacked tumors, whereas the remaining animals had small nodules that had not progressed at 2 mo. The CBE11 animals treated without IFN-γ were similar to the CBE11 + IFN-γ group at 30 d; however, these mice eventually developed slowly growing tumors. There were statistically significant differences between the control or IFN-γ–treated groups and the CBE11-treated groups, whereas no significant differences were observed between the saline, IFN-γ, or the control anti–human LFA3 mAb (1E6) + IFN-γ groups. The 1E6 and CBE11 mAbs are both IgG1s, and since the 1E6 mAb effectively coats the tumor line yet did not block tumor

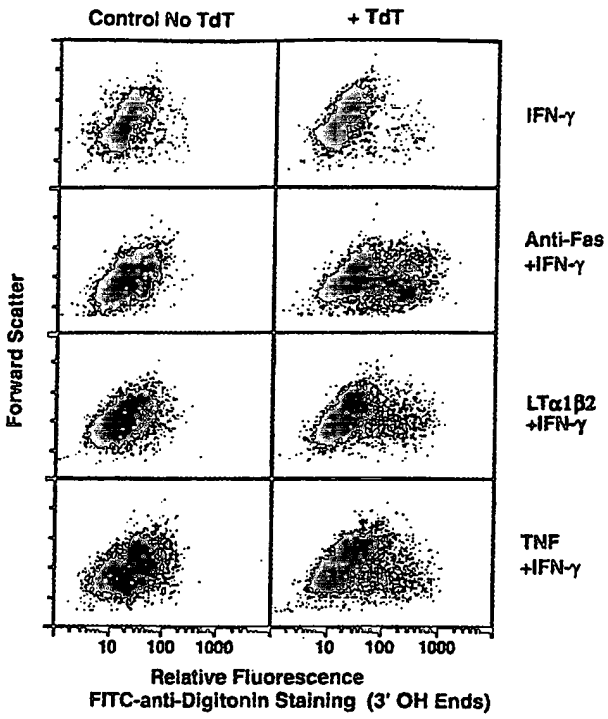

Figure 3. FACS® analysis of TUNEL staining of DNA fragmentation occurring in response to Fas, TNF, or LT-α_1/β_2 signaling. HT-29 cells were exposed to 80 U/ml of IFN-γ for 3 d, 50 ng/ml anti-Fas mAb and IFN-γ for 2 d, 50 ng/ml LT-α_1/β_2 and IFN-γ for 3 d, or 10 ng/ml TNF with IFN-γ for 2 d. All cells in the culture were stained using the Apo-Tag™ kit (Oncor, Inc.) without or with terminal deoxynucleotidyl transferase addition.

growth, we can exclude complement- or NK cell–mediated events as the basis for the tumor inhibition. The efficacy of CBE11 in the absence of IFN-γ was unexpected since there was an absolute dependence on IFN-γ for any LT-β-R based in vitro cytotoxic effect. Either there is some crossover of mouse IFN-γ onto human IFN-γ receptors, or other mechanisms are involved in vivo. The mechanism(s) by which LT-β-R signaling prevents tumor growth in vivo effects are being investigated. The ability of combined IFN-γ/CBE11 treatment to inhibit the growth of an established tumor was demonstrated (Fig. 6 *B*). Mice were inoculated with 10^6 WiDr cells, and after 15 d, treatment was initiated. At this point the average tumor volume was 0.076 cc or an average diameter of 0.532 cm. Treated tumors stopped growing, and after three injections of antibody over 3 wk, growth was arrested out to 7 wk after inoculation, at which point the experiment was terminated.

Discussion

Activation of the receptors of the TNF family can direct cells into a proliferative or differentiation type response, or it can induce cell death sometimes even in the same cell type depending on the conditions (4, 22, 44). In this work, we have shown that signaling through the LT-β-R leads to the death of the HT-29 and WiDr human adenocarcinoma cell lines and is at least growth inhibitory to two other lines. This activity represents the first observed effect of LT-β-R signaling and is important not only because of the current interest in cytotoxic events, but because it provides a biological assay for characterizing various reagents. There was no evidence that LT-β-R signaling was cytostatic to

Table 2. *Summary of Mouse Anti–Human LT-β-R mAbs*

mAb group	mAb name	Cell staining*	Blocking receptor binding‡	HT-29 cytotoxicity		
				mAb immobilized on Plastic§	Soluble mAb alone	Soluble mAb with LT-$\alpha_1\beta_1$
I	BDA8	+++	+++	+	+/−¶	Inhibits
I	AGH1	+++	+++	+	+/−	Inhibits
II	BCG6	+++	++	+	+/−	Mixed
II	BHA10	+++	+++	+	+/−	Mixed
III	BKA11	+++	+/−	+	−	Potentiates
III	CDH10	+++	+/−	+	+/−	Potentiates
IV	CBE11	+++	+++	+	+/−	No effect
Controls						
	MOPC21	−	−	−	−	No effect
	HT29/26	−	ND	−	−	No effect
	TS 2/9#	ND	ND	−	−	No effect

*FACS® staining of CHO cells transfected with LT-β-R.
‡Assay assessed whether antibody blocks binding of soluble receptor to the activated T cell hybridoma II-23.
§HT-29 cells were grown with IFN-γ on anti–LT-β-R–coated plates as described in Materials and Methods.
¶Variable, partial inhibition in some assays, no effects in others.
#Anti–human LFA-3, a mouse IgG1.

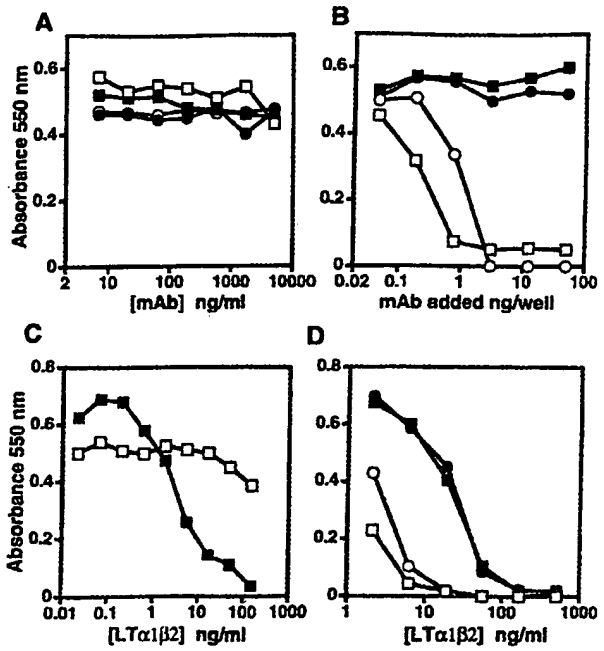

Figure 4. Effects of various anti-LT-β-R mAbs on HT-29 growth. *A* shows the effects of soluble anti-LT-β-R mAbs alone on the growth of HT-29 cells: control IgG1 (●), HT-29/26, a mAb to an irrelevant abundant surface Ag on HT-29 cells (■), BDA8 (○), and CDH10 (□). *B* illustrates the direct cytotoxic effects of these two anti-LT-β-R mAbs on HT-29 cells when immobilized on the plastic surface. Plates were coated with IgG1 (●), HT-29/26 (■), BDA8 (○), and CDH10 (□). *C* shows the LT-α_1/β_2 antiproliferative effects on HT-29 cells in the presence of 2 μg/ml control IgG1 (■) or anti-LT-β-R mAb BDA8 (□). BDA8 exhibits some agonist activity even at low concentrations. *D* shows the effects of CDH10 as an example of a group III anti-LT-β-R mAb that potentiates the effects of LT-α_1/β_2. LT-α_1/β_2 effects were measured in the presence of no mAb (●), 0.5 μg/ml control IgG1 (■), 0.05 μg/ml CDH10 (○), and 0.5 μg/ml (□) CDH10.

Table 3. *Effect of Pairs of Anti-LT-β-R mAbs on HT-29/WiDr Growth*

mAb	Concentration	mAb	Concentration	Cell growth
	(ng/ml)		*(ng/ml)*	*(OD 550 nm)*
IgG1	200			0.77 (HT-29)
BDA8	100	—	—	0.33*
—	—	BCG6	100	0.50
BDA8	100	BCG6	100	0.05
IGG1	50	—	—	0.85 (HT-29)
CDH10	33	—	—	0.525
—	—	AGH1	50	0.49
CDH10	33	AGH1	50	0.23
IgG1	100	—	—	0.80 (HT29)
CDH10	10	—	—	0.86
IgG1	50	CDH10	10	0.81
—	—	CBE11	50	0.58
CDH10	10	CBE11	50	0.21
BHA10	10	—	—	0.85
BHA10	10	CBE11	50	0.09
IgG1	50	—	—	0.62 (WiDr)
CDH10	33	—	—	0.36
—	—	AGH1	50	0.36
CDH10	33	AGH1	50	0.16

Dotted lines indicate separate experiments.
*Typically, further increases in the mAb concentration did not increase the amount of growth inhibition.

nontransformed cells, and signaling could actually drive growth in some situations. This pattern of cell sensitivity to LT-α_1/β_2 basically resembles the effects of TNF. The data we have obtained suggest that the cytotoxicity mediated by the LT-β-R will be limited to transformed cells. Recently, signaling through TNF-R75 has been reported to mediate an unusually slow death of nontransformed activated lymphocytes (23, 24), indicating that TNF-induced death may not be limited to transformed cells. In contrast, nontransformed lymphocytes can be induced to undergo rapid apoptosis after Fas signaling, and this event is most likely to be involved in the deletion of certain lymphocyte populations in the periphery (22, 45). Whether the slow events involving LT-β-R or TNF-R75 are physiologically important will require further investigation. Surface LT is abundant on lymphokine activated T cells, i.e., LAK cells (12, 46). Currently, cell mediated cytotoxicity is thought to be mediated through the perforin and/or Fas pathways (47). A classic LT-β-R–positive NK/LAK target, K562, was found to be completely resistant to the action of soluble LT-α_1/β_2, suggesting that neither surface LT is not involved in NK-like cytotoxicity. Genetic disruption of LT-α and the two TNF-R does not impair CTL-mediated cell death supporting the hypothesis that TNF/LT signaling is not involved in cell–cell killing (13). Further experimental work will be required to determine whether LT signaling via direct cell–cell contact supports these conclusions.

The LT system with its heterotrimeric ligand is unusual. The cytotoxic activity resides primarily in the LT-α_1/β_2 form, with the LT-α_2/β_1 complex being much less active. The crystal structure of LT-α complexed with the TNF-R55 revealed that the receptor lies in the groove between two adjacent subunits (48). The higher potency of the LT-α_1/β_2 form suggests that the β/β cleft, which is unique in the LT-α_1/β_2 heterotrimer, must interact with the LT-β-R. Biochemical analyses of this interaction have confirmed that there is a high affinity interaction of LT-β-R with LT-α_1/β_2 and a lower affinity interaction with LT-α_2/β_1 (Browning, J.L., M. Zafari, C. Benjamin, W. Meier, D. Griffiths, and K. Miatkowski, unpublished observations). The exact nature of the signaling complex is currently unclear.

Antibodies to the TNF-R55 (49, 50), Fas receptor (21, 35, 51), CD27 (52), and CD40 (53) have been shown to have receptor-activating properties. Presumably antibodies

Table 4. *Summary of the Effects of TNF, Anti-Fas, LT-α_1/β_2, and Anti-LT-β-R on the Growth of Various Cells in the Presence of IFN-γ*

Name	Type	Growth inhibition by			
		TNF	Anti-Fas	LT-α_1/β_2	Anti-LT-β-R
Brain					
U118	Glioblastoma	+/−	+/−	−	−
SW1783	Astrocytoma	−	++	−	−
SW1088	Astrocytoma	+	+/−	−	−
Skin					
A375	Melanoma	−	−	−	ND
SK-MEL-1	Melanoma	−	−	−	−
Colorectal					
HT29	Adenocarcinoma	++	++	++	++
WiDr	Adenocarcinoma	++	++	++	++
SK-Co-1	Adenocarcinoma	++	++	−	−
SW 403	Adenocarcinoma	−	++	−	−
SW 480	Adenocarcinoma	+	+	−	−
SW 620	Adenocarcinoma	−	−	*‡	−
SW 837	Adenocarcinoma	+/−	+/−	−	−
SW 1116	Adenocarcinoma	−	+	−	ND
SW 1417	Adenocarcinoma	−	−	‡	ND
Colo 320DM	Adenocarcinoma	−	ND	−	ND
LoVo	Adenocarcinoma	+	+/−	−	−
DLD-1	Adenocarcinoma	+	+	−	+/−
LS 174T	Adenocarcinoma	++	+/−	−	−
LS 123	Adenocarcinoma	+	−	−	ND
T84	Carcinoma	+	++	−	−
HCT 116	Carcinoma	+/−	−	−	ND
NCI H508	Adenocarcinoma	++	+	−	ND
CACO-2	Adenocarcinoma	−	−	−	−
Breast					
BT-20	Carcinoma	++	−	−	ND
SK-BR-3	Carcinoma	+/−	−	+/−‡§‖	−
MCF-7	Adenocarcinoma	++	+	+/−‡‖	ND
MDA-MB-468	Adenocarcinoma	++	ND	+/−§	+
Cervix					
ME180	Carcinoma	+	+	+/−‖	+
HT-3	Carcinoma	++	−	++‡	+/−
MS751	Carcinoma	+§	+/−	−	ND
Ovary					
SK-OV-3	Adenocarcinoma	−	−	−	−
Pancreas					
PANC-1	Epitheloid carcinoma	+	+	−	−
Capan-1	Adenocarcinoma	−	++	−	−
Capan-2	Adenocarcinoma	−	++	−	−
Lung					
A549	Carcinoma	+/−	ND	−	ND
Lymphoid					
U937	Histiocytic	++	+/−	+/−§	ND
K562	Promyelocytic	−	−	−	−

*Some growth stimulation.
‡Altered morphology.
§Heterogenous cell population, responders and nonresponders present.
‖Unconfirmed if LT-α component.

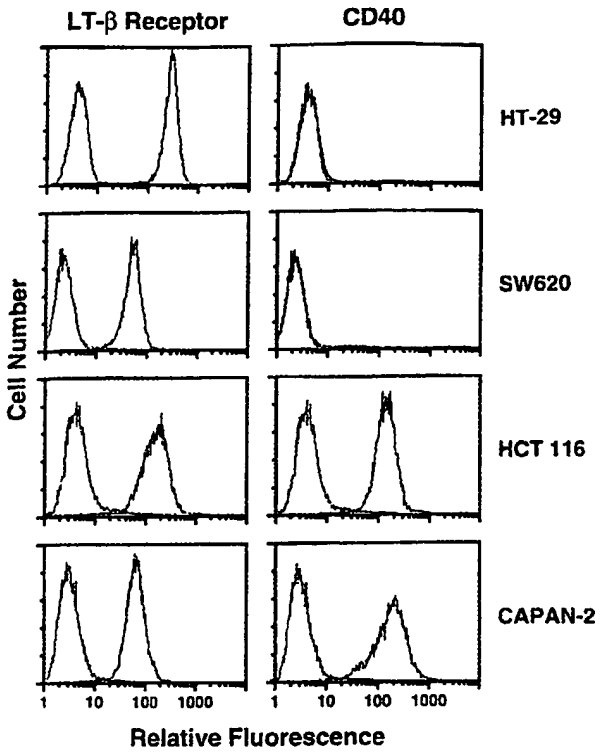

Figure 5. FACS® analysis comparing CD40 and LT-β-R levels on three colorectal carcinoma lines, HT-29, SW620, HCT 116, and the pancreatic carcinoma CAPAN-2. Untreated cells were stained with anti-CD40 (BB20), anti-LT-β-R (BDA8), or a control mAb (MOPC 21). Control antibody staining is the curve with the lowest staining in each panel.

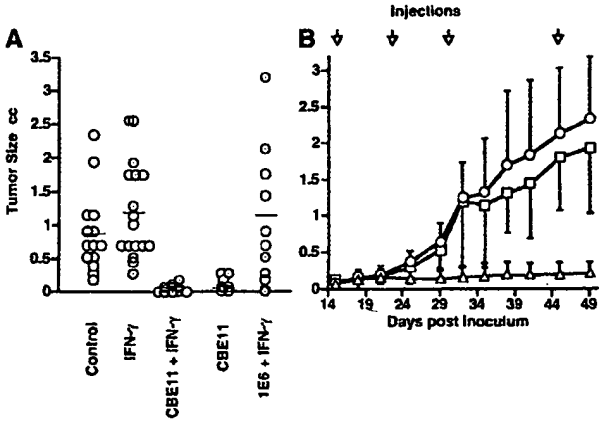

Figure 6. Growth of the human adenocarcinoma WiDr tumor in SCID mice. *A* shows the size of tumors 30 d after inoculation. Mice were treated on days 0 and 1 with saline, IFN-γ alone, an anti–LT-β-R mAb CBE11 with and without IFN-γ, and a control anti–human LFA3 mAb 1E6 with IFN-γ. Animals treated with CBE11 or 1E6, represented by circles with dots, received 10 μg/mouse per injection of antibody instead of 50 μg for the open-circle animals. The mean of each group is indicated by a crossbar. Means, standard deviations, and (number of animals) for the five groups (*left* to *right*) were 0.88 ± 0.59 (14), 1.21 ± 0.7 (21), 0.041 ± 0.052 (16), 0.11 ± 0.1 (12) and 0.98 ± 1.16 (12). *B* shows the growth of WiDr tumors as per *A*, however, the tumors were grown to an average diameter of 0.53 cm (0.076 cc) without any treatment, then intraperitoneal injections were started on day 15 and continued as indicated by the arrows. Animals were treated with IFN-γ alone (10^6 U/injection) (□), IFN-γ with 50 μg 1E6 anti-LFA-3 (○), or IFN-γ with 50 μg CBE11 anti–LT-β-R (Δ). Means and standard deviations are indicated for groups of 12 animals.

capable of cross-linking the receptors in the right orientation will generate receptor aggregates that can signal. Dimerization of the TNF-R55 may be sufficient to trigger TNF signaling; however, in the Fas receptor case, larger aggregates need to be formed (54). When immobilized on a plastic surface, all the anti–LT-β-R mAbs were able to induce death, including those that blocked ligand binding. Similar patterns were shown for anti-Fas receptor mAbs (51). In contrast, the anti–LT-β-R mAbs were not very effective in solution unless mAbs to two different epitopes were mixed together. In this case, it can be envisioned that aggregates larger than dimers could form, resulting in more productive signaling. When combined with the LT-α_1/β_2 ligand, some antibodies blocked activity, presumably by directly blocking the binding site, e.g., BDA8 and AGH1, although there was some evidence for mixed agonistic/antagonistic effects even in this case. At the other end of the spectrum, some mAbs, e.g., CDH10 and BKA11, potentiated the killing induced by ligand. Again, cross-linking of the receptor into small aggregates presumably facilitates the ability of ligand to productively cross-link and signal. Interestingly, the synergistic effect of the anti–LT-β-R mAbs with the LT-α_1/β_2 ligand also occurred between anti–LT-β-R mAbs and TNF. We do not have any evidence that the TNF receptors are involved in LT-β-R signaling, and therefore we interpret the effects on TNF signaling as resulting from more complex priming-like events at the intracellular level. Anti–LT-β-R mAbs can trigger NF-κB activation without inducing cell death (MacKay, F., manuscript submitted for publication), thus it is possible that both the LT-β-R and TNF-R intracellular signal transduction pathways utilize some common elements resulting in synergistic cross talk. Along with the soluble ligands and LT-β-R–Fc forms, the anti–LT-β-R mAbs are good tools for either activating or inhibiting the LT-β-R signaling pathway.

TNF can induce necrosis, apoptosis, or mixed mechanisms, depending on the cell line (55, 56), whereas Fas-triggered death is generally described as occurring by apoptosis. TNF can have either fast or slow effects on cells, probably reflecting multiple mechanisms (57). The experiments described here showed a lack of classical DNA laddering, although some DNA cleavage was detected using TUNEL techniques. The nuclei appear to condense, yet the cytoplasm balloons out in a manner characteristic of necrosis. It is possible that the ballooning occurs long after the death event and is observed in these assays, which are relatively long term compared with conventionally studied apoptotic events. Morphologically, the death induced by TNF, anti-Fas receptor, and LT-α_1/β_2 are similar, differing only kinetically. The signaling pathways initiated in each case may be different, as shown previously for Fas and TNF receptors (58, 59). The action of TNF is often accelerated by

the addition of cycloheximide to the culture, and the HT-29 cells are no exception. In contrast, LT-α_1/β_2 lacked activity in the standard short term cycloheximide-containing assay. Either the LT-α_1/β_2 action required protein synthesis, or the cytotoxic events are simply too slow to manifest themselves in the short-term assay format. In the TNF case, the signaling pathways leading to death are likely to be different depending on whether or not cycloheximide is present (60). The effects of cycloheximide and the slow pace of LT-β-R–induced death relative to TNF and Fas suggest that LT-β-R acts via a different pathway. This concept is intriguing since the LT-β-R lacks a canonical death domain. Either receptor cytoplasmic domains lacking the death domain can signal death, or the LT-β-R undergoes complex ill-defined interactions with other receptors. In light of the recent observations on the slow death mediated by TNF-R75 (23, 24), which also lacks a canonical death domain, it is possible that there are other death pathways used by some TNF family members distinct from that typified by the well-studied Fas system.

The ability to induce death selectively in tumor cells is an attractive goal. The signaling mediated by the TNF family of receptors is intriguing since this is one of relatively few cases in which a normal physiological signal can induce cell death as opposed to the loss of a signal, e.g., IL-2 or IL-3 removal. The use of TNF to treat cancers was predicated on this concept even before the emergence of programmed cell death as an important physiological process. Activation of the LT-β-R with the CBE11 mAb in vivo blocked the growth of WiDr cells inoculated into SCID mice. Since the anti–human LT-β-R mAb cannot bind to mouse cells, the growth inhibition mechanism must directly target the tumor cell. Likewise, the exogenously added IFN-γ can act only on the tumor cells since mouse IFN-γ does not bind to human IFN-γ receptors (61) and human IFN-γ does not bind to mouse IFN-γ receptors. Therefore, because of the lack of an absolute requirement for IFN-γ, it remains unclear whether the in vivo effect reflects direct cytotoxicity as observed in vitro or whether other mechanisms are contributing. If other mechanisms are involved, a wider range of tumors may be affected in vivo than would be forecast by the in vitro analyses. Generally, more primary tumors were found to be affected by TNF in in vivo models than would be surmised from the analysis of in vitro cultured tumor lines (62).

An LT-β-R–based antitumor strategy may be important when considered in the context of recent advances. TNF, Fas, and LT-α_1/β_2 are clearly cytotoxic to tumor types with mutant p53 such as HT-29 (63), and, moreover, the TNF signaling pathway in cells of fibroblastoid or epithelial origin is not sensitive to the protective effects of bcl-2 (64). Therefore, the induction of a death sequence might occur via a route that circumvents the wild-type p53 dependency of some chemotherapeutic approaches (65). A proper understanding of these signaling processes may lead to alternative strategies for controlling cancer. Clinically, isolated limb perfusion with TNF dramatically demonstrated the soundness of the approach (66), but unfortunately the systemic application of TNF was frustrated by dose-limiting toxicity resulting from activation of inflammatory cascades. Likewise, the Fas receptor is widely distributed, and anti-Fas mAbs can be very potent inducers of apoptosis; however, receptor activation also leads to rapid necrosis of normal liver cells and death in mice. This activity would certainly complicate its therapeutic application (67). The LT-β-R is present on most transformed cell types, and its activation also presents a potential anticancer therapy. Moreover, it is likely that sufficient IFN-γ exists in the tumor environment to synergize with LT-α_1/β_2 without exogenous administration (68). Our preliminary data indicate that LT-α_1/β_2 does not effectively activate primary human endothelial cells to express the VCAM or E-selectin adhesion molecules, and hamster anti–m-LT-β-R mAbs do not cause death (Hochman, P., G. Majean, F. Mackay, and S. Browning, manuscript submitted for publication); therefore, LT-β-R signaling should lack TNF-type toxicity. If the physiological activity of LT-α_1/β_2 is limited to more subtle regulatory effects on lymph node function, it is conceivable that an LT-α_1/β_2 therapy may provide an alternative therapy for some adenocarcinomas.

We thank Chris Ambrose for her analysis of the D50N mutant system, Paula Hochman for a critical reading of the manuscript, and also for her and Gerry Majeau's experiments on the effects of LT-α_1/β_2 signaling on endothelial cells. We also thank Carl Ware and coworkers for their advice, insight, and advance knowledge of their work, and Apinya Ngam-ek for her studies on LT-β-R regulation.

Address correspondence to Jeffrey L. Browning, Department of Immunology and Inflammation, Biogen, 14 Cambridge Center, Cambridge, MA 02142.

Received for publication 6 September 1995 and in revised form 1 November 1995.

References

1. Smith, C.A., T. Farrah, and R.G. Goodwin. 1994. The TNF receptor superfamily of cellular and viral proteins: activation, costimulation, and death. *Cell.* 76:959–962.
2. Beyaert, R., and W. Fiers. 1994. Molecular mechanisms of tumour necrosis factor-induced cytotoxicity. *FEBS (Fed. Eur. Biochem. Soc.) Lett.* 340:9–16.
3. Fiers, W. 1991. Tumor necrosis factor. Characterization at the molecular, cellular and in vivo level. *FEBS (Fed. Eur. Biochem. Soc.) Lett.* 285:199–212.
4. Tracey, K.J., and A. Cerami. 1993. Tumor necrosis factor,

other cytokines and disease. *Annu. Rev. Cell Biol.* 9:317–343.
5. Tartaglia, L.A., D.V. Goeddel, C. Reynolds, I.S. Figari, R.F. Weber, B.M. Fendly, and M.A. Palladino, Jr. 1993. Stimulation of human T-cell proliferation by specific activation of the 75-kDa tumor necrosis factor receptor. *J. Immunol.* 151: 4637–4641.
6. Pimentel-Muinos, F.X., J. Mazana, and M. Fresno. 1995. Biphasic control of nuclear factor-kappa B activation by the T cell receptor complex: role of tumor necrosis factor alpha. *Eur. J. Immunol.* 25:179–186.
7. Paul, N.L., and N.H. Ruddle. 1988. Lymphotoxin. *Annu. Rev. Immunol.* 6:407–438.
8. Browning, J.L., A. Ngam-ek, P. Lawton, J. DeMarinis, R. Tizard, E.P. Chow, C. Hession, G.B. O'Brine, S.F. Foley, and C.F. Ware. 1993. Lymphotoxin beta, a novel member of the TNF family that forms a heteromeric complex with lymphotoxin on the cell surface. *Cell.* 72:847–856.
9. Browning, J.L., I. Dougas, E.A. Ngam, P.R. Bourdon, B.N. Ehrenfels, K. Miatkowski, M. Zafari, A.M. Yampaglia, P. Lawton, W. Meier, et al. 1995. Characterization of surface lymphotoxin forms. Use of specific monoclonal antibodies and soluble receptors. *J. Immunol.* 154:33–46.
10. Androlewicz, M.J., J.L. Browning, and C.F. Ware. 1992. Lymphotoxin is expressed as a heteromeric complex with a distinct 33-kDa glycoprotein on the surface of an activated human T cell hybridoma. *J. Biol. Chem.* 267:2542–2547.
11. Ware, C.F., P.D. Crowe, M.H. Grayson, M.J. Androlewicz, and J.L. Browning. 1992. Expression of surface lymphotoxin and tumor necrosis factor on activated T, B, and natural killer cells. *J Immunol.* 149:3881–3888.
12. Ware, C.F., T.L. VanArsdale, P.D. Crowe, and J.L. Browning. 1995. The ligands and receptors of the lymphotoxin system. *Curr. Top. Microbiol. Immunol.* 198:175–218.
13. Abe, Y., A. Horiuchi, Y. Osuka, S. Kimura, G.A. Granger, and T. Gatanaga. 1992. Studies of membrane-associated and soluble (secreted) lymphotoxin in human lymphokine-activated T-killer cells in vitro. *Lymphokine Cytokine Res.* 11:115–121.
14. Crowe, P.D., T.L. VanArsdale, B.N. Walter, C.F. Ware, C. Hession, B. Ehrenfels, J.L. Browning, W.S. Din, R.G. Goodwin, and C.A. Smith. 1994. A lymphotoxin-beta-specific receptor. *Science (Wash. DC).* 264:707–710.
15. De Togni, P., J. Goellner, N.H. Ruddle, P.R. Streeter, A. Fick, S. Mariathasan, S.C. Smith, R. Carlson, L.P. Shornick, J. Strauss-Schoenberger, J.H. Russell, R. Karr, and D.D. Chaplin. 1993. Abnormal development of peripheral lymphoid organs in mice deficient in lymphotoxin. *Science (Wash. DC).* 264:703–706.
16. Banks, T.A., B.T. Rouse, M.K. Kerley, P.J. Blair, V.L. Godfrey, N.A. Kuklin, D.M. Bouley, J. Thomas, S. Kanangat, and M.L. Mucenski. 1995. Lymphotoxin-alpha-deficient mice: effects on secondary lymphoid development and humoral immune responsiveness. *J. Immunol.* 155:1685–1693.
17. Miyawaki, S., Y. Nakamura, H. Suzuka, M. Koba, R. Yasumizu, S. Ikehara, and Y. Shibata. 1994. A new mutation, aly, that induces a generalized lack of lymph nodes accompanied by immunodeficiency in mice. *Eur. J. Immunol.* 24:429–434.
18. Pfeffer, K., T. Matsuyama, T.M. Kundig, A. Wakeham, K. Kishihara, A. Shahinian, K. Wiegmann, P.S. Ohashi, M. Kronke, and T.W. Mak. 1993. Mice deficient for the 55 kd tumor necrosis factor receptor are resistant to endotoxic shock, yet succumb to *L. monocytogenes* infection. *Cell.* 73:457–467.
19. Erickson, S.L., F.J. de Sauvage, K. Kikly, K. Carver-Moore, S. Pitts-Meek, N. Gillett, K.C.F. Sheehan, R.D. Schreiber, D.V. Goeddel, and M. Moore. 1994. Decreased sensitivity to tumour-necrosis factor but normal T-cell development in TNF receptor-2-deficient mice. *Nature (Lond.).* 372:560–563.
20. Itoh, N., S. Yonehara, A. Ishii, M. Yonehara, S. Mizushima, M. Sameshima, A. Hase, Y. Seto, and S. Nagata. 1991. The polypeptide encoded by the cDNA for human cell surface antigen Fas can mediate apoptosis. *Cell.* 66:233–243.
21. Trauth, R.C., C. Klas, A.M.J. Peters, S. Matzku, P. Moeller, W. Falk, K.-M. Debatin, and P.H. Krammer. 1989. Monoclonal antibody-mediated tumor regression by induction of apoptosis. *Science (Wash. DC).* 245:301–305.
22. Nagata, S., and P. Golstein. 1995. The Fas death factor. *Science (Wash. DC).* 267:1449–1458.
23. Sarin, A., M. Conan-Cibotti, and P.A. Henkart. 1995. Cytotoxic effect of TNF and lymphotoxin on T lymphoblasts. *J. Immunol.* 155:3716–3718.
24. Zheng, L., G. Fisher, R.E. Miller, J. Peschon, D.H. Lynch, and M.J. Lenardo. 1995. Induction of apoptosis in mature T cells by tumour necrosis factor. *Nature (Lond.).* 377:348–351.
25. Cleveland, J.L., and J.N. Ihle. 1995. Contenders in FasL/TNF death signaling. *Cell.* 81:479–482.
26. Funakoshi, S., D.L. Longo, M. Beckwith, D.K. Conley, G. Tsarfaty, I. Tsarfaty, R.J. Armitage, W.C. Fanslow, M.K. Spriggs, and W.J. Murphy. 1994. Inhibition of human B-cell lymphoma by CD40 stimulation. *Blood.* 83:2787–2794.
27. Smith, C.A., H.J. Gruss, T. Davis, D. Anderson, T. Farrah, E. Baker, G.R. Sutherland, C.I. Brannan, N.G. Copeland, N.A. Jenkins, et al. 1993. CD30 antigen, a marker for Hodgkin's lymphoma, is a receptor whose ligand defines an emerging family of cytokines with homology to TNF. *Cell.* 73:1349–1360.
28. Browning, M.J., P. Krausa, A. Rowan, D.C. Bicknell, J.G. Bodmer, and W.F. Bodmer. 1993. Tissue typing the HLA-A locus from genomic DNA by sequence specific PCR: comparison of HLA genotype and surface expression on colorectal tumor cell lines. *Proc. Natl. Acad. Sci. USA.* 90:2842–2845.
29. Miller, G.T., P.S. Hochman, W. Meier, R. Tizard, S.A. Bixler, M.D. Rosa, and B.P. Wallner. 1993. Specific interaction of lymphocyte function associated antigen-3 with CD2 can inhibit T cell responses. *J. Exp. Med.* 178:211–222.
30. Browning, J., and A. Ribolini. 1989. Studies on the differing effects of tumor necrosis factor and lymphotoxin on the growth of several human tumor lines. *J. Immunol.* 143:1859–1867.
31. Crowe, P.D., T.L. VanArsdale, B.N. Walter, K.M. Dahms, and C.F. Ware. 1994. Production of lymphotoxin (LT alpha) and a soluble dimeric form of its receptor using the baculovirus expression system. *J. Immunol. Methods.* 168:79–89.
32. Johne, B., M. Gadnell, and K. Hansen. 1993. Epitope mapping and binding kinetics of monoclonal antibodies studied by real time biospecific interaction analysis using surface plasmon resonance. *J. Immunol. Methods.* 160:191–198.
33. Lee, S.H., B.B. Aggarwal, E. Rinderknecht, F. Assisi, and H. Chiu. 1984. The synergistic anti-proliferative effect of gamma-interferon and human lymphotoxin. *J. Immunol.* 133:1083–1086.
34. Dealtry, G.B., M.S. Naylor, W. Fiers, and F.R. Balkwill. 1987. DNA fragmentation and cytotoxicity caused by tumor necrosis factor is enhanced by interferon-gamma. *Eur. J. Immunol.* 17:689–693.
35. Yonehara, S., A. Ishii, and M. Yonehara. 1989. A cell-killing monoclonal antibody (anti-fas) to a cell surface antigen co-downregulated with the receptor of tumor necrosis factor. *J. Exp. Med.* 169:1747–1756.
36. Ashkenazi, A., S.A. Marsters, D.J. Capon, S.M. Chamow,

I.S. Figari, D. Pennica, D.V. Goeddel, M.A. Palladino, and D.H. Smith. 1991. Protection against endotoxic shock by a tumor necrosis factor receptor immunoadhesin. *Proc. Natl. Acad. Sci. USA.* 88:10535–10539.

37. Loetscher, H., R. Gentz, M. Zulauf, A. Lustig, H. Tabuchi, E.J. Schlaeger, M. Brockhaus, H. Gallati, M. Manneberg, and W. Lesslauer. 1991. Recombinant 55-kDa tumor necrosis factor (TNF) receptor. Stoichiometry of binding to TNF alpha and TNF beta and inhibition of TNF activity. *J. Biol. Chem.* 266:18324–18329.
38. Goh, C.R., C.S. Loh, and A.G. Porter. 1991. Aspartic acid 50 and tyrosine 108 are essential for receptor binding and cytotoxic activity of tumour necrosis factor beta (lymphotoxin). *Protein Eng.* 4:785–791.
39. Oberhammer, F., J.W. Wilson, C. Dive, I.D. Morris, J.A. Hickman, A.E. Wakeling, P.R. Walker, and M. Sikorska. 1993. Apoptotic death in epithelial cells: cleavage of DNA to 300 and/or 50 kb fragments prior to or in the absence of internucleosomal fragmentation. *EMBO (Eur. Mol. Biol. Organ.) J.* 12:3679–3684.
40. Dusenbury, C.E., M.A. Davis, T.S. Lawrence, and J. Maybaum. 1991. Induction of megabase DNA fragments by 5-fluorodeoxyuridine in human colorectal tumor (HT29) cells. *Mol. Pharmacol.* 39:285–289.
41. Bortner, C.D., N.B.E. Oldenburg, and J.A. Cidlowski. 1995. The role of DNA fragmentation in apoptosis. *Trends Cell Biol.* 5:21–26.
42. Ledbetter, J., L.S. Grosmaire, D. Hollenbaugh, A. Aruffo, and S.G. Nadler. 1995. Agonistic and antagonistic properties of CD40 mAb G28-5 are dependent on binding valency. *Circ. Shock.* 44:67–72.
43. Raitano, A.B., P. Scuderi, and M. Korc. 1991. Upregulation of interferon-gamma binding by tumor necrosis factor and lymphotoxin: disparate potencies of the cytokines and modulation of their effects by phorbol ester. *J. Interferon Res.* 11:61–67.
44. Lynch, D. 1995. Biology of Fas. *Circ. Shock.* 44:63–66.
45. Crispe, I.N. 1994. Fatal interactions: Fas-induced apoptosis of mature T cells. *Immunity.* 1:347–349.
46. Horiuchi, A., Y. Abe, M. Miyake, K. Kimura, Y. Hitsumoto, N. Takeuchi, and S. Kimura. 1994. Role of membrane-associated lymphotoxin (mLT) in the killing activity of lymphokine-activated killer (LAK) cells towards various tumour cell lines. *Clin. Exp. Immunol.* 96:152–157.
47. Henkardt, P.A. 1994. Lymphocyte-mediated cytoxicity: two pathways and multiple effector molecules. *Immunity.* 1:343–346.
48. Banner, D.W., A. D'Arcy, W. Janes, R. Gentz, H.J. Schoenfeld, C. Broger, H. Loetscher, and W. Lesslauer. 1993. Crystal structure of the soluble human 55 kd TNF receptor-human TNF beta complex: implications for TNF receptor activation. *Cell.* 73:431–445.
49. Engelmann, H., H. Holtmann, C. Brakebusch, Y.S. Avni, I. Sarov, Y. Nophar, O. Hadas, O. Leitner, and D. Wallach. 1990. Antibodies to a soluble form of a tumor necrosis factor (TNF) receptor have TNF-like activity. *J. Biol. Chem.* 265: 14497–14504.
50. Shalaby, M.R., A. Sundan, H. Loetscher, M. Brockhaus, W. Lesslauer, and T. Espevik. 1990. Binding and regulation of cellular functions by monoclonal antibodies against human tumor necrosis factor receptors. *J. Exp. Med.* 172:1517–1520.
51. Alderson, M.R., T.W. Tough, S. Braddy, T. Davis-Smith, E. Roux, K. Schooley, R.E. Miller, and D.H. Lynch. 1994. Regulation of apoptosis and T cell activation by Fas-specific mAb. *Int. Immunity.* 6:1799–1806.
52. van Lier, R.A.W., M.O. Pool, P. Kabel, S. Mous, F. Terpstra, M.A. De Ric, C.J. Melief, and F. Miedema. 1988. Anti-CD27 monoclonal antibodies identify two functionally distinct populations within the $CD4^+$ T cell subset. *Eur. J. Immunol.* 18:811–816.
53. Gordon, J., M.J. Millsum, G.R. Guy, and J.A. Ledbetter. 1988. Resting B lymphocytes can be triggered directly through the CDw40 (Bp50) antigen. *J. Immunol.* 140:1425–1430.
54. Dhein, J., P.T. Daniel, B.C. Trauth, A. Oehm, P. Moller, and P.H. Krammer. 1992. Induction of apoptosis by monoclonal antibody anti-APO-1 class switch variants is dependent on cross-linking of APO-1 cell surface antigens. *J. Immunol.* 149:3166–3173.
55. Laster, S.M., J.G. Wood, and L.R. Gooding. 1988. Tumor necrosis factor can induce both apoptotic and necrotic forms of cell lysis. *J. Immunol.* 141:2629–2634.
56. Fady, C., A. Gardner, F. Jacoby, K. Briskin, Y. Tu, I. Schmid, and A. Lichtenstein. 1995. Atypical apoptotic cell death induced in L929 targets by exposure to tumor necrosis factor. *J. Interferon Cytokine Res.* 15:71–80.
57. Reid, T.R., F.M. Tortis, and G.M. Ringold. 1989. Evidence for two mechanisms by which tumor necrosis factor kills cells. *J. Biol. Chem.* 264:4583–4589.
58. Wong, G.H.W., and D.V. Goeddel. 1994. Fas antigen and p55 TNF receptor signal apoptosis through distinct pathways. *J. Immunol.* 152:1751–1755.
59. Grell, M., P.H. Krammer, and P. Scheurich. 1994. Segregation of APO-1/Fas antigen and tumor necrosis factor receptor mediated apoptosis. *Eur. J. Immunol.* 24:2563–2566.
60. Reid, T., P. Louie, and R.A. Heller. 1994. Mechanisms of tumor necrosis factor cytotoxicity and the cytotoxic signals transduced by the p75 tumor necrosis factor receptor. *Circ. Shock.* 44:84–90.
61. Peska, S., J.A. Langer, K.C. Zoon, and C.E. Samuel. 1987. Interferons and their actions. *Annu. Rev. Biochem.* 56:727–777.
62. Fiers, W. 1991. Tumor necrosis factor, characterization at the molecular, cellular and in vivo level. *FEBS (Fed. Eur. Biochem. Soc.) Lett.* 285:199–212.
63. Park, D.J., H. Nakamura, A.M. Chumakov, J.W. Said, C.M. Miller, D.L. Chen, and H.P. Koeffler. 1994. Transactivational and DNA binding activities of endogenous p53 in p53 mutant cell lines. *Oncogene.* 9:1899–1906.
64. Vanhaesebroeck, B., J.C. Reed, V.D. De, J. Grooten, T. Miyashita, S. Tanaka, R. Beyaert, R.F. Van, and W. Fiers. 1993. Effect of bcl-2 proto-oncogene expression on cellular sensitivity to tumor necrosis factor-mediated cytotoxicity. *Oncogene.* 8:1075–1081.
65. Lowe, S.W., H.E. Ruley, T. Jacks, and D.E. Housman. 1993. p53-dependent apoptosis modulates the cytotoxicity of anticancer agents. *Cell.* 74:957–967.
66. Lejeune, F., D. Lienard, A. Eggermont, H. Schraffordt, B. Kroon, J. Gerain, F. Rosenkaimer, and P. Schmitz. 1994. Clinical experience with high dose tumor necrosis factor alpha in regional therapy of advanced melanoma. *Circ. Shock.* 43:191–197.
67. Ogasawara, J., F.R. Watanabe, M. Adachi, A. Matsuzawa, T. Kasugai, Y. Kitamura, N. Itoh, T. Suda, and S. Nagata. 1993. Lethal effect of the anti-Fas antibody in mice. *Nature (Lond.).* 364:806–809.
68. Dighe, A.S., E. Richards, L.J. Old, and R.D. Schreiber. 1994. Enhanced in vivo growth and resistance to rejection of tumor cells expressing dominant negative IFNgamma receptors. *Immunity.* 1:447–456.

EXHIBIT E

Journal of Clinical Immunology, Vol. 11, No. 3, 1991

Special Article

Monoclonal Antibody Therapy of Human Cancer: Taking the HER2 Protooncogene to the Clinic

H. MICHAEL SHEPARD,[1,4] GAIL D. LEWIS,[1] JAY C. SARUP,[1] BRIAN M. FENDLY,[1] DANIEL MANEVAL,[1] JOYCE MORDENTI,[1] IRENE FIGARI,[1] CLAIRE E. KOTTS,[1] MICHAEL A. PALLADINO, JR.,[1] AXEL ULLRICH,[2] and DENNIS SLAMON[3]

Accepted: January 22, 1991

The HER2 protooncogene encodes a 185-kDa transmembrane protein ($p185^{HER2}$) with extensive homology to the epidermal growth factor (EGF) receptor. Clinical and experimental evidence supports a role for overexpression of the HER2 protooncogene in the progression of human breast, ovarian, and non-small cell lung carcinoma. These data also support the hypothesis that $p185^{HER2}$ present on the surface of overexpressing tumor cells may be a good target for receptor-targeted therapeutics. The anti-$p185^{HER2}$ murine monoclonal antibody (muMAb) 4D5 is one of over 100 monoclonals that was derived following immunization of mice with cells overexpressing $p185^{HER2}$. The monoclonal antibody is directed at the extracellular (ligand binding) domain of this receptor tyrosine kinase and presumably has its effect as a result of modulating receptor function. *In vitro* assays have shown that muMAb 4D5 can specifically inhibit the growth of tumor cells only when they overexpress the HER2 protooncogene. MuMAb 4D5 has also been shown to enhance the TNF-α sensitivity of breast tumor cells that overexpress this protooncogene. Relevant to its clinical application, muMAb 4D5 may enhance the sensitivity of $p185^{HER2}$-overexpressing tumor cells to cisplatin, a chemotherapeutic drug often used in the treatment of ovarian cancer. *In vivo* assays with a nude mouse model have shown that the monoclonal antibody can localize at the tumor site and can inhibit the growth of human tumor xenografts which overexpress $p185^{HER2}$. Modulation of $p185^{HER2}$ activity by muMAb 4D5 can therefore reverse many of the properties associated with tumor progression mediated by this putative growth factor receptor. Together with the demonstrated activity of muMAb 4D5 in nude mouse models, these results support the clinical application of muMAb 4D5 for therapy of human cancers characterized by the overexpression of $p185^{HER2}$.

KEY WORDS: HER2; *neu*; TNF-α; monoclonal antibody therapy.

[1]Department of Developmental Biology, Genentech, Inc., 460 Point San Bruno Boulevard, South San Francisco, California 94080.
[2]Max Planck Institute for Biochemistry, Martinsreid, Germany.
[3]Department of Hematology and Oncology, University of California, Los Angeles, California 90024.
[4]To whom correspondence should be addressed.

BACKGROUND: THE HER2 PROTOONCOGENE AND HUMAN CANCER

Cellular protooncogenes encode proteins that are thought to regulate normal cellular proliferation and differentiation. Alterations in their structure or amplification of their expression lead to abnormal cellular growth and have been associated with carcinogenesis (1–4). Protooncogenes were first identified by either of two approaches. First, molecular characterization of the genomes of transforming retroviruses showed that the genes responsible for the transforming ability of the virus in many cases were altered versions of genes found in the genomes of normal cells. The normal version is the protooncogene, which is altered by mutation to give rise to the oncogene. An example of such a gene pair is represented by the EGF receptor and the v-erbB gene product. The virally encoded v-erbB gene product has suffered truncation and other alter-

0271-9142/91/0500-0117$06.50/0

ations that render it constitutively active and endow it with the ability to induce cellular transformation (5).

The second method for detecting cellular transforming genes that behave in a dominant fashion involves transfection of cellular DNA from tumor cells of various species into nontransformed target cells of a heterologous species. Most often this was done by transfection of human, avian, or rat DNAs into the murine NIH 3T3 cell line (1–5). Following several cycles of genomic DNA isolation and retransfection, the human or other species DNA was molecularly cloned from the murine background and subsequently characterized. In some cases, the same genes were isolated following transfection and cloning as those identified by the direct characterization of transforming viruses. In other cases, novel oncogenes were identified. An example of a novel oncogene identified by this transfection assay is the *neu* oncogene. It was discovered by Weinberg and colleagues in a transfection experiment in which the initial DNA was derived from a carcinogen-induced rat neuroblastoma (6,7). Characterization of the *neu* oncogene revealed that it had the structure of a growth factor receptor tyrosine kinase, had homology to the EGF receptor, and differed from its normal counterpart, the *neu* protooncogene, by an activating mutation in its transmembrane domain (8).

The association of the HER2 protooncogene with cancer was established by yet a third approach, that is, its association with human breast cancer. The HER2 protooncogene was first discovered in cDNA libraries by virtue of its homology with the EGF receptor, with which it shares structural similarities throughout (5). When radioactive probes derived from the cDNA sequence encoding $p185^{HER2}$ were used to screen DNA samples derived from breast cancer patients, amplification of the HER2 protooncogene was observed in about 30% of patient samples (9). Further studies have confirmed this original observation and extended it to suggest an important correlation between HER2 protooncogene amplification and/or overexpression and worsened prognosis in ovarian cancer and non-small cell lung cancer (10–14).

The association of HER2 amplification/overexpression with aggressive malignancy, as described above, implies that it may have an important role in progression of human cancer; however, many tumor-related cell surface antigens have been described in the past, few of which appear to have a direct role in the genesis or progression of disease (15,16). The data which support a role of HER2 overexpression in the basic mechanisms of human cancer are summarized below.

Amplified expression of $p185^{HER2}$ can lead to cellular transformation as assessed by morphological alterations and growth of $p185^{HER2}$-overexpressing cells in soft agar and in nude mice (17,18). In addition, NIH 3T3 fibroblasts overexpressing $p185^{HER2}$ have an increased resistance to cytotoxicity mediated by activated macrophages or recombinant human TNF-α (19), the cytokine that appears to be mainly responsible for macrophage-mediated tumor cell cytotoxicity (20). This observation extends also to breast tumor cells, which overexpress $p185^{HER2}$ (19), and suggests that high levels of $p185^{HER2}$ expression may be related to tumor cell resistance to at least one component of the host's antitumor surveillance armamentarium, the activated macrophage. This work has been reviewed previously (21), and similar data have recently been reported for ovarian tumor cell lines which overexpress $p185^{HER2}$ (22). Further support for a role of $p185^{HER2}$ or the related *neu* oncogene-encoded tyrosine kinase in tumorigenesis comes from work with transgenic mice that have been manipulated to overexpress one or the other of these two related genes. Transgenic mice expressing the activated form of the rat *neu* protooncogene, under the control of a steroid inducible promoter, uniformly develop mammary carcinoma (23). In another transgenic mouse model the HER2 protooncogene product, "activated" by point mutation analogous to the rat *neu* oncogene product, or an unaltered form of the HER2 protooncogene, has been expressed in mice (24). The main malignancies induced in this model were either lung adenocarcinoma or lymphoma but not mammary carcinoma. While it is not known why the different transgenic mouse models give such distinct results, the latter model may be of particular significance given the recent report of an association between $p185^{HER2}$ overexpression and poor prognosis in nonsmall cell lung cancer (14). These differing results suggest some difference in the activity of activated *neu* and HER2-encoded tyrosine kianses, although effects due to mouse strain differences cannot be excluded.

The structural similarities between $p185^{HER2}$ and the EGF receptor suggest that function of $p185^{HER2}$ may be regulated similarly to the EGF receptor. In particular, one expects that the tyrosine kinase activity associated with the cytoplasmic domain of

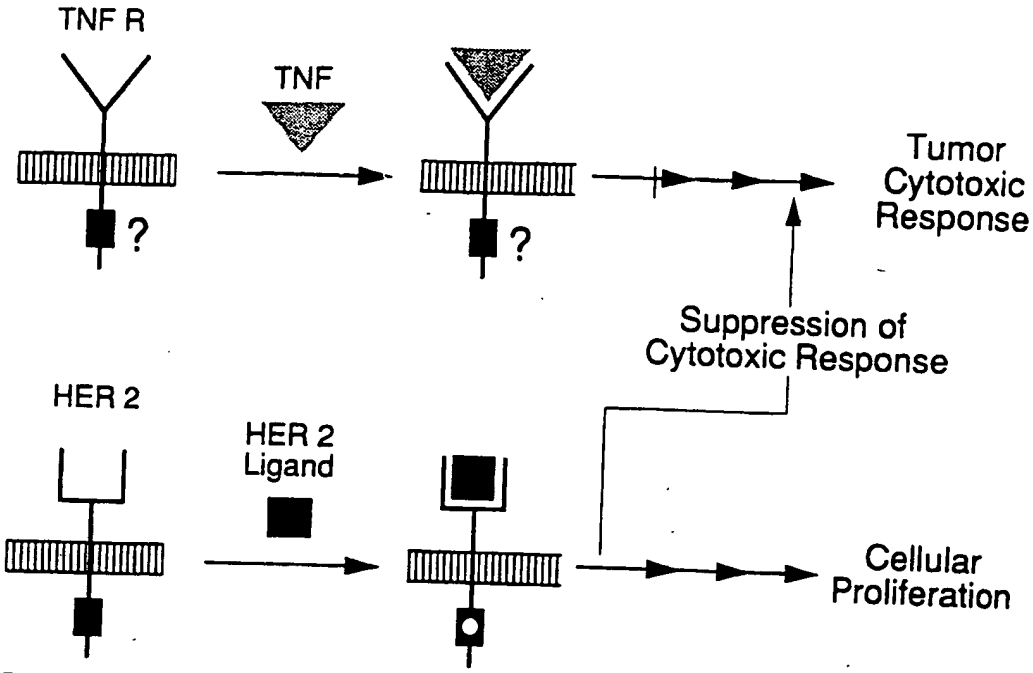

Fig. 1. Suppression of the TNF cytotoxic response by activation of $p185^{HER2}$. The schematic shows both the TNF cytotoxic pathway (top) and the $p185^{HER2}$-stimulated cell proliferation/transformation pathway (bottom). Signaling from the TNF receptor following interaction with TNF has not been characterized. Binding of ligand to $p185^{HER2}$ is shown to activate the receptor-associated tyrosine kinase activity, resulting in stimulation of cellular proliferation and suppression of the tumor cell cytotoxic response to TNF.

the receptor would be ligand activated. This proposal receives support from recent work describing a ligand for $p185^{HER2}$ (25). These data lead to a model (Fig. 1) wherein antagonists that downregulate the function of $p185^{HER2}$ should have the effect of inhibiting growth of tumor cells dependent upon $p185^{HER2}$ function and of increasing the sensitivity of such tumor cells to TNF-α. By analogy with previous work done with two related tyrosine kinases, the EGF receptor (26) and the activated *neu* protooncogene product (27), we hypothesized that monoclonal antibodies targeted to the extracellular domain of $p185^{HER2}$ may have the desired properties.

DERIVATION OF muMAb 4D5

A family of monoclonal antibodies focused against the extracellular domain of $p185^{HER2}$ were prepared (28). To do this, an NIH 3T3 fibroblast cell line that overexpresses $p185^{HER2}$ [NIH 3T3/HER2-3-400 (18)] was used to immunize BALB/c mice. The mice were subsequently boosted with NIH 3T3/HER2-3-400 and, finally, with a preparation enriched for $p185^{HER2}$ by wheat germ agglutinin chromatography of membrane extracts of this cell line. Following splenocyte fusion with a mouse myeloma partner, the hybridomas were cultured in 96-well microtiter plates. Hybridomas positive for anti-$p185^{HER2}$ activity, but with little or no anti-EGFR activity, were detected by ELISA (Fig. 2). A critical property of an anti-$p185^{HER2}$ monoclonal antibody with potential for therapy would be its lack of cross-reactivity with the closely related EGF receptor, which is expressed at elevated levels in multiple tissues (29). To select further monoclonal antibodies with this characteristic, a number of assays were performed, including immunoprecipitation assays utilizing *in vivo* labeled EGF receptor and $p185^{HER2}$ (Fig. 3A) and FACS analysis of antibody binding to tumor cells overexpressing either $p185^{HER2}$ or the EGFR (Fig. 3B). The screening results are summarized in Table I. Based upon these results, nine of the $p185^{HER2}$ monoclonal antibodies were chosen for further characterization, including a cell growth inhibition assay utilizing the SK-BR3 human breast adenocarcinoma cell line, which greatly overexpress $p185^{HER2}$. The monoclo-

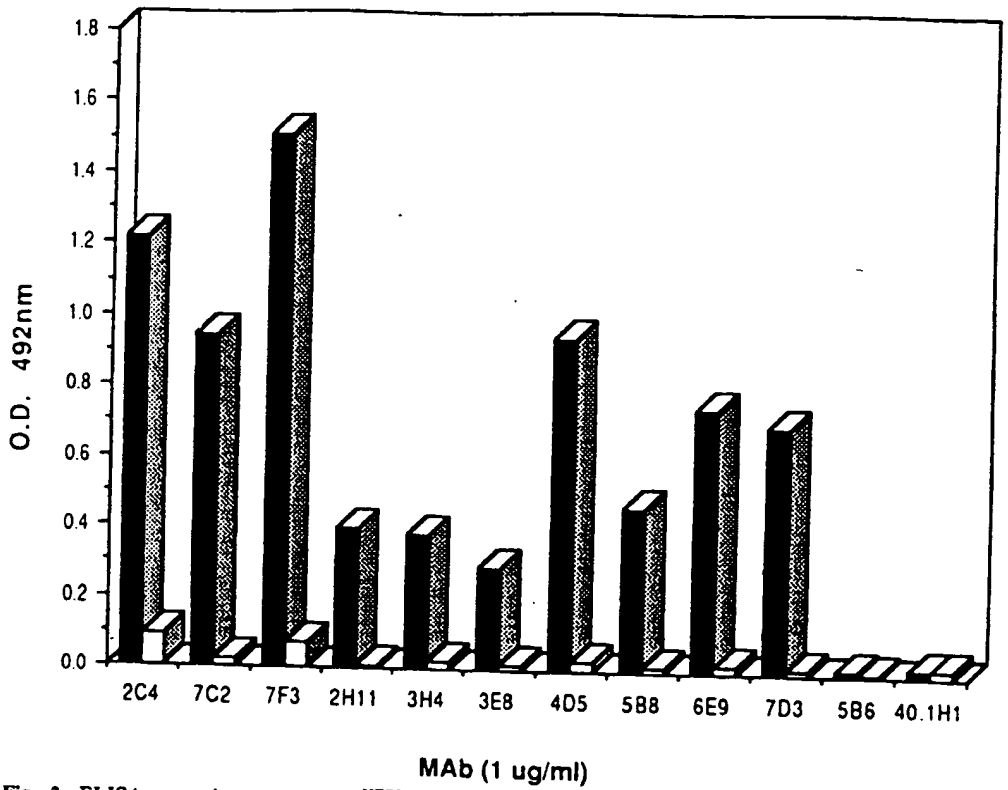

Fig. 2. ELISA screening of anti-p185^{HER2} monoclonal antibodies. Results shown measure the relative reactivities of the purified anti-p185^{HER2} monoclonal antibodies (added to 1 μg/ml) with membrane extracts enriched in EGF receptor (open bars; from A431 squamous carcinoma cells) or enriched in p185^{HER2} (filled bars; from NIH 3T3/HER2-3-400).

nal antibody, muMAb 4D5, was clearly the most effective of the group in this assay (Table II).

The initial results characterizing the growth inhibitory activity of these monoclonal antibodies were extended by comparing them for activity against a battery of human breast and ovarian tumor cell lines that expressed varying levels of p185^{HER2}. These results reveal that the monoclonal antibodies can be growth inhibitory, they may have no affect on cell proliferation, or they may stimulate the proliferation of breast tumor cells. Growth inhibition appears to depend upon overexpression (Table III). This property, in particular, is shared by the monoclonal antibodies 4D5 and 3H4. These monoclonal antibodies may exert their effects on cell growth by similar mechanisms since they compete for binding to the receptor (Tables I and III) (28) and, therefore, may recognize the same or overlapping epitopes. The other monoclonal antibodies vary in their ability to inhibit proliferation, but 7C2 and 6E9 are consistently less active in this respect.

The potent growth inhibitory activity of 2C4 for MDA-MB-175 breast tumor cells is not understood at present but may represent cross-reactivity with another receptor expressed on these cells. Similarly, the properties that distinguish 7C2 from the other antibodies with regard to its ability to stimulate the proliferation of several of the tumor cell lines shown in Table III has not been determined. The 6E9 monoclonal antibody has been shown to bind to the extracellular domain of p185^{HER2}, although only to a subset of receptors on the surface of SK-BR-3 tumor cells (30). The functional significance of this subset of receptors is unclear. In addition to its activity on breast tumor cells, which overexpress p185^{HER2}, muMAb 4D5 is also clearly the most active of the monoclonal antibodies with respect to its ability to inhibit growth of SKOV-3, a human ovarian adenocarcinoma cell line that overexpresses p185^{HER2} (Table III). Experiments are currently planned to try to understand in more detail how these monoclonal antibodies may exert

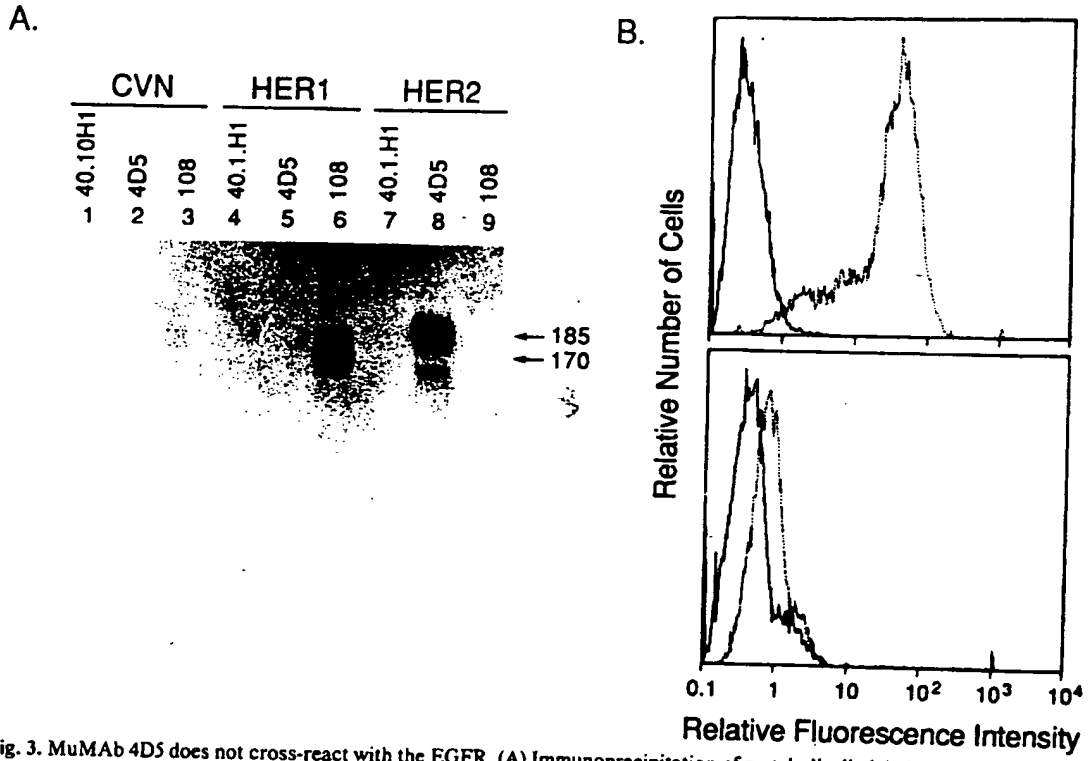

Fig. 3. MuMAb 4D5 does not cross-react with the EGFR. (A) Immunoprecipitation of metabolically labelelled NIH 3T3 cells transfected by control plasmid (CVN), by a plasmid encoding the EGFR (HER1) or a plasmid encoding $p185^{HER2}$ (HER2). MuMAb 40.1.H1 is directed against hepatitis B surface antigen (lanes 1, 4, 7); muMAb 4D5 is directed against $p185^{HER2}$ (lanes 2, 5, 8); muMAb 108 is directed against the EGFR (lanes 3, 6, 9). (B) Fluorescence-activated cell sorter histograms of muMAb 40.1.H1 (solid lines) or muMAb 4D5 (dotted lines) reacted with SK-BR-3 tumor cells (approx. 2×10^6 receptors per cell; upper panel) or the same antibodies reacted with the A431 squamous carcinoma cell line (approx. 2×10^6 EGFR per cell; lower panel).

distinct effects on tumor cell proliferation. The *in vitro* results summarized in Table III clearly show that when the monoclonal antibodies are compared for efficacy, as measured by their abilities to inhibit growth of breast and ovarian tumor cells overexpressing $p185^{HER2}$, muMAb 4D5 is usually the most potent and is therefore a good candidate for further characterization in other models that may be predictive of its efficacy in human clinical trials. Interestingly, the most dramatic activity of the antibody is seen in cell lines that overexpress greater than fivefold the level observed in MCF-7 breast tumor cell lines [a low expressor control cell line; Table III (19)]. Patients who overexpress greater than fivefold the normal level of $p185^{HER2}$ have been shown to have a very poor prognosis (10). These results will aid in choosing patients who are most likely to respond in clinical trials.

The model depicted in Fig. 1 predicts that downregulation of $p185^{HER2}$ by a monoclonal antibody or other reagent should result in decreased cellular proliferation, as shown in Table III, but also increased sensitivity to TNF-α. Results of experiments in which tumor cells overexpressing $p185^{HER2}$ were treated with muMAb 4D5 or a control monoclonal antibody, alone and in combination with TNF-α, suggest the validity of this model (Fig. 4) (31). MuMAb 4D5 treatment of breast tumor cells overexpressing $p185^{HER2}$ resulted in enhanced sensitivity of these cells to TNF-α. The growth and the TNF-α sensitivity of normal cells or tumor cells that do not overexpress the receptor were unaltered.

In addition to the relationship between TNF-α resistance and $p185^{HER2}$ overexpression, a possible relationship between protoncogene expression and resistance to the chemotherapeutic drug cisplatin has been investigated. A correlation between HER2 protooncogene overexpression and resistance to chemotherapeutic drugs rests on the grounds that

Table I. Summary Table of Monoclonal Antibodies Described

MAb	Isotype	ELISA[a]		RIP[b]		Epitope[c]	FACS[d]
		EGFR	p185^{HER2}	EGFR	p185^{HER2}		
4D5	IgG1,k	–	++	–	++	I(p/c)	+++
2C4	IgG1,k	–	+++	–	++	F(p/c)	+++
2H11	IgG2a,k	–	+	–	++	H(p/c)	++
3E8	IgG2a,k	–	+	–	+++	H(p/c)	+++
3H4	IgG1,k	–	+	–	+	I(p)	+
SB8	IgG1,k	–	+	–	++	nd(p)	+
6E9	IgG1,k	–	++	–	+	nd(p)	–
7C2	IgG1,k	–	++	–	++	G(p)	+++
7D3	IgG1,k	–	++	–	++	F(p/c)	+++
7F3	IgG1,k	–	+++	–	+++	G/F(p/c)	+++

[a]Summary of OD 492 nm: (–) <0.1; (+) 0.11–0.50; (++) 0.51–1.0; (+++) >1.0.
[b]Summary of autoradiography from immunoprecipitations: (–) bands equal to negative control; (+) weak bands but darker than negative control; (++) moderately exposed bands; (+++) strongly exposed bands.
[c]Letters were assigned to represent individual epitopes A through I (nd, not done). MAbs were considered to share an epitope if each blocked binding of the other by 50% or greater in comparison to an irrelevant MAb control. The epitope composition recognized by immunoprecipitations with each MAb from tunicamycin-treated cells is shown. The letters p, c, or p/c in parentheses indicate that the monoclonal antibody binds only to the polypeptide (p), the carbohydrate (c), or both (p/c) moieties in the extracellular domain of p185^{HER2}.
[d]Fluorescence staining of SK-BR-3 cells by the anti-p185^{HER2} monoclonal antibodies: (–) MAbs equal to the negative control MAbs; (+) 1- to 9-fold higher than the negative controls; (++) 10- to 99-fold higher than the negative controls; (+++) >100-fold higher than the negative controls.

patients exhibiting overexpression appear to have a worsened prognosis, especially in ovarian cancer (10, 13). In addition, recent work with the EGF receptor (32) has indicated that when the anti-EGFR monoclonal antibody 108.4 was added together with cisplatin, the antitumor effect of the antibody was greatly enhanced. Because the 108.4 monoclonal antibody and muMAb 4D5 appear to share the ability to inhibit soft agar growth of tumor cells overexpressing their respective receptors, it seemed possible that such an interaction may also occur in the HER2 protooncogene system. The *in vitro* results (Fig. 5) show that treatment of SK-BR-3 breast tumor cells with muMAb 4D5 enhances their sensitivity to cisplatin.

Table II. Inhibition of SK-BR-3 Proliferation by Anti-p185^{HER2} Monoclonal Antibodies[a]

Monoclonal antibody	Relative cell proliferation[b]
4D5	44.2 ± 4.4
7C2	79.3 ± 2.2
2C4	79.5 ± 4.4
7D3	83.8 ± 5.9
3E8	66.2 ± 2.4
6E9	98.9 ± 3.6
7F3	62.1 ± 1.4
3H4	66.5 ± 3.9
2H11	92.9 ± 4.8
40.1 H1[c]	105.8 ± 3.8
4F4	94.7 ± 2.8

[a]SK-BR-3 breast tumor cells were plated at a density of 4 × 10^4 cells per well into 96-well microdilution plates, allowed to adhere, and then treated with monoclonal antibody (10 μg/ml).
[b]Relative cell proliferation was determined by crystal violet staining of the monolayers after 72hr. Values are expressed as a percentage of results with untreated control cultures (100%).
[c]Control monoclonal antibodies 40.1H1 and 4F4 are directed against hepatitis B surface antigen and human interferon-γ, respectively (27).

IN VIVO PRECLINICAL EFFICACY

A critical part of the rationale supporting the application of muMAb 4D5 to human cancer therapy is its ability to inhibit the growth of tumor cells overexpressing p185^{HER2} *in vivo*. A human tumor xenograft model was used to test this property of muMAb 4D5 and to compare its activities with those of the other monoclonal antibodies in a relevant model of human disease. In this model, a human breast tumor, characterized with respect to HER2 protooncogene amplification and expression, was grafted into the subrenal capsules of nude mice. Therapy was initiated 1 week postimplantation. In order to be active in this model, the monoclonal antibody must be able to localize to the overexpressing tumor cells in the lesion and subsequently exert a growth regulatory effect mediated through p185^{HER2}. Growth inhibition occurs only with tumors that overexpress the receptor. Heterotransplants (approximately 1 mg) of Murray breast tumor [a high expresser of the HER2 gene product (10)] were implanted into the subrenal capsule of 48

Table III. Inhibition of Human Breast and Ovarian Tumor Cell Growth by Monoclonal Antibodies Directed Against the Extracellular Domain of $p185^{HER2}$

Cell line	Relative $p185^{HER2}$ expression[a]	Cell proliferation (% control)[b]					
		4D5[c]	3H4[c]	2C4[d]	7F3[d]	7C2[e]	6E9[f]
MCF7	1	94	101	101	97	106	110
ZR-75-1	3	106	113	104	100	149	113
MDA-MB-175	4	61	84	24	48	87	103
MDA-MB-453	7	62	68	91	84	78	101
MDA-MB-361	17	60	68	65	73	113	113
BT474	20	23	25	53	20	74	94
SK-BR-3	33	42	56	66	64	92	105
SK-OV-3	17	77	85	87	91	97	99

[a]Based on FACS assay using muMAb 4D5 and fluorescence-labeled goat anti-murine IgG1 polyclonal antibody.
[b]Five-day assay with 10 μg/ml of indicated monoclonal antibody (SE, ~10%). Other methods as described in the footnotes to Table II.
[c]4D5 and 3H4 define epitope "I."
[d]2C4 and 7F3 will partially block one another, 2C4 is assigned epitope "F," and 7F3 is assigned epitope "F/G."
[e]7C2 defines epitope "G" and will partially block 7F3 binding.
[f]6E9 epitope determination not done.

athymic mice on day 0. Groups of eight animals were injected intravenously with tissue culture-derived muMAb 4D5 (36.4 mg/kg), PBS, or control monoclonal antibody, muMAb 5B6 (directed against gp120; 36.4 mg/kg), as single agents in equally divided doses on days 7, 10, and 13. Four mice from each group were sacrificed on day 20, and the remainder of the animals were sacrificed on day 34. Tumor sizes were measured using ocular micrometer and gravimetric techniques. A summary of the tumor weights (mean ± SD) from animals sacrificed on days 20 and 34 is shown in Table IV. On day 20, average tumor weights of animals receiving muMAb 4D5 were significantly less than those receiving the same dose of the control antibody muMAb 5B6. Interactive effects between muMAb 4D5 and cisplatin have also been observed in this model (33). These studies in athymic mice bearing human breast tumor xenografts have demonstrated efficacy and suggested an enhanced effect when muMAb 4D5 is given in combination with cisplatin.

MECHANISM OF ACTION

The results described above are consistent with muMAb 4D5 having receptor antagonist activity. Surprisingly, however, muMAb 4D5 treatment of SK-BR3 tumor cells stimulates receptor tyrosine kinase activity (Table V) (30, 34). In addition, it can mediate the phosphorylation of intracellular substrates by $p185^{HER2}$ (34). Consistent with its ability to stimulate receptor activity, muMAb 4D5 treatment of SK-BR-3 or SK-OV-3 tumor cells results in a modulation of intracellular second messengers, including diacylglycerol. Diacylglycerol (DAG) is a product of phospholipase C breakdown of phosphatidylinositol-4,5-bisphosphate. It is a cofactor

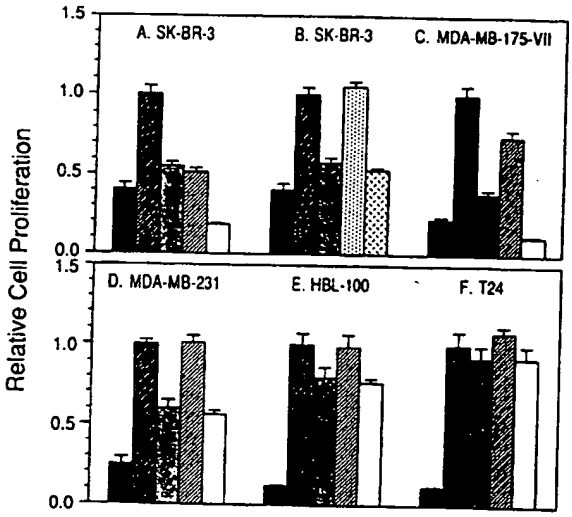

Fig. 4. Monoclonal antibody 4D5 sensitizes breast tumor cells to the cytotoxic effects of TNF-α. Filled bars, cell number at initiation of the assay; dark cross-hatching, untreated control; dark stipples, TNF-α alone; light cross-hatching, MuMAb 4D5; open bars, MuMAb 4D5 combined with TNF-α. (B) Lack of growth inhibition of SK-BR3 tumor cells by muMAb 40.1 H1 (anti-hepatitis B antigen; light stipples) and failure of the 40.1 H 1 to enhance SK-BR-3 tumor cell sensitivity to TNF-α (broken cross-hatching). SK-BR-3 and MDA-MB-175-VII overexpress p185HER2 (see Table III). MDA-MB-231 and HBL-100 are breast cell lines which do not overexpress $p185^{HER2}$, and T24 is a nonoverexpressing human bladder carcinoma cell line. The assay was performed as described in Ref. 31.

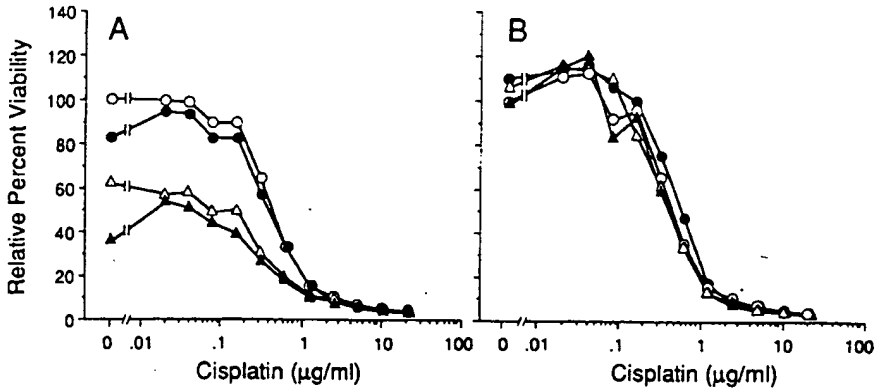

Fig. 5. Treatment of SK-BR-3 breast tumor cells with muMAb 4D5 enhances sensitivity to cisplatin. MuMAb 4D5 (A) or muMAb 6E9 (control; B) and cisplatin were added at the indicated concentrations to SK-BR-3 breast tumor cells. The plate cultures were incubated for 3 days and relative cell proliferation was determined as described (31). No antibody (○); 0.156 μg/ml muMAb 4D5 or muMAb 6E9 (●); 0.625 μg/ml muMAb 4D5 or muMAb 6E9 (△); 2.5 μg/ml muMAb 4D5 or muMAb 6E9 (▲).

for activation of protein kinase C and has been closely associated with growth factor activity (35). As may be predicted from its effect on cell proliferation, muMAb 4D5 treatment of SK-BR-3 tumor cells results in downregulation of intracellular pools of DAG (Table VI) (30). This result is consistent with overall antagonist activity, as is inhibition of tumor cell proliferation. Other data suggest that muMAb 4D5 may inhibit association of ligand with the receptor (25). Similar monoclonal antibodies have been reported for the EGFR system (26, 28). Further work is under way to characterize the ligand(s) that binds $p185^{HER2}$ and the mechanism of action of muMAb 4D5.

While the ability of muMAb 4D5 to stimulate phosphorylation of $p185^{HER2}$ is consistent with an agonist of receptor function, it is important to note that our current data suggest that it does not behave as an agonist in our cell growth assays *in vitro* or in nude mice. The results of an experiment that compares the effects of muMAb 4D5 on the growth of MCF-7 and SK-BR-3 breast tumor cells are shown in Fig. 6. These data demonstrate that muMAb 4D5 has no effect on the growth of nonoverexpressing tumor cells (MCF-7; Tables III, VII) at any of the doses tested between 0.7 p*M* and 67 n*M*. Also, whatever allows the muMAb 4D5 to have differential effects on overexpressing tumor cells, this difference does not lie in different receptor affinities for the monoclonal antibody. Table VII clearly shows that SK-BR-3 and SK-OV-3, both $p185^{HER2}$ overexpressors, which are growth inhibited by 4D5, and MCF-7, which is not, all have similar affinities for muMAb 4D5. The clearest difference between these cell lines is the number of binding sites per tumor cell. These data are consistent with other work that has been previously reported with tumor cells in monolayer culture or in soft agar (18, 19, 25).

A possible mechanistic explanation, which takes many of our experimental observations into account, is a model in which muMAb 4D5 binds

Table IV. MuMAb 4D5 Inhibits the Growth of a Human Breast Tumor (Murray) in Athymic Mice[a]

Group (n = 4)	Tumor weight (mg)[b]	
	Day 20	Day 34
PBS	6.79 ± 9.79	36.0 ± 30.7
Control IgG (muMAb5B6)	7.11 ± 5.48	88.1 ± 91.4
muMAb4D5	1.48 ± 1.10	6.5 ± 6.4

[a]Administered as equally-divided intravenous doses on days 7, 10, and 13 post tumor implantation.
[b]Data are mean ± standard deviation (SD) (n = 4).

Table V. Effect of muMAb 4D5 on Phosphoamino Acid Content of $p185^{HER2}$ in SK-BR-3 Cells

Treatment	Phospho-tyrosine		Phospho-serine		Phospho-threonine	
	cpm[a]	%[b]	cpm	%	cpm	%
None	11	1.5	564	75	176	23.5
muMAb4D5	827	14.0	3,658	62.0	1,429	24.0

[a]Phosphoamino acids as cpm are expressed following background subtraction (17 cpm for none, 21 cpm for muMAb 4D5).
[b]Percentage of total phosphoamino acids.

Table VI. Effect of muMAb 4D5 or 6E9 Monoclonal Antibodies on *sn*-1,2-diacylglycerol levels in SK-BR-3 Cells

Time	Treatment	pmol *sn*-1,2-DAG/10^6 cells	% change
5 min	Vehicle	111.0 ± 10	0
5 min	muMAb4D5	133.2 ± 11.3	+20
5 min	muMAb6E9	133.3 ± 12.9	+20
24 hr	Vehicle	98.6 ± 9.6	0
24 hr	muMAb4D5	62.1 ± 7.4	−37
24 hr	muMAb6E9	92.0 ± 12.7	−7

[a]Following incubation with monoclonal antibody (33 n*M*) or vehicle (PBS) control, the reactions were terminated by aspirating the media and adding 1 ml of ice-cold 100% MeOH. Cells were scraped from the plates and transferred to 13 × 100-mm glass tubes containing 1 ml 100% chloroform. Plates were rinsed with an additional 1 ml of cold methanol, and the rinses combined and mixed thoroughly. Following phase separation at room temperature for 30 min, 1 ml methanol and 1 ml NaCl were added, the samples were centrifuged at 3000 rpm for 5 min, and the top aqueous layer was aspirated. The remaining organic phase was assayed for *sn*-1,2-diacylglycerol by standard procedures.

tightly to $p185^{HER2}$, excludes ligand binding, stimulates receptor internalization, and downregulates receptor signaling pathways as a result of constitutive activation of tyrosine kinase activity that results from nondissociation of the muMAB 4D5/$p185^{HER2}$ complex during receptor cycling. This hypothesis has additional support from our observations that the monoclonal antibody is not degraded following internalization (30) and, in the nude mouse experiments, localizes to and remains at the tumor site for more than 7 days following a single administration of antibody (D.M., personal communication). Such downregulation could result from activation of the serine–threonine protein kinase C, which is known to downregulate the function of other receptor tyrosine kinases (5). The mechanism of action of muMAb 4D5 remains a subject for continuing work.

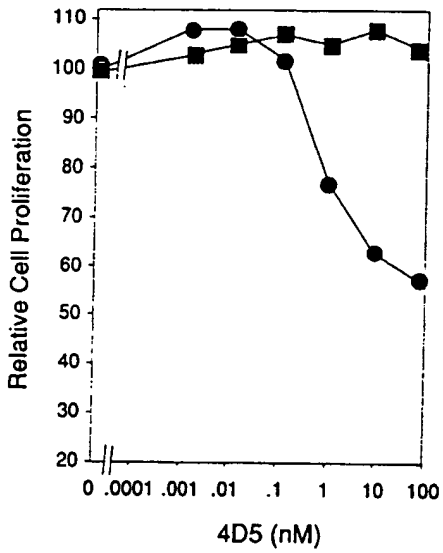

Fig. 6. MuMAb 4D5 does not stimulate proliferation of breast tumor cells. Cells were plated and the assay performed as described (31). MCF-7 breast tumor cells (squares) are compared with the SK-BR-3 tumor cell line (circles). MCF-7 expresses a low amount of $p185^{HER2}$, while SK-BR-3 expresses about 33-fold more (Table III). Coefficient of variation was less than 10%.

Table VII. Monoclonal Antibody Binding to Cultured Human Adenocarcinoma Cells

Cell line	Antibody	K_d (n*M*)	Receptor no. (sites/cell)	Growth inhibition[a]
SK-BR-3	muMAb4D5	6.0	926,650	—*
SK-OV-3	muMAb4D5	5.0	428,930	—*
MCF7	muMAb4D5	1.2	5,525	–

[a]Growth inhibition was measured as described in the footnotes to Table II.
*Statistically significant inhibition of growth ($P<0.05$) as compared to an untreated control.

SUMMARY AND CONCLUSIONS

A convincing body of clinical and experimental evidence supports the role of $p185^{HER2}$ in the progression of human cancers characterized by the overexpression of this protooncogene product. Important aspects of this evidence include the worsened prognosis of breast, ovarian, and non-small cell lung carcinoma patients whose tumors overexpress $p185^{HER2}$, as well as observations that indicate that modulation of $p185^{HER2}$ activity by muMAb 4D5 can reverse many of the properties associated with tumor progression mediated by a growth factor receptor. The properties of muMAb 4D5 that indicate its potential usefulness for the therapy of human cancers characterized by the overexpression of $p185^{HER2}$ are as follows: (i) downregulation of receptors from the cell surface (30); (ii) reversal of the transformed phenotype [as measured by inhibition of colony formation in soft agar of $p185^{HER2}$ overexpressing tumor cells (25, 31)]; (iii) inhibition of the proliferation of overexpressing breast and ovarian tumor cells in monolayer culture (Tables II, III); (iv) reversal of the TNF-α resistant phenotype of breast tumor cells overexpressing $p185^{HER2}$ (Fig. 4) (31); (v) enhancement of the sensitivity to cisplatin of the SK-BR-3 breast tumor cell line *in vitro* (Fig. 5); and (vi)

inhibition of the growth of breast tumor xenografts in a nude mouse model, which may be enhanced when the animals bearing human breast xenografts are also treated with cisplatin (Tables IV, V).

The evidence supporting a role for $p185^{HER2}$ overexpression in human cancer makes this receptor an attractive target for development of cancer therapeutics. Our first exploration of this system with muMAb 4D5 will allow us to obtain information regarding antibody localization and possibly efficacy in combination with cisplatin or as a result of induction of macrophage sensitivity. The muMAb 4D5 also serves as a template for antibody engineering efforts to construct humanized versions more suitable for chronic therapy or other molecules which may be directly cytotoxic for tumor cells overexpressing the HER2 protooncogene.

REFERENCES

1. Bishop JM: The molecular genetics of cancer. Science 235:305–311, 1987
2. Rhim JS: Viruses, oncogenes, and cancer. Cancer Detect Prev 11:139–149, 1988
3. Nowell PC: Mechanisms of tumor progression. Cancer Res 46:2203–2207, 1986
4. Nicolson GL: Tumor cell instability, diversification, and progression to the metastatic phenotype: From oncogene to oncofetal expression. Cancer Res 47:1473–1487, 1987
5. Yarden Y, Ullrich AL: Growth factor receptor tyrosine kinases. Annu Rev Biochem 57:443–478, 1988
6. Padhy L, Shih C, Cowing D, Finkelstein R, Weinberg RA: Identification of a phosphoprotein specifically induced by the transforming DNA of rat neuroblastomas. Cell 28:865–871, 1982
7. Schechter AL, Stern DF, Vaidyanatha L, Decker SJ, Drebin JA, Greene MI, Weinberg RA: The neu oncogene: An erb-B related gene encoding a 185,000-M_r tumour antigen. Nature 312:513–516, 1984
8. Bargmann CI, Hung MC, Weinberg RA: Multiple independent activations of the *neu* oncogene by a point mutation altering the transmembrane domain of p185. Cell 45:649–657, 1986
9. Slamon DJ, Clark GM, Wong SG, Levin WJ, Ullrich A, McGuire WL: Human breast cancer: Correlation of relapse and survival with amplification of the HER2/*neu* oncogene. Science 235:177–182, 1987
10. Slamon DJ, Godolphin W, Jones LA, Holt JA, Wong SG, Keith DE, Levin WJ, Stuart SG, Udove J, Ullrich A, Press M: Studies of the HER2/*neu* proto-oncogene in human breast and ovarian cancer. Science 244:707–712, 1989
11. Wright C, Angus B, Nicholson S, Sainsbury JRC, Cairns J, Gullick WJ, Kelley P, Harris AL, Horne CHW: Expression of cerbB-2 oncoprotein: A prognostic indicator in human breast cancer. Cancer Res 49:2087–2090, 1989
12. Paik S, Hazan R, Fisher ER, Sass RE, Fisher B, Redmond C, Schlessinger J, Lippman ME, King CR: Pathologic findings from the national surgical adjuvant breast and bowel project: Prognostic significance of erbB-2 protein overexpression in primary breast cancer. J Clin Oncol 8:103–112, 1990
13. Berchuck A, Kamel A, Whitaker R, Kerns B, Olt G, Kinney R, Soper JT, Dodge R, Clarke-Pearson DL, Marks P, McKenzie S, Yin S, Bast RC: Overexpression of HER2/*neu* is associated with poor survival in advanced epithelial ovarian cancer. Cancer Res 50:4087–4091, 1990
14. Kern JA, Schwartz DA, Nordberg JE, Weiner DB, Greene MI, Torney L, Robinson RA: $p185^{neu}$ expression in human lung adenocarcinomas predicts shortened survival. Cancer Res 50:5184–5191, 1990
15. Schlom J, Hand PH, Greiner JW, Colcher D, Shrivastav S, Carrasquillo JA, Reynolds JC, Larso SM, Raubitschek, A: Innovations that influence the pharmacology of monoclonal antibody guided tumor targeting. Cancer Res 50:820–827, 1990
16. Szala S, Froehlich M, Scollon M, Kasai Y, Steplewski Z, Koprowski H, Linnenbach AJ: Molecular cloning of cDNA for the carcinoma-associated antigen GA733-2. Proc Natl Acad Sci 87:3542–3546
17. Di Fiore PP, Pierce JH, Kraus MH, Segatto O, King CR, Aaronson, SA: erbB-2 is a potent oncogene when overexpressed in NIH/3T3 cells. Science 237:178–182, 1987
18. Hudziak RM, Schlessinger J, Ullrich A: Increased expression of the putative growth factor receptor p185HER2 causes transformation and tumorigenesis of NIH 3T3 cells. Proc Natl Acad Sci USA 84:7159–7163, 1987
19. Hudziak RM, Lewis GD, Shalaby MR, Eessalu TE, Aggarwal BB, Ullrich A, Shepard HM: Amplified expression of the HER2/ErbB2 oncogene induces resistance to tumor necrosis factor-α in NIH3T3 cells. Proc Natl Acad Sci USA 85:5102–5106, 1988
20. Urban JL, Shepard HM, Rothstein JL, Sugarman BJ, Schreiber H: Tumor necrosis factor: A potent effector molecule for tumor cell killing by activated macrophages. Proc Natl Acad Sci USA 83:5233–5237, 1986
21. Shepard HM, Lewis GD: Resistance of tumor cells to tumor necrosis factor. J Clin Immunol 8:1–9, 1988
22. Lichtenstein A, Berenson J, Gera JF, Waldburger K, Martiniz-Maza D, Berek JS: Resistance of human ovarian cancer cells to tumor necrosis factor and lymphokine-activated killer cells: Correlation with expression of HER2/*neu* oncogenes. Cancer Res 50:7364–7370, 1990
23. Muller WJ, Sin E, Pattengale PK, Wallace R, Leder P: Single-step induction of mammary adenocarcinoma in transgenic mice bearing the activated c-*neu* oncogene. Cell 54:105–115, 1988
24. Suda Y, Aizawa S, Furuta Y, Yagi T, Ikawa Y, Saitoh K, Yamada Y, Toyoshima K, Yamamoto T: Induction of a variety of tumors by c-erbB2 and clonal nature of lymphomas even with the mutated gene (Val^{659} Glu^{659}). EMBO J 9:181–190, 1990
25. Lupu R, Colomer R, Zugmaier G, Sarup J, Shepard M, Slamo D, Lippman ME: Direct intraction of a ligand for the erbB2 oncogene product with the EGF receptor and $p185^{erbB2}$. Science 249:1552–1555, 1990
26. Gill GN, Kawamoto T, Cochet C, Le A, Sato JD, Masui H, MacLeod C, Mendelsohn J: Monoclonal anti-epidermal growth factor receptor antibodies which are inhibitors of epidermal growth binding and antagonists of epidermal growth factor-stimulated tyrosine protein kinase activity. J Biol Chem 259:7755–7760, 1984

27. Drebin JA, Link VC, Stern DF, Weinberg RA, Greene MI: Down-modulation of an oncogene protein product and reversion of the transformed phenotype by monoclonal antibodies. Cell 41:695–706, 1985
28. Fendly BM, Winget M, Hudziak RM, Lipari MT, Napier MA, Ullrich A: Characterization of murine monoclonal antibodies reactive to either the human epidermal growth factor receptor or HER2/neu gene product. Cancer Res 50:1550–1558, 1990
29. Mendelsohn J: Anti-EGF receptor monoclonal antibodies: Biological studies and potential clinical applications. Trans Am Clin Climatol Assoc 100:31–38, 1988
30. Sarup JC, Johnson RM, King KL, Fendly BM, Lipari MT, Napier MA, Shepard HM: Growth regulation, 1991, in press
31. Hudziak RM, Lewis GD, Winget M, Fendly BM, Shepard HM, Ullrich A: p185HER2 monoclonal antibody has antiproliferative effects *in vitro* and sensitizes human breast tumor cells to tumor necrosis factor. Mol Cell Biol 9:1165–1172; 1989
32. Aboud-Pirak E, Hurwitz E, Pirak ME, Bellot F, Schlessinger J, Sela M: Efficacy of antibodies to epidermal growth factor receptor against KB carcinoma *in vitro* and in nude mice. J Natl Cancer Inst 80:1605–1611, 1988
33. Slamon D: Personal communication
34. Scott GK, Dodson JM, Johnson RM, Sarup JC, Fendly BM, Worig WL, Shepard HM, Benz CC: Manuscript in preparation
35. Ullrich A, Schlessinger J: Signal transduction by receptors with tyrosine kinase activity. Cell 61:203–212, 1990

EXHIBIT F

FIGURE 1

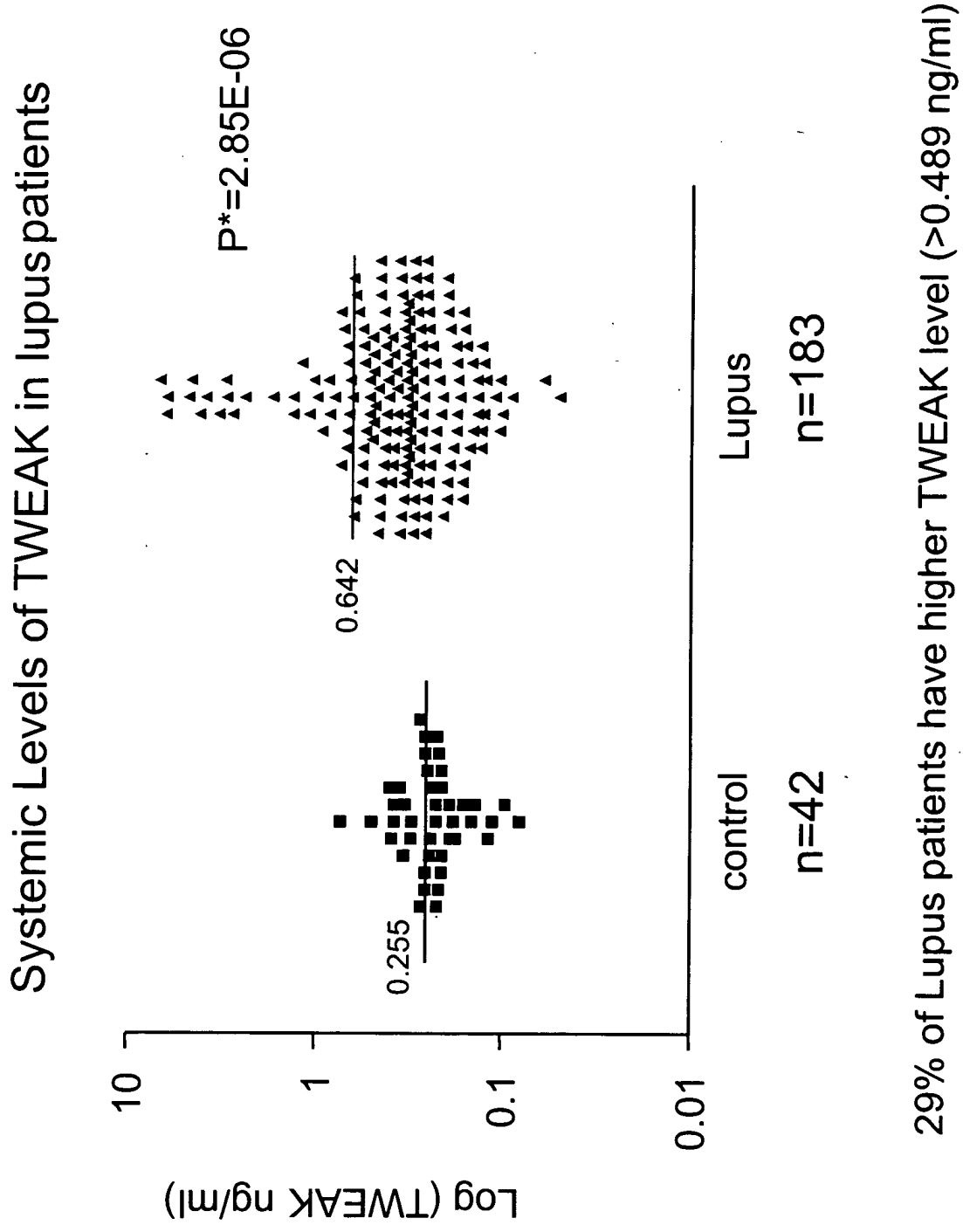
Systemic Levels of TWEAK in lupus patients
P*=2.85E-06
0.642
0.255
10
1
0.1
0.01
Log (TWEAK ng/ml)
control
Lupus
n=42
n=183
29% of Lupus patients have higher TWEAK level (>0.489 ng/ml)

EXHIBIT G

ARTHRITIS & RHEUMATISM
Vol. 43, No. 12, December 2000, pp 2648–2659

COMBINATION BENEFIT OF TREATMENT WITH THE CYTOKINE INHIBITORS INTERLEUKIN-1 RECEPTOR ANTAGONIST AND PEGylated SOLUBLE TUMOR NECROSIS FACTOR RECEPTOR TYPE I IN ANIMAL MODELS OF RHEUMATOID ARTHRITIS

ALISON M. BENDELE, ELIZABETH S. CHLIPALA, JON SCHERRER, JANET FRAZIER, GINA SENNELLO, WILLIAM J. RICH, and CARL K. EDWARDS, III

Objective. **To determine the potential for additive or synergistic effects of combination therapy with the recombinant anticytokine agents interleukin-1 receptor antagonist (IL-1Ra) and PEGylated soluble tumor necrosis factor receptor type I (PEG sTNFRI) in established type II collagen–induced arthritis (CIA) and developing adjuvant-induced arthritis (AIA) in rats.**

Methods. **Rats with established CIA or developing AIA were treated with various doses of IL-1Ra in a slow-release hyaluronic acid vehicle or with PEG sTNFRI, either alone or in combination with the IL-1Ra. The effects of treatment were monitored by sequential caliper measurements of the ankle joints or hind paw volumes, final paw weights, and histologic evaluation with particular emphasis on bone and cartilage lesions.**

Results. **Combination therapy with IL-1Ra and PEG sTNFRI in rats with CIA resulted in an additive effect on clinical and histologic parameters when moderately to highly efficacious doses of each protein were administered. Greater-than-additive effects were seen when an inactive dose of IL-1Ra was given in combination with moderately to minimally active doses of PEG sTNFRI. Plasma levels associated with the latter effect (for both proteins) were similar to those seen in rheumatoid arthritis (RA) patients in clinical trials with these agents. Combination therapy in the AIA model generally resulted in additive effects, but some parameters showed a greater-than-additive benefit.**

Conclusion. **The results provide preclinical support for the hypothesis that IL-1Ra administered in combination with PEG sTNFRI might provide substantially more clinical benefit to RA patients than either agent alone at blood levels that are currently achievable in patients.**

Rheumatoid arthritis (RA) is a chronic disease characterized by inflammation of the joints with concomitant destruction of cartilage and bone. The involvement of cytokines, particularly interleukin-1 (IL-1) and tumor necrosis factor α (TNFα), in the pathogenesis of RA is now well accepted as a result of numerous studies in animal models as well as in humans with the disease (1–11). The IL-1 receptor antagonist (IL-1Ra) is a specific receptor antagonist that competitively inhibits the binding of IL-1β and IL-1α to human and animal types I and II IL-1 receptors (12). Several clinical trials have been completed in which IL-1Ra has been administered long term to patients with RA (13,14). The results indicate that treatment with IL-1Ra lowers the levels of acute-phase proteins and the counts of swollen joints and may inhibit radiographic progression of disease (14,15). This protein has proved efficacious in various animal models of arthritis, both alone (10,11) and in combination with methotrexate (16), where the potential for additive effects was demonstrated.

Treatment with soluble TNF receptors (sTNFR) and antibodies to TNF has been shown to be clinically efficacious in RA patients (17–21). Animal models of arthritis in which these agents were evaluated predicted the excellent clinical response in humans (22–27). Several animal studies have focused on the efficacy of the high-affinity, monomeric PEGylated type I TNFR (PEG

Alison M. Bendele, DVM, PhD, Elizabeth S. Chlipala, BS, Gina Sennello, BS (current address for Dr. Bendele, Ms Chlipala, and Ms Sennello: BolderPath, Inc., University of Colorado, Boulder): Amgen Colorado, Boulder; Jon Scherrer, BS, Janet Frazier, BS, William J. Rich, MS, Carl K. Edwards, III, PhD: Amgen Inc., Thousand Oaks, California.

Address reprint requests to Carl K. Edwards, III, PhD, Amgen, Inc., One Amgen Center Drive, Thousand Oaks, CA 91320-1799.

Submitted for publication February 16, 2000; accepted in revised form July 28, 2000.

TNFRI) administered alone (28) or in combination with other agents, such as methotrexate, dexamethasone, and indomethacin (29,30), where the potential for additive or synergistic effects was shown.

The purpose of the present study was to determine the potential benefit of combination treatment with the specific cytokine inhibitors IL-1Ra and PEG sTNFRI when given at dosages designed to achieve clinically relevant blood levels in order to support the clinical investigation of this approach.

MATERIALS AND METHODS

Animals. Female and male Lewis rats (175–225 gm; Charles River, Portage, MI) were used in these studies. Animals were allowed to acclimate for at least 7 days prior to initiation of experiments. Rats were housed in polycarbonate cages (2–4 per cage) and were allowed ad libitum access to food and water. All animal use was in accordance with the United States Department of Agriculture guidelines for humane care.

Materials. Recombinant IL-1Ra in hyaluronic acid (HA; 20 or 100 mg/ml) (10) and PEG recombinant sTNFRI (3, 1, or 0.3 mg/ml) (31) were produced at Amgen (Thousand Oaks, CA). Freund's complete adjuvant and Freund's incomplete adjuvant were obtained from Sigma (St. Louis, MO) and Difco (Detroit, MI), respectively. The synthetic adjuvant *N,N*-dioctylddecyl-*N',N-bis*(2-hydroxyethyl)propanediamine (LA) was from BolderPath (Boulder, CO). Type II collagen was purchased from Elastin Products (Owensville, MO).

Induction and treatment of collagen-induced arthritis (CIA) and evaluation of clinical effects. Female rats (8 per group) were given intradermal/subcutaneous (SC) injections of bovine type II collagen (2 mg/ml in Freund's incomplete adjuvant) at a single site at the base of the tail and over the back at 2 sites (250 μl in divided doses) on day 0 and day 7. Arthritis onset occurred on days 12, 13, and 14; as rats developed disease, they were randomized to study groups. Treatment was initiated on the first day that clinical signs of arthritis were clearly visible, as evidenced by ankle joint swelling.

IL-1Ra in the sustained-release delivery system of HA and PEG sTNFRI in phosphate buffered saline (PBS) vehicle were given alone and in combination. Treatment with IL-1Ra (100 or 20 mg/kg) in HA was administered SC beginning on day 1 of arthritis and continuing through day 6. Treatment with PEG sTNFRI (3, 1, or 0.3 mg/kg) was given intraperitoneally (IP) in PBS on days 1, 3, and 5 of clinical arthritis. Vehicle-treated control rats were given HA (SC on days 1–6) or PBS (IP on days 1, 3, and 5).

Caliper measurements of ankle joint diameter were made prior to the onset of arthritis, on the day of randomization (day 1 of arthritis), and on each subsequent study day until termination of the study on day 7 of arthritis. At termination, the tibiotarsal joint was transected at the level of the medial and lateral malleolus for determination of paw weights as another measure of inflammation. Hind paws and knee joints were then collected into formalin for histopathologic evaluation.

Induction and treatment of adjuvant-induced arthritis (AIA) and evaluation of clinical effects. Male rats (5–7 per group) were given a single SC (base of tail) injection of 100 μl of Freund's complete adjuvant to which 5 mg/ml of LA had been added. In this model, systemic inflammatory disease occurs in various tissues, including the spleen and liver, as well as in most joints (32–34).

IL-1Ra in the sustained release delivery system of HA and PEG sTNFRI in PBS were given alone and in combination. Treatment with IL-1Ra (100 mg/kg) in HA was administered SC beginning on day 8 post–adjuvant injection and continuing through day 13. Treatment with PEG sTNFRI (3 or 1 mg/kg) in PBS was given IP on days 9, 11, and 13.

Caliper measurements of ankle joint width were made prior to the onset of arthritis, and then every other day until the study was terminated on day 15 post–adjuvant injection. Hind paw volumes and body weights were measured on days 9, 11, 12, 14, and 15. At termination, the tibiotarsal joint was transected at the level of the medial and lateral malleolus for determination of paw weights as another measure of inflammation. Spleen and liver were trimmed of extraneous tissue and weighed. The hind paws and spleen were then collected into formalin for histopathologic evaluation.

Histopathology. Ankle joints (CIA and AIA) and knee joints (CIA only) were collected into 10% neutral buffered formalin and maintained for at least 24 hours prior to placement in SurgiPath Decalcifier I solution (Grayslake, IL) for ~1 week. When decalcification was complete, the digits were trimmed, and the ankle joint was transected in the longitudinal plane to give 2 approximately equal portions. Knee joints were transected in the frontal plane to give 2 approximately equal portions. These were processed for paraffin embedding, sectioned, and stained with hematoxylin and eosin for general evaluation and with toluidine blue for specific evaluation of cartilage changes. Multiple sections were prepared to ensure that the distal tibia was present with both cortices and that abundant distal tibial medullary space was available for evaluation.

Ankles from rats with AIA were scored for inflammation and bone resorption according to the following criteria (0–5 scales) (34). For bone resorption, scores were 0 = normal, 1 = minimal—small areas of resorption in distal tibial trabecular or cortical bone, not readily apparent on low magnification, rare osteoclasts, 2 = mild—more numerous areas of resorption in distal tibial trabecular or cortical bone, not readily apparent on low magnification, osteoclasts more numerous, 3 = moderate—obvious resorption of medullary trabecular and cortical bone without full-thickness defects in the cortex, loss of some medullary trabeculae, lesion apparent on low magnification, osteoclasts more numerous, 4 = marked—full-thickness defects in cortical bone, often with distortion of profile of the remaining cortical surface, marked loss of medullary bone of the distal tibia, numerous osteoclasts, no resorption in smaller tarsal bones, and 5 = severe—full-thickness defects in cortical bone, often with distortion of profile of the remaining cortical surface, marked loss of medullary bone of the distal tibia, numerous osteoclasts, resorption also present in smaller tarsal bones.

For inflammation, scores were 0 = normal, 1 =

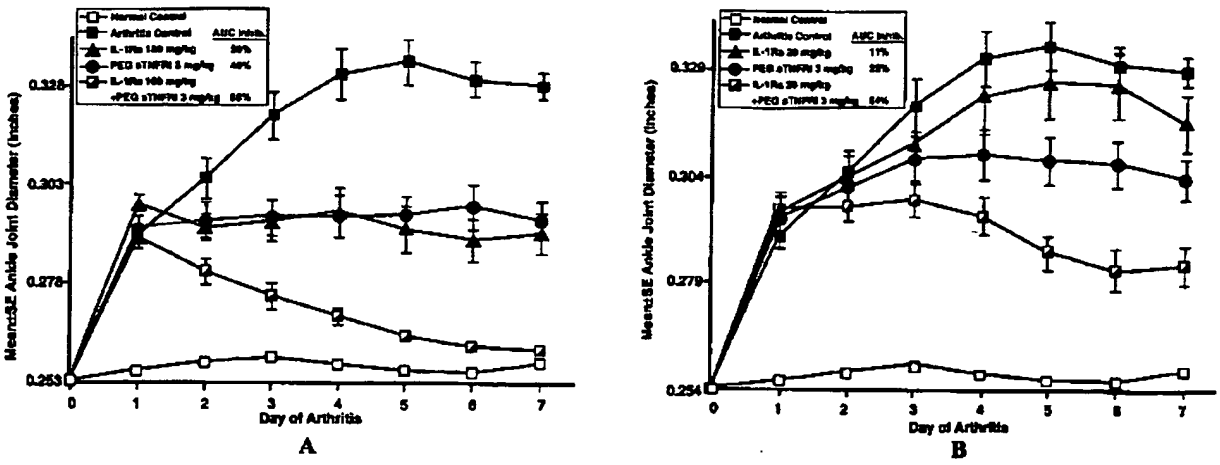

Figure 1. Changes in ankle joint diameter over time in rats with type II collagen–induced arthritis. A, Rats were treated with vehicles alone (hyaluronic acid [HA] for interleukin-1 receptor antagonist [IL-1Ra] subcutaneously [SC] every day and phosphate buffered saline for PEGylated soluble tumor necrosis factor α receptor type I [PEG sTNFRI] intraperitoneally [IP] every other day), with 100 mg/kg of IL-1Ra SC every day and vehicle IP every other day, with 3 mg/kg of PEG sTNF-RI IP every other day and HA SC every day, or with IL-1Ra and PEG sTNFRI in combination. The combination therapy produced additive benefits for ankle swelling, with the final measurements being similar to those of normal rats. B, Rats were treated with vehicles alone, with 20 mg/kg of IL-1Ra SC every day and vehicle IP every other day, with 0.3 mg/kg of PEG sTNFRI IP every other day and HA SC every day, or with the combination of IL-1Ra and PEG sTNFRI. Combination therapy produced additive benefits on ankle joint swelling over time. AUC = area under the curve; Inhib = inhibition; n = 8 rats per group.

minimal infiltration of inflammatory cells in periarticular tissue, 2 = mild infiltration, 3 = moderate infiltration with moderate edema, 4 = marked infiltration with marked edema, and 5 = severe infiltration with severe edema.

Cartilage damage was not scored in the AIA model because we have generally found this to be a minor feature and therefore not reliable for evaluation of potential treatment effects.

Histopathologic scoring for the tibiotarsal and knee joints of rats with CIA was similar to the inflammation and bone resorption scoring system used for rats with AIA. In addition, cartilage damage and pannus were scored because of the nature of the pathology in the CIA model. Cartilage damage was scored according to the following criteria (0–5 scale): 0 = normal, 1 = minimal-to-mild loss of toluidine blue staining with no obvious chondrocyte loss or collagen disruption, 2 = mild loss of toluidine blue staining with focal mild (superficial) chondrocyte loss and/or collagen disruption, 3 = moderate loss of toluidine blue staining with multifocal moderate (to middle-zone depth) chondrocyte loss and/or collagen disruption, 4 = marked loss of toluidine blue staining with multifocal marked (to deep-zone depth) chondrocyte loss and/or collagen disruption, and 5 = severe diffuse loss of toluidine blue staining with multifocal severe (to tidemark depth) chondrocyte loss and/or collagen disruption.

Spleens from rats with AIA were stained with hematoxylin and eosin and evaluated microscopically for inhibition of the classic AIA pathology (lymphoid atrophy, increased extramedullary hematopoiesis, and pyogranulomatous inflammation in the white pulp) (32).

The total histologic score comprises the composite total score of histologic parameters of inflammation, pannus formation, cartilage changes, and bone resorption (11,34).

Plasma IL-1Ra determination. Blood samples for determinations of plasma levels of IL-1Ra were collected from the tail veins of isoflurane-anesthetized rats at various times postdosing with 20 or 100 mg/kg of IL-1Ra in HA. Samples were analyzed using an enzyme-linked immunosorbent assay with an antibody to IL-1Ra prepared (R&D Systems, Minneapolis, MN). The sensitivity of the assay was 22 pg/ml.

Statistical analysis. Clinical data for ankle width and paw volumes in each model were analyzed by determining the area under the dosing curve (AUC), with subsequent application of Student's *t*-test to these values. Paw, spleen, and liver weights and histopathology parameters for each group (mean ± SEM) were analyzed for differences using Student's *t*-test.

RESULTS

Effects of combination therapy on established CIA. All animals had arthritis of similar severity at study inception, as evidenced by comparable mean ankle joint diameters on day 1, when randomization occurred and treatment was initiated (Figures 1A and B). Rats given daily doses of 100 mg/kg of IL-1Ra in HA had good inhibition of paw swelling over time (expressed as the AUC) and final paw weights, while those treated with 20 mg/kg IL-1Ra in HA had minimal beneficial effects on these clinical parameters (Table 1).

Table 1. Summary of data from rats with CIA treated with IL-1Ra and PEG sTNFRI alone and in combination*

Treatment group	Body weight change (gm)	Hind paw weight			Ankle diameter, AUC for % inhibition from arthritis control	Composite total histologic score			
						Ankle		Knee	
		Absolute (gm)	AUC for swelling (gm)	Final, % inhibition from arthritis control		Total (gm)	% inhibition from arthritis control	Total (gm)	% inhibition from arthritis control
Normal control rats	5.41 ± 0.95†	1.317 ± 0.012†	1.293 ± 0.004†	100.0	100.0	0.0 ± 0.0†	100.0	0.0 ± 0.0†	100.0
Rats with CIA									
HA + vehicle control IP/SC	−23.23 ± 3.4	1.850 ± 0.036	1.632 ± 0.025	–	–	14.0 ± 0.7	–	7.8 ± 1.2	–
Vehicle + IL-1Ra									
100 mg/kg	−15.88 ± 2.4	1.495 ± 0.045†	1.462 ± 0.025†	66.0	50.0	8.0 ± 1.1†	43.0	0.9 ± 0.6†	88.0
20 mg/kg	−18.16 ± 2.6	1.756 ± 0.060	1.595 ± 0.038	17.0	11.0	13.4 ± 1.3	4.0	5.8 ± 1.3	26.0
HA + PEG sTNFRI									
3 mg/kg	−13.11 ± 4.36	1.602 ± 0.048†	1.477 ± 0.024†	46.0	46.0	8.8 ± 1.2†	37.0	6.4 ± 1.1	18.0
1 mg/kg	−16.70 ± 4.9	1.653 ± 0.041†	1.507 ± 0.022†	36.0	37.0	9.9 ± 1.3†	29.0	6.9 ± 1.1	12.0
0.3 mg/kg	−18.51 ± 3.25	1.700 ± 0.039†	1.533 ± 0.026†	28.0	29.0	11.0 ± 1.0†	21.0	7.9 ± 1.4	0.0
IL-1Ra 100 mg/kg + PEG sTNFRI									
3 mg/kg	−7.69 ± 3.06†	1.346 ± 0.017†	1.342 ± 0.009†	93.0	88.0	1.8 ± 0.4†	87.0	0.0 ± 0.0†	100.0
1 mg/kg	−8.99 ± 2.2†	1.340 ± 0.013†	1.371 ± 0.008†	94.0	77.0	2.3 ± 0.5†	84.0	0.0 ± 0.0†	100.0
0.3 mg/kg	−5.54 ± 3.04†	1.388 ± 0.022†	1.392 ± 0.014†	88.0	71.0	2.6 ± 0.5†	81.0	0.0 ± 0.0†	100.0
IL-1Ra 20 mg/kg + PEG sTNFRI									
3 mg/kg	−6.46 ± 3.56†	1.387 ± 0.036†	1.395 ± 0.018†	86.0	70.0	3.1 ± 0.7†	78.0	0.0 ± 0.0†	100.0
1 mg/kg	−1.43 ± 2.84	1.421 ± 0.042†	1.429 ± 0.020†	79.0	60.0	4.4 ± 0.7†	69.0	0.2 ± 0.1†	97.0
0.3 mg/kg	−8.38 ± 3.4†	1.485 ± 0.041†	1.449 ± 0.020†	67.0	54.0	5.4 ± 0.9†	61.0	1.0 ± 0.3†	87.0

* Paw weight represents the final paw weight (in grams). Composite total histologic score represents the scores for inflammation, pannus, cartilage damage, and bone resorption. All groups contained 8 rats each. CIA = (type II) collagen-induced arthritis; IL-1Ra = interleukin-1 receptor antagonist; PEG sTNFRI = PEGylated soluble tumor necrosis factor receptor type I; AUC = area under the curve (in inches); HA = hyaluronic acid; IP = intraperitoneal; SC = subcutaneous.
† $P = 0.05$ versus vehicle control, by Student's 2-tailed t-test.

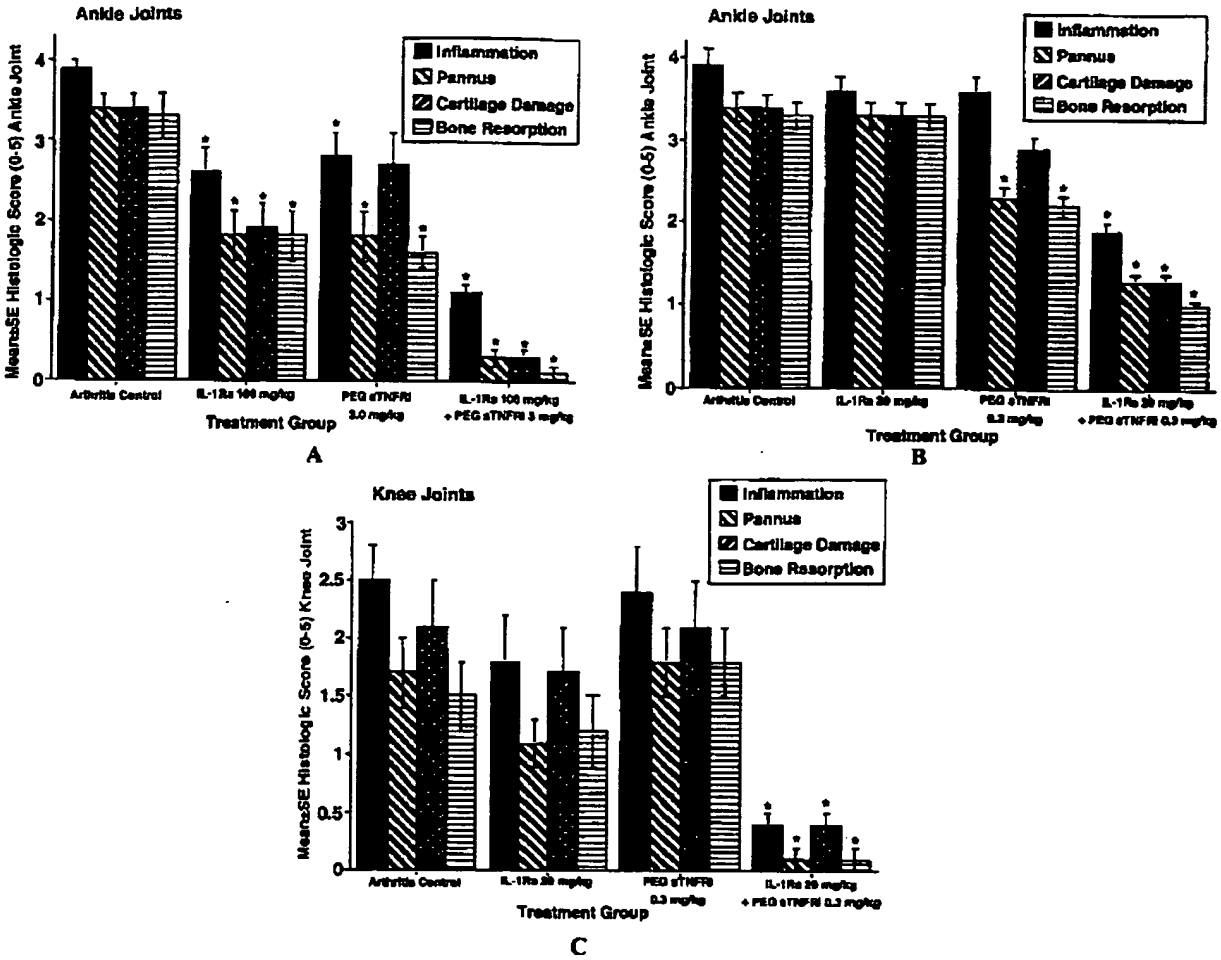

Figure 2. Changes in histologic parameters in the ankle joints (A and B) and knee joints (C) of rats with type II collagen–induced arthritis. A, Rats were treated with vehicles alone (HA for IL-1Ra SC every day and phosphate buffered saline for PEG sTNFRI vehicle IP every other day), with 100 mg/kg of IL-1Ra SC every day and vehicle IP every other day, with 3 mg/kg of PEG sTNFRI IP every other day and HA SC every day, or with IL-1Ra and PEG sTNFRI in combination. Combination therapy produced additive benefits on all parameters, resulting in dramatic inhibition of ankle joint pathology. B, Rats were treated with vehicles alone, with 20 mg/kg of IL-1Ra SC every day and vehicle IP every other day, with 0.3 mg/kg of sTNFRI IP every other day and HA SC every day, or with IL-1Ra and PEG sTNFRI in combination. Combination therapy produced greater-than-additive benefits on all parameters, resulting in good inhibition of ankle joint pathology. C, Rats were treated as in B, at the same dosages and protocol. Combination therapy produced greater-than-additive benefits on all parameters, resulting in excellent inhibition of knee joint pathology. * = $P \leq 0.05$ versus control, by Student's 2-tailed t-test; $n = 8$ rats per group. See Figure 1 for definitions.

Microscopic evaluation of joints revealed good inhibition of ankle pathology and excellent inhibition of knee lesions in rats treated with 100 mg/kg of IL-1Ra. The magnitude of inhibition of cartilage and bone lesions was generally similar at this dosage (Figures 2A–C). Treatment with IL-1Ra at 20 mg/kg had little beneficial effect on histologic parameters in the ankle and the knee joints (Table 1). There was no beneficial effect on body weight gain with either dose of IL-1Ra (Table 1).

Treatment with PEG sTNFRI (3, 1, or 0.3 mg/kg) resulted in dose-responsive inhibition of the AUC for paw swelling, final paw weights, and total histologic scores for ankle joints (Table 1). Knee joint pathology

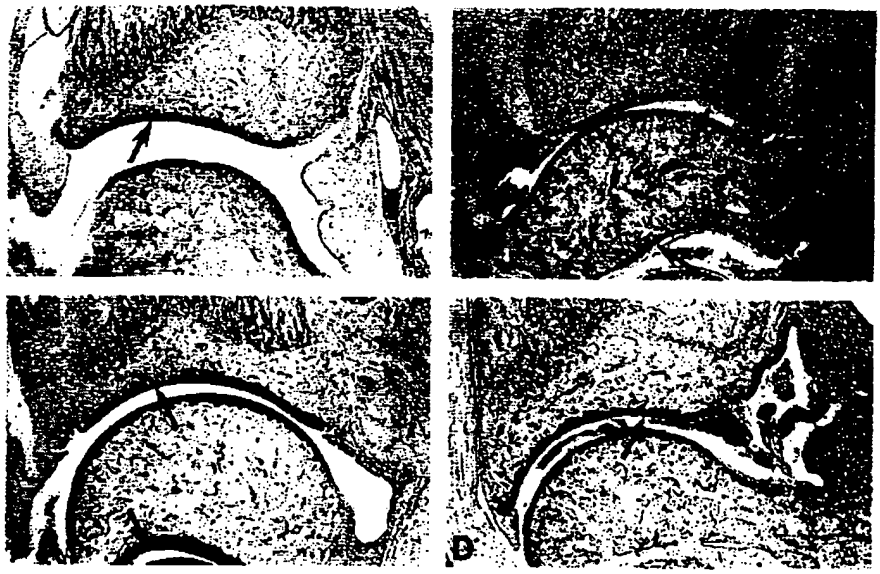

Figure 3. Photomicrographs of toluidine blue–stained ankle joints from rats with type II collagen–induced arthritis. A, Normal control rat, showing intense staining of normal articular cartilage (arrow) and absence of infiltrate in the synovium. B, Arthritic, vehicle-treated control rat, showing severe infiltration of inflammatory cells into the synovium and markedly diminished overall toluidine blue staining of the cartilage, as well as pannus formation and destruction (arrows) of cartilage and subchondral bone. C, Arthritic rat treated with the combination of IL-1Ra 100 mg/kg and PEG sTNFRI 3 mg/kg, showing largely intact (arrows) articular cartilage and subchondral bone, with mild inflammatory cell infiltration into the synovium. D, Arthritic rat treated with IL-1Ra 20 mg/kg and PEG sTNFRI 0.3 mg/kg, showing mild loss of proteoglycan from the articular cartilage, as evidenced by diminished toluidine blue staining. However, the collagenous portion of the cartilage is largely intact (arrow), and there is little evidence of subchondral bone resorption. The synovium has moderate inflammatory cell infiltration. See Figure 1 for definitions.

was not inhibited significantly by any dosage of PEG sTNFRI (Table 1). The magnitude of inhibition of bone resorption was consistently greater than that of cartilage damage at all doses of PEG sTNFRI in both the knee and the ankle joints. There was no beneficial effect on body weight gain with any dose of PEG sTNFRI alone.

Combination therapy with IL-1Ra 100 mg/kg and PEG sTNFRI (all doses) resulted in additive beneficial effects on the AUC for paw swelling and final paw weights, with all combinations resulting in excellent amelioration of the clinical signs of arthritis (Table 1). In addition, significant benefit was also observed on body weight gain (Table 1). Additive effects on ankle swelling (resulting in 88% inhibition of the AUC) over time were found for the combination of 100 mg/kg IL-1Ra and 3 mg/kg PEG sTNFRI (Figure 1A). Additive effects were generally seen on the histologic parameters, except that rats treated with the combination of 100 mg/kg IL-1Ra and 0.3 mg/kg PEG sTNFRI had greater-than-additive effects on the histologic scores in both the ankle and the knee (Table 1). Additive effects on histologic parameters for the combination of 100 mg/kg IL-1Ra and 3 mg/kg PEG sTNFRI are shown in Figure 2A.

Combination therapy with IL-1Ra 20 mg/kg and PEG sTNFRI (all doses) resulted in greater-than-additive beneficial effects on the AUC for paw swelling and the final paw weights, with all combinations resulting in good-to-excellent amelioration of the clinical signs of arthritis (Table 1). In addition, significant benefit on body weight gain (Table 1) was also observed. Additive effects on ankle swelling (resulting in 54% inhibition of the AUC) over time are shown for the combination of 20 mg/kg IL-1Ra and 0.3 mg/kg PEG sTNFRI in Figure 1B. Effects seen on the histologic parameters with these combinations were much greater than additive and were excellent in all cases (Table 1). Greater-than-additive

Table 2. Summary of data from rats with AIA treated with IL-1Ra and PEG sTNFRI alone or in combination*

		Paw weight		Spleen weight		Liver weight		Histology			
								Bone resorption		Inflammation	
Treatment group	Body weight change	Absolute weight, mean ± SEM	Final, % inhibition from arthritis control	Relative weight, mean ± SEM	Final, % inhibition from arthritis control	Relative weight, mean ± SEM	Final, % inhibition from arthritis control	Score, mean ± SEM	% inhibition from arthritis control	Score, mean ± SEM	% inhibition from arthritis control
Normal control rats, IP/SC	91.2 ± 0.81	1.813 ± 0.009	100	0.207 ± 0.005	100	5.706 ± 0.120	100	0 ± 0	100	0 ± 0	100
Rats with AIA											
HA + vehicle control IP/SC	29.8 ± 2.01	3.132 ± 0.081	0	0.572 ± 0.036	0	7.119 ± 0.281	0	3.07 ± 0.27	0	3.21 ± 0.21	0
IL-1Ra 100 mg/kg SC	42.2 ± 2.01	2.952 ± 0.060	14.0	0.481 ± 0.043	25	6.996 ± 0.188	9	1.75 ± 0.43†	43	2.5 ± 0.23†	22
PEG sTNFRI											
3 mg/kg IP	40.9 ± 2.23	2.671 ± 0.035†	35.0	0.413 ± 0.016†	44	6.498 ± 0.182	44	1.36 ± 0.25†	56	1.86 ± 0.18†	42
1 mg/kg IP	36.7 ± 2.98	2.825 ± 0.069†	23.0	0.398 ± 0.021†	48	6.414 ± 0.061†	50	2.14 ± 0.46	30	2.64 ± 0.27	18
sTNFRI 100 mg/kg SC + IL-1Ra											
3 mg/kg IP	46.9 ± 4.04	2.279 ± 0.033†	65.0	0.348 ± 0.016†	61	5.991 ± 0.142†	80	0 ± 0†	100	1.0 ± 0†	69
1 mg/kg IP	46.5 ± 2.64	2.583 ± 0.038†	42.0	0.362 ± 0.012†	58	6.110 ± 0.159†	71	1.21 ± 0.32†	60	1.71 ± 0.19†	47

* All groups contained 8 rats each. AIA = adjuvant-induced arthritis; IL-1Ra = interleukin-1 receptor antagonist; PEG sTNFRI = PEGylated soluble tumor necrosis factor receptor type I; IP = intraperitoneal; SC = subcutaneous; HA = hyaluronic acid.
† $P = 0.05$ versus vehicle control, by Student's 2-tailed t-test.

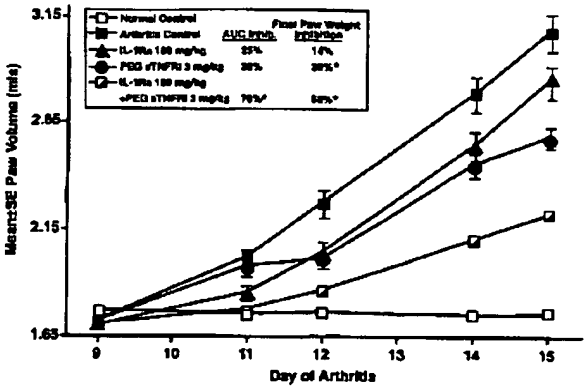

Figure 4. Changes in ankle paw volume over time in rats with adjuvant-induced arthritis treated with vehicles alone (HA for IL-1Ra SC every day and phosphate buffered saline for PEG sTNFRI IP every other day), with 100 mg/kg of IL-1Ra SC every day and vehicle IP every other day, with 3 mg/kg of PEG sTNFRI IP every other day and HA SC every day, or with IL-1Ra and PEG sTNFRI in combination. Combination therapy produced additive to slightly greater than additive benefits on ankle swelling over time. * = $P \leq 0.05$ versus control, by Student's 2-tailed t-test; n = 8 rats per group. See Figure 1 for definitions.

effects on histologic parameters for the combination of 20 mg/kg IL-1Ra and 0.3 mg/kg PEG sTNFRI are shown in Figures 2B and C, as well as in Figure 3.

Effects of combination therapy on developing AIA. Treatment with IL-1Ra alone resulted in minimal inhibition of ankle joint swelling in rats with AIA. Treatment with 3 mg/kg PEG sTNFRI resulted in 35% inhibition of final paw weights (Table 2 and Figure 4). Combination therapy yielded 70% inhibition of paw swelling over time (expressed as the AUC) and 65% inhibition of final paw weights. Combination benefit was also seen on inhibition of inflammation in the spleen and liver, as assessed by the weights of these organs (Table 2). Histopathologic evaluation of the spleen confirmed that the beneficial effects of treatment on spleen weights were associated with a return to normal morphology in animals given the combination therapy (results not shown). Body weight change associated with AIA showed modest benefit with either treatment alone and mildly increased benefit with combination treatment (data not shown).

Histologic parameters of inflammation and bone resorption were moderately decreased with either treatment alone and dramatically decreased when the treatments were administered in combination (Figure 5 and Table 2). Administration of a lower dose of PEG sTNFRI (1 mg/kg) in combination with IL-1Ra also resulted in additive effects on the various parameters (Table 2).

Plasma levels of IL-1Ra in rats treated with 20 or 100 mg/kg of IL-1Ra in HA. Peak levels of IL-1Ra after a single SC injection of 100 mg/kg were 9 μg/ml at 6 hours postdosing (Figure 6) and fell below 1 μg/ml 24 hours after injection. Peak levels of IL-1Ra after a single SC injection of 20 mg/kg were 2 μg/ml at 3 hours postdosing (Figure 6) and fell below 0.08 μg/ml 24 hours after injection.

DISCUSSION

The findings of the present study demonstrate that combination therapy with higher, more efficacious doses of IL-1Ra and PEG sTNFRI results in additive effects in rats with established CIA. Minimally effective doses of PEG sTNFRI (0.3 mg/kg) in combination with ineffective doses of IL-1Ra (20 mg/kg) result in much greater than additive effects on all parameters and excellent overall inhibition of established arthritis.

IL-1 appears to be an important mediator of CIA in rats. In rats treated with daily doses of 100 mg/kg of IL-1Ra in HA, 50% inhibition (by AUC) to 66% inhibition (by paw weight) of clinical parameters of estab-

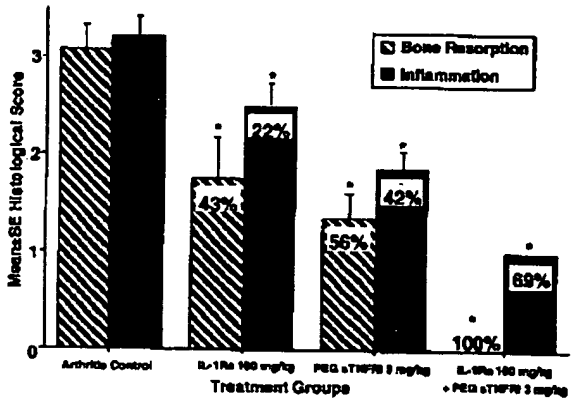

Figure 5. Changes in histologic parameters of inflammation and bone resorption in rats with adjuvant-induced arthritis treated with vehicles alone (HA for IL-1Ra SC every day and phosphate buffered saline for PEG sTNFRI IP every other day), with 100 mg/kg of IL-1Ra SC every day and vehicle IP every other day, with 3 mg/kg of PEG sTNFRI IP every other day and HA SC every day, or with IL-1Ra and PEG sTNFRI in combination. Combination therapy produced additive benefits on inflammation and bone resorption, resulting in 100% inhibition of the aggressive bone resorption that occurs in this disease and excellent inhibition of periarticular inflammation. * = $P \leq 0.05$ versus controls, by Student's 2-tailed t-test; n = 8 rats per group. See Figure 1 for definitions.

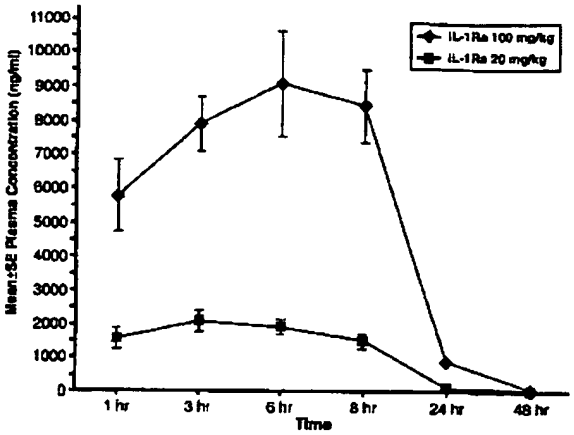

Figure 6. Plasma concentrations of interleukin-1 receptor antagonist (IL-1Ra) in rats treated with single subcutaneous doses of 20 mg/kg or 100 mg/kg in the slow-release vehicle hyaluronic acid.

lished arthritis was achieved. Histologic changes in knee joints were dramatically suppressed (88%) at this dosage. This dosing regimen results in blood levels of 6–9 μg/ml for 1–8 hours after the dose is administered, with the blood levels falling to 0.875 μg/ml at 24 hours, when the next dose is due. Although administration of IL-1Ra in HA dramatically improves the pharmacokinetic profile over that seen with aqueous vehicles (10), continuous-infusion studies in which blood levels are maintained at ~5 μg/ml have shown even greater inhibition of this established arthritis (11).

Since it is unlikely that similar continuously high blood levels would be achieved clinically, we chose to perform these combination studies using a regimen that more closely approximates the pharmacokinetic profile seen in humans given 2 mg/kg of IL-1Ra (in its current aqueous vehicle), which results in approximate levels of 1.2–1.6 μg/ml at 12 hours, 0.8 μg/ml at 18 hours, and 0.2 μg/ml at 24 hours, when the next dose would be given (Bendele A: unpublished observations). The blood levels in rats treated with 100 mg/kg IL-1Ra in HA are much higher (especially peak levels) than those seen in humans given 1–2 mg/kg. Blood levels (for the first 8 hours postdosing) in rats given 20 mg/kg are similar to those in humans in current clinical trials who are receiving daily doses of 1–2 mg/kg, but trough levels at 24 hours are much lower than those in humans. Therefore, the data from this study of combination therapy demonstrate efficacy in rodent models at blood levels of IL-1Ra that are much higher than, as well as blood levels that are comparable to, those achieved with the 1–2 mg/kg dose currently being utilized in monotherapy trials with this agent, in which efficacy has been demonstrated (11,14,15).

TNFα also appears to be an important mediator of established CIA in rats. Forty-six percent inhibition (by AUC and paw weight) of clinical parameters of established arthritis was achieved when rats were treated every other day with 3 mg/kg doses of PEG sTNFRI. This dosing regimen results in peak blood levels of 6.8 μg/ml at 24 hours, with the levels falling to 4.2 μg/ml at 48 hours, when the next dose is due (28). These blood levels are high compared with those being achieved in early phase I trials of this agent in humans (35). However, the peak blood levels in rodents given 0.3 mg/kg (0.5 μg/ml) to 1 mg/kg (2.5 μg/ml) every other day are comparable to the peak levels in humans treated with similar weekly doses of PEG sTNFRI (28,35,36). Efficacy data are not currently available for PEG sTNFRI; however, results of a previous trial with a dimeric PEG construct in which efficacy was measured suggested that average blood levels of ~0.6 μg/ml were associated with swollen joint counts that were 55% of baseline (21).

Therefore, this study of combination therapy in rats with established CIA demonstrates efficacy in association with blood levels of both biologic agents that range from higher to lower than those that are currently being achieved in humans, thus providing a full range of potential scenarios. When both agents are given together at the highest dosages (100 mg/kg of IL-1Ra and 3 mg/kg of PEG sTNFRI), near-total suppression of this aggressive established arthritis occurs, with the effects being additive compared with either agent alone. The combinations of 100 mg/kg of IL-1Ra and either 1 mg/kg or 0.3 mg/kg of PEG sTNFRI (producing blood levels that are reasonably close to those seen in humans, especially with PEG sTNFRI), resulted in excellent additive (1 mg/kg) to greater-than-additive (0.3 mg/kg, histologic parameters only) effects on all aspects of CIA. When IL-1Ra was given at a completely inactive dosage of 20 mg/kg (which results in blood levels that are much lower than the levels currently achieved in humans) in combination with the clinically relevant dosages of 1 mg/kg or 0.3 mg/kg of PEG sTNFRI, patterns of efficacy were consistently greater than additive for all parameters. These data suggest a potential for synergistic clinical effects at dosages of IL-1Ra that are lower than those currently used and at dosages of PEG sTNFRI potentially lower than the dosages that have been proposed.

Evaluation of efficacy in the rat model of developing AIA utilized dosages of 100 mg/kg of IL-1Ra and

either 3 mg/kg or 1 mg/kg of PEG sTNFRI. Additive to greater-than-additive effects were seen for all parameters with both combinations.

Although there are no human trials to date, the combination of 2 anticytokines, such as IL-1Ra and an sTNFR, may offer greater efficacy than either agent alone (37,38). In a previously published animal study, the combination of IL-1Ra with a dimeric TNFRI (TNFRI p55), TNF binding protein (21), or an anti-TNFα antibody significantly reduced disease activity in a murine model of streptococcal cell wall–induced arthritis (39).

Further insight into the role of TNFα and IL-1 in inflammation and cartilage destruction has emerged from studies of experimental arthritis. In murine models, using zymosan, immune complexes, or T cell allergens as arthritogenic stimuli, it was shown that cartilage destruction was highly dependent on IL-1, whereas TNFα involvement was limited (9,40). Finally, in a recently published study, the effects of neutralization of either TNFα or IL-1 on joint structures in established CIA in the murine model were studied (41). Both treatment with soluble TNF binding protein and treatment with anti–IL-1 ameliorated disease activity when administered shortly after the onset of CIA. Serum analysis revealed that early treatment with anti-TNFα did not decrease the disease activity in the cartilage, as indicated by the elevated levels of cartilage oligomeric matrix protein (41).

The biologic activities of IL-1 are synergistic with other cytokines and growth factors; however, the synergism of IL-1 plus TNFα is highly consistent and has been frequently reported. The synergism between IL-1 and TNFα is often observed in vivo (42,43), whereas the synergism between IL-1 and various growth factors relates mostly to cytokine production and prostanoid synthesis and is primarily an in vitro finding (43). The mechanism for synergy may involve receptor modulation, but TNF receptors are down-regulated by IL-1 (44,45). Synergism may also be explained at the level of signal transduction (46). Since the signaling mechanism of IL-1 and TNFα appear to be similar, additive rather than synergistic effects should be observed. Part of the synergism in vivo may be explained by the ability of TNFα to induce IL-1 and vice versa (47). For example, during heat-killed *Staphylococcus epidermidis*–induced shock in rabbits, IL-1Ra administration reduced circulating levels of TNFα (48), suggesting that endogenous IL-1 induces TNFα. In baboons with *Escherichia coli*–induced shock, anti-TNFα treatment reduced circulating levels of IL-1β (49).

At present, there is no single molecular mechanism that would explain the synergism of IL-1 and TNFα. However, this synergism may explain why the combination of IL-1Ra plus sTNFR was more effective in blocking disease in animal studies than either strategy alone. These findings require confirmation in humans.

The basis for attributing part of the success of TNFα neutralization in RA to a decrease in the production of bioactive IL-1 can be found in a classic paper by Brennan et al (50). In that study, mixed cells from patients' synovial fluid or synovial tissues were cultured in the presence of neutralizing antibodies to human TNFα or lymphotoxin. Anti-TNFα dramatically reduced the spontaneous production of IL-1 activity, whereas anti-lymphotoxin did not (51). In RA patients treated with anti-TNFα agents, the reduction in circulating IL-1β confirms Brennan's observation that IL-1 production in RA is under the control of TNFα. However, it would not be unexpected that some of the TNFα production in RA is also under the control of IL-1.

Our results in 2 well-established animal models of arthritis that have been reasonably predictive of clinical efficacy (34), using dosing protocols that result in realistic blood levels with respect to clinical applicability, support the clinical investigation of combination therapy with the specific cytokine inhibitors IL-1Ra and PEG sTNFRI in RA patients.

REFERENCES

1. Arend WP, Dayer J-M. Inhibition of the production and effects of interleukin-1 and tumor necrosis factor α in rheumatoid arthritis. Arthritis Rheum 1995;38:151–60.
2. Eastgate JA, Wood NC, di Giovine FS, Symons JA, Grinlinton JA, Duff GW. Correlation of plasma interleukin-1 levels with disease activity in rheumatoid arthritis. Lancet 1988;24:706–9.
3. Khale P, Saal JG, Schaudt K. Determination of cytokines in synovial fluids: correlation with diagnosis and histomorphological characteristics of synovial tissue. Ann Rheum Dis 1992;51:731–4.
4. Van de Loo FAJ, Arntz OJ, Otterness IG, van den Berg WB. Protection against cartilage proteoglycan synthesis inhibition by antiinterleukin 1 antibodies in experimental arthritis. J Rheumatol 1992;19:348–56.
5. Joosten LAB, Helsen MMA, van de Loo FAJ, van den Berg WB. Amelioration of established type II collagen-induced arthritis with anti-IL-1. Agents Actions 1994;41:C174–6.
6. Van de Loo AAJ, Arntz OJ, Otterness IG, van den Berg WB. Proteoglycan loss and subsequent replenishment in articular cartilage after a mild arthritic insult by IL-1 in mice: impaired proteoglycan turnover in the recovery phase. Agents Actions 1994;41:200–8.
7. Van de Loo FAJ, Joosten LAB, van Lent PLEM, Arntz OJ, van den Berg WB. Role of interleukin-1, tumor necrosis factor α, and interleukin-6 in cartilage proteoglycan metabolism and destruction: effect of in situ blocking in murine antigen- and zymosan-induced arthritis. Arthritis Rheum 1995;38:164–72.
8. Van de Loo FAJ, Arntz OJ, Bakker AC, van Lent PLEM, Jacobs

MJM, van den Berg WB. Role of interleukin-1 in antigen-induced exacerbations of murine arthritis. Am J Pathol 1995;146:239–49.
9. Joosten LAB, Helsen MMA, van de Loo FAJ, van den Berg WB. Anticytokine treatment of established type II collagen-induced arthritis in DBA/1 mice: a comparative study using anti-TNFα, anti-IL-1α/β, and IL-1Ra. Arthritis Rheum 1996;39:797–809.
10. Bendele A, McAbee T, Woodward M, Scherrer J, Collins D, Frazier J, et al. Effects of interleukin-1 receptor antagonist in a slow-release hylan vehicle on rat type II collagen arthritis. Pharm Res 1998;15:1557–61.
11. Bendele A, McAbee T, Sennello G, Frazier J, Chlipala E, McCabe D. Efficacy of sustained blood levels of interleukin-1 receptor antagonist in animal models of arthritis: comparison of efficacy in animal models with human clinical data. Arthritis Rheum 1999; 42:498–506.
12. Eisenberg SP, Evans RJ, Arend WP. Primary structure and functional expression from complementary DNA of a human interleukin-1 receptor antagonist. Nature 1990;343:341–5.
13. Campion GV, Lebsack ME, Lookabaugh J, Gordon G, Catalano M, and the IL-1Ra Arthritis Study Group. Dose-range and dose-frequency study of recombinant human interleukin-1 receptor antagonist in patients with rheumatoid arthritis. Arthritis Rheum 1996;39:1092–101.
14. Bresnihan B, Alvaro-Gracia JM, Cobby M, Doherty M, Domljan Z, Emery P, et al. Treatment of rheumatoid arthritis with recombinant human interleukin-1 receptor antagonist. Arthritis Rheum 1998;41:2196–204.
15. Jiang Y, Genant HK, Watt I, Cobby M, Bresnihan B, Aitchison R, et al. A multicenter, double-blind, dose-ranging, randomized, placebo-controlled study of recombinant human interleukin-1 receptor antagonist in patients with rheumatoid arthritis: radiologic progression and correlation of Genant and Larsen scores. Arthritis Rheum 2000;43:1001–9.
16. Bendele A, Sennello, G, McAbee T, Frazier J, Chlipala C, Rich B. Effects of interleukin-1 receptor antagonist alone and in combination with methotrexate in adjuvant arthritic rats. J Rheumatol 1999;26:1225–9.
17. Moreland LW, Baumgartner SW, Schiff MH, Tindall EA, Fleischmann RM, Weaver AL, et al. Treatment of rheumatoid arthritis with a recombinant human tumor necrosis factor receptor (p75)-Fc fusion protein. N Engl J Med 1997;337:141–7.
18. Moreland LW, Margolies G, Heck LW Jr, Tindall EA, Fleischmann RM, Weaver AL, et al. Recombinant soluble tumor necrosis factor receptor (p80) fusion protein: toxicity and dose finding trial in refractory rheumatoid arthritis. J Rheumatol 1996;23:1849–55.
19. Elliott MJ, Maini RN, Feldmann M, Long-Fox A, Charles P, Katsikis P, et al. Treatment of rheumatoid arthritis with chimeric monoclonal antibodies to tumor necrosis factor α. Arthritis Rheum 1993;36:1681–90.
20. Moreland LW, Schiff MH, Baumgartner SW, Tindall EA, Fleischmann RM, Bulpitt KJ, et al. Etanercept therapy in rheumatoid arthritis: a randomized, controlled trial. Ann Intern Med 1999;130: 478–86.
21. Moreland LW, McCabe DP, Caldwell JR, Sack M, Weisman M, Henry G, et al. Phase I/II trial of recombinant methionyl human tumor necrosis factor binding protein PEGylated dimer in patients with active refractory rheumatoid arthritis. J Rheumatol 2000;27: 601–9.
22. Thorbecke GJ, Shah R, Leu CH, Kuruvilla AP, Hardison AM, Palladino MA. Involvement of endogenous tumor necrosis factor alpha and transforming growth factor beta during induction of collagen arthritis in mice. Proc Natl Acad Sci U S A 1992;89: 7375–9.
23. Williams RO, Feldmann M, Maini RN. Anti-tumor necrosis factor ameliorates joint disease in murine collagen-induced arthritis. Proc Natl Acad Sci U S A 1992;89:9784–8.
24. Piguet PF, Grau GE, Vesin C, Loetscher H, Gentz R, Lesslauer W. Evolution of collagen arthritis in mice is arrested by treatment with anti-tumor necrosis factor (TNF) antibody or a recombinant soluble TNF receptor. Immunology 1992;77:510–4.
25. Wooley PH, Dutcher J, Widmer MB, Gillis S. Influence of a recombinant human soluble tumor necrosis factor receptor FC fusion protein on type II collagen-induced arthritis in mice. J Immunol 1993;151:6602–7.
26. Issekutz AC, Meager A, Otterness I, Issekutz TB. The role of tumor necrosis factor alpha and IL-1 in polymorphonuclear leukocyte and T lymphocyte recruitment to joint inflammation in adjuvant arthritis. Clin Exp Immunol 1994;97:26–32.
27. Mori L, Iselin S, de Libero GD, Lesslauer W. Attenuation of collagen-induced arthritis in 55-kDa TNF receptor type I (TNFRI)-deficient mice. J Immunol 1996;22:3178–82.
28. McComb J, Gould T, Chlipala L, Sennello G, Frazier J, Kieft G, et al. Antiarthritic activity of soluble tumor necrosis factor receptor type I in adjuvant arthritis: correlation of plasma levels with efficacy. J Rheumatol 1999;26:1347–51.
29. Bendele A, McComb J, Gould T, Frazier J, Chlipala L, Seely J, et al. Combination benefit of PEGylated soluble tumor necrosis factor receptor type I (PEG sTNF-RI) and dexamethasone or indomethacin in adjuvant arthritic rats. Inflamm Res 1999;48:453–60.
30. Bendele A, McComb J, Gould T, Guy M, Chlipala L, Sennello R, et al. Effects of PEGylated soluble tumor necrosis factor receptor type I (PEG sTNF-RI) alone and in combination with methotrexate in adjuvant arthritic rats. Clin Exp Rheumatol 1999;17:553–60.
31. Edwards CK III. PEGylated recombinant human soluble tumor necrosis factor receptor type I (r-Hu-sTNF-RI): a novel high-affinity TNF receptor designed for one chronic inflammatory diseases. Ann Rheum Dis 1999;58 Suppl I:173–81.
32. Pearson CM. Development of arthritis, periarthritis and periostitis in rats given adjuvants. Proc Soc Exp Biol Med 1956;91:95–100.
33. Benslay DN, Bendele AM. Development of a rapid screen for detecting and differentiating immunomodulatory vs. anti-inflammatory compounds in rats. Agents Actions 1991;34:254–6.
34. Bendele A, McComb J, Gould T, Chlipala L, Sennello R, McAbee T, et al. Animal models of arthritis: relevance to human disease. Toxicol Pathol 1999;27:134–42.
35. Martin SW, Sommers JS, Macri MJ, Newmark RD, Jelaca-Maxwell K, Turner SA, et al. The pharmacokinetics of subcutaneous injections of PEGylated recombinant methionyl human soluble tumor necrosis factor-type I receptor in subjects with active rheumatoid arthritis [abstract]. Arthritis Rheum 1999;42 Suppl 9:S79.
36. Caldwell JR, Davis MW, Jelaca-Maxwell K, Wang A, Wason S, Chase W, et al. A phase 1 study of PEGylated soluble tumor necrosis factor receptor type I (PEG sTNF-RI [p55]) in subjects with rheumatoid arthritis [abstract]. Arthritis Rheum 1999;42 Suppl 9:S236.
37. Van den Berg WB, Joosten LAB, Kollias G, van de Loo FAJ. Role of tumor necrosis factor-α in experimental arthritis: separate activity of interleukin 1β in chronicity and cartilage destruction. Ann Rheum Dis 1999;58 Suppl 1:140–8.
38. Van den Berg WB, Joosten LAB, van de Loo FAJ. TNFα and IL-1β are separate targets in chronic arthritis. Clin Exp Rheumatol 1999;17 Suppl 18:S105–14.
39. Kuiper SL, Joosten LAB, Bendele AM, Edwards CK III, Arntz OJ, Helsen MMA, et al. Different roles of TNFα and IL-1 in murine streptococcal cell wall arthritis. Cytokine 1998;10:690–702.
40. Van Lent PLEM, van de Loo FAJ, Holthuysen EM, van den Bersselaaer LAM, van den Berg WB. Major role of interleukin-1 but not tumor necrosis factor in early cartilage degradation in immune-complex arthritis in mice. J Rheumatol 1995;22:2250–8.
41. Joosten LAB, Helsen MMA, Saxne T, van de Loo FAJ, Heinegard D, van den Berg WB. IL-1αβ blockade prevents cartilage and bone destruction in murine type II collagen-induced arthritis, whereas

TNF-α blockade only ameliorates joint inflammation. J Immunol 1999;163:5049–55.
42. Okusawa S, Gelfand JA, Ikejima T, Connolly RJ, Dinarello CA. Interleukin 1 induces a shock-like state in rabbits: synergism with tumor necrosis factor and the effect of cyclooxygenase inhibition. J Clin Invest 1988;81:1162–72.
43. Movat HZ, Burrowes CE, Cybulsky MI, Dinarello CA. Acute inflammation and a Shwartzman-like reaction induced by interleukin-1 and tumor necrosis factor: synergistic action of the cytokines in the induction of inflammation and microvascular injury. Am J Pathol 1987;1129:463–76.
44. Holtmann H, Wallach D. Down regulation of the receptors for tumor necrosis factor by interleukin-1 and 4 beta-phorbol-12-myristate-13-acetate. J Immunol 1987;139:1161–7.
45. Brakebusch C, Varfolomeev EE, Batkin M, Wallach D. Structural requirements for inducible shedding of the p55 tumor necrosis factor receptor. J Biol Chem 1994;269:32488–96.
46. Dinarello CA. Blocking IL-1 and TNF. J Endotoxin Res 1999;5: 174–6.
47. Ikejima T, Ikusawa S, Ghezzi P, van der Meer JWM, Dinarello CA. IL-1 induces TNF in human PBMC in vitro and a circulating TNF-like activity in rabbits. J Infect Dis 1990;162:215–21.
48. Aiura K, Gelfand JA, Wakabayashi G, Burke JF, Thompson RC, Dinarello CA. Interleukin-1 (IL-1) receptor antagonist prevents Staphylococcus epidermidis-induced hypotension and reduces circulating levels of tumor necrosis factor and IL-1β in rabbits. Infect Immun 1993;61:3342–50.
49. Fong Y, Tracey KJ, Moldawer LL, Hesse DG, Manogue KB, Kenny JS, et al. Antibodies to cachectin/tumor necrosis factor reduce interleukin 1 beta and interleukin 6 appearance during lethal bacteremia. J Exp Med 1989;170:1627–33.
50. Brennan FM, Chantry D, Jackson A, Maini R, Feldmann M. Inhibitory effect of TNF alpha antibodies on synovial cell interleukin-1 production in rheumatoid arthritis. Lancet 1989;2: 244–7.
51. Charles P, Elliott MJ, Davis D, Potter A, Kalden JR, Antoni C, et al. Regulation of cytokines, cytokine inhibitors, and acute phase proteins following anti-TNF-α therapy in rheumatoid arthritis. J Immunol 1999;163:1521–8.

EXHIBIT H

Cell Death and Differentiation (2001) 8, 679–686

www.nature.com/cdd

Therapeutic neutralization of CD95-ligand and TNF attenuates brain damage in stroke

A Martin-Villalba*,[1,2], M Hahne[4], S Kleber[2], J Vogel[2], W Falk[3], J Schenkel[2] and PH Krammer[1]

[1] Tumorimmunology Programm, German Cancer Research Center (DKFZ), Heidelberg, Germany
[2] Department of Physiology, University of Heidelberg, Heidelberg, Germany
[3] Department of Internal Medicine I, University of Regensburg, Regensburg, Germany
[4] Department of Immunology, National Center of Biotechnology, Madrid
* Corresponding author: A Martin-Villalba, German Cancer Research Center (DKFZ), Im Neuenheimer Feld 280, 69120 Heidelberg, Germany. Tel: +49 6221 423766; Fax: +49 6221 411715; E-mail: c50@ix.urz.uni-heidelberg.de

Received 9.3.01; revised 22.3.01; accepted 27.3.01
Edited by G Melino

Abstract

Stroke is the third most common cause of death in the Western world. The mechanisms of brain damage in the affected areas are largely unknown. Hence, rational treatment strategies are limited. Previous experimental evidence suggested that cerebral lesions were less prominent in CD95 (APO-1/Fas)-deficient (lpr) than in wild-type mice. Additional results strongly suggested that the CD95-ligand (CD95L) was a major cause of neuronal autocrine suicide in the penumbra. These data and the assumption that death-receptor systems might determine stroke-related damage in the brain prompted us to examine these systems in *in vitro* and *in vivo* models of ischemia. We showed that hybrids of TNF-deficient and *gld* mice were strongly resistant towards stroke-induced damage. To determine the mechanism of action of TNF and CD95L, we separately investigated their influence on primary ischemic death and secondary inflammatory injury. Inhibition of both TNF and CD95L *in vitro* prevented death of primary neurons induced by oxygen-glucose deprivation and reperfusion. The recruitment of inflammatory cells to the ischemic hemisphere was abrogated in the absence of both TNF and CD95L. Significantly, mice injected with a mixture of neutralizing anti-TNF and anti-CD95L antibodies 30 min after induction of stroke showed a marked decrease in both infarct volumes and mortality. Accordingly, the locomotor performance of these animals was not significantly impaired in comparison to sham-operated animals. These data reveal that inhibition of TNF and CD95L blocks stroke-related damage at two levels, the primary ischemic and the secondary inflammatory injury. These results offer new approaches in stroke treatment. *Cell Death and Differentiation* (2001) 8, 679–686.

Keywords: CD95-ligand; TNF; stroke; apoptosis; stroke therapy; *gld*; *tnf*-ko

Abbreviations: CD95L, CD95-ligand; MCA, middle cerebral artery; TNF, tumor necrosis factor-α

Introduction

Stroke is the third most common cause of death in the Western world and the most important single cause of severe disability.[1] Current data show that there is a variable therapeutic window that may exceed 6–8 h.[2] This interval is determined by formation of the ischemic penumbra. Evidence has accumulated that neurons in the ischemic penumbra undergo apoptosis.[3] Thus, neuroprotective strategies towards suppression of apoptosis may alleviate disease severity in stroke patients.

Tumor necrosis factor-receptor-1 (TNFR1, p55, CD120a) and CD95 (APO-1, Fas) are members of the TNF-R superfamily involved in triggering apoptosis.[4–6] Like other death receptors, they show a homologous cytoplasmic sequence crucial for the transduction of the apoptotic signal, the 'death domain'.[7] Their natural ligands, CD95-ligand (CD95L) and TNF are structurally related type II transmembrane proteins. Ligation of receptors by trimerized ligands leads to recruitment of the adaptor protein FADD (Fas-associated death domain, MORT1)[8] and caspase-8 into a death inducing signaling complex.[9] Caspase-8 in the DISC is activated through self-cleavage[10] and commits the cell to apoptosis by activation of downstream effector caspases. Activation and cleavage of caspase-3 has been detected in the postischemic brain,[11] but controversy exists with regard to the steps upstream of caspase activation.

Following brain ischemia, expression of TNF, CD95L and CD95 is increased in the ischemic penumbra.[12–16] The role of TNF in ischemic brain injury *in vivo*, however, is controversial. On the one hand, neutralization of endogenous TNF is reported to reduce infarct volume.[17–20] On the other hand, mice lacking TNF-receptor-1 (TNF-R1; also called p55) or both TNF-R1 and TNF-R2 (also called p75) showed enhanced ischemic damage.[21,22] It is consistent with these data that administration of TNF prior to the ischemic insult significantly reduced infarct size.[23] In contrast, the role of CD95/CD95L in ischemic brain disease seems to be deleterious. *lpr* mice, lacking functional CD95, exhibited a profound reduction of infarct size.[14] In addition, in microglia, TNF facilitates CD95L-induced apoptosis.[24] Whether these two ligand/receptor systems cooperate or counteract each other in the induction of ischemic damage remains unclear.

In the present study we show that mice deficient for TNF ($tnf^{-/-}$) or functional CD95L (*gld*) are protected against brain ischemia. This protection is greatly enhanced in mice lacking both ligand/receptor systems ($gld/tnf^{-/-}$). Most importantly, treatment of wild-type mice after induction of ischemia with antibodies against TNF and CD95L

diminished infarct volumes and significantly improved survival of the animals. Intact functionality of rescued neurons *in vivo* was demonstrated by an almost normal locomotor performance of the treated animals 3 days after stroke. Thus, simultaneous neutralization of CD95L and TNF may alleviate the consequences of stroke.

Results

CD95L and TNF induce neuronal death

To investigate the role of CD95L and TNF in ischemic brain damage, we took advantage of an *in vitro* model of oxygen-glucose deprivation (OGD). OGD in primary neuronal cultures is a common *in vitro* model for studying early mechanisms of vascular stroke damage in a system mostly consisting of neurons.[25] Primary cortical neurons were obtained from mice carrying a targeted disruption of the *tnf* gene ($tnf^{-/-}$),[26] from mice with mutated CD95L and impaired ability to successfully interact with CD95 (*gld*),[27] from mice deficient in TNF with mutated CD95L ($gld/tnf^{-/-}$), and from wild-type mice (wt). Neuronal cultures were then subjected to 6 h OGD and 3, 18 and 24 h reperfusion. Whereas the absence of TNF markedly protected against OGD/reperfusion damage, protection due to the absence of a functional CD95L was less profound (Figure 1a). For as yet unknown reasons, despite frequent attempts neuronal cells derived from $gld/tnf^{-/-}$ mice could not be grown in culture.

$Tnf^{-/-}$ and *gld* mice exhibit normal development and anatomy of the brain. This apparently normal 'cerebral-phenotype' may be due to compensatory mechanisms, which might non-specifically protect against brain ischemia. To exclude this possibility, wild-type neurons were treated with CD95-Fc or TNF-R2-Fc proteins 15 min prior to induction of OGD. Administration of both CD95-Fc and TNF-R2-Fc had toxic effects for the cultures, as it has also been the experience of other groups. After 6 h of OGD and 18 h reperfusion scavenging of either CD95L or TNF-α reduced neurotoxicity of the cultures by 55 and 80%, respectively, compared to IgG1 (immunoglobulin G_1) treated controls (Figure 1b). Therefore, inhibition of TNF and CD95L activity can specifically block OGD/reperfusion-induced neuronal death.

CD95L and TNF synergistically promote cell death following brain ischemia

To examine the *in vivo* role of TNF and CD95L and their possible interaction in ischemic brain damage we used $tnf^{-/-}$, *gld*, $gld/tnf^{-/-}$, and wild-type mice (wt), all on C57BL/6 background. $gld/tnf^{-/-}$ mice showed no structural or morphological abnormalities of the brain as assessed by Nissl staining of coronal cryostat sections (data not shown).

wt, *gld*, $tnf^{-/-}$ and $gld/tnf^{-/-}$ mice underwent 90 min occlusion of the middle cerebral artery (MCA) and 24 h reperfusion. Physiological parameters such as blood pressure, blood pH, pO_2, pCO_2 and glucose measured before, during and after MCA occlusion did not significantly differ between the different animal groups (data not shown).

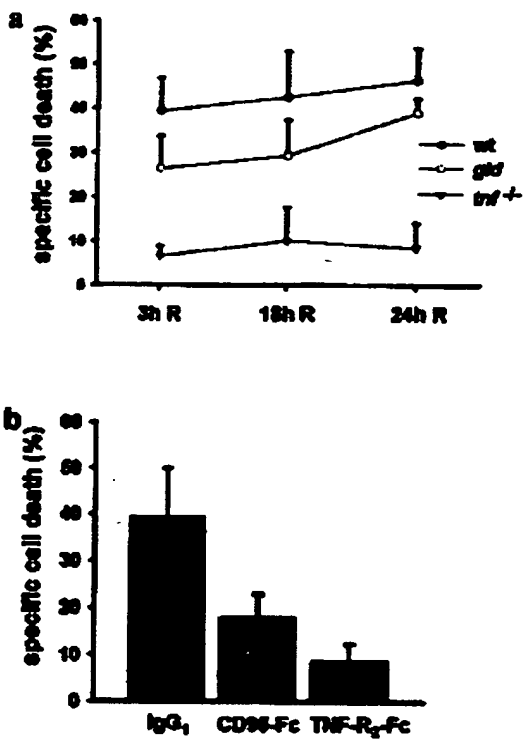

Figure 1 Protection against ischemic death in an *in vitro* model of vascular stroke. (a) Cortical neurons from wild-type, *gld* and $tnf^{-/-}$ mice were subjected to 6 h of oxygen-glucose deprivation (OGD) and increasing reperfusion periods (R). Specific death was assessed at 3, 18 and 24 h of reperfusion (R). (b) Cortical neurons from wild-type animals were incubated with CD95-Fc and TNF-R2-Fc proteins (20 μg/ml each) prior to induction of 6 h OGD and 18 h of reperfusion; specific death was assessed at the end of the reperfusion period. Incubation with control immunoglobulin (IgG_1) did not have any effect on neurotoxicity of the cultures. Cell death was assessed by trypan-blue exclusion and given as the means $\pm$ S.D. (n=3). Differences between per cent of cell death in wt and *gld* and $tnf^{-/-}$ animals were statistically significant ($P<0.05$ and $P<0.00009$, respectively). The same applied to the treated groups: IgG1 and CD95-Fc and TNF-R2-Fc treated cells ($P<0.009$ and $P<0.0001$, respectively) as assessed by student *t*-test

The mean infarct volume exhibited by wt-animals was in good concordance with that obtained by other groups in similar models.[21,28] Data from mice which did not exhibit an ischemic lesion (10% wt, 30% *gld* and 40% $tnf^{-/-}$ and $gld/tnf^{-/-}$ mice) or from mice who died before the end of the 24 h observation period (Figure 2a) were not included in the analyses of infarct volume.

In *gld* and $tnf^{-/-}$ mice the infarct volume was significantly reduced by about 54 and 67%, respectively, compared to wt mice (23.23 ± 4.97 mm^3, n=8, and 16.44 ± 7.24 mm^3, n=7, *versus* 54.66 ± 6.32 mm^3, n=9, respectively, both $P<0.01$; Figure 2b). Surprisingly, neuroprotection was greatly enhanced by the absence of both CD95L and TNF. $gld/tnf^{-/-}$ mice exhibited a mean infarct volume significantly smaller than wt animals (3.97 ± 1.52 mm^3, n=8; $P<0.0001$; Figure 2b). TNF and CD95L have an additive effect in infarct extension as assessed by two factorial variance analysis.

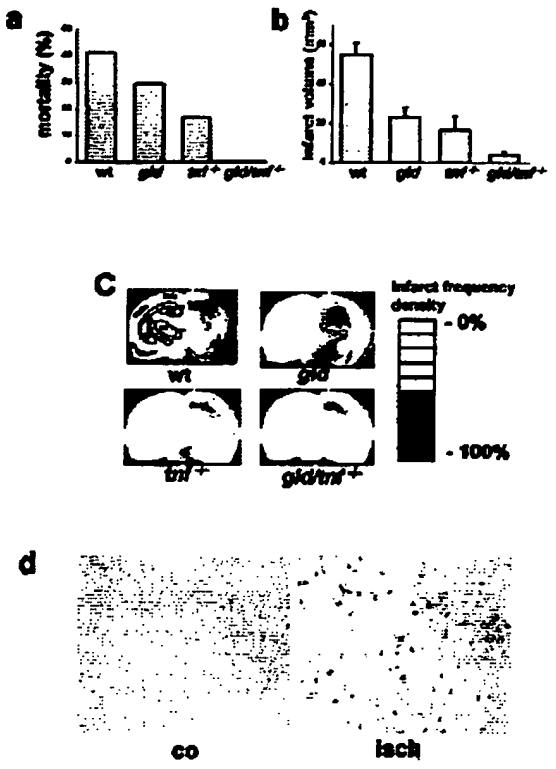

Figure 2 Ischemic brain damage is reduced in *gld*, $tnf^{-/-}$ and *gld*/$tnf^{-/-}$ mice. (a) mortality within 24 h after occlusion of the middle cerebral artery (MCA) in wild-type (n=14), *gld* (n=17), $tnf^{-/-}$ (n=13), and *gld*/$tnf^{-/-}$ (n=15) mice. (b) Infarct volume after transient focal ischemia in wild-type (n=9), *gld* (n=8), $tnf^{-/-}$ (n=7), and *gld*/$tnf^{-/-}$ (n=8) mice. Animals were subjected to 90 min occlusion of the MCA and 24 h reperfusion as described. Cryostat coronal sections, 20 μm thick and 400 μm apart from each other were silver-stained. The volume of infarction was determined by numeric integration of areas of marked pallor with section thickness. Data are presented as the means ± S.E.M. Significance was determined by comparing *gld*, $tnf^{-/-}$, and *gld*/$tnf^{-/-}$ mice to wild-type mice by using the Mann-Whitneys' U-test ($P<0.01$, $P<0.01$, and $P<0.0001$, respectively). (c) Image analysis of the regional infarct frequencies of the coronal section at bregma −2.3 mm from wild-type, *gld*, $tnf^{-/-}$, and *gld*/$tnf^{-/-}$ mice reveals a relative sparing of the motor and somatosensory cortex and striatum in *gld* mice and of the entire adjacent neocortex, striatum and thalamus in $tnf^{-/-}$ mice. In *gld*/$tnf^{-/-}$ mice the hippocampus was almost the only affected area. MCx, motor cortex; SSCx, somatosensory cortex; Hc, hippocampus; Th, thalamus; St, Striatum. (d) Immunohistochemical analysis for CD95L was performed in brain sections from wild-type subjected to 90 min MCA occlusion and 24 h reperfusion. CD95L was found in cells in the ischemic penumbra (isch) but not in the corresponding region in the contralateral hemisphere (co)

The regional infarct distribution in the coronal plane was analyzed by averaging infarct areas (coronal section at bregma −2.3 mm). The resulting frequency density map reveals a relative sparing of the motor and somatosensory cortex and striatum in *gld* mice and a relative sparing of the entire adjacent neocortex, striatum and thalamus in $tnf^{-/-}$ mice (Figure 2c). In *gld*/$tnf^{-/-}$ mice striatum, cortex and thalamus remain unaffected by the ischemic insult and damage is mainly restricted to the hippocampus (Figure 2c).

The spared areas in the $tnf^{-/-}$ and *gld* mice belong to the ischemic penumbra – a region surrounding the necrotic core with diminished cerebral blood flow where neurons are at risk of undergoing apoptosis. In these areas TNF has been reported to be expressed in neurons.[13] With regard to CD95L we already showed expression of this protein in the ischemic penumbra in the rat.[14] Here we found that in wt mice subjected to 90 min MCA occlusion and 24 h reperfusion, CD95L is expressed in the regions surrounding the necrotic core but not in the corresponding regions in the contralateral hemisphere (Figure 2d). Expression of CD95L was not detectable in the brains of sham-operated animals or in control stainings performed with isotype control IgG or without the first antibody, whereas it was found in tumors transfected with murine-CD95L and in the mouse thymus (data not shown).

CD95L and TNF mediate the recruitment of inflammatory cells following stroke

In vivo, cytokine production and adhesive events occur early following cerebral blood flow reduction.[29] TNF, produced by the ischemic parenchyma, contributes to the expression of cellular adhesion molecules of endothelial cells such as, intercellular adhesion molecule-1 (ICAM-1), vascular cell adhesion molecule-1 (VCAM-1) and endothelial-leukocyte adhesion molecule-1 (E-selectin); adhesion molecules facilitate the recruitment of inflammatory cells to the ischemic lesion. Similar chemotactic properties have been described for CD95L in tumors.[30,31] These data prompted us to ask whether in addition to the death promoting role of CD95L and TNF following ischemia, these two molecules could contribute to the ischemic injury through the recruitment of inflammatory cells. To address this question in brain sections from wt, *gld*, $tnf^{-/-}$ and *gld*/$tnf^{-/-}$ mice (each n=3) that underwent focal ischemia (90 min MCA occlusion and 24 h reperfusion) the number of infiltrating granulocytes and lymphocytes was determined by immunoautoradiography (Figure 3). Control stainings without first antibody or of brain sections from sham-operated animals were negative (data not shown). Quantitative analysis of autoradiograms standardized by infarcted volume, revealed a decreased granulocyte infiltration in $tnf^{-/-}$ and *gld*/$tnf^{-/-}$ mice (Figure 3). The extent of lymphocyte infiltration was similar in wt, in *gld* and in $tnf^{-/-}$ animals and higher in *gld*/$tnf^{-/-}$ mice, possibly due to persistent survival rather than to increased infiltration (Figure 3). These data confirm the chemotactic effect of TNF towards granulocytes following ischemia.

Treatment with anti-TNF and anti-CD95L antibodies reduces ischemic injury

To find out whether the data obtained from knockout animals can be the basis for therapy, we also investigated the effect of *in vivo* therapeutic neutralization of TNF and CD95L following focal ischemia *in vivo*. Wild type mice were i.p. injected with anti-TNF and anti-CD95L antibodies (50 μg each) 30 min after occlusion of MCA – a time point which would reflect later time points in humans, since the basal metabolic rate in humans is lower than in rodents.[32] This led to a significant

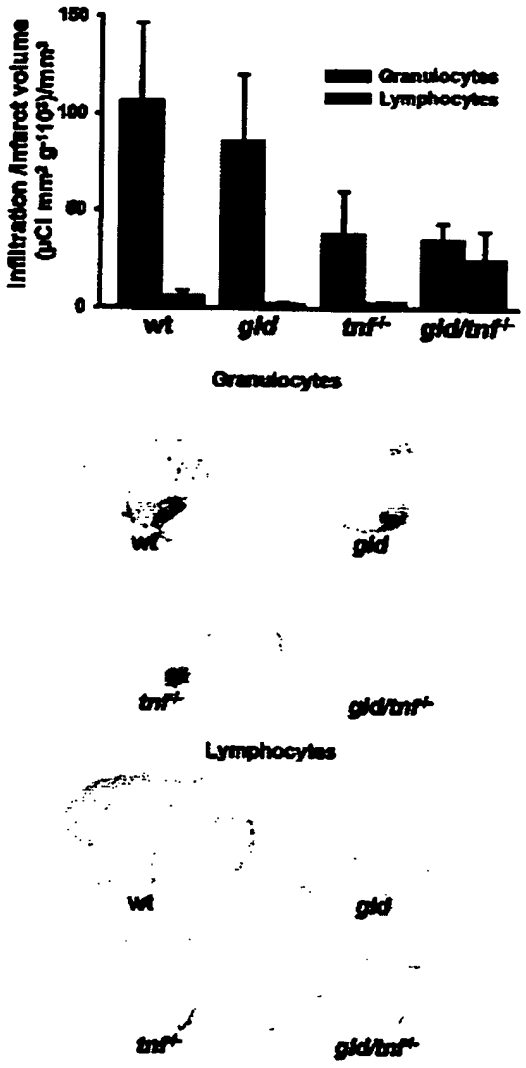

Figure 3 Infiltration by inflammatory cells of the ischemic brain. Infiltration by granulocytes or lymphocytes of the ischemic brains from wild-type, *gld*, *tnf*$^{-/-}$ and *gld/tnf*$^{-/-}$ mice (each n=3) was quantified by autoimmunoradiography. Brain sections from brains subjected to focal ischemia (90 min MCA occlusion and 24 h reperfusion) were incubated with primary antisera against GR1 (for granulocytes) or CD3 (for lymphocytes). Stainings were revealed by autoradiography (representative autoradiography, lower panel). Inflammatory infiltrates in the ischemic hemisphere were quantified by measuring the area and the optical density (OD) of the infiltrates (upper panel) divided by the mean infarct volume of the examined animals. Data are presented as the means ± S.E.M. (n=3)

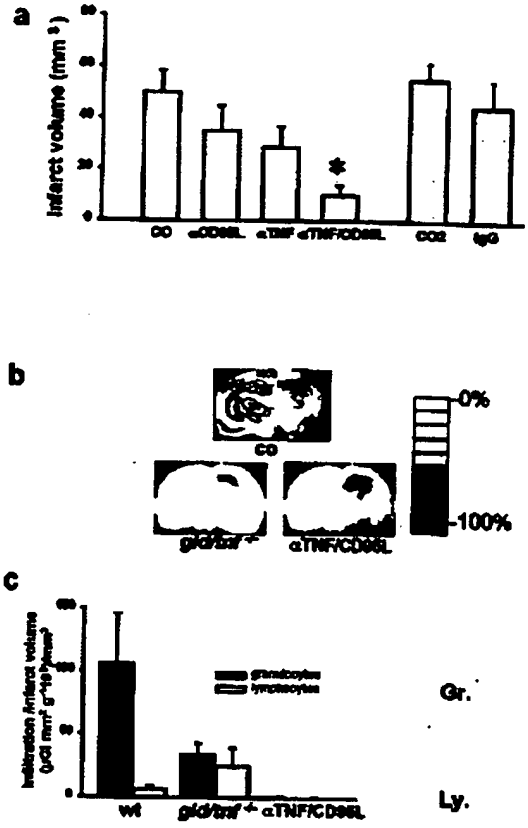

Figure 4 Infarct extension and inflammatory infiltrates of the ischemic brain are significantly reduced by anti-TNF and anti-CD95L antibodies. Wild-type animals subjected to 90 min MCA occlusion and 24 h reperfusion were i.p. treated 30 min after occlusion with saline (co; n=9), or with antibodies against TNF (αTNF), CD95L (αCD95L) or both (αTNF/CD95L) (n=10 each group) in a double blind manner. In a second series of experiments animals were either treated with saline (co2; n=9) or IgG (IgG; n=7). Animals who did not exhibit an infarct (27, 40, 40, 50 and 10% of co, αTNF, αCD95L and αTNF/CD95L and IgG, respectively) or died before the 24 h period (33, 10, 10, 30 and 20% of co, αTNF, αCD95L, co2 and IgG) were not included in the examination of infarct volumes. Cryostat brain coronal section from 20 μm thick, 400 μm apart from each other, were silver-stained. (a) The volume of infarction was determined by numeric integration of areas of marked pallor with section thickness. Data are presented as the means ± S.E.M. Significance was determined by comparing saline-treated animals with the other groups by using the Mann-Whitney's test (*P<0.004). (b) Image analysis of the regional infarct frequencies of the coronal section at bregma −2.3 mm from co, αTNF/CD95L and gld/tnf$^{-/-}$ mice reveals a relative sparing of the motor and somatosensory cortex and striatum in αTNF/CD95L-treated mice. MCx, motor cortex; SSCx, somatosensory cortex; Hc, hippocampus; Th, thalamus; St, Striatum. (c) The number of granulocytes and lymphocytes in the ischemic hemisphere were quantified by autoimmunoradiography. Brain sections from animals subjected to focal ischemia (90 min MCA occlusion and 24 h reperfusion) were incubated with primary antibodies against GR1 (for granulocytes) and CD3 (for lymphocytes). Stainings were revealed by autoradiography (representative autoradiography, right panel). Inflammatory infiltrates in the ischemic hemisphere were quantified by measuring the area and the optical density (OD) of the infiltrates (left panel) divided by the mean infarct volume of the examined animals. Data are presented as the means ± S.E.M. (n=3)

reduction in the infarct volume by 70% in double treated compared to saline treated animals (18.04 ± 4.87 mm^3, n=5 in treated mice *versus* z50.66 ± 6.32 mm^3, n=9, P<0.004; Figure 4a). Inhibition of CD95L and TNF activities had an additive effect in reducing infarct volumes, as assessed by two factorial variance analysis. By contrast, separate inhibition of CD95L or TNF did not significantly reduce infarct volumes. In a second series of experiments was found that the injection of control IgG did not influence infarct volumes when compared to saline-treated animals (Figure 4a).

The regional infarct distribution in the coronal plane of anti-TNF/CD95L-treated animals was analyzed by averaging infarct areas (at the coronal level bregma −2.3 mm). The resulting frequency density map shows a sparing of the motor cortex, the lateral thalamic nuclei and the striatum (Figure 4b). Also, in these animals, inflammatory infiltrates were nearly undetectable (Figure 4c).

The functionality of rescued neurons was examined by testing the motor coordination of treated mice 3 days after reperfusion. Thus, anti-TNF and anti-CD95L antibodies (50 μg each) were injected twice i.p. 30 min and 24 h after occlusion of MCA. All mice in which focal ischemia was induced and that were not antibody-treated died before the end of the observation period (n=5), whereas mortality in the treated group (n=10) was only 30% (Figure 5a). Six non-treated sham-operated animals (so-utr) and five anti-TNF/CD95L-treated mice which underwent 90 min occlusion of MCA and 3 day reperfusion were tested on a rotarod and on stationary rods. Retention times on the rotarod displayed by treated animals did not significantly differ from those exhibited by sham-operated animals (Figure 5b). Motor coordination on stationary rods paralleled these results (data not shown). Likewise, maintenance of axial balance, as assessed by the first swimming experience of the mice, was comparable in untreated sham-operated and stroke-treated animals (data not shown). Even animals with low retention time on the rotarod exhibited unimpaired axial balance.

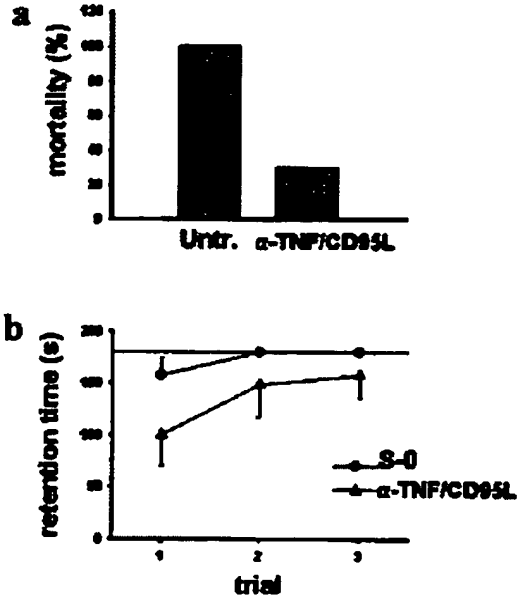

Figure 5 Neutralization of CD95L and TNF reduces mortality and improves motor performance of stroke animals. (a) Percentage of mortality within 3 days after occlusion of the MCA in animals untreated (n=5; wt) or treated with anti-TNF and anti-CD95L antibodies (n=10; α-TNF/CD95L). (b) Retention times on accelerated rotarod for untreated sham-operated animals (s-o; n=6) and treated animals (α-TNF/CD95L; n=5)

Discussion

In this study we report that TNF and CD95L additively contribute to ischemic damage, both by triggering ischemic cell death and by recruiting inflammatory cells to the site of the lesion. Moreover, the therapeutic neutralization of these ligands leads to preservation of neuron functionality and increased survival of the animals.

CD95-L and TNF additively induce ischemic brain damage

The protection provided by the absence of TNF disagrees with the report by Bruce *et al.* (1996) of an enhanced ischemic damage in mice lacking TNF-receptor-1 (TNF-R1; also called p55) or both TNF-R1 and TNF-R2 (also called p75). Something that might be due to the use of a different mouse strain (C57BL/6 × 129) and a shorter occlusion time of 1 h by this group.

In previous studies we have shown that apoptotic cells in the penumbra are mostly neurons and express CD95L.[14] Here, we report that CD95L is also generated in the ischemic penumbra in the mouse (Figure 2). Expression of TNF mRNA and protein already occurs within 2 h after induction of ischemia[12,13,33,34] and is followed by the expression of CD95L at 12 h.[14] CD95L expression may be induced by TNF, e.g. through transcription factors such as c-Jun or NF-κB,[35,36] like it has been described in human astrocytes.[37] Thus, these two ligands, TNF and CD95L might compliment each other in the induction of stroke damage. Nevertheless, the fact that neurons from *gld/tnf*$^{-/-}$ could not be cultured *in vitro*, indicate that these ligand might have other functions in neurons besides the triggering of the death program that should be elucidated in further studies.

The deleterious effect of the CD95 and the TNF system may indeed be related to effects not directed to neurons themselves but to other cells such as microglia, which would in turn produce killer chemokines,[38] or leucocytes. In support of this idea is recent work which shows that inhibition of caspase-1 induces long-lasting neuroprotection in cerebral ischemia by reducing apoptosis and proinflammatory cytokines.[39] Nevertheless, the decrease in cell death *in vitro* in primary neurons in the absence of a functional CD95 or TNF system suggests a harmful role of these systems, at least in part, directed to neurons. Besides, one could argue that the dramatic protection exhibited by *gld/tnf*$^{-/-}$ mice is due to a primary defect in the glia/neuron interaction arising from the mutation in the CD95L and the TNF ligands. This is excluded by the enhanced neuroprotection also achieved by the acute therapeutic neutralization of both CD95 and TNF systems in wild-type animals.

Analysis of infarct frequencies in the coronal plane in *gld/tnf*$^{-/-}$ mice (Figure 1c) reveals that hippocampus was almost the only affected area. Hippocampus is the most vulnerable brain area following ischemia possibly due to its higher density of glutamate receptors. Prominent glutamate stimulation through the ischemic insult can favor severe excitotoxicity in which CD95 and TNF systems may play a minor role.

CD95L and TNF promote inflammation in the ischemic brain

Ischemia-mediated breakdown of the blood-brain barrier (BBB)[40-42] leads to the unique exposure of relatively sequestered CNS antigens to the peripheral circulation. This results in a deleterious immune response that enhances neuronal damage[43] and underlies the transition from ischemic to inflammatory injury. Among inflammatory cells, granulocytes invade the infarct and its boundary zone within hours with a peak at 24 h, whereas T cells start infiltrating the infarct region from day 1 onwards, with a peak around day 7.[44] Granulocyte infiltration is preceded by an increased expression of cytokine-induced neutrophil chemoattractant (CINC).[44] Accordingly, at 24 h after MCA occlusion, we detected inflammatory infiltration with a nearly exclusive participation of granulocytes in the ischemic hemisphere. This infiltration could be reduced in the absence of TNF and/or CD95L, consistent with the known chemotactic properties of these two ligands.[30,31,45] The recruitment of inflammatory cells to the site of the lesion, like the induction of ischemic neuronal death *in vitro*, was more effectively inhibited in the absence of TNF than in the absence of CD95L.

Strikingly, however, infarct volumes in *tnf*$^{-/-}$ and *gld* mice were not significantly different. This similar outcome might be explained by the additional ability of CD95L to activate the cytotoxic machinery of granulocytes.[30,31] Thus, CD95L might enhance the induction of inflammatory damage by TNF in stroke.

Possible consequences for the treatment of stroke

Currently, neuroprotective strategies strive to maintain viability of ischemic neurons until reperfusion can be normally re-established. However, cerebral reperfusion is followed by destruction of microvasculature and subsequent inflammatory events. Therefore, protection towards both reperfusion damage and ischemic death emerges as the ideal therapy for stroke either in combination with thrombolytic therapy or alone if thrombolysis is precluded.

In the microcirculatory failure and the inflammatory events that follow reperfusion different effectors participate, such as the intercellular adhesion molecule-1 (ICAM-1) or CD18 (the beta2-integrin subunit on granulocytes and ligand for ICAM-1). The absence of ICAM-1 or CD18 mitigates stroke damage by improving microcirculation in the ischemic penumbra.[46,47] Moreover, in ICAM-1 knockout animals, further granulocyte depletion enhances protection.[46] Interestingly, ICAM-1 expression in the ischemic brain is enhanced by TNF.[20] Early studies in a rabbit model of acute stroke indicated the potential of the combination of thrombolytic therapy with anti-ICAM-1 antibodies.[48] In comparison, neutralization of TNF and CD95L, not only attenuates reperfusion damage but also helps to maintain neuronal viability until reperfusion is achieved.

Apoptotic cell death and inflammation are also important components of the pathophysiology of other acute and chronic neurodegenerative diseases such as Parkinson's, Alzheimer's and Prion diseases, HIV encephalopathy, and multiple sclerosis. Therefore, the therapeutical neutralization of CD95L and TNF might have a more global application in acute neurodestruction as well as in chronic neurodegenerative diseases.

Materials and Methods

Cell culture and experimental treatment *in vitro*

Primary neuronal cultures were prepared from day 15 to 17 fetal mice as previously described.[14] In brief, cortical neurons were obtained after trituration in MEM medium with 20% horse serum, 25 mM glucose and 2 mM L-glutamine (all from Gibco/Life Technologies, Scotland) following a 30 min digestion in 0.025 trypsin/saline solution. Cells were plated in 24 well plates coated with polyornithine (Sigma, Germany). After 4 days, cells were treated with cytosine-arabinoside (5 μM) for another 4 days to inhibit proliferation of non-neuronal cells. Thereafter, cell cultures were maintained in MEM, 10% horse serum, 5% fetal bovine serum, 25 mM glucose and 2 mM L-glutamine in a 8% CO_2 humidified incubator at 37°C. Neurons were allowed to mature for at least 8 days in culture before being used for experiments. The proportion of glial cells in the cultures was less than 10%, as assessed by an antibody against glial-fibrillary-acidic protein (GFAP; data not shown).

Oxygen-glucose deprivation *in vitro*

Combined oxygen-glucose deprivation (OGD) was performed as previously described[25] with minor modifications. The culture medium was replaced with MEM, 1% horse serum and 2 mM L-glutamine. The cultures were kept in an anaerobic chamber for 6 h containing the gas mixture, 5% H_2/90% N_2/5% CO_2, and GasPak Catalyst replacement charges (Becton Dickinson, Germany), maintained at 37°C and 100% humidity. Combined oxygen-glucose deprivation was terminated by removal of the cultures from the chamber and adding horse and fetal bovine serum and glucose to a final concentration of 10%, 5% and 25 mM, respectively. The cultures were returned to a humidified incubator containing 8% CO_2 and atmospheric oxygen at 37°C for another 3, 18 or 24 h. Human IgG1 (Sigma, Deisenhofen, Germany), CD95-Fc and TNF-R2-Fc (20 μg/ml each) were added to the culture medium 5 min prior to the induction of OGD.

Due to the impossibility to analyze cell death in primary neurons by forward side scatter analysis (FACS) the percentage of cell death was assessed by Trypan-blue exclusion and given as % of specific death. This was calculated as follows:

$$\%\ \text{specific death} = \frac{(\text{assessed death} - \text{spontaneous death})}{(100 - \text{spontaneous death})} \times 100$$

Spontaneous cell death was of 12% ± 0.09 for neurons from *tnf*$^{-/-}$ mice, 10% ± 0.73 for neurons from *gld* mice and of 15% ± 0.87 for neurons from C57BL/6 wild-type mice. All data are given as the means ± S.D. (n=3).

Ischemic animal model

In wild-type, *gld*, *tnf*$^{-/-}$ and *gld/tnf*$^{-/-}$ mice, all matched for age (mean 100 days) and weight (mean 24 g), focal cerebral ischemia was induced by occlusion of the middle cerebral artery (MCA) as described previously.[14] A surgical nylon thread was advanced from the lumen of the common carotid artery up to the anterior cerebral artery to block the origin of the MCA for 90 min. MCA blood flow was restored by withdrawing the nylon thread. Deep anesthesia was reached by

Ketamin and Rompun (150 mg/kg body weight each). Animals were kept under anesthesia and rectal temperature was controlled at or near 37°C with a Heating lamp throughout both the surgical procedure and the MCA occlusion period up to the time the animals recovered from anesthesia. A reduction of cerebral blood flow in the animals included in the study was indirectly confirmed by a reduction in the silver infarct staining intensity.[49] After different reperfusion periods animals were deeply reanesthetized and killed by decapitation. To obtain physiological parameters, the right femoral artery was cannulated under ongoing anesthesia, blood pressure continually recorded, and samples for blood gas and glucose analysis taken 15 min before, 1 h after begin and 30 min after the end of MCA occlusion. Mice gender varied due to the availability in our animal facilities. Infarct outcome was not influenced by the sex of the animal (data not shown). All mice were on a C57BL/6 background to avoid known differences in infarct susceptibility dependent on the mice strain.[50]

For treatment experiments, anti-CD95L antibody (MFL3; Pharmingen, Germany) and anti-TNF antibody (V1q)[51] 50 μg each, were either i.p. injected 30 min and 24 h after occlusion of the MCA in 12-week-old male C57BL/6 in a double blind manner. In a second series of experiments mice were i.p. treated with saline or control hamster IgG (Pharmingen).

Measurement of infarct extension

Mice were subjected to MCA filament occlusion for 90 min and reperfused for 24 h as described. The time point of 24 h was chosen for reasons of practicability (number of animals and amounts of purified proteins used) and because at this time the major damage has already taken place and infarct volumes do not significantly differ from those thereafter. Forebrains were cut and cryostat coronal sections 20 μm thick 400 μm apart from each other, were silver-stained. In brief, sections were impregnated with a silvernitrate/lithiumcarbonate solution for 2 min and developed with a hydrochinone/formaldehyde solution for 3 min.[49] Stained sections were directly scanned (MCID-M4, 3.0; Imaging res. Inc.). The volume of infarction was determined by numeric integration of the scanned areas of marked pallor corrected for brain edema x section thickness using digital planimetry. All data are given as mean $\pm$ standard error of the mean. Significance was measured using the Mann-Whitney *U*-test. To generate infarct frequency distribution maps,[52] the respective sections of each series were scanned, infarcts delineated, and projected on a mask. Averaging was done with Scion Image β 3.b.

Immunohistochemical analysis of CD95L and TNF expression

Coronal cryostat sections (20 μm) from wild type mice that underwent 90 min MCA occlusion and 24 h reperfusion were processed for immunohistochemistry. Sections were incubated with a polyclonal antibody against CD95L (P62).[53] Immunoreactivity of CD95L protein was visualized by diaminobenzidine (Alexis, Germany). Neither CD95L nor TNF were detectable in the brains of sham-operated animals or in control stainings performed without the first antibody or isotype control IgG, whereas it was detectable in the mouse thymus and in sections from tumors transfected with murine-CD95L (data not shown).

Detection of infiltration of inflammatory cells

Coronal cryostat sections (20 μm) from wt, *gld*, *tnf*$^{-/-}$ and *gld/tnf*$^{-/-}$ mice that underwent 90 min MCA occlusion and 24 h reperfusion were processed for immunoautoradiography. Sections were incubated for 24 h with a monoclonal antibody against GR1 (Ly-1, Pharmingen, Germany) or a monoclonal antibody against CD3 (Chemicon, USA). Thereafter, sections were incubated with a ^{125}I-labeled secondary antibody (Biotrend, Germany). Sections were exposed together with a [I^{125}] standard set on a Kodak MinR1 x-ray film for 21 days. Granulocyte or lymphocyte infiltration in the ischemic hemisphere was assessed by measuring the optical density and the area of the infiltrates with an image analyzing system (MCID, Imaging Research Inc., Ontario, Canada).

Motor coordination

Male C57BL/6 mice 12–16-week-old were placed on a fixed horizontal wood rod or a plexiglass rod (1 cm diameter, 50 cm length, and 40 cm above ground), and the time the animal remained on the rod was measured. For the rotarod examination (Ugo Basile Biol. Res. App.), the mouse was placed on a gritted plastic roller, which was accelerated from 4 to 40 r.p.m. in 5 min. Retention times were recorded for 180 s.

Acknowledgements

TNF k.o. mice were kindly provided by M Mike. This work was supported by a grant of the University of Heidelberg to A Martin-Villalba.

References

1. Poungvarin N (1998) Stroke in the developing world. Lancet 352: 19–22
2. Ginsberg MD (1995) The concept of the therapeutic window: a synthesis of critical issues. In: Moskowitz MA, Caplan LR, eds. (Cerebrovascular disease. 19th Princetown Stroke Conference. Newton: Butterworth Heinemann), pp.331–352
3. Linnik MD, Zobrist RH and Hatfield MD (1993) Evidence supporting a role for programmed cell death in focal cerebral ischemia in rats. Stroke 24: 2002–2008
4. Itoh N and Nagata S (1993) A novel protein domain required for apoptosis. J. Biol. Chem. 268: 10932–10937
5. Oehm A, Behrmann I, Falk W, Pawlita M, Maier G, Klas C, Li-Weber M, Richards S, Dhein J, Trauth BC, Martin-Villalba A, Hahne M, Kleber S, Vogel J, Schenkel J and Krammer PH. (1992) Purification and molecular cloning of the APO-1 cell surface antigen, a member of the tumor necrosis factor/nerve growth factor receptor superfamily. Sequence identity with the Fas antigen. J. Biol. Chem. 267: 10709–10715
6. Smith CA, Davis T, Anderson D, Solam L, Beckmann MP, Jerzy R, Dower SK, Cosman D and Goodwin RG (1990) A receptor for tumor necrosis factor defines an unusual family of cellular and viral proteins. Science 248: 1019–1023
7. Tartaglia LA, Ayres TM, Wong GH and Goeddel DV (1993) A novel domain within the 55 kd TNF receptor signals cell death. Cell 74: 845–853
8. Kischkel FC, Hellbardt S, Behrmann I, Germer M, Pawlita M, Krammer PH and Peter ME (1995) Cytotoxicity-dependent APO-1 (Fas/CD95)-associated proteins form a death-inducing signaling complex (DISC) with the receptor. EMBO J. 14: 5579–5588
9. Medema JP, Scaffidi C, Kischkel FC, Shevchenko A, Mann M, Krammer PH and Peter ME (1997) FLICE is activated by association with the CD95 death-inducing signaling complex (DISC). EMBO J. 16: 2794–2804
10. Scaffidi C, Fulda S, Srinivasan A, Friesen C, Li F, Tomaselli KJ, Debatin KM, Krammer PH and Peter ME (1998) Two CD95 (APO-1/Fas) signaling pathways. EMBO J. 17: 1675–1687
11. Namura S, Zhu J, Fink K, Endres M, Srinivasan A, Tomaselli KJ, Yuan J and Moskowitz MA (1998) Activation and cleavage of caspase-3 in apoptosis induced by experimental cerebral ischemia. J. Neurosci. 18: 3659–3668

12. Buttini M, Appel K, Sauter A, Gebicke-Haerter PJ and Boddeke HW (1996) Expression of tumor necrosis factor alpha after focal cerebral ischemia in the rat. Neuroscience 71: 1–16
13. Liu T, Clark RK, McDonnell PC, Young PR, White RF, Barone FC and Feuerstein GZ (1994) Tumor necrosis factor α expression in ischemic neurons. Stroke 25: 1481–1488
14. Martin-Villalba A, Herr I, Jeremias I, Hahne M, Brandt R, Vogel J, Schenkel J, Herdegen T and Debatin KM (1999) CD95 ligand (Fas-L/APO-1L) and tumor necrosis factor-related apoptosis-inducing ligand mediate ischemia-induced apoptosis in neurons. J. Neurosci. 19: 3809–3817
15. Matsuyama T, Hata R, Yamamoto Y, Tagaya M, Akita H, Uno H, Wanaka A, Furuyama J and Sugita M (1995) Localization of Fas antigen mRNA induced in postischemic murine forebrain by in situ hybridization. Mol. Brain Res. 34: 168–172
16. Saito K, Suyama K, Nishida K, Sei Y and Basile AS (1996) Early increases in TNF-alpha, IL-6 and IL-1 beta levels following transient cerebral ischemia in gerbil brain. Neurosci. Lett. 206: 149–152
17. Nawashiro H, Martin D and Hallenbeck JM (1997) Neuroprotective effects of TNF binding protein in focal cerebral ischemia. Brain Res. 778: 265–271
18. Meistrell ME, Botchkina GJ, Wang H, Di Santo E, Cockroft KM, Bloom O, Vishnubhakat JM, Ghezzi P and Tracey KJ (1997) Tumor necrosis factor is a brain damaging cytokine in cerebral ischemia. Shock 8: 341–348
19. Barone FC, Arvin B, White RF, Miller A, Webb CL, Willette RN, Lysko PG and Feuerstein GZ (1997) Tumor necrosis factor-alpha. A mediator of focal ischemic brain injury. Stroke 28: 1233–1244
20. Yang GY, Gong C, Qin Z, Ye W, Mao Y and Bertz AL (1998) Inhibition of TNFα attenuates infarct volume and ICAM-1 expression in ischemic mouse brain. NeuroReprot 9: 2131–2134
21. Bruce AJ, Boling W, Kindy MS, Peschon J, Kraemer PJ, Carpenter MK, Holtsberg FW and Mattson MP (1996) Altered neuronal and microglial responses to excitotoxic and ischemic brain injury in mice lacking TNF receptors. Nat. Med. 2: 788–794
22. Gary DS, Bruce-Keller AJ, Kindy MS and Mattson MP (1998) Ischemic and excitotoxic brain injury is enhanced in mice lacking the p55 tumor necrosis factor receptor. J. Cereb. Blood Flow Metab. 18: 1283–1287
23. Nawashiro H, Tasaki K, Ruetzler CA and Hallenbeck JM (1997) TNF-alpha pretreatment induces protective effects against focal cerebral ischemia in mice. J. Cereb. Blood Flow Metab. 17: 483–490
24. Spanaus KS, Schlapbach R and Fontana A (1998) TNF-alpha and IFN-gamma render microglia sensitive to Fas ligand-induced apoptosis by induction of Fas expression and down-regulation of Bcl-2 and Bcl-xL. Eur. J. Immunol. 28: 4398–4408
25. Monyer H, Giffard RG, Hartley DM, Dugan LL, Goldberg MP and Choi DW (1992) Oxygen or glucose deprivation-induced neuronal injury in cortical cell cultures is reduced by tetanus toxin. Neuron. 8: 967–973
26. Marino MW, Dunn A, Grail D, Inglese M, Noguchi Y, Richards E, Jungbluth A, Wada H, Moore M, Williamson B, Basu S and Old LJ (1997) Characterization of tumor necrosis factor-deficient mice. Proc. Natl. Acad. Sci. USA 94: 8093–8098
27. Cohen PL and Eisenberg RA (1991) Lpr and gld: single gene models of systemic autoimmunity and lymphoproliferative disease. Annu. Rev. Immunol. 9: 243–269
28. Eliasson MJ, Sampei K, Mandir AS, Hurn PD, Traystman RJ, Bao J, Pieper A, Wang ZQ, Dawson TM, Snyder SH and Dawson VL (1997) Poly (ADP-ribose)polymerase gene disruption renders mice resistant to cerebral ischemia. Nature Med. 3: 1089–1095
29. del Zoppo GJ (1997) Microvascular responses to cerebral ischemia/inflammation. Ann. NY Acad. Sci. 823: 132–147
30. Seino K, Kayagaki N, Okumura K and Yagita H (1997) Antitumor effect of locally produced CD95 ligand. Nat. Med. 3: 165–170
31. Chen JJ, Sun Y and Nabel GJ (1998) Regulation of the proinflammatory effects of Fas ligand (CD95L). Science 282: 1714–1717
32. Siesjö BK (1992) Pathophysiology and treatment of focal cerebral ischemia. Part I: Pathophysiology. J. Neurosurg. 77: 169–184
33. Szaflarski J, Burtrum D and Silverstein FS (1995) Cerebral hypoxia-ischemia stimulates cytokine gene expression in perinatal rats. Stroke 26: 1093–1100
34. Feuerstein GZ, Wang X and Barone FC (1997) Inflammatory gene expression in cerebral ischemia and trauma. Potential new therapeutic targets. Ann. NY Acad. Sci. 825: 179–193
35. Le-Niculescu H, Bonfoco E, Kasuya Y, Claret FX, Green DR and Karin M (1999) Withdrawal of survival factors results in activation of the JNK pathway in neuronal cells leading to Fas ligand induction and cell death. Mol. Cell. Biol. 19: 751–763
36. Li-Weber M, Laur O, Dern K and Krammer PH (2000) T cell activation-induced and HIV tat-enhanced CD95(APO-1/Fas) ligand transcription involves NF-kappaB. Eur. J. of Immunology 30: 661–670
37. Choi C, Park J, Lee J, Lim JH, Shin EC, Ahn YS, Kim CH, Kim SJ, Kim JD, Choi IS and Choi IH (1999) Fas ligand and Fas are expressed constitutively in human astrocytes and the expression increases with IL-1, IL-6, TNF-alpha, or IFN-gamma. J. Immunol. 162: 1889–1895
38. Kaul M and Lipton SA (1999) Chemokines and activated macrophages in HIV gp120-induced neuronal apoptosis. Proc. Natl. Acad. Sci. USA 96: 8212–8216
39. Rabuffetti M, Sciorati C, Tarozzo G, Clementi E, Manfredi AA and Beltramo M (2000) Inhibition of caspase-1-like activity by Ac-Tyr-Val-Ala-Asp-Chloromethyl ketone induces long-lasting neuroprotection in cerebral ischemia through apoptosis reduction and decrease of proinflammatory cytokines. J. Neurosci. 20: 4398–4404
40. Hohlbaum AM, Moe S and Marshak-Rothstein A (2000) Opposing effects of transmembrane and soluble Fas ligand expression on inflammation and tumor cell survival. J. Exp. Med. 191: 1209–1220
41. Dobbin J, Crockard HA and Ross-Russell R (1989) Transient blood-brain barrier permeability following profound temporary global ischaemia: an experimental study using 14C-AIB. J. Cereb. Blood Flow Metab. 9: 71–78
42. Nagahiro S, Goto S, Korematsu K, Sumi M, Takahashi M and Ushio Y (1994) Disruption of the blood-cerebrospinal fluid barrier by transient cerebral ischemia. Brain Res. 633: 305–311
43. Becker KJ, McCarron RM, Ruetzler C, Laban O, Sternberg E, Flanders KC and Hallenbeck JM (1997) Immunologic tolerance to myelin basic protein decreases stroke size after transient focal cerebral ischemia. Proc. Natl. Acad. Sci. USA 94: 10873–10878
44. Stoll G, Jander S and Schroeter M (1998) Inflammation and glial responses in ischemic brain lesions. Progr. Neurobiol. 56: 149–171
45. Mano-Hirano Y, Sato N, Sawasaki Y, Haranaka K, Satomi N, Narfuchi H and Goto T (1987) Inhibition of tumor-induced migration of bovine capillary endothelial cells by mouse and rabbit tumor necrosis factor. J. Natl. Cancer Inst. 78: 115–120
46. Kitagawa K, Matsumoto M, Mabuchi T, Yagita Y, Ohtsuki T, Hori M and Yanagihara T (1998) Deficiency of intercellular adhesion molecule 1 attenuates microcirculatory disturbance and infarction size in focal cerebral ischemia. J. Cereb. Blood Flow Metab. 18: 1336–1345
47. Prestigiacomo CJ, Kim SC, Connolly Jr ES, Liao H, Yan SF and Pinsky DJ (1999) CD18-mediated neutrophil recruitment contributes to the pathogenesis of reperfused but not nonreperfused stroke. Stroke 30: 1110–1117
48. Bowes MP, Rothlein R, Fagan SC and Zivin JA (1995) Monoclonal antibodies preventing leukocyte activation reduce experimental neurologic injury and enhance efficacy of thrombolytic therapy. Neurology 45: 815–819
49. Vogel J, Mobius C and Kuschinsky W (1999) Early delineation of ischemic tissue in rat brain cryosections by high-contrast staining. Stroke 30: 1134–1141
50. Connolly ES, Winfree CJ, Stern DM, Solomon RA and Pinsky DJ (1996) Procedural and strain-related variables significantly affect outcome in a murine model of focal cerebral ischemia. Neurosurgery 38: 523–531
51. Echtenacher B, Falk W, Mannel DN and Krammer PH (1990) Requirement of endogenous tumor necrosis factor/cachectin for recovery from experimental peritonitis. J. Immunol. 145: 3762–3768
52. Schneider A, Martin-Villalba A, Weih F, Vogel J, Wirth T and Schwaninger M (1999) NF-kappaB is activated and promotes cell death in focal cerebral ischemia. Nat. Med. 5: 554–559
53. Hahne M, Rimoldi D, Schroter M, Romero P, Schreier M, French LE, Schneider P, Bornand T, Fontana A, Lienard D, Cerottini J and Tschopp J (1996) Melanoma cell expression of Fas(Apo-1/CD95) ligand: implications for tumor immune escape. Science 274: 1363–1368

EXHIBIT I

THE JOURNAL OF BIOLOGICAL CHEMISTRY
Vol. 272, No. 51, Issue of December 19, pp. 32401–32410, 1997
Printed in U.S.A.

TWEAK, a New Secreted Ligand in the Tumor Necrosis Factor Family That Weakly Induces Apoptosis*

(Received for publication, July 10, 1997, and in revised form, September 22, 1997)

Yves Chicheportiche‡, Paul R. Bourdon§, Haoda Xu§, Yen-Ming Hsu§, Hamish Scott¶, Catherine Hession§, Irene Garcia‡, and Jeffrey L. Browning§‖

From the ‡Department of Pathology and ¶Department of Genetics and Microbiology, University of Geneva, 1211 Geneva 4, Switzerland and the §Departments of Cell Biology, Molecular Genetics, and Protein Chemistry, Biogen, Cambridge, Massachusetts 02142

The members of the tumor necrosis factor (TNF) family play pivotal roles in the regulation of the immune system. Here we describe a new ligand in this family, designated TWEAK. The mouse and human versions of this protein are unusually conserved with 93% amino acid identity in the receptor binding domain. The protein was efficiently secreted from cells indicating that, like TNF, TWEAK may have the long range effects of a secreted cytokine. TWEAK transcripts were abundant and found in many tissues, suggesting that TWEAK and TRAIL belong to a new group of widely expressed ligands. Like many members of the TNF family, TWEAK was able to induce interleukin-8 synthesis in a number of cell lines. The human adenocarcinoma cell line, HT29, underwent apoptosis in the presence of both TWEAK and interferon-γ. Thus, TWEAK resembles many other TNF ligands in the capacity to induce cell death; however, the fact that TWEAK-sensitive cells are relatively rare suggests that TWEAK along with lymphotoxins α/β and possibly CD30L trigger death via a weaker, non-death domain-dependent mechanism.

Cytokines of the TNF[1] family are mediators of host defense and immune regulation. Members of this family act either locally through direct cell-to-cell contact or as secreted proteins capable of diffusing to more distant targets. These proteins are synthesized as type II membrane proteins with the extracellular C-terminal region mediating binding to the receptors of the TNF receptor (TNF-R) family (1). The TNF family of ligands and receptors comprises at least 14 unique signaling pathways including TNF, lymphotoxins (LT), Fas, CD27, CD30, CD40, 4–1BB, OX-40, TRAMP (also DR3, WSL-1, Apo-3), CAR-1, TRAIL, GITR, HVEM, osteoprotegerin, and NGF (2–12). Excluding NGF, each of these signaling pathways is likely to be involved in critical functions related to both the function and development of the immune system. For example, TNF acts primarily as an inflammatory cytokine coordinating host defenses in response to aggression by pathogens by activating a wide range of immunological and non-immunological mechanisms (13). The LT system is involved in the development of the peripheral lymphoid organs and the organization of splenic architecture (14, 15). CD40 is a key element in the regulation of the immunoglobulin response (16), and Fas signaling has been implicated in the mechanisms controlling peripheral tolerance and thymic selection (17, 18). Other members such as OX-40, 4–1BB, CD27, and CD30 are also involved in the control of various aspects of the immune system (19–22).

Some of these receptors upon activation can directly trigger the apoptotic death of many transformed cells, *e.g.* TNF-R55, Fas, TRAIL-R, and TRAMP (23). Clearly, Fas and possibly TNF-R55 and CD30 activation can induce cell death in non-transformed lymphocytes, which may play an immunoregulatory function (22–25). In general, death is triggered following the aggregation of death domains that reside on the cytoplasmic side of the TNF receptors. The death domain orchestrates the assembly of various signal transduction components that result in the activation of the caspase cascade (23). Some receptors lack canonical death domains, *e.g.* LTβ receptor and CD30 (26, 27), yet can induce cell death, albeit more weakly. It is likely that these receptors function primarily to induce cell differentiation *in vivo* and the death is an aberrant consequence in some transformed cell lines, although this picture is unclear, as studies on the CD30 null mouse suggest a role in death during negative selection in the thymus (22). Conversely, signaling through other pathways such as CD40 is required to maintain cell survival.

In this paper, we describe the mouse and human versions of a new member of this family, which we have called TWEAK. Like TNF, TWEAK is readily secreted from cells. Furthermore, we have prepared a recombinant soluble form of the molecule and used it to show that TWEAK signaling can induce cell death in an adenocarcinoma cell line.

EXPERIMENTAL PROCEDURES

Cells and Reagents—All cells were obtained from the American Type Culture Collection (ATCC, Rockville, MD) and grown in the recommended medium except for WEHI 164 clone 13, which was obtained from Dr. Kawashima (Geneva Biomedical Research Institute, Geneva, Switzerland). The HT29 subclone (HT29–14) and II-23 T cell hybridoma have been described previously (26, 28), and the TNF-sensitive ME180 subclone was obtained from Dr. Carl Ware. Recombinant FLAG-labeled hTRAIL was a generous gift from Dr. J. Tschopp (3), and anti-FLAG M2 monoclonal antibody was purchased from Eastman Kodak Corp. Anti-Fas CH11 was purchased from Kamiya Biomedical Co. (Seattle, WA), and LTα1/β2 was prepared as described previously (29).

Mouse TWEAK Cloning—The antisense oligonucleotide primer 5′-GTTCCAGGCCAGCCTGGG-3′ from the mouse erythropoietin se-

* This work was supported in part by Grants 31-42275.94 and 32-41729.94 (to I. G.) from the Swiss National Fund. The costs of publication of this article were defrayed in part by the payment of page charges. This article must therefore be hereby marked "*advertisement*" in accordance with 18 U.S.C. Section 1734 solely to indicate this fact.

The nucleotide sequence(s) reported in this paper has been submitted to the GenBank™/EBI Data Bank with accession number(s) AF030099 and AF030100.

‖ To whom correspondence should be addressed: Biogen, 12 Cambridge Center, Cambridge, MA 02142. E-mail: jeff_browning@biogen.com.

[1] The abbreviations used are: TNF, tumor necrosis factor; IL, interleukin; TNF-R, TNF receptor; NGF, nerve growth factor; RACE, rapid amplification of cDNA ends; LT, lymphotoxin; PCR, polymerase chain reaction; bp, base pair(s); kb, kilobase pair(s); EST, expressed sequence tag; PAGE, polyacrylamide gel electrophoresis; PBS, phosphate-buffered saline; FACS, fluorescence-activated cell sorting; IFN, interferon; EBNA, Epstein-Barr virus nuclear antigen; DAPI, 4′,6-diamidino-2-phenylindole.

quence was used in a 5'-RACE protocol following the recommendation of the manufacturer (5'-RACE system from Life Technologies, Inc.) in association with the Life Technologies-designed anchor primer. Template cDNA was made from RNA from 1-h adherent peritoneal macrophage RNA. After a 5-min denaturation at 94 °C, the cycling conditions were as follows: 35 cycles of 30 s at 94 °C, 30 s at 55 °C, and 3 min at 72 °C followed by a terminal extension step at 72 °C. Analysis of the PCR products on an agarose gel revealed two amplified fragments of 650 and 500 bp. The two fragments were excised from the gel, inserted in pBS-T vectors and sequenced. Northern hybridizations with ^{32}P-labeled random-primed fragments indicated that the 500-bp fragment hybridizing to a 1.4-kb RNA in macrophages. To determine the orientation of the cDNA, ^{32}P-labeled riboprobes in both directions were used in Northern hybridization. From the determined orientations and sequences, we derived two internal primers for the 1.4-kb mRNA: 5'-TCAGGTGCACTTTGATGAGG-3' and 5'-CTGTCAGCTCCTCCTGAG-3', which were used in 3'- and 5'-RACE PCR, respectively. The 3'-RACE experiment revealed a 750-bp fragment, which was inserted in a pBS-T vector and sequenced. It corresponded to the 3' end of the 1.4-kb RNA since the sequence possessed a poly(A) addition signal just prior to the poly(A) tract. The 5'-RACE did not revealed any band. The CLONTECH Marathon cDNA amplification kit was used to prepare a cDNA library from 1-h adherent macrophages. PCR used a 1040-bp TWEAK PCR fragment and the universal primer from the kit. The 1040-bp TWEAK PCR fragment was isolated using sense and antisense oligonucleotide primers from the determined cDNA sequence (5'-AGCAGGAGCCT-TCTCAGGAG-3' and 5'-GATCCAGGGAGGAGCTTGTCC-3'). This method resulted in the isolation of a fragment 60 bp longer on the 5' end than the original 1040-bp fragment.

Human TWEAK Cloning—A search of the EST data base revealed 1 human clone that was clearly homologous to the murine sequence. The clone 154742 (GenBank™ accession no R55379) has a 345-bp sequence 89% homologous to the murine cDNA. Two primers derived from the EST (5'-CCCTGCGCTGCCTGGAGGAA-3' and 5'-AGACCAGGGCC-CCTCAGTGA-3') were used in RT-PCR reactions to screen different tissues and libraries for the presence of hTWEAK transcripts. Products of the correct size were obtained from liver, spleen, lymph node, THP-1, and tonsil, but not from U937 mRNA. The 201-bp product was cloned and used to screen a λgt10 human tonsil cDNA library. One million plaque-forming units were plated at 10^5 plaque-forming units/plate. Duplicate lifts were made onto 20 × 20-cm nitrocellulose filters and hybridized with a probe prepared by random priming. The filters were hybridized overnight at 65 °C in plaque screen buffer (50 mM Tris, pH 7.5, 1 M NaCl, 0.1% sodium pyrophosphate, 0.2% polyvinylpyrrolidone, and 0.2% Ficoll) containing 10% dextran sulfate, 100 μg/ml tRNA, and 6×10^5 cpm/ml of probe. They were washed twice with plaque screen buffer and twice with 2 × SSC, 0.1% SDS at 65 °C. λ miniprep DNAs were prepared from positive colonies, and the clones with the largest inserts were selected for large scale DNA purification and DNA sequencing. The inserts were subcloned into the *Not*I site of pBlueScript SK+.

RNA Analysis—Either a 0.45-kb *Ppu*MI/*Bst*XI or a 1.25-kb *Nar*I/*Not*I fragment of the hTWEAK cDNA was labeled by random priming and used to probe human adult tissue and cell Northern blots purchased from CLONTECH. Blots were probed as per the manufacturer's instructions and given a final wash at 0.1 × SSC with 0.1% SDS at 50 °C.

Chromosomal Assignment—A panel of DNA from monochromosomal cell hybrids (HGMP Resource Center, Hinxton, Cambridge, UK) was used to amplify a 329-bp fragment with primers chosen in 3'-untranslated region that are not homologous to the murine sequence (5'-AGTCGTCCCAGGCTGCCGGCT-3' and 5'-CCTGAAGTGGGGTCTT-CTGGA-3'). Amplification was done for 40 cycles, 30 s at 94 °C, 90 s at 65 °C, and 90 s at 72 °C. Additional mapping was carried out using the same PCR primers on the Genebridge 4 Radiation Hybrid DNA panel (HGMP Resource Center), and the results were analyzed using the RHMAPPER program at the Whitehead Institute.

Expression of Recombinant hTWEAK Protein—A soluble expression construct combining the VCAM leader sequence, the Myc peptide tag, and the extracellular domain of hTWEAK was prepared similar to that described for LTβ (29). The following DNA fragments were isolated or synthesized, a *Not*I/blunt fragment encoding the VCAM leader, a pair of oligonucleotides encoding the Myc tag (5' blunt, 3' *Ppu*MI site; 5'-GAACAGAAACTCATCTCTGAAGAAGACCTG and 5'-GTCCAGGT-CTTCTTCAGAGATGAGTTTCTGTTC), a 0.45-kb *Ppu*MI/*Bst*XI fragment of TWEAK, and a 0.65-kb *Bst*XI/*Not*I fragment of TWEAK. The four fragments were ligated into a *Not*I/phosphatased pBlueScript vector. The *Not*I insert from this vector was transferred into the pFastBac1 vector (Life Technologies, Inc.) and used to generate recombinant baculovirus. Soluble TWEAK was prepared by infecting HiFiveTM insect cells at a multiplicity of infection of 10, and the medium was harvested after 2 days. The following items were added to the media: HEPES buffer to a final concentration of 25 mM, pH 7.4, 1 mM 4-(2-aminoethyl)benzenesulfonyl fluoride (AEBSF, Calbiochem), and 1 μg/ml pepstatin. The media was filtered and concentrated 10-fold by ultrafiltration over a Amicon 10-kDa cut-off filter. The concentrated medium was loaded directly onto a Fast S column, washed with 25 mM HEPES buffer, pH 7.4, with 0.4 M NaCl, and eluted with 0.7 M NaCl in the same buffer. N-terminal amino acid sequencing was performed on blot transfers following SDS-PAGE.

Analysis of TWEAK Secretion—Vectors for EBNA-based expression were constructed using the vector CH269, which is a modified version of the pCEP4 (Invitrogen) from which the EBNA gene was removed. A 0.71-kb fragment of hTNF in the pFastBac vector was provided by Dr. P. Pesavento and A. Goldfeld (Dana Farber Cancer Institute). The *Sna*BI/*Xho*I insert was ligated into the *Pvu*II/*Xho*I site of CH269. A 1.8-kb *Not*I insert of hTWEAK clone A2A, a 0.98-kb *Not*I fragment containing the hCD40L cDNA provided by Dr. E. Garber (Biogen), and a 1.46-kb *Not*I insert containing hLTα (30) were each ligated into the *Not*I site of CH269. A 0.81-kb *Hin*dIII insert containing the hLTβ coding region with a modified start site (30) was ligated into the *Hin*dIII site of CH269. 293-EBNA cells (Invitrogen) were transfected with the various CH269 vectors using LipofectAMINE, and after 2–3 days cells were either removed with Ca/Mg-free PBS with 5 mM EDTA for FACS analysis or subjected to metabolic labeling. Twice as much total DNA was used in the LTα/LTβ cotransfection experiments as in the single vector experiments.

A rabbit anti-TWEAK serum was prepared by immunizing rabbits with recombinant hTWEAK in complete Freund's adjuvant by intralymph node injection, boosting subcutaneously after 3 weeks with TWEAK in incomplete Freund's adjuvant, followed by bleeding 7 days later. This serum was functional in FACS, immunoprecipitation, and Western formats. An IgG fraction of this serum was isolated and used *versus* purified rabbit IgG fraction as a control. Both the FACS and immunoprecipitation procedures in addition to the rabbit anti-TWEAK utilized the following antibodies: 104c (anti-hTNF), AG9 (anti-hLTα), B9 (anti-LT), 5C8 (anti-CD40L); purified isotype-matched mAbs were used as controls (30, 31). FACS analysis was carried out in RPMI medium containing 10% FBS and 50 μg/ml heat-aggregated human IgG with the antibodies at 5 μg/ml. Phycoerythrin-labeled anti-mouse or rabbit IgG (Jackson ImmunoResearch) was used to detect antibody binding and cells were counterstained with 7-amino-actinomycin D for live gate exclusion of dead cells. For immunoprecipitation, 2 days after transfection, the cells were washed with PBS and transfered into Met/Cys-free minimal essential medium with glutamine, 10% dialyzed fetal bovine serum, and 200 μCi/ml each of Tran^{35}S-label (ICN) and [^{35}S]cysteine except for TNF and TWEAK, where only [^{35}S]cysteine was provided. After 3 h of labeling, the cells were chased for an additional 3 h with cold cysteine/methionine. The supernatants and cells were harvested, lysed in 1% Nonidet P-40, and subjected to immunoprecipitation and SDS-PAGE analysis as described (30).

Analysis of Interleukin-8 Secretion—Cells were grown to confluence in six-well plates, at which point various cytokines were added in a total of 5 ml of medium. Aliquots were taken at various time points and assayed using a human IL-8-specific enzyme-linked immunosorbent assay that has been described previously (32).

Cytotoxicity Assays—Cell growth assays were carried out as described previously (33). For microscopy, HT29–14 cells were seeded into two-chamber slide well plates at a density of 100,000 cells/well and grown for 2 days. Human TWEAK, TNF, or anti-Fas (CH11, Kamaya) were added along with 80 units/ml human interferon-γ. After 24 h, the medium was removed and it was observed that slides treated with cytokine or anti-Fas antibody included many dead cells that had detached from the plastic. The remaining cells were acetone-fixed and washed into PBS containing 1 μg/ml DAPI dye. After 2 min, the dye was removed, and cells were washed into PBS and examined by fluorescence microscopy.

RESULTS

Isolation of Mouse and Human TWEAK cDNAs—During the course of a study intended to clone a RNA that hybridized to an erythropoietin probe (34), we isolated several unrelated cDNAs from mouse peritoneal macrophage mRNA. One of these cDNAs was a TNF family member, as defined using the Prosite program to identify TNF sequence motifs. This new protein was thus named TWEAK in view of its TNF relatedness and

A

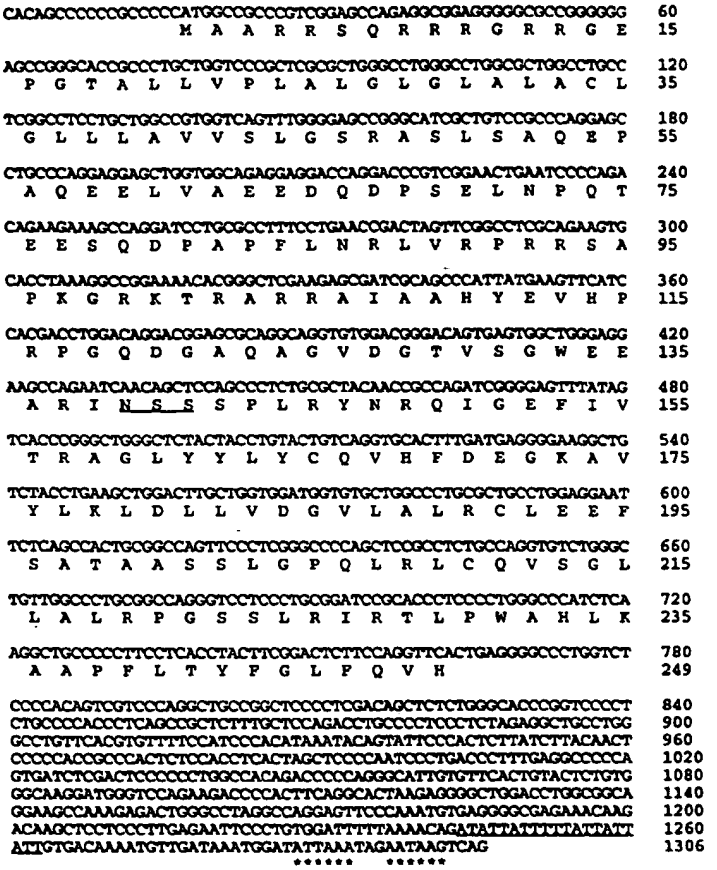

B

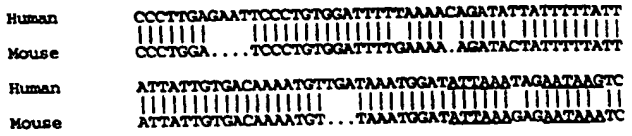

FIG. 1. *A*, nucleotide and predicted amino acid sequence of human TWEAK. A potential *N*-linked glycosylation site is *underlined*, as is the AU-rich sequence in the 3′-untranslated region. Possible polyadenylation signal sites are indicated with *asterisks*. *B*, a comparison of mouse and human 3′-untranslated sequence in region of the AU-rich and polyadenylation sites.

weak ability to induce cell death. The 1.18-kb cDNA contained the entire coding region except for an estimated 20–25 amino acids from the N terminus. A homologous human EST sequence was identified from which a PCR probe was prepared and used to screen human tonsil and fetal liver libraries. Three 1.9-kb and two 1.3-kb hTWEAK cDNAs were isolated that encoded the predicted polypeptide sequence shown in Fig. 1*A*. The 3′-untranslated region was identical in all six clones, and one of these clones possessed a poly(A) tail. In Fig. 1*A*, the two potential polyadenylation sites are indicated. In the mouse clone, polyadenylation occurred 15 bp 3′ of the second region indicating utilization of this site, which is an exact AATAAA sequence in the mouse gene. In the one polyadenylated human TWEAK cDNA clone, polyadenylation occurred 14 bp from the first site, and therefore the ATTAAA is functional. Immediately upstream of the first possible polyadenylation site lies an extensive AU-rich region that resembles an adenylate/uridylate-rich element (35). These regions can destabilize the mRNA and are found in many genes including several cytokines involved in inflammatory responses. This region in TWEAK is very well conserved between mouse and man (Fig. 1*B*). By Northern analysis, the primary mRNA species is 1.4–1.5 kb and the long 5′ region in the 1.9-kb clones is most likely an artifact. In three of the human clones, the region 5′ of the transmembrane region contained an open reading frame extending for 42 amino acids beyond that shown in Fig. 1*A* and the initiating AUG shown here is the second AUG in this reading frame. The second AUG is preceded by a reasonable Kozak consensus sequence, which does not exist in front of the first AUG (36). The two 1.3-kb clones lacked the first AUG, leading us to suspect that the N terminus of TWEAK is that shown in Fig. 1*A*.

The lack of a hydrophobic leader sequence, yet the presence of a single internal hydrophobic domain of 27 amino acids in the N-terminal region, indicated that TWEAK is a type II membrane protein (Fig. 2*A*). All members of the TNF family of ligands appear to be type II membrane proteins, which in the cases of TNF and LTα are readily cleaved from the transmembrane region. The predicted short N-terminal hydrophilic 18 amino acids are very basic, a feature that is commonly observed in TNF family members and is suggestive of a stop transfer function. The transmembrane domain was linked to the receptor binding domain via a stalk region containing a high proportion of basic amino acids, suggesting that this region could be sensitive to proteolysis. The C-terminal extracellular do-

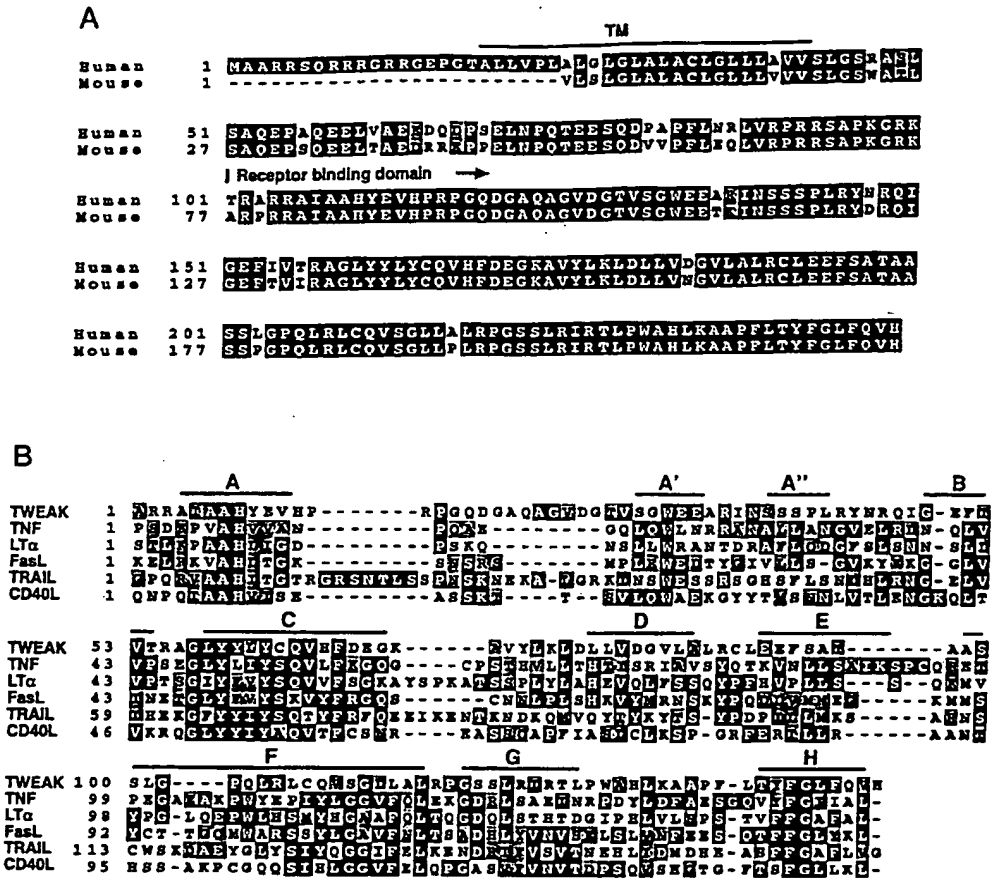

FIG. 2. **Comparison of protein sequences in the TNF ligand family.** *A*, comparison of mouse and human TWEAK amino acid sequences where identical residues are in *black* and conserved residues *shaded*. *B*, ClustalW alignment of human TWEAK to several members of the TNF family. Identical residues are in *black*, and conserved residues are *shaded*. The β sheet structures of LTα are indicated by the *bars* using the labeling defined previously (43).

main possessed a single N-terminal glycosylation site at position 139, which is a somewhat unusual location for a sugar in this structure, and this site is utilized. An amino acid sequence comparison of human and mouse TWEAK (Fig. 2*A*) showed 93% identity in the extracellular receptor binding domain (from amino acid 101 in Fig. 1). This high level of identity is very unusual within the family. For example, a similar comparison of TNF, TRAIL, Fas ligand, and CD40 ligand showed the mouse and human receptor binding sequences to be 79%, 75%, 86%, and 75% identical, respectively. Alignment of the human TWEAK sequence with the members of the TNF family revealed considerable structural similarity, especially in several regions previously described as characteristic of TNF family members (Fig. 2*B*) (5).

To determine the genomic location of hTWEAK, genomic DNA from monochromosomal somatic cell hybrids was analyzed by PCR using specific hTWEAK primers situated in the 3′-untranslated region. This analysis showed that the hTWEAK gene lies on chromosome 17 (data not shown). Further mapping using the Genebridge 4 Radiation Hybrid DNA panel showed that the gene was localized to the tip of the p13 region of chromosome 17 (LOD score 15) as shown in Fig. 3. Human TWEAK does not cluster with any of the known TNF ligands, and, while NGF is located on chromosome 17, it is on the other arm. Mouse chromosome 11 is syntenic with this region.

TWEAK mRNA Expression in Tissues—The 1.4–1.5-kb hTWEAK mRNA was found to be abundant in most tissues, and this pattern resembles that of TRAIL, albeit with some tissue-specific differences (Fig. 4). Message was abundant in human heart, pancreas, colon, small intestine, lung, ovary, and prostate, while kidney, testis, and liver contained the lowest levels of TWEAK. The lymphoid organs including spleen, lymph node, appendix, and peripheral blood lymphocytes contained abundant TWEAK mRNA, whereas less was found in thymus and bone marrow. This pattern suggests that, within the immune system, the secondary immune system predominantly expresses TWEAK. In a parallel analysis of mouse tissue Northern blots, a 1.4-kb TWEAK mRNA species was also abundant in heart tissue, but there were several differences from the human pattern, *e.g.* expression was low in the mouse spleen and high in the lung. The basis for these discrepancies is not clear.

Among human cell lines, the nonlymphoid tumor cells expressed TWEAK, while the hematopoietic lineage lines HL60, K562, MOLT4, and Raji exhibited very weak or no expression (Fig. 4). Analyses of various mouse cell lines indicated that freshly isolated thioglycollate-induced peritoneal macrophages expressed a 1.4-kb TWEAK transcript and a limited survey suggested that among the hematopoietically derived T, B, and monocytic lineages, primarily monocytes express TWEAK. Additional work will be required to properly evaluate the expression pattern in primary cells.

TWEAK Can Be Secreted—To analyze whether TWEAK is a secreted or cell associated cytokine, we compared TWEAK to two cell-surface ligands, *i.e.* CD40 ligand (CD40L) and the heteromeric LTα/β complex, and two secreted ligands, *i.e.* TNF

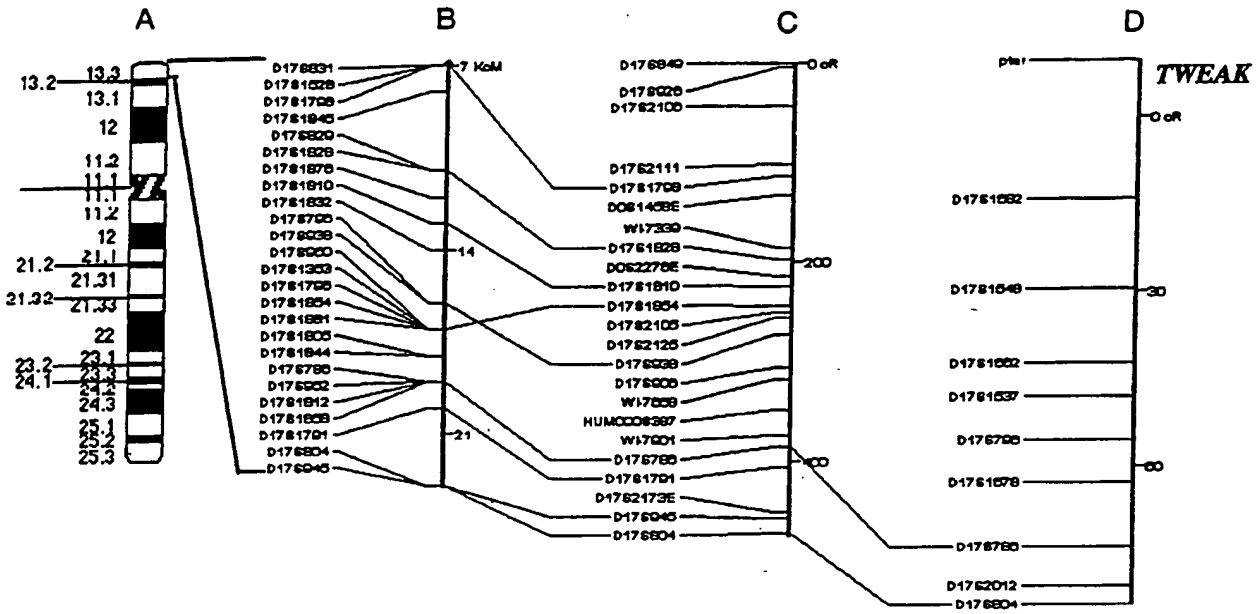

FIG. 3. **Chromosomal location of human TWEAK.** *A*, schematic diagram of human chromosome 17; *B*, the Genethon chromosome 17 linkage map; *C*, the Stanford human genome center map; *D*, the Whitehead DR11 radiation hybrid map. The Genebridge 4 radiation mapping panel was used to map TWEAK 38.7 cR telomeric to the framework marker D17S1682 (WI-9674) placing TWEAK distal to the genetic markers D17S786. Although radiation hybrid maps are not anchored to the cytogenetic maps, the most likely location of TWEAK is 17p13.3.

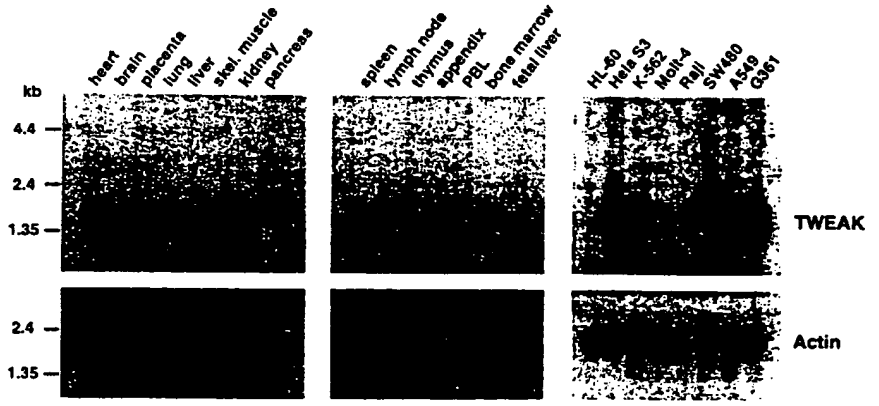

FIG. 4. **Northern analysis of hTWEAK expression in various tissues.** The 1.4-kb hTWEAK and actin transcripts are indicated. The cell line blot probed with hTWEAK was exposed longer than the other blots to reveal the low level signals in some of the lymphoid lines.

and LTα. Full-length constructs of TWEAK, TNF, CD40L, LTα, LTβ, and LTα plus LTβ were transfected into 293-EBNA human embryonic kidney cells. Vector-alone controls were negative in all analyses (data not shown). FACS analysis of the cells showed that the heteromeric LTα/β complex and CD40L were retained on the cell surface at high levels (Fig. 5). TWEAK and TNF were also detectable on the cell surface, although there was variation from experiment to experiment in the levels on the cell surface. Fig. 5 shows roughly the highest levels of surface TWEAK ever observed; sometimes, no TWEAK forms were present. With TNF, sometimes higher surface levels were noted. Upon continued culturing of the transfected cells, TNF and TWEAK expression disappeared, whereas surface CD40L and LTα/β complex were long-lived. Cells from the same transfection were metabolically labeled with [^{35}S]cysteine and methionine, and the secreted and cell-associated forms were examined by immunoprecipitation. An 18-kDa TWEAK form was immunoprecipitated from the 293-EBNA cell supernatants representing secreted TWEAK. Total TWEAK expression was low relative to the CD40L or LT ligands, possibly reflecting the presence of adenylate/uridylate-rich element motifs in the full-length construct. An additional complication is the presence of only cysteine residues in the secreted TNF and TWEAK forms and the relative labeling efficiencies of methionine *versus* cysteine may give the appearance of poor expression. As expected, 17-kDa TNF and 25-kDa LTα were found in the supernatant and upon cotransfection with LTβ, secreted LTα levels appeared to decrease substantially, possibly indicating that LTα prefers being complexed on the cell surface. LTβ and CD40L were not readily detected in the supernatant which is consistent with their primarily cell-to-cell contact specific roles (a relatively small amount of secreted 18–20-kDa CD40L was observed with long exposures). As can be seen by the intensities of the background bands, the exposures for the TNF and TWEAK supernatants are longer than those shown for the cell lysates in Fig. 5, reflecting inefficient secretion of these ligands. PhosphorImager quantitation of the bands in this experiment showed that of the total 18-kDa TWEAK synthesized, about 5% was in the supernatant. This value was comparable to the TNF case where about 4–5% of the total TNF synthesized was cleaved to the 17-kDa form and of this amount 3–4% was secreted. Presumably, low levels of the TNF-converting enzymes and TWEAK-processing enzymes limit secretion in this cell line. In other experiments, up to 25–50% of the total la-

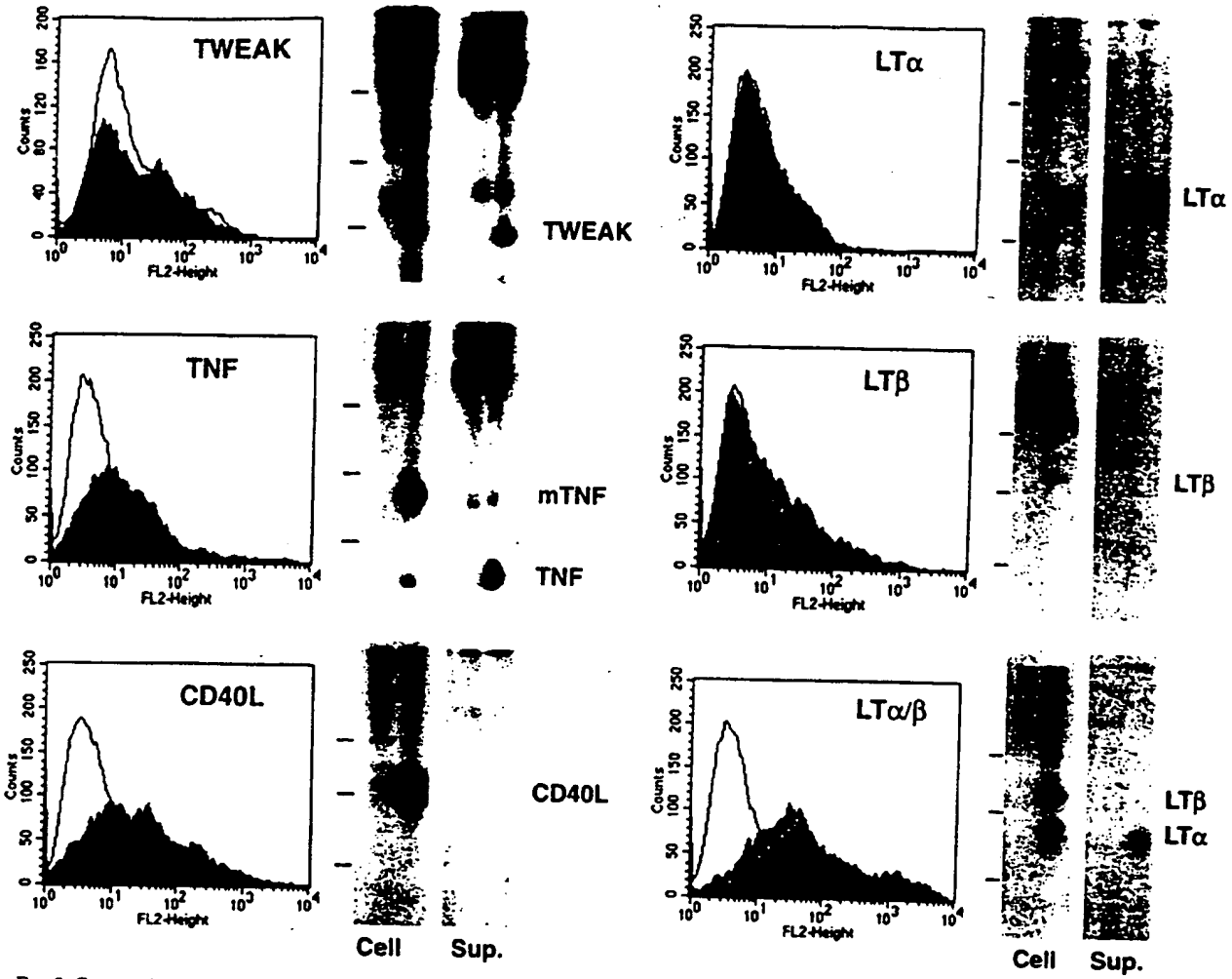

FIG. 5. **Comparison of the cell-associated and secreted forms of TWEAK, LTs, TNF, and CD40L from transfected 293-EBNA cells.** Each panel shows FACS analysis of human embryonic kidney cells transfected with TWEAK, TNF, CD40 ligand, LTα alone, LTβ alone, and LTα plus LTβ expression vectors. Cells were stained with specific antibodies (*solid histograms*) or control antibodies (*open histograms*) to each protein. In the *LT panels*, the cells were stained with anti-LTβ (*gray histogram*) or anti-LTα (*black histogram*). Next to the FACS profile is a SDS-PAGE analysis of the metabolically labeled immunoprecipitates from the cell lysates and the supernatants from the same cells. The *first* and *second lanes* in each panel result from the control antibody and anti-ligand antibody immunoprecipitations respectively. The positions of the 43-, 30-, and 18-kDa molecular size markers are indicated. In the *TNF panel*, 17-kDa secreted and 26-kDa membrane forms of TNF are indicated as *TNF* and *mTNF*, respectively. The entire immunoprecipitates from the cells and supernatants were loaded onto the gel allowing direct comparison of the relative amounts of secreted *versus* cell-associated material. Exposures were as follows: all LT panels and CD40L cells, 4 h; CD40L supernatant, TWEAK cells, and TNF cells, 20 h; TWEAK and TNF supernatants, 72 h.

beled TWEAK was secreted.

Immunoprecipitation of the ligands from cell lysates showed TNF to be present in its expected 26-kDa membrane form, and the LTα and CD40L ligands also were present at their expected 22–25- and 31–33-kDa sizes (30, 31). Cell-associated TWEAK existed in a 18-kDa processed form and in 30- and 35-kDa forms, presumably with intact transmembrane domains. A series of intermediate cleavage products were observed in this experiment. In a similar study of Fas ligand secretion from Cos cells, a low percentage of Fas ligand was cleaved, and like the TNF data presented here only a small of material was secreted (37). In contrast, even in pulse-chase experiments, it is not possible to see uncleaved LTα forms. TWEAK resembles the LTα case, since much of the cell-associated material is already cleaved away from the transmembrane region. We conclude that TWEAK, like LTα, is cleaved early during synthesis and transits to the outside, but, like TNF, some uncleaved molecules are retained on the cell. These observations indicate that TWEAK is primarily a secreted cytokine like TNF and LTα.

Further evidence for this contention was provided during the course of preparing recombinant TWEAK. A soluble molecule was prepared by deleting the N-terminal and transmembrane domains and then adding a VCAM signal sequence followed by a 11-amino acid Myc peptide tag to amino acid 67 of hTWEAK to create a secreted form basically as described for the LTβ ligand (29). Following expression in insect cells, the protein was purified from the supernatant. Two proteins were isolated, a 29-kDa full-length form wherein the VCAM leader was properly processed from the Myc-tagged N terminus and a second 17-kDa form resulting from proteolytic cleavage after Arg^{93} (Fig. 6). The stalk region between the transmembrane domain and the β sheet extracellular receptor binding domain is very rich in basic amino acids in both the human and mouse proteins, and the Arg^{92}-Arg^{93} sequence renders the full-length protein very susceptible to proteolysis in the insect cell supernatants. This putative cleavage region is identical in the mouse TWEAK structure. The amount of TWEAK N-terminal peptide remaining in the processed form that precedes the folded β

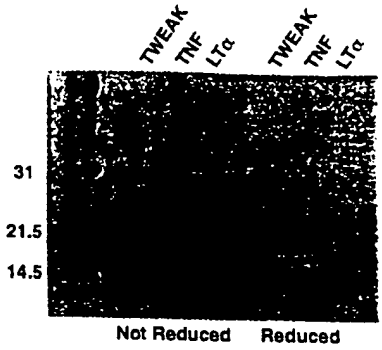

FIG. 6. **Purification of secreted hTWEAK.** SDS-PAGE of recombinant human TNF, LTα, and insect cell-derived TWEAK under reduced and nonreduced conditions.

TABLE I
Induction of IL-8 secretion by TWEAK and other TNF family members

Activating agent	Concentration of IL-8 in the media[a] from cell lines:				
	Concentration	HT29	A375	WI-38	A549
			ng/ml		
None		0.18	1.5	3.4	1.8
TWEAK	100 ng/ml	1.2	110	11	1.3
TWEAK boiled	100 ng/ml	0.14	4.5	3.4	1.4
TNF	50 ng/ml	15	625	275	110
TRAIL[b]	50 ng/ml	0.8	42	3.4	6.5
LTα1/β2	100 ng/ml	0.26	40	16.5	14
Anti-Fas	100 ng/ml	2.5	5.5	3.5	2.0
IFNγ	100 units/ml	nd	13	3.4	1.6

[a] The IL-8 concentration in the cell supernatant was measured 2 days after addition of the activating agent.
[b] FLAG-TRAIL was added with 1 μg/ml M2 anti-FLAG antibody.

sheet structure resembles TNF closely. When recombinant 17-kDa TWEAK was added directly to the metabolically labeled material secreted from 293-EBNA cells, the radiolabeled form of TWEAK migrated about 1 kDa larger than the 17-kDa recombinant TWEAK in the SDS-PAGE analysis. Therefore either this same Arg-Arg site is utilized and carbohydrate differences account for the small M_r disparity or a more N-terminal residue is the site of processing in a mammalian system. Mass spectroscopic analysis of recombinant TWEAK forms indicated that a *N*-linked glycosylated form is present (data not shown). The protein is very basic and sticks to most gel exclusion chromatographic matrices under low salt conditions. Gel exclusion chromatographic analysis of TWEAK under high salt conditions was consistent with the bulk of the protein being in a trimeric form (dat not shown).

TWEAK Can Induce Chemokine Secretion—Several of the TNF family members are known to induce chemokine secretion from various cell types (38, 39), and four cell lines were surveyed for the secretion of IL-8 in response to TNF, anti-Fas, TRAIL, LTα1/β2, or TWEAK treatment. Table I shows the levels of IL-8 secreted within a 2-day period from the HT29, A375, A549 and WI-38 lines, which are, respectively, a colon carcinoma, melanoma, lung carcinoma, and fibroblast lines. TNF was the best inducer of IL-8 release in all four cell lines. All cell lines except the A549 cells responded to TWEAK signaling with increased IL-8 release, and, in this capacity, TWEAK resembles LTα1/β2 and Trail. The A375 line exhibited the largest induction of IL-8, and here both TWEAK and LTα1/β2 had maximal effects in the 50–100 ng/ml range. The TWEAK effects peaked by 2 days, and boiling inactivated TWEAK's activity. Therefore, TWEAK has the potential to trigger chemokine production *in vivo* by selective target cells.

Cytotoxic Activity of TWEAK—Purified TWEAK induced the

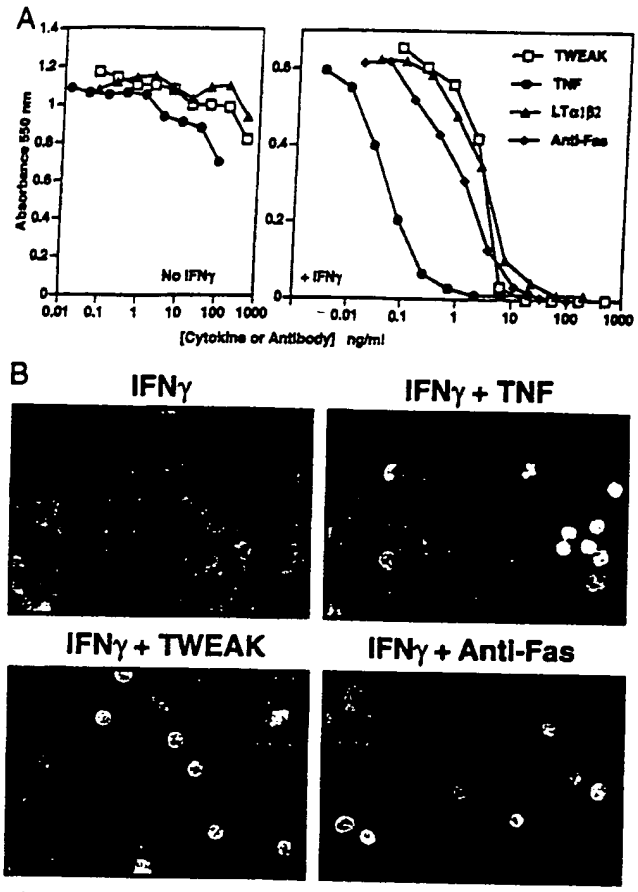

FIG. 7. **TWEAK is cytotoxic to the human adenocarcinoma line HT29.** *A*, ability of the TNF, TWEAK, LTα/β, and anti-Fas (CH11) to block the growth of the HT29 line in the presence of human IFNγ. Cells were grown for 4 days in the presence of the various agents, and growth was assessed by MTT staining. *B*, morphology of the cells undergoing cell death. Cells were pregrown for 2 days and then treated for 24 h with 80 units/ml IFN-γ with either no further addition, 20 ng/ml hTNF, 100 ng/ml hTWEAK, or 100 ng/ml anti-Fas antibody CH1 in the *bottom panel*. DAPI staining of of the nuclei of acetone-fixed cells shows nuclear condensation characteristic of apoptosis in the TNF-, TWEAK-, and anti-Fas-treated panels. One mitotic figure is visible in the TWEAK panel.

death of HT29 cells when cultured with human interferon-γ (Fig. 7*A*). This cell is also sensitive to the activation of the TNF, LTβ, and Fas receptors as well as the TRAIL receptor.[2] In the presence of these agents, HT29 cells undergo apoptosis as indicated by nuclear condensation, *i.e.* small DAPI dye bright nuclei (Fig. 7*B*). Furthermore, we had previously shown that TNF and Fas receptor activation led to TUNEL-positive staining in these cells again indicative of an apoptotic event (26). The morphology of the dying cells was similar in the presence of an anti-Fas antibody, TNF, or TWEAK. The HT29 cells died within 16–30 h in the presence of TWEAK, which was similar to TNF- and Fas-induced cell death yet faster than LTα/β-induced death. Addition of soluble TNF-R55, TNF-R75, Fas, and LTβR immunoglobulin fusion proteins had no effect on TWEAK-induced cell death indicating that these receptors do not bind TWEAK. Preliminary surveys have shown that TWEAK does not bind to TRAMP (DR3/WSL-1/Apo-3)[2] or HVEM.[3] No other cell lines were observed to die in the presence of TWEAK, although an anti-proliferative effect was seen on

[2] J. Tschopp, personal communication.
[3] C. Ware, personal communication.

A375 cells (Table II). HeLa cells underwent a morphology change yet did not die, suggestive of a differentiation type event. Notably, hTWEAK was not cytotoxic to any lymphoid cell lines or to the mouse WEHI 164 fibroblastoid cells, which are extremely sensitive to TNF and LT. Preliminary analysis of TWEAK binding to cell surfaces suggests that a putative TWEAK receptor is present on many nonlymphoid cell lines. Thus, the simple presence of receptor does not necessarily confer on a cell the ability to induce cell death, which has been a common observation in the TNF field.

DISCUSSION

This paper describes the molecular cloning, expression, and biological activity of a new member of the TNF family. Both the murine and human TWEAK proteins exhibit all the characteristics of this family, *i.e.* a type II membrane protein organization and conservation of the sequence motifs involved in the folding of the protein into the TNF anti-parallel β-sheet structure. All members of the TNF ligand family are believed to be compact trimers, and our biochemical analysis of TWEAK is consistent with this quaternary structure. A striking feature of TWEAK is the extensive sequence conservation of the receptor binding domain between mouse and man, and only the Fas ligand approaches this level of conservation. It is enticing to speculate that this sequence conservation reflects a critical functional role for TWEAK. Within the genome, both ligands and receptors in this family are often found in clusters of genes; however, the TWEAK gene does not lie within any known cluster, nor is it in a region with known disease linkage.

TNF family members can best be described as master switches in the immune system controlling both cell survival and differentiation, although the recent description of bone density regulation by the TNF family member osteoprotegerin certainly suggests broader roles (12). There may be some clues to TWEAK's functional role from the limited characterization presented here. Only TNF and LTα and possibly Fas ligand are currently recognized as secreted cytokines, contrasting with the other predominantly membrane anchored members. While a membrane form of TNF has been well characterized and is likely to have a unique biological role, secreted TNF functions as a general alarm signaling to cells more distant from the site of the triggering event. Thus, TNF secretion can amplify a primary inflammatory event leading to the well described changes in the vascular lining and and consequent cell trafficking. In contrast, the membrane-bound members of the family send signals through the TNF type receptors only to cells in direct contact. For example T cells probably provide CD40-mediated "help" only to those B cells brought into contact via cognate interactions. The fact that TWEAK appears to be efficiently secreted suggests that its role will resemble that of TNF, *i.e.* to provide a long range signal. The presence of a possible AU-rich motif may indicate involvement in host defense.

TWEAK RNA is abundantly expressed in many organs in a pattern reminiscent of TRAIL (5). Other TNF family members are typically more difficult to detect in tissue Northern blots, *e.g.* CD40 ligand or TNF, where expression is limited to very specific circumstances. While TWEAK RNA is abundant, it remains to be seen if protein expression is equally abundant. TWEAK and TRAIL expression patterns suggest more constitutive functions for these TNF family members, possibly indicating that they form a subclass within the family. The relative lack of TWEAK expression in hematopoietically derived tumor lines also points to a divergence from the standard TNF family ligand, which is typically expressed in lymphoid cells.

TWEAK can induce chemokine secretion, which is likely to be a common feature of members of the TNF family. Chemokine regulation by TNF members may underlie several key aspects of their biology as is well described for TNF (38, 39), but may also extend to the LT system and BRL-1-interacting chemokines (40). The ability to induce programmed cell death is also an important and well studied feature of several members of the TNF family. Fas-mediated apoptosis appears to play a role in the regulation of autoreactive lymphocytes in the periphery and possibly the thymus (18, 23), and recent work has also implicated the TNF and CD30 systems in the survival of T cells and large cell anaplastic lymphoma lines (22, 24, 25, 41). TWEAK induced cell death in a human adenocarcinoma cell line, HT29. We and others had previously shown that the death of this line in response to TNF, Fas, or LTβ receptor signaling has the features of apoptosis (26, 39) and the death induced by TWEAK was similar to that triggered by Fas or TNF receptor activation. In contrast to the broad spectrum of Fas ligand- or TRAIL-sensitive cells, other TWEAK-sensitive cells were not readily found, and this pattern is similar to that described for LTβ receptor activation. Whether TWEAK has a function similar to Fas remains to be seen; however, the inability to kill the sensitive Jurkat and SKW 6.4 lines suggests that regulation of lymphocyte death or survival is not its role. LTβ receptor activation can induce growth arrest in some cell lines (38), and our studies on the effects of LTβ receptor activation on the growth of tumors *in vivo* are also consistent with growth arrest as opposed to direct cell death.[4] For these reasons, TWEAK is likely to induce cell differentiation *in vivo* and probably not cell death.

TABLE II
Cytotoxic effects of human TWEAK on various cell lines

Cell line	Type	Cytotoxicity[a]
Hematopoietic		
Jurkat	T lymphoma	–
SKW 6.4	EBV B cell	–
Namalwa	Burkitt lymphoma	–
K562	Promyelocytic	–
THP-1	Monocytic leukemia	–
Nonhematopoietic		
HT29	Colon adenocarcinoma	++[b]
ME-180	Cervical carcinoma	–
HeLa	Cervical carcinoma	–[c]
MCF-7	Breast adenocarcinoma	–
A375	Melanoma	–[d]
293	Embryonic kidney cells	–
WEHI 164	Mouse fibroblast	–

[a] 3–5 day proliferation assay in the presence and absence of human IFNγ using a range of protein concentrations.
[b] Cytotoxicity was only observed in the presence of IFNγ.
[c] Morphology changes.
[d] Some anti-proliferative effect.

[4] F. Mackay and J. Browning, unpublished observations.

TABLE III
Grouping of various TNF family signaling pathways by cytotoxicity patterns

Group	Receptor
Potent inducers of apoptosis in many cell types	TNF-R55, Fas, TRAIL-RI (DR4), TRAIL-RII (DR5), TRAMP (DR3)
Weak inducers of apoptosis in a few cell types	LTβ-R, TWEAK-R,[a] CD30, CD27, TNF-R75
Do not induce cell death	CD40, OX-40, 4–1BB

[a] TWEAK-R is presumed to exist.

It is possible to segregate the TNF receptor pairs into three groups based on their ability to induce cell death (Table III). First, TNF-R55, Fas, TRAIL-RI (DR4), TRAIL-RII (DR5), and TRAMP (DR3/WSL-1/Apo-3) receptors can efficiently induce cell death in many lines, and these receptors have canonical death domains (8–10, 23). Next, there are those receptors that trigger a weaker death signal limited to a few cell types; the TWEAK, CD30, LTβ, and possibly the TNF-R75 (42, 43) and CD27 receptors (44) are examples of this class. Finally, there are those members that cannot efficiently deliver a death signal, and the possibility must be considered that these receptors have simply not been studied as well. Probably all groups can exhibit antiproliferative effects on some cell types consequent to inducing cell differentiation, *e.g.* CD40 (45).

How the "weak death" group can trigger cell death in the absence of a canonical death domain is an interesting question and prompts speculation that an alternative entry point into the death-inducing caspase cascade exists. Specifically, in the case of HT29 cells, why does receptor signaling lead to death only in the presence of IFNγ? It is possible that these weak death receptors may activate the conventional death domain-mediated pathways via induction of the expression of Fas and Fas ligand or other receptor/ligands in the strong death group. In support of this concept, Fas expression is known to be up-regulated by IFNγ on HT29 cells, and the expression of Fas ligand by tumor lines as a possible immune surveillance escape mechanism has been described (46–48), although the anti-hFas-L blocking antibody, NOK-1, did not affect cell death in this system (data not shown). We have also observed that activation of the LTβ receptor can potentiate TNF signaling possibly reflecting favorable cross-talk between signaling pathways (26, 49). Alternatively, weak death receptor signaling may differentiate the line into a state of unfulfilled growth factor dependence or cell cycle confusion with consequent initiation of the death pathway. A fourth possibility lies in the recent observations on the ability of NF-κB activation to inhibit the death signal delivered by death domain bearing receptors and IFNγ treatment may relieve the death repression by NF-κB (23). Since anti-Fas-induced HT29 cell death is IFNγ-dependent yet Fas signaling does not lead to NF-κB activation (23), regulation of downstream NF-κB-mediated events is less likely. Finally, and most likely, death may be initiated by other "non-FLICE"-initiated signaling pathways such as the ceramide or JNK/stress-activated protein kinase pathways (50, 51). Whatever the mechanism, further exploration of the death trigger initiated by these weak death receptors may provide an additional approach to cancer therapy.

The TNF family has grown dramatically in recent years to encompass at least 14 different ligand/receptor signaling pathways that regulate host defense and the immune system. The widespread expression patterns of TWEAK and TRAIL indicate that there may be considerably more functional variety to be uncovered in this family. This aspect was highlighted recently with the discovery of two new TNF receptors that affect the ability of Rous sarcoma and herpes simplex virus to productively infect cells along with the discovery of a bone density regulating receptor. When coupled with the historical observations that TNF itself has anti-viral activity and that pox viruses encode for decoy TNF receptors to avoid host defense, it appears that viral pathology and the functions of the TNF are interwoven (6, 7, 13, 52). The generation of soluble TWEAK and the eventual identification of the TWEAK receptor should provide the tools to elucidate the biological function of this new pathway.

Acknowledgments—We thank Jeff Thompson, Werner Meier, and Konrad Miatkowski for help with the purification and characterization of TWEAK; the protein and DNA sequencing groups at Biogen; Sarah Bixler and Christine Ambrose for the initial studies of mTWEAK; Ellen Garber for the hCD40L cDNA; Anne Goldfeld and Patricia Pesavento for the wild type TNF cDNA insert; and Carl Ware and Jurg Tschopp for testing the binding of TWEAK to HVEM and TRAMP (DR3/WSL-1), respectively.

REFERENCES

1. Smith, C. A., Farrah, T., and Goodwin, R. G. (1994) *Cell* **76**, 959–962
2. Chinnaiyan, A. M., O'Rourke, K., Yu, G.-L., Lyons, R. H., Garg, M., Duan, D. R., Xing, L., Gentz, R., Ni, J., and Dixit, V. M. (1996) *Science* **274**, 990–992
3. Bodmer, J.-L., Burns, K., Schneider, P., Hofmann, K., Steiner, V., Thome, M., Bornand, T., Hahne, M., Schroeter, M., Becker, K., Wilson, A., French, L. E., Browning, J. L., MacDonald, H. R., and Tschopp, J. (1997) *Immunity* **6**, 79–88
4. Kitson, J., Raven, T., Jiang, Y.-P., Goeddel, D. V., Giles, K. M., Pun, K.-T., Grinham, C. J., Brown, R., and Farrow, S. N. (1996) *Nature* **384**, 372–375
5. Wiley, S. R., Schooley, K., Smolak, P. J., Din, W. S., Huang, C.-P., Nicholl, J. K., Sutherland, G. R., Smith, T. D., Rauch, C., Smith, C. A., and Goodwin, R. G. (1995) *Immunity* **3**, 673–682
6. Montgomery, R. I., Warner, M. S., Lum, B. J., and Spear, P. G. (1996) *Cell* **87**, 427–436
7. Brojatsch, J., Naughton, J., Rolls, M. M., Zingler, K., and Young, J. A. T. (1996) *Cell* **87**, 845–855
8. Pan, G., O'Rourke, K., Chinnaiyan, A. M., Gentz, R., Ebner, R., Ni, J., and Dixit, V. M. (1997) *Science* **276**, 111–113
9. Pan, G., Ni, J., Wei, Y.-F., Yu, G.-L., Gentz, R., and Dixit, V. M. (1997) *Science* **277**, 815–818
10. Sheridan, J. P., Marsters, S. A., Pitti, R. M., Gurney, A., Skubatch, M., Baldwin, D., Ramakrishnan, L., Gray, C. L., Baker, K., Wood, W. I., Goddard, A. D., Godowski, P., and Ashkenazi, A. (1997) *Science* **277**, 818–821
11. Nocentini, G., Giunchi, L., Ronchetti, S., Krausz, L. T., Bartoli, A., Moraca, R., Migliorati, G., and Riccardi, C. (1997) *Proc. Natl. Acad. Sci. U. S. A.* **94**, 6216–6221
12. Simonet, W. S., Lacey, D. L., Dunstan, C. R., Kelley, M., Chang, M.-S., Luethy, R., Nguyen, H. Q., Wooden, S., Bennett, L., Boone, T., Shimamoto, G., DeRose, M., Elliot, R., Colombero, A., Tan, H.-L., Trail, G., Sullivan, J., Davy, E., Bucay, N., Renshaw-Gegg, L., Hughes, T. M., Hill, D., Pattison, W., Campbell, P., Sander, S., Van, G., Tarpley, J., Derby, P., Lee, R., and Boyle, W. J. (1997) *Cell* **89**, 309–319
13. Vassalli, P. (1992) *Annu. Rev. Immunol.* **10**, 411–452
14. De Togni, P., Goellner, J., Ruddle, N. H., Streeter, P. R., Fick, A., Mariathasan, S., Smith, S. C., Carlson, R., Shornick, L. P., Strauss-Schoenberger, J., Russell, J. H., Karr, R., and Chaplin, D. D. (1994) *Science* **264**, 703–707
15. Koni, P. A., Sacca, R., Lawton, P., Browning, J. L., Ruddle, N. H., and Flavell, R. A. (1997) *Immunity* **6**, 491–500
16. Foy, T. M., Aruffo, A., Bajorath, J., Buhlmann, J. E., and Noelle, R. J. (1996) *Annu. Rev. Immunol.* **14**, 591–617
17. Nagata, S., and Golstein, P. (1995) *Science* **267**, 1449–1458
18. Castro, J. E., Listman, J. A., Jacobson, B. A., Wang, Y., Lopez, P. A., Ju, S., Finn, P. W., and Perkins, D. L. (1996) *Immunity* **5**, 617–627
19. Strueber, E., and Strober, W. (1996) *J. Exp. Med.* **183**, 979–989
20. DeBenedette, M. A., Chu, N. R., Pollok, K. E., Hurtako, J., Wade, W. F., Kwon, B. S., and Watts, T. H. (1995) *J. Exp. Med.* **181**, 985–992
21. Agematsu, K., Kobata, T., Yang, F.-C., Nakazawa, T., Fukushima, K., Kitahara, M., Mori, T., Sugita, K., Morimoto, C., and Komiyama, A. (1995) *Eur. J. Immunol.* **25**, 2825–2829
22. Amakawa, R., Hakem, A., Kundig, T. M., Matsuyama, T., Simard, J. J. L., Timms, E., Wakeham, A., Mittruecker, H.-W., Griesser, H., Takimoto, H., Schmits, R., Shahinian, A., Ohashi, P. S., Penninger, J. M., and Mak, T. W. (1996) *Cell* **84**, 551–562
23. Nagata, S. (1997) *Cell* **88**, 355–365
24. Zheng, L., Fisher, G., Miller, R. E., Peschon, J., Lynch, D. H., and Lenardo, M. J. (1995) *Nature* **377**, 348–351
25. Sytwu, H.-K., Liblau, R. S., and McDevitt, H. O. (1996) *Immunity* **5**, 17–30
26. Browning, J. L., Miatkowski, K., Sizing, I., Griffiths, D., Zafari, M., Benjamin, C. D., Meier, W., and Mackay, F. (1996) *J. Exp. Med.* **183**, 867–878
27. Lee, S. Y., Park, C. G., and Choi, Y. (1996) *J. Exp. Med.* **183**, 669–674
28. Browning, J. L., Androlewicz, M. J., and Ware, C. F. (1991) *J. Immunol.* **147**, 1230–1237
29. Browning, J. L., Miatkowski, K., Griffiths, D. A., Bourdon, P. R., Hession, C., Ambrose, C. M., and Meier, W. (1996) *J. Biol. Chem.* **271**, 8618–8626
30. Browning, J. L., Dougas, I., Ngam-ek, A., Bourdon, P. R., Ehrenfels, B. N., Miatkowski, K., Zafari, M., Yampaglia, A. M., Lawton, P., Meier, W., Benjamin, C. P., and Hession, C. (1995) *J. Immunol.* **154**, 33–46
31. Hsu, Y.-M., Lucci, J., Su, L., Ehrenfels, B., Garber, E., and Thomas, D. (1997) *J. Biol. Chem.* **272**, 911–915
32. Santos, A. A., Scheltinga, M. R., Lynch, E., Brown, E. F., Lawton, P. L., Chambers, E., Browning, J., Dinarello, C. A., Wolff, S. M., and Wilmore, D. W. (1993) *Arch. Surg.* **128**, 138–144
33. Browning, J., and Ribolini, A. (1989) *J. Immunol.* **143**, 1859–1867
34. Chicheportiche, Y., Ody, C., and Vassalli, P. (1995) *Biochim. Biophys. Res. Commun.* **209**, 1076–1081
35. Chen, C.-Y. A., and Shyu, A.-B. (1995) *Trends Biol. Sci.* **20**, 465–470
36. Kozak, M. (1990) *Proc. Natl. Acad. Sci. U. S. A.* **87**, 8301–8305
37. Tanaka, M., Suda, T., Takahashi, T., and Nagata, S. (1995) *EMBO J.* **14**, 1129–1135
38. Degli-Esposti, M., Davis-Smith, T., Din, W. S., Smolak, P. J., Goodwin, R. G., and Smith, C. A. (1997) *J. Immunol.* **158**, 1756–1762
39. Abreu-Martin, M. T., Vidrich, A., Lynch, D. H., and Targan, S. R. (1995)

J. Immunol. **155**, 4147–4154
40. Forster, R., Mattis, A. E., Kremmer, E., Wolf, E., Brem, G., and Lipp, M. (1996) *Cell* **87**, 1037–1047
41. Gruss, H. J., Boiani, N., Williams, D. E., Armitage, R. J., Smith, C. A., and Goodwin, R. G. (1994) *Blood* **83**, 2045–2056
42. Medvedev, A. E., Sundan, A., and Espevik, T. (1994) *Eur. J. Immunol.* **24**, 2842–2849
43. Grell, M., Zimmermann, G., Hulser, D., Pfizenmaier, K., and Scheurich, P. (1994) *J. Immunol.* **153**, 1963–1972
44. Prasad, K. V. S., Ao, Z., Yoon, Y., Wu, M. X., Rizk, M., Jacquot, S., and Schlossman, S. F. (1997) *Proc. Natl. Acad. Sci. U. S. A.* **94**, 6346–6351
45. Funakoshi, S., Longo, D. L., Beckwith, M., Conley, D. K., Tsarfaty, G., Tsarfaty, I., Armitage, R. J., Fanslow, W. C., Spriggs, M. K., and Murphy, W. J. (1994) *Blood* **83**, 2787–2794
46. Yonehara, S., Ishii, A., and Yonehara, M. (1989) *J. Exp. Med.* **169**, 1747–1756
47. Strand, S., Hofmann, W. J., Hug, H., Mueller, M., Otto, G., Strand, D., Mariani, S. M., Stremmel, W., Krammer, P. H., and Galle, P. R. (1996) *Nat. Med.* **2**, 1361–1366
48. Hahne, M., Rimoldi, D., Schroeter, M., Romero, P., Schreier, M., French, L. E., Schneider, P., Bornand, T., Fontana, A., Lienard, D., Cerottini, J.-C., and Tschopp, J. (1996) *Science* **274**, 1363–1366
49. Mackay, F., Bourdon, P. R., Griffiths, D. A., Lawton, P., Zafari, M., Sizing, I. D., Miatkowski, K., Ngam-ek, A., Benjamin, C. D., Hession, C., Ambrose, C. M., Meier, W., and Browning, J. L. (1997) *J. Immunol.* **159**, 3299–3310
50. Hannun, Y. A. (1996) *Nature* **274**, 1855–1859
51. Yang, X., Khosravi-Far, R., Chang, H. Y., and Baltimore, D. (1997) *Cell* **89**, 1067–1076
52. Smith, G. L. (1994) *Trends Microbiol.* **3**, 81–88

EXHIBIT J

Cancer Investigation, 19(7), 732–738 (2001)

MINISERIES/SPECIAL ARTICLE

The Role of CXC Chemokines in the Regulation of Tumor Angiogenesis

Sergio Dias, Ph.D., Margaret Choy, B.A., and Shahin Rafii, M.D.*

Division of Hematology/Oncology, Weill Medical College of Cornell University, New York, New York

KEY WORDS: *Angiogenesis; CXC chemokines; Tumor metastasis.*

THE CHEMOKINE FAMILY

Chemokines comprise a small group of secreted, heparin-binding proteins containing four highly conserved cysteine residues. These cytokines have a typical triple-stranded, β-sheet three-dimensional structure (1) and have been classified based on the positions of their N-terminal cysteine residues. The CC chemokines, which represent the majority of chemokines identified to date, are characterized by the presence of two adjacent cysteines at the amino terminal end. On the other hand, CXC chemokines have a single nonconserved amino acid separating the two N-terminal cysteines (see reference 2 for an updated review on the structure of chemokines).

FUNCTIONS OF CHEMOKINES

Chemokines are primarily known for their capacity to induce leukocyte recruitment and activation in processes that require active cell migration, such as inflammatory responses, bacterial or viral infections, and wound healing (3–6). Other functions of chemokines have been described more recently, particularly for the CXC chemokines, and include their ability to regulate angiogenesis directly—through interaction with their receptors on endothelial cells (7)—or indirectly, by attracting inflammatory cells which release angiogenic factors such as basic fibroblast growth factor (bFGF) and vascular endothelial growth factor (VEGF) (8,9).

Members of the CXC chemokine subfamily exhibit angiogenic or angiostatic properties, based on the presence or absence of a structural and functional motif, which led to the creation of a novel chemokine classification. CXC chemokines can be subdivided based on the presence of the ELR (Glu-Leu-Arg) motif, which precedes the first cysteine residue on the N-terminus of these chemokines (10). ELR$^+$ chemokines are generally potent neutrophil chemoattractants with pro-angiogenic proper-

* Corresponding author. Shahin Rafii, M.D., Division of Hematology/Oncology, Room C-606, Weill Medical College of Cornell University, 1300 York Avenue, New York, NY 10021. Fax: (212) 746-8866; E-mail: srafii@mail.med.cornell.edu

Table 1

Examples of CXC Chemokines with Angiogenic (ELR⁺) or Angiostatic (ELR⁻) Properties

ELR⁺ Chemokines	ELR⁻ CXC Chemokines
IL-8	PF-4
ENA-78	IP-10
GRO-α	MIG
GRO-β	SDF-1
GRO-γ	
GCP-2	

IL-8, interleukin 8; ENA-78, epithelial neutrophil activating protein-78; GRO-α, growth related gene-α; GCP-2, granulocyte chemotactic protein 2; PF-4, platelet factor 4; IP-10, interferon inducible protein; MIG, monokine induced by interferon-γ; SDF-1, stromal cell-derived factor-1.

ties, whereas CXC chemokines, which lack the ELR motif (ELR⁻), are generally monocyte and T-cell chemoattractants with potent angiostatic properties (2,10) (Table 1).

CELLULAR PATHWAYS INVOLVED IN TUMOR ANGIOGENESIS

Tumor growth requires sustenance of established endothelium, as well as proliferation of new blood vessels, a process referred to as angiogenesis (11–13). Formation of new blood vessels facilitates rapid and timely delivery of nutrients and oxygen, as well as removal of waste products; these processes, in turn, enhance tumor proliferation and sustenance. By releasing endothelial survival and growth factors, tumor cells promote neo-angiogenesis, which supports their own growth and determines the size of the tumor mass.

Tumor angiogenesis results from the balance between endothelial cell apoptosis and proliferation (14,15). Tumor cells, by elaboration of a wide variety of stimulatory factors including VEGF and FGFs, promote proliferation and suppress apoptosis of endothelial cells. Therefore, inhibition of stimulatory signals and/or induction of apoptotic signals will result in a decrease in endothelial cell mass with a concomitant decrease in tumor cell mass (15).

CXC CHEMOKINES AND PHYSIOLOGICAL/"NORMAL" ANGIOGENESIS

The strongest experimental evidence supporting a role for chemokines in normal angiogenesis comes from wound healing studies. It is well established that angiogenesis is required for efficient scarring and healing of wounds, a process that involves recruitment and activation of inflammatory cells.

Previous studies demonstrated intense chemokine expression in wounds, and showed a correlation with the recruitment of inflammatory cells. For instance, monocyte chemotactic protein-1 (MCP-1) has been implicated in mast cell infiltration (16), whereas macrophage inflammatory protein-1α (MIP-1α) attracts macrophages to the wound healing site (17,18). By attracting pro-inflammatory cells that can release angiogenic growth factors, chemokines may thus contribute to the neovascularization process required for efficient wound healing.

Elevated chemokine levels have also been detected in processes that require physiological/normal angiogenesis, such as the menstrual cycle. It was shown that levels of MCP-1 are highest premenstrually, and decrease with the increase in estrogen levels as the cycle starts (19). Finally, chemokine levels are elevated and correlate with an abundant leukocyte infiltrate in the mouse uterus during pregnancy (20).

Given their role as potent leukocyte and other inflammatory cell chemoattractants, and the pro-angiogenic properties of these cells, it is not surprising that chemokines may be involved in physiological/normal angiogenesis. However, few studies have tried to address these issues, and further experimental evidence is required to conclude whether chemokines play a crucial role in regulating physiological angiogenesis.

CHEMOKINES AND TUMOR ANGIOGENESIS

In contrast to the lack of experimental data on chemokines and normal angiogenesis, there is ample evidence supporting a role for chemokines in tumor/malignant angiogenesis. Chemokine expression, particularly for the CXC chemokines containing the ELR motif (ELR⁺), is increased in a variety of tumors, and correlates with a more invasive (metastatic) and more vascularized (angiogenic) tumor phenotype (Table 2). A list of cancer types, the most abundant ELR⁺ CXC chemokine detected, and the phenotypic changes in the tumors associated with increased chemokine expression are shown in Table 2. These studies have suggested that the level of expression of ELR⁺ CXC chemokines may regulate different aspects of tumor biology such as tumorigenesis, the onset of me-

Table 2

The Role of ELR⁺ CXC Chemokines in Regulating Different Aspects of Tumor Biology; Shows Different Cancer Types, the Chemokine Detected at Highest Level in the Tumor, and the Change in Tumor Phenotype Associated with Such Expression

Type of Cancer	Chemokine	Phenotype	Reference
Melanoma	IL-8	Angiogenesis, tumor growth, metastasis	21
Gastric carcinoma	IL-8	Angiogenesis, tumorigenesis	22
Pancreatic cancer	IL-8	Tumorgenesis, metastasis	23
Head and Neck	IL-8	Large primary tumor	24
NSCLC	IL-8	Angiogenesis	25
NSCLC	ENA-78	Tumor progression	26
Ovarian carcinoma	IL-8	Tumor progression	27
Prostate	IL-8	Tumor progression	28
Mesothelioma	IL-8	Tumor progression	29
Glioblastoma	IL-8	Tumor progression	30

tastasis, and the acquisition of a more angiogenic phenotype.

As noted in Table 2, most studies identified interleukin-8 (IL-8) as the main pro-angiogenic chemokine expressed in human tumors. Therefore, initial reports on the role of chemokines in tumor angiogenesis focused mostly on IL-8. It was first shown that IL-8 had the capacity to mediate endothelial cell chemotaxis, proliferation, and induce angiogenesis in vitro and in vivo (31,32). Note that these effects were observed in the absence of inflammation, suggesting a direct effect on endothelial cells.

A role for IL-8 in tumor angiogenesis was subsequently investigated in tumor models in vivo. Neutralizing antibodies against IL-8 blocked the growth and formation of metastasis by human prostate and lung tumors in severe combined immunodeficiency syndrome (SCID) mice (33). Other studies have reinforced the importance of IL-8 in regulating tumor growth. For instance, transfection of human gastric carcinoma (34) and melanoma (35) cells with IL-8 increased angiogenesis, tumorigenesis, and formation of metastasis in nude mice. In melanoma cells, increased IL-8 expression was shown to regulate the activity of matrix metalloproteinase-2 (MMP-2), which may explain the increased metastatic behavior of the transfected cells (36). Furthermore, in pancreatic cancer, IL-8 is regulated by acidosis and hypoxia, and an increase in its expression is correlated with a more tumorigenic and metastatic behavior of human pancreatic cancer cells in nude mice (23).

Note that IL-8, as for other CXC chemokines, has been suggested not to act directly on the tumor cells, suggesting that its tumor growth-promoting effects involve an increase in angiogenesis. However, expression of IL-8 receptors has been detected both on tumors as well as endothelial cells in breast cancer biopsies (37), whereas human colonic epithelium also expresses chemokine-related receptor-4 (CXCR4), a receptor for stromal cell-derived factor-1 (SDF-1) (38). Furthermore, despite experimental evidence suggesting that the angiogenic effects of IL-8 are exerted at the endothelial cell level, neither IL-8 binding nor IL-8-induced calcium flux was demonstrated on human umbilical vein or dermal microvascular endothelial cells and, even by reverse transcriptase-polymerase chain reaction (RT-PCR), IL-8 receptors could not be detected on these cells (39).

ELR⁻ CXC CHEMOKINES BLOCK TUMOR ANGIOGENESIS

As mentioned above, ELR⁺ CXC chemokines such as IL-8 stimulate angiogenesis. Indeed, it has been suggested that the presence of this amino acid ELR motif may confer the angiogenic nature of chemokines. This hypothesis received further support from studies which demonstrated that ELR⁻ CXC chemokines such as interferon inducible protein-10 (IP-10), platelet factor-4 (PF-4), and monokine induced by interferon (MIG) have angiostatic properties both in vitro and in vivo (2,32,40,41).

Furthermore, in order to establish whether the presence of the ELR motif was critical for the angiogenic or angiostatic role of CXC chemokines, site-directed mutagenesis was used to insert amino acid residues from IP-10 or PF-4 into the ELR motif of wild-type IL-8 (32). Conversely, using a similar approach, a mutant MIG protein containing the ELR motif immediately adjacent to the first cysteine in its primary structure was created. As predicted, the mutated ELR⁻ IL-8 had angiostatic activity, whereas the mutant MIG produced positive angiogenic responses both in vitro and in vivo (32).

These initial studies have also shown that ELR⁻ CXC chemokines block endothelial cell chemotaxis and are ac-

MARCEL DEKKER, INC.
270 Madison Avenue, New York, New York 10016

tually capable of blocking the angiogenic effects of IL-8, epithelial neutrophil-activating protein (ENA)-78, and bFGF. The angiostatic action of these chemokines was demonstrated in established in vivo angiogenesis assays such as the corneal micropocket assay (42,43), and growth factor-induced neovascularization of subcutaneously implanted Matrigel plugs in nude mice (44). In the corneal micropocket assay, implantation of pellets containing chemokines such as IL-8, ENA-78, growth-related protein (GRO)-α or granulocyte chemotactic protein (GCP)-2, VEGF, or bFGF produced positive angiogenic responses (42,43). When combined with IP-10, MIG, or SDF-1, the angiogenic properties of ELR$^+$ CXC chemokines, VEGF, or bFGF were markedly abrogated (45). Because there was no evidence of increased inflammation, these results suggested that the angiogenic and/or angiostatic effects of CXC chemokines were produced independent of their role in leukocyte chemoattraction.

Given the powerful in vitro and in vivo angiostatic effects of ELR$^-$ CXC chemokines, namely IP-10 and MIG, there has been considerable interest in exploiting these properties in tumor models as a way to block tumor angiogenesis. Intratumor administration of recombinant IP-10 was shown to decrease tumor growth and angiogenesis in mice bearing aggressive adenocarcinomas (45), and in non-small cell lung cancer-bearing mice, higher tumor and plasma IP-10 levels correlated with a decrease in tumor incidence and delayed tumor progression (46). Also in a model of human non-small cell lung cancer, overexpression of the ELR$^-$ CXC chemokine MIG resulted in decreased angiogenesis and tumor growth (41).

It was suggested from these studies that by modulating the level of angiogenic versus angiostatic chemokines at the tumor site, it might be possible to decrease or block tumor angiogenesis and delay tumor growth. This may be achieved by systemic or local delivery of angiostatic chemokines, or alternatively by administration of agents known to modulate chemokine expression. Subsequently, monitoring the angiogenic versus angiostatic chemokine levels in tumors may give a prediction of the therapeutic outcome.

This approach has been employed in preclinical studies using the antitumor cytokine IL-12. In models of murine breast cancer (47) and human lymphoma (48), the levels of the antiangiogenic chemokines IP-10 and MIG correlated with decreased angiogenesis, delayed tumor growth, and in some cases, cure after IL-12 therapy.

CHEMOKINE RECEPTORS AND ANGIOGENESIS

Although most cell types produce different chemokines, chemokine receptors have considerable ligand specificity profiles. This is particularly striking for the ELR$^+$ CXC angiogenic chemokines (which bind CXCR-2) versus the ELR$^-$ CXC angiostatic chemokines, which bind CXCR-3 (see Fig. 1; reviewed in references 2 and 49). IL-8 does, however, also bind CXCR-1, and SDF-1 binds CXCR-4 (2,50). This apparent receptor specificity in angiogenic versus angiostatic chemokines has received further support from studies on the pathophysiology of Kaposi's sarcoma (KS).

The KS-associated herpesvirus (KSHV) is detected in all KS biopsies, and has been implicated in the pathogenesis of KS (51). In particular, certain oncogenic proteins encoded by the virus have been suggested to confer the angiogenic phenotype seen in KS lesions. One such protein, encoded by the viral ORF74, is a G-coupled receptor

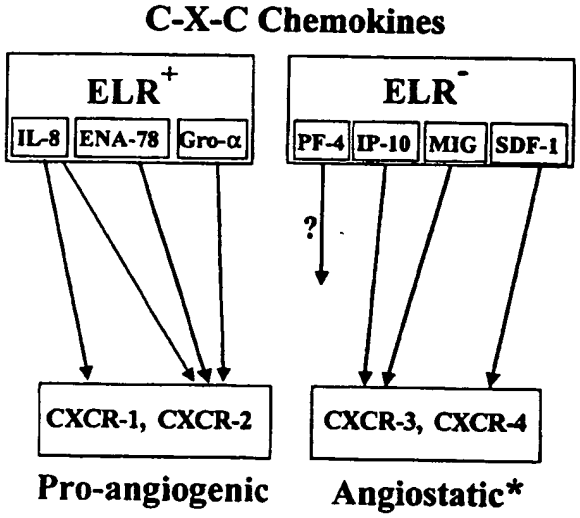

Figure 1. Some of the CXC chemokine family members, divided according to the presence or absence of the ELR motif in their primary structure, their receptor specificity, and pro-angiogenic or angiostatic properties. IL-8, interleukin 8; ENA-78, epithelial neutrophil activating protein-78; GRO-α, growth related gene-α; PF-4, platelet factor 4; IP-10, interferon inducible protein; MIG, monokine induced by interferon-γ; SDF-1, stromal cell-derived factor-1. ?: The receptor for PF-4 has not been identified. *Although SDF-1 is an ELR$^-$ chemokine, there is little evidence supporting an angiostatic versus a pro-angiogenic function.

which stimulates intracellular signaling leading to proliferation, and has been shown to induce an angiogenic phenotype when transfected into normal cells (52). Note that this KSHV-G-protein-coupled receptor has a high degree of homology with CXCR-2 (52).

Given their receptor-binding specificity, the angiostatic chemokines IP-10 (and possibly MIG) have also been suggested to represent unique members of the chemokine family. In addition to CXCR-3, these chemokines bind a specific heparin sulfate proteoglycan-associated receptor on endothelial cells, exerting their angiostatic activity by inducing cell cycle arrest (53).

GENE TARGETING OF CHEMOKINE AND CHEMOKINE-RECEPTOR GENES

Despite significant evidence supporting a role for chemokines in angiogenesis, chemokine as well as chemokine receptor-deficient mice have not been reported to have any major angiogenesis defects. Actually, there is an absence of chemokine knock-out studies documenting its effects on angiogenesis in normal or pathological conditions. The CXCR-4 (receptor for SDF-1) knock-out mice provide the exception, because these mice have hematopoietic deficiencies, cardiac defects, as well as defective vascularization of the brain (54). Finally, IP-10-overexpressing transgenic mice have defective post-wound healing neovascularization (55), highlighting the angiostatic properties of this chemokine described in other models.

CONCLUSIONS

A considerable amount of evidence supports a role for chemokines in tumor angiogenesis, whereas for physiological/normal angiogenesis, further experimental evidence is lacking. In tumors, the expression and activity of ELR^+ CXC chemokines may also regulate tumor progression and the formation of metastasis. These properties of chemokines may provide a basis for antitumor strategies aimed at blocking chemokine production or secretion by tumor as well as accessory cells. A diagram showing some of the CXC chemokines, and the ELR^+ (pro-angiogenic) and ELR^- (angiostatic) members and their receptors can be seen in Figure 1.

Finally, given the apparent specificity of pro-angiogenic versus angiostatic chemokine receptors, it is legitimate to hypothesize that these may also have different downstream signaling pathways. Inhibitors for specific signaling intermediates or strategies to block receptor function may thus have antiangiogenic as well as antitumor effects.

REFERENCES

1. Clore, G.M.; Gronenborn, A.M. Three-Dimensional Structures of Alpha and Beta Chemokines. FASEB J. **1995**, *9*, 57–62.
2. Baggiolini, M.; Dewald, B.; Moser, B. Human Chemokines: An Update. Annu. Rev. Immunol. **1997**, *15*, 675–705.
3. Ebnet, K.; Vestweber, D. Molecular Mechanisms That Control Leukocyte Extravasation: The Selectins and the Chemokines. Histochem. Cell Biol. **1999**, *112*, 1–23.
4. Nelson, P.J.; Krensky, A.M. Chemokines, Lymphocytes and Viruses: What Goes Around, Comes Around. Curr. Opin. Immunol. **1998**, *10*, 265–270.
5. Dieu-Nosjean, M.C.; Vicari, A.; Lebecque, S.; Caux, C. Regulation of Dendritic Cell Trafficking: A Process That Involves the Participation of Selective Chemokines. J. Leukoc. Biol. **1999**, *66*, 252–262.
6. Cyster, J.G.; Ngo, V.N.; Ekland, E.H.; Gunn, M.D.; Sedgwick, J.D.; Ansel, K.M. Chemokines and B-Cell Homing to Follicles. Curr. Top. Microbiol. Immunol. **1999**, *246*, 87–92, 93.
7. Gupta, S.K.; Lysko, P.G.; Pillarisetti, K.; Ohlstein, E.; Stadel, J.M. Chemokine Receptors in Human Endothelial Cells. Functional Expression of CXCR4 and Its Transcriptional Regulation by Inflammatory Cytokines. J. Biol. Chem. **1998**, *273*, 4282–4287.
8. Goede, V.; Brogelli, L.; Ziche, M.; Augustin, H.G. Induction of Inflammatory Angiogenesis by Monocyte Chemoattractant Protein-1. Int. J. Cancer **1999**, *82*, 765–770.
9. Polverini, P.J. Role of the Macrophage in Angiogenesis-Dependent Diseases. EXS **1997**, *79*, 11–28.
10. Keane, M.P.; Arenberg, D.A.; Moore, B.B.; Addison, C.L.; Strieter, R.M. CXC Chemokines and Angiogenesis/Angiostasis. Proc. Assoc. Am. Physicians **1998**, *110*, 288–296.
11. Folkman, J. The Role of Angiogenesis in Tumor Growth. Semin. Cancer Biol. **1992**, *3*, 65–71.
12. Folkman, J. Angiogenesis and Angiogenesis Inhibition: An Overview. EXS **1997**, *79*, 1–8.
13. Hanahan, D.; Folkman, J. Patterns and Emerging Mechanisms of the Angiogenic Switch During Tumorigenesis. Cell **1996**, *86*, 353–364.
14. Hager, J.H.; Hanahan, D. Tumor Cells Utilize Multiple Pathways to Down-Modulate Apoptosis. Lessons from a Mouse Model of Islet Cell Carcinogenesis [in process citation]. Ann. N.Y. Acad. Sci. **1999**, *887*, 150–163.
15. Hanahan, D.; Weinberg, R.A. The Hallmarks of Cancer. Cell **2000**, *100*, 57–70.
16. Trautmann, A.; Toksoy, A.; Engelhardt, E.; Brocker, E.B.; Gillitzer, R. Mast Cell Involvement in Normal Hu-

man Skin Wound Healing: Expression of Monocyte Chemoattractant Protein-1 Is Correlated with Recruitment of Mast Cells Which Synthesize Interleukin-4 In Vivo. J. Pathol. **2000**, *190*, 100–106.

17. DiPietro, L.A.; Burdick, M.; Low, Q.E.; Kunkel, S.L.; Strieter, R.M. MIP-1 Alpha as a Critical Macrophage Chemoattractant in Murine Wound Repair. J. Clin. Invest. **1998**, *101*, 1693–1698.
18. DiPietro, L.A. Wound Healing: The Role of the Macrophage and Other Immune Cells. Shock **1995**, *4*, 233–40.
19. Arici, A.; Senturk, L.M.; Seli, E.; Bahtiyar, M.O.; Kim, G. Regulation of Monocyte Chemotactic Protein-1 Expression in Human Endometrial Stromal Cells by Estrogen and Progesterone. Biol. Reprod. **1999**, *61*, 85–90.
20. Wood, G.W.; Hausmann, E.H.; Kanakaraj, K. Expression and Regulation of Chemokine Genes in the Mouse Uterus During Pregnancy. Cytokine **1999**, *11*, 1038–1045.
21. Ijland, S.A.; Jager, M.J.; Heijdra, B.M.; Westphal, J.R.; Peek, R. Expression of Angiogenic and Immunosuppressive Factors by Uveal Melanoma Cell Lines. Melanoma Res. **1999**, *9*, 445–450.
22. Kitadai, Y.; Haruma, K.; Sumii, K.; Yamamoto, S.; Ue, T.; Yokozaki, H.; Yasui, W.; Ohmoto, Y.; Kajiyama, G.; Fidler, I.J.; Tahara, E. Expression of Interleukin-8 Correlates with Vascularity in Human Gastric Carcinomas. Am. J. Pathol. **1998**, *152*, 93–100.
23. Shi, Q.; Abbruzzese, J.L.; Huang, S.; Fidler, I.J.; Xiong, Q.; Xie, K. Constitutive and Inducible Interleukin 8 Expression by Hypoxia and Acidosis Renders Human Pancreatic Cancer Cells More Tumorigenic and Metastatic. Clin. Cancer Res. **1999**, *5*, 3711–3721.
24. Chen, Z.; Malhotra, P.S.; Thomas, G.R.; Ondrey, F.G.; Duffey, D.C.; Smith, C.W.; Enamorado, I.; Yeh, N.T.; Kroog, G.S.; Rudy, S.; McCullagh, L.; Mousa, S.; Quezado, M.; Herscher, L.L.; Van Waes, C. Expression of Proinflammatory and Proangiogenic Cytokines in Patients with Head and Neck Cancer. Clin. Cancer Res. **1999**, *5*, 1369–1379.
25. Yatsunami, J.; Tsuruta, N.; Ogata, K.; Wakamatsu, K.; Takayama, K.; Kawasaki, M.; Nakanishi, Y.; Hara, N.; Hayashi, S. Interleukin-8 Participates in Angiogenesis in Non-Small Cell, but Not Small Cell Carcinoma of the Lung. Cancer Lett. **1997**, *120*, 101–108.
26. Arenberg, D.A.; Keane, M.P.; DiGiovine, B.; Kunkel, S.L.; Morris, S.B.; Xue, Y.Y.; Burdick, M.D.; Glass, M.C.; Iannettoni, M.D.; Strieter, R.M. Epithelial-Neutrophil Activating Peptide (ENA-78) Is an Important Angiogenic Factor in Non-Small Cell Lung Cancer. J. Clin. Invest. **1998**, *102*, 465–472.
27. Yoneda, J.; Kuniyasu, H.; Crispens, M.A.; Price, J.E.; Bucana, C.D.; Fidler, I.J. Expression of Angiogenesis-Related Genes and Progression of Human Ovarian Carcinomas in Nude Mice. J. Natl. Cancer Inst. **1998**, *90*, 447–454.
28. Ferrer, F.A.; Miller, L.J.; Andrawis, R.I.; Kurtzman, S.H.; Albertsen, P.C.; Laudone, V.P.; Kreutzer, D.L. Angiogenesis and Prostate Cancer: In Vivo and In Vitro Expression of Angiogenesis Factors by Prostate Cancer Cells. Urology **1998**, *51*, 161–167.
29. Antony, V.B.; Hott, J.W.; Godbey, S.W.; Holm, K. Angiogenesis in Mesotheliomas. Role of Mesothelial Cell Derived IL-8. Chest **1996**, *109*, 21S–22S.
30. Desbaillets, I.; Diserens, A.C.; Tribolet, N.; Hamou, M.F.; Van Meir, E.G. Upregulation of Interleukin 8 by Oxygen-Deprived Cells in Glioblastoma Suggests a Role in Leukocyte Activation, Chemotaxis, and Angiogenesis. J. Exp. Med. **1997**, *186*, 1201–1212.
31. Koch, A.E.; Polverini, P.J.; Kunkel, S.L.; Harlow, L.A.; DiPietro, L.A.; Elner, V.M.; Elner, S.G.; Strieter, R.M. Interleukin-8 as a Macrophage-Derived Mediator of Angiogenesis. Science **1992**, *258*, 1798–1801.
32. Strieter, R.M.; Polverini, P.J.; Kunkel, S.L.; Arenberg, D.A.; Burdick, M.D.; Kasper, J.; Dzuiba, J.; Van Damme, J.; Walz, A.; Marriott, D.; et al. The Functional Role of the ELR Motif in CXC Chemokine-Mediated Angiogenesis. J. Biol. Chem. **1995**, *270*, 27348–27357.
33. Arenberg, D.A.; Kunkel, S.L.; Polverini, P.J.; Glass, M.; Burdick, M.D.; Strieter, R.M. Inhibition of Interleukin-8 Reduces Tumorigenesis of Human Non-Small Cell Lung Cancer in SCID Mice. J. Clin. Invest. **1996**, *97*, 2792–2802.
34. Kitadai, Y.; Takahashi, Y.; Haruma, K.; Naka, K.; Sumii, K.; Yokozaki, H.; Yasui, W.; Mukaida, N.; Ohmoto, Y.; Kajiyama, G.; Fidler, I.J.; Tahara, E. Transfection of Interleukin-8 Increases Angiogenesis and Tumorigenesis of Human Gastric Carcinoma Cells in Nude Mice. Br. J. Cancer **1999**, *81*, 647–653.
35. Bar-Eli, M. Role of Interleukin-8 in Tumor Growth and Metastasis of Human Melanoma. Pathobiology **1999**, *67*, 12–18.
36. Luca, M.; Huang, S.; Gershenwald, J.E.; Singh, R.K.; Reich, R.; Bar-Eli, M. Expression of Interleukin-8 by Human Melanoma Cells Up-Regulates MMP-2 Activity and Increases Tumor Growth and Metastasis. Am. J. Pathol. **1997**, *151*, 1105–1113.
37. Miller, L.J.; Kurtzman, S.H.; Wang, Y.; Anderson, K.H.; Lindquist, R.R.; Kreutzer, D.L. Expression of Interleukin-8 Receptors on Tumor Cells and Vascular Endothelial Cells in Human Breast Cancer Tissue. Anticancer Res. **1998**, *18*, 77–81.
38. Jordan, N.J.; Kolios, G.; Abbot, S.E.; Sinai, M.A.; Thompson, D.A.; Petraki, K.; Westwick, J. Expression of Functional CXCR4 Chemokine Receptors on Human Colonic Epithelial Cells. J. Clin. Invest. **1999**, *104*, 1061–1069.
39. Petzelbauer, P.; Watson, C.A.; Pfau, S.E.; Pober, J.S. IL-8 and Angiogenesis: Evidence That Human Endothelial Cells Lack Receptors and Do Not Respond to IL-8 In Vitro. Cytokine **1995**, *7*, 267–272.
40. Strieter, R.M.; Polverini, P.J.; Arenberg, D.A.; Kunkel, S.L. The Role of CXC Chemokines as Regulators of Angiogenesis. Shock **1995**, *4*, 155–160.

41. Addison, C.L.; Arenberg, D.A.; Morris, S.B.; Xue, Y.Y.; Burdick, M.D.; Mulligan, M.S.; Iannettoni, M.D.; Strieter, R.M. The CXC Chemokine, Monokine Induced by Interferon-Gamma, Inhibits Non-Small Cell Lung Carcinoma Tumor Growth and Metastasis. Hum. Gene Ther. **2000**, *11*, 247–61.
42. Strieter, R.M.; Kunkel, S.L.; Arenberg, D.A.; Burdick, M.D.; Polverini, P.J. Interferon Gamma-Inducible Protein 10 (IP-10), a Member of the CXC Chemokine Family, Is an Inhibitor of Angiogenesis. Biochem. Biophys. Res. Commun. **1995**, *210*, 51–57.
43. Arenberg, D.A.; Polverini, P.J.; Kunkel, S.L.; Shanafelt, A.; Strieter, R.M. In Vitro and In Vivo Systems to Assess Role of CXC Chemokines in the Regulation of Angiogenesis. Methods Enzymol. **1997**, *288*, 190–220.
44. Angiolillo, A.L.; Sgadari, C.; Taub, D.D.; Liao, F.; Farber, J.M.; Maheshwari, S.; Kleinman, H.K.; Reaman, G.H.; Tosato, G. Human Interferon-Inducible Protein 10 Is a Potent Inhibitor of Angiogenesis In Vivo. J. Exp. Med. **1995**, *182*, 155–162.
45. Moore, B.B.; Arenberg, D.A.; Addison, C.L.; Keane, M.P.; Strieter, R.M. Tumor Angiogenesis Is Regulated by CXC Chemokines. J. Lab. Clin. Med. **1998**, *132*, 97–103.
46. Arenberg, D.A.; Kunkel, S.L.; Polverini, P.J.; Morris, S.B.; Burdick, M.D.; Glass, M.C.; Taub, D.T.; Iannettoni, M.D.; Whyte, R.I.; Strieter, R.M. Interferon-Gamma-Inducible Protein 10 (IP-10) Is an Angiostatic Factor That Inhibits Human Non-Small Cell Lung Cancer (NSCLC) Tumorigenesis and Spontaneous Metastases. J. Exp. Med. **1996**, *184*, 981–992.
47. Dias, S.; Thomas, H.; Balkwill, F. Multiple Molecular and Cellular Changes Associated with Tumour Stasis and Regression During IL-12 Therapy of a Murine Breast Cancer Model. Int. J. Cancer **1998**, *75*, 151–157.
48. Angiolillo, A.L.; Sgadari, C.; Tosato, G. A Role for the Interferon-Inducible Protein 10 in Inhibition of Angiogenesis by Interleukin-12. Ann. N.Y. Acad. Sci. **1996**, *795*, 158–167.
49. Ward, S.G.; Westwick, J. Chemokines: Understanding Their Role in T-Lymphocyte Biology. Biochem. J. **1998**, *333*, 457–470.
50. Nagasawa, T.; Tachibana, K.; Kishimoto, T. A Novel CXC Chemokine PBSF/SDF-1 and Its Receptor CXCR4: Their Functions in Development, Hematopoiesis and HIV Infection. Semin. Immunol. **1998**, *10*, 179–185.
51. Chang, Y.; Cesarman, E.; Pessin, M.S.; Lee, F.; Culpepper, J.; Knowles, D.M.; Moore, P.S. Identification of Herpesvirus-Like DNA Sequences in AIDS-Associated Kaposi's Sarcoma. Science **1994**, *266*, 1865–1869.
52. Bais, C.; Santomasso, B.; Coso, O.; Arvanitakis, L.; Raaka, E.G.; Gutkind, J.S.; Asch, A.S.; Cesarman, E.; Gerhengorn, M.C.; Mesri, E.A. G-Protein-Coupled Receptor of Kaposi's Sarcoma-Associated Herpesvirus Is a Viral Oncogene and Angiogenesis Activator. Nature **1998**, *391*, 86–89.
53. Luster, A.D.; Greenberg, S.M.; Leder, P. The IP-10 Chemokine Binds to a Specific Cell Surface Heparin Sulfate Site Shared with Platelet Factor 4 and Inhibits Endothelial Cell Proliferation. J. Exp. Med. **1995**, *182*, 219–231.
54. Zou, Y.R.; Kottmann, A.H.; Kuroda, M.; Taniuchi, I.; Littman, D.R. Function of the Chemokine Receptor CXCR4 in Haematopoiesis and in Cerebellar Development. Nature **1998**, *393*, 595–599.
55. Luster, A.D.; Cardiff, R.D.; MacLean, J.A.; Crowe, K.; Granstein, R.D. Delayed Wound Healing and Disorganized Neovascularization in Transgenic Mice Expressing the IP-10 Chemokine. Proc. Assoc. Am. Physicians **1998**, *110*, 183–196.

MARCEL DEKKER, INC.
270 Madison Avenue, New York, New York 10016

EXHIBIT K

The CXC Chemokines IP-10 and Mig Are Necessary for IL-12-Mediated Regression of the Mouse RENCA Tumor[1]

Charles S. Tannenbaum,[2]* Raymond Tubbs,*‡ David Armstrong,* James H. Finke,* Ronald M. Bukowski,*† and Thomas A. Hamilton*

The role of the non-ELR-containing CXC chemokines IP-10 and Mig in antitumor activity induced by systemic treatment with IL-12 was examined in mice bearing the murine renal adenocarcinoma RENCA. IL-12 treatment produces a potent antitumor effect that is associated with tumor infiltration by $CD8^+$ T lymphocytes. The regression of tumor is associated with the elevated expression of the IFN-γ-inducible chemokines IP-10 and Mig within the tumor tissue. IP-10 and Mig have been shown to function as chemoattractants for activated T lymphocytes. In animals treated with rabbit polyclonal Abs specific for IP-10 and for Mig, the IL-12-induced regression of RENCA tumors was partially abrogated. This effect was associated with a dramatic inhibition of T cell infiltration. Thus, it appears that IL-12-dependent, T cell-mediated antitumor activity requires the intermediate expression of IP-10 and Mig to recruit antitumor effector T cells to the tumor site. *The Journal of Immunology,* **1998, 161: 927–932.**

Many cytokines, either administered systemically or expressed as transgenes by tumors, have been shown to promote significant antitumor activity in rodents (1–6). IL-12 is one of the most effective cytokines in such settings and results in high frequency cure of established, poorly immunogenic tumors (6–12). The mechanisms by which IL-12 induces antitumor function are believed to include the promotion of potent antitumor immunity in which T cells of the Th1 phenotype predominate (13–17). IL-12-mediated antitumor activity is dependent upon the presence of both $CD4^+$ and $CD8^+$ T lymphocytes and upon the production of IFN-γ (7, 10, 11). A recent report from this laboratory demonstrated that the antitumor response stimulated by IL-12 correlated strongly with the production of the IFN-γ-inducible chemokine IP-10 by cells within the tumor bed (6). IP-10 is a member of the CXC family of chemokines but is missing the ELR amino acid sequence motif that has been linked with neutrophil chemotaxis. The absence of this function reflects the inability of non-ELR CXC chemokines to bind with the IL-8R (CXCR1[3] and CXCR2) (18–20). Recently, a receptor exhibiting specificity for IP-10 and a related, non-ELR CXC chemokine termed Mig (21, 22) has been identified (CXCR3) whose expression is restricted to activated T cells (23). This finding suggested the hypothesis that IL-12 induces expression of IP-10 and Mig chemokines secondary to the production of IFN-γ and thereby stimulates enhanced recruitment of effector immune cells to the tumor site.

The goal of the present study was to test this hypothesis by examining the antitumor activity of IL-12 in animals given Abs to block the function of IP-10 and Mig. In BALB/c mice bearing established RENCA tumors, IL-12 treatment produces effective tumor regression (6, 7). Treatment with a mixture of rabbit polyclonal Abs that recognize IP-10 and Mig produced a significant abrogation of the IL-12-mediated antitumor function that was associated with a marked reduction in the infiltration of the tumor tissue with perforin-expressing $CD8^+$ T cells.

Materials and Methods

Reagents

Dulbecco's PBS was purchased from Mediatech (Washington DC). Agarose, SDS, guanidine isothiocyanate, cesium chloride, and phenol were purchased from Life Technologies (Gaithersburg, MD). Boehringer Mannheim (Indianapolis, IN) was the source of restriction endonucleases, proteinase K, nick translation kits, random primer kits, reverse transcriptase, RNase inhibitor, and Taq polymerase. [^{32}P]dCTP was purchased from DuPont-New England Nuclear Research Products (Boston, MA). Reagents for SDS-PAGE and protein determination were obtained from Bio-Rad Laboratories (Richmond, CA). Recombinant murine IL-12 was provided by both Genetics Institute (Boston, MA) and Dr. Michael Brunda (Hoffmann-La Roche, Nutley, NJ). Vector Laboratories (Burlingame, CA) was the source of biotinylated goat anti-rat IgG. Peroxidase-labeled streptavidin, biotinylated anti-rat IgG, and chromogenic substrate for immunohistology were purchased from Ventana Medical Systems (Tuscon, AZ). Rat mAbs against mouse CD4 and CD8 were purchased from Becton Dickinson (Mountain View, CA), and a mAb against mouse CD31 was provided by Dr. Alberto Mantovani (Mario Negri Institute, Milan, Italy).

Animals

Male BALB/c mice, 6 to 8 wk old, were purchased from the National Institutes of Health (Bethesda, MD) and housed in a specific pathogen-free animal facility. Animals were maintained in microisolator cages with autoclaved food and bedding to minimize exposure to viral and microbial pathogens (24).

Tumors

RENCA is a spontaneously arising murine renal cell carcinoma and was isolated and maintained as described previously (25). Routinely, 4×10^5 tumor cells in 0.1 ml of PBS were inoculated s.c. Fourteen days following tumor inoculation, animals received 0.5 μg of recombinant murine IL-12 i.p. daily for the duration of the experiment, while control animals received vehicle alone. Tumor volumes were measured daily with a micrometer in two dimensions, and tumor size was estimated according to the formula: $(\text{smallest diameter})^2 \times (\text{longest diameter})$. Tumor growth under different treatment conditions was statistically analyzed using the Wilcoxon rank sum test. The p values obtained represent the two-sided value.

*Department of Immunology, Lerner Research Institute; and Departments of †Hematology-Oncology and ‡Anatomic Pathology, Cleveland Clinic Foundation, Cleveland, OH 44195

Received for publication September 22, 1997. Accepted for publication March 11, 1998.

The costs of publication of this article were defrayed in part by the payment of page charges. This article must therefore be hereby marked *advertisement* in accordance with 18 U.S.C. Section 1734 solely to indicate this fact.

[1] This work was supported by U.S. Public Health Service Grant CA39621 and funds from the Cleveland Clinic Cancer Center.

[2] Address correspondence and reprint requests to Dr. Charles S. Tannenbaum, Department of Immunology, NN10, Cleveland Clinic Foundation, 9500 Euclid Ave., Cleveland, OH 44195.

[3] Abbreviation used in this paper: CXCR, receptor for CXC chemokine.

0022-1767/98/$02.00

Preparation of Abs

Rabbit polyclonal Abs to Mig and IP-10 were produced by Biosynthesis (Lewisville, TX) using synthetic peptides selected from the IP-10 and Mig protein sequences (CIHIDDGPVRMRAIGK and CISTSRGTIHYKSLK DLKQFAPS, respectively) coupled to carrier protein KLH.

Western blot analysis

RENCA cells in 100-mm diameter petri dishes were cultured in serum- and protein-free hybridoma medium (Sigma, St. Louis, MO) with or without stimulation by IFN-γ for 24 h. Supernatant medium was dialyzed overnight against 25 mM NaPO4, pH 7.4, and then mixed with a 40-μl (bed volume) aliquot of heparin-Sepharose beads for 16 h at room temperature. The beads were washed in buffer and then boiled in the presence of 2% SDS sample buffer (26), and the eluted samples were separated by SDS-PAGE (15%). Proteins were then transferred to Nitrobind transfer membranes (Micron Separations, Westborough, MA) using a semidry transfer cell (Bio-Rad) for 45 min at 450 mA constant current in transfer buffer (48 mM Tris, 39 mM glycine, and 20% methanol, pH 9.2). Blots were blocked with 5% nonfat milk in TBST (0.15 M NaCl, 0.1% Tween-20, and 50 mM Tris, pH 7.4) at 20°C for 2 h, then incubated overnight with rabbit polyclonal Abs against IP-10 or Mig in 5% nonfat milk TBST solution (in some reactions, peptide against which the Ab was initially raised was included as a competitor at 1 μg/ml). After washing three times in TBST, filters were incubated at room temperature for 1 h with goat anti-rabbit IgG conjugated to horseradish peroxidase and then washed again as described above. Ab binding was detected using the ECL kit from Amersham (Arlington Heights, IL).

Immunohistologic analysis

Immunohistology was performed as previously described (6, 25, 27). Tissues were snap-frozen in isopentane precooled in liquid nitrogen until sectioned. Frozen tissue sections (6 μm) were prepared, air-dried, fixed in cold reagent grade acetone for 10 min, and air dried. Rat mAbs against mouse CD8 or CD31 were applied at concentrations optimally titrated against mouse thymus or mouse lung, respectively, and linked to streptavidin-peroxidase by biotinylated rabbit anti-rat IgG using the Ventana 320 automated immunostainer (Ventana, Tuscon, AZ). The chromogenic substrate aminocarbazole/H_2O_2 followed by hematoxylin counterstaining was used to visualize positive reactivity. To quantify T cell infiltration into tumor tissues, the number of cells showing anti-CD8 reactivity in a series of high power fields was counted in several tumors from each experiment. Because the tumor tissue exhibited variable degrees of necrosis and variable distribution of T cell infiltrates, only fields of nonnecrotic tumor containing the highest T cell numbers for each experimental condition were included in the analysis.

Plasmids

Plasmids with inserts encoding murine IP-10 and perforin were previously described (6). A DNA fragment encoding a portion of the murine Mig mRNA sequence was obtained by RT-PCR using primers flanking the coding region and RNA derived from IFN-γ-stimulated mouse peritoneal macrophages. The PCR product was cloned into the plasmid pGEM 4Z. The methods for plasmid DNA preparation were previously described (6).

Analysis of mRNA expression in tumor tissue

Total cellular RNA was extracted from 0.3 to 0.5 g of whole tumor tissue by homogenization with a Polytron sonicator/homogenizer (Brinkmann Instruments, Westbury, NY) for 1 min in guanidine isothionate followed by ultracentrifugation through cesium chloride according to previously described methods (28, 29). Northern hybridization analysis was conducted as described previously (30, 31). Equal amounts of RNA (20 μg) were denatured, separated by electrophoresis in an agarose-formaldehyde gel, and blotted by capillary transfer onto nylon membranes. The blots were prehybridized 6 to 18 h at 42°C in 50% formamide, 1% SDS, 5× SSC, 1× Denhardt's solution (0.02% Ficoll, 0.02% BSA, and 0.02% polyvinylpyrrolidine), 0.25 mg/ml denatured salmon sperm DNA, and 50 mM sodium phosphate buffer, pH 6.5. Hybridization was conducted at 42°C for 12 to 18 h with 10^7 cpm of denatured probe. The filters were washed twice for 15 min each time at 55°C in 0.1% SDS-0.5× SSC. The blots were then exposed using XAR-5 x-ray film (Eastman Kodak, Rochester, NY) with DuPont (Wilmington, DE) Cronex Lightening Plus intensifying screens at −70°C. Expression of glyceraldehyde-3-phosphate dehydrogenase (GAPDH) mRNA was used as an internal control and was applied in all experiments.

Semiquantitative RT-PCR analysis of perforin mRNA was conducted as reported previously (6, 25, 32). One microgram of total RNA was amplified using an oligo(dT) antisense primer and AMV reverse transcriptase at 42°C for 1 h. The RT reaction products were used undiluted or at a 1/10 dilution for PCR amplification using 20 mM sense and antisense primers (see below) and Taq polymerase. PCR reactions were conducted in a Perkin-Elmer/Cetus DNA Thermal Cycler for 15 cycles (denaturation, 1 min, 94°C; annealing, 1 min, 60°C; amplification, 2 min, 72°C). The primer sequences used were as follows: perforin antisense primer, GGTGGAGT GGAGGTTTTTGTACC; and perforin sense primer, CAGAATGCAAG CAGAAGCACAAG (perforin product size, 486 bp). These primers were chosen from separate exons to ensure that products derived from mRNA and contaminating genomic DNA could be distinguished. The PCR products were separated by agarose gel electrophoresis and visualized by Southern hybridization analysis using radiolabeled cDNA encoding a portion of the perforin gene sequence.

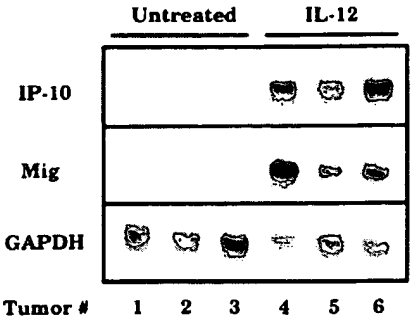

FIGURE 1. Expression of IP-10 and Mig mRNA in tumor tissue from untreated and IL-12-treated mice. BALB/c mice were inoculated with 4×10^5 RENCA cells s.c. Groups of six animals were not treated or were treated i.p. with IL-12 (0.5 μg/mouse/day) beginning on day 14 for 10 days before harvest of tumor tissue and preparation of total RNA. Twenty micrograms of RNA from each animal was subjected to Northern hybridization analysis as described in *Materials and Methods*, using radiolabeled cDNAs corresponding to the indicated mRNAs. Similar results were obtained in three separate experiments.

Results

BALB/c mice were injected s.c with 4×10^5 RENCA tumor cells, and IL-12 treatment (0.5 μg/day i.p.) was initiated on day 14. Tumors in animals receiving saline vehicle grew progressively, while tumors in IL-12-treated animals regressed following a modest delay, confirming previous work (6). To examine the expression of chemokines at the tumor site, total RNA was prepared from tumor tissue isolated from control or IL-12-treated animals and analyzed for the expression of the IFN-γ-inducible chemokine mRNAs by Northern hybridization (Fig. 1). IP-10 and Mig mRNA were readily detected in tumor tissue from IL-12-treated animals, but not in tumors from untreated animals.

To determine the functional importance of chemokine expression in the IL-12-mediated antitumor activity, Abs against mouse IP-10 and Mig were raised in rabbits as described in *Materials and Methods*. The Abs were characterized by examining reactivity in Western blots with proteins secreted by cultured RENCA cells stimulated with IFN-γ (Fig. 2). While Ab to IP-10 reacts with a single band of approximately 8 kDa present only in the medium from IFN-γ-stimulated cells, the Ab to Mig showed specific recognition of three IFN-γ-inducible peptide species of approximately 14, 10, and 8 kDa. Specificity was further demonstrated by competition with peptides used as immunogens (Fig. 2). The heterogeneity evident in the Mig protein may derive from post-translational modification and/or from degradation following secretion.

These Abs were subsequently employed to assess the roles of IP-10 and Mig in IL-12-mediated regression of RENCA tumors. BALB/c mice bearing 14-day-old RENCA tumors were treated with IL-12 (0.5 μg/animal/day) for 15 days with or without control

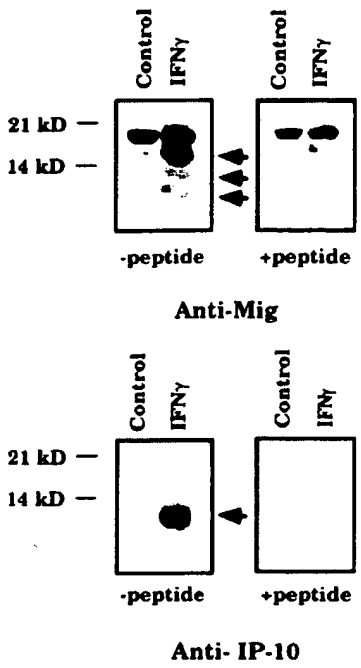

FIGURE 2. Analysis of IP-10 and Mig protein expression in RENCA cells in culture. Confluent cultures of RENCA cells in 100-mm petri dishes were not treated or were treated with 100 U/ml of murine IFN-γ for 18 h in serum- and protein-free culture medium. Supernatant medium from each sample was dialyzed, adsorbed to heparin-Sepharose beads, eluted, and separated by 15% SDS-PAGE. Proteins were transferred to nitrocellulose filters and analyzed separately for reactivity with Abs against IP-10 or Mig in presence or the absence of specific peptide immunogen (1 μg/ml) as indicated. Similar results were obtained in two separate experiments.

or anti-chemokine Ig. Animals in groups of 12 received 1 mg of nonimmune Ig or anti-Mig and/or anti-IP-10 Ig i.p. 1 day before the initiation of IL-12 treatment and at 3-day intervals (0.5 mg each) through the completion of the experiment. Tumors grew progressively in otherwise untreated mice and in mice that were given nonimmune rabbit Ig, while growth of tumors in animals treated with IL-12 was inhibited (Fig. 3). In two separate experiments, the combination of anti-IP-10 and anti-Mig significantly reduced the IL-12-mediated inhibition of tumor growth ($p \leq 0.005$ for the group treated with IL-12 and nonimmune Ig vs that treated with IL-12 and anti-IP-10 and anti-Mig Ig). Indeed, by day 15 of treatment, tumors from animals receiving both anti-chemokine Abs were approximately fivefold larger than tumors from animals treated with IL-12 alone or with nonimmune Ig. While treatments with anti-IP-10 alone had no detectable effect on IL-12-driven antitumor function, use of Ab to Mig alone produced a small reduction of the response to IL-12, which was not statistically significant. These results indicate that Mig and IP-10 may be necessary for IL-12-mediated anti-tumor activity.

It has recently been shown that Mig and IP-10 mediate chemotaxis of activated T cells via interaction with the CXCR3 receptor (22, 23, 33). Furthermore, the antitumor activity of IL-12 is heavily dependent on T cells (7, 10). To determine whether the observed inhibition of IL-12-mediated antitumor activity by Abs against Mig and IP-10 might result from abrogation of T cell recruitment into the tumor bed, tumor tissue from animals treated with IL-12 along with control or anti-chemokine Abs was analyzed for T cell infiltration by immunohistology. Tumors prepared from IL-12-treated animals were heavily infiltrated with $CD8^+$ T cells, confirming previous findings (6) (Fig. 4*A*). Tumor tissue from animals receiving Abs to both IP-10 and Mig throughout the course of IL-12 treatment exhibited a dramatic reduction in $CD8^+$ T cell infiltration (this effect was observed in all four RENCA tumors examined and in two separate experiments). Quantification of $CD8^+$ T cell infiltration was conducted by comparing numbers of T cells in sections of tumors from different treatment conditions (Fig. 4*B*). In each treatment group regions of the tumor that contained the highest level of T cell infiltration were identified, and the $CD8^+$ T cells were enumerated in a series of high power fields. Regions of the tumor that exhibited necrosis were excluded. This analysis confirms the reduction in T cell numbers within tumors from mice receiving IL-12 plus anti-IP-10 and anti-Mig compared with those in animals receiving IL-12 alone or in the presence of nonspecific Ab. Furthermore, an intermediate reduction in T cell infiltration was observed in animals receiving IL-12 and only anti-Mig Ab. The number of $CD4^+$ T cells infiltrating the tumors in IL-12-treated animals was also reduced in animals receiving the anti-chemokine Ig (data not shown).

Previous studies from this laboratory demonstrated that perforin mRNA was strongly expressed in regressing RENCA tumors from mice treated with IL-12 (6). Perforin is a product of cytotoxic T cells and NK cells and may contribute to the antitumor activity of IL-12 (34–37). Portions of the RENCA tumors from the experiments shown in Figure 4 were used to prepare total RNA for semiquantitative analysis of perforin mRNA levels using RT-PCR. The results obtained provide further confirmation of the histologic data

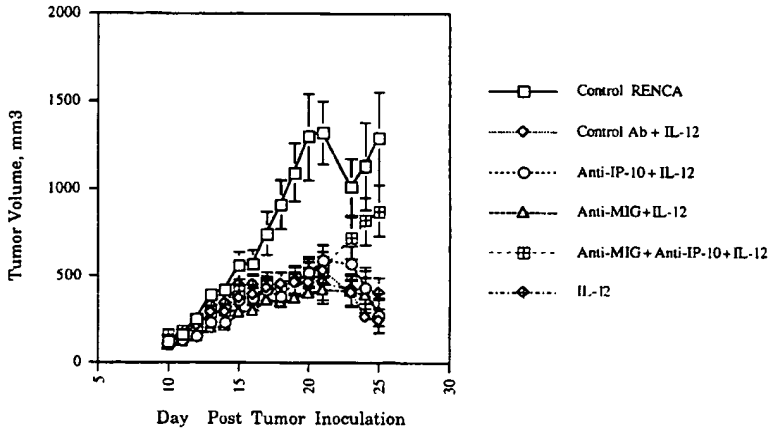

FIGURE 3. Abs to IP-10 and Mig inhibit IL-12-mediated antitumor activity. BALB/c mice were inoculated with 4×10^5 RENCA cells s.c. On day 14, groups of 12 animals were treated with IL-12 alone or with control or anti-chemokine Abs as indicated. IL-12 (0.5 μg/animal/day) was administered daily, and Abs were given 1 day before IL-12 and at 3-day intervals thereafter. Tumor size was measured as described in *Materials and Methods* daily through 15 days of treatment. Results are presented as the mean ± SEM. Similar results were obtained in two separate experiments.

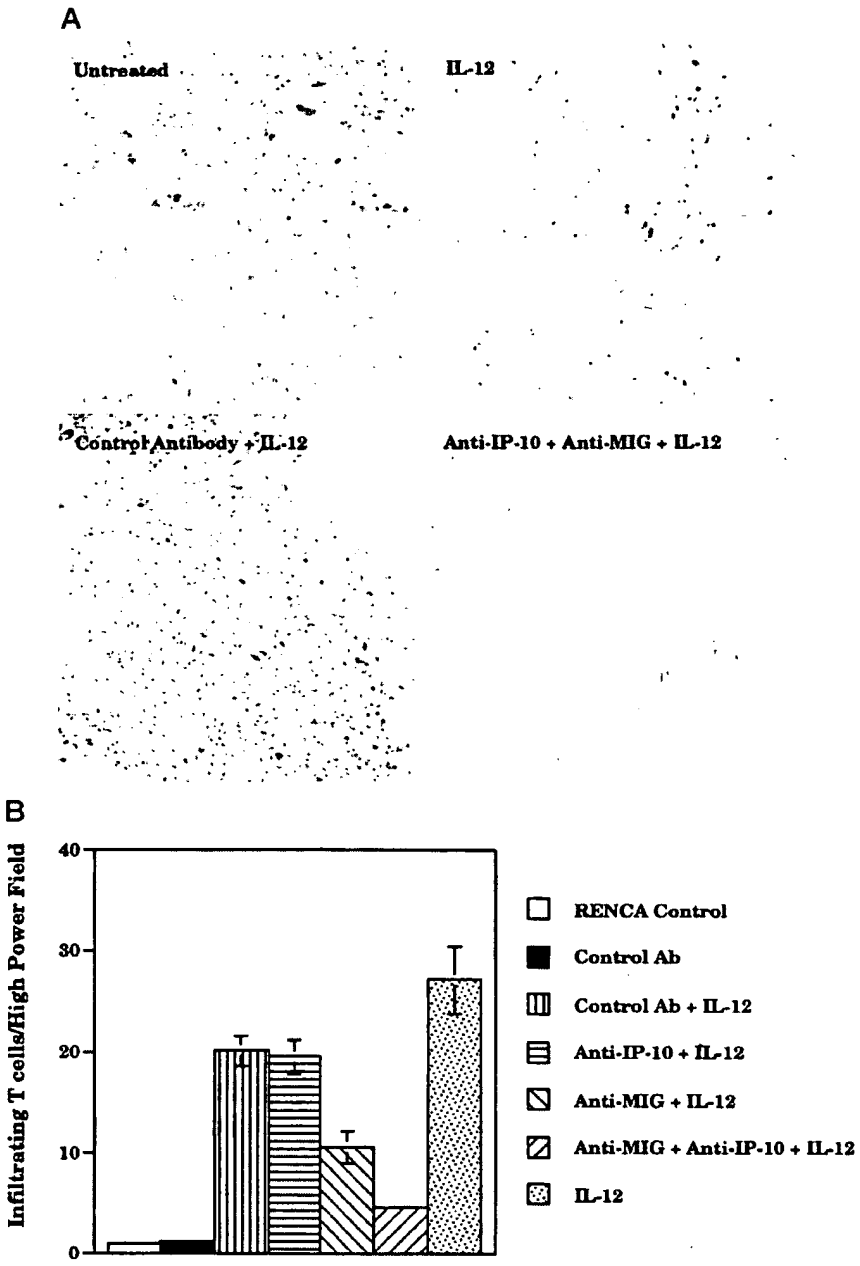

FIGURE 4. Abs to IP-10 and Mig block $CD8^+$ T cell infiltration in IL-12-treated RENCA tumors. *A*, RENCA tumors were obtained from animals treated, or not, with IL-12 in the presence or the absence of either control or anti-IP-10 and anti-Mig Abs and were processed for immunohistology to detect the presence of $CD8^+$ T cells as described in *Materials and Methods*. *B*, High power fields from each histologic section were analyzed for T cell infiltration as described in *Materials and Methods*. Results are presented as the mean ± SEM. Similar results were obtained in two separate experiments.

(Fig. 5). Tumors from IL-12-treated mice had high levels of perforin mRNA compared with untreated tumors, in which perforin mRNA was not detectable. Tumor tissue from animals treated with IL-12 and nonimmune rabbit Ig also expressed high levels of perforin mRNA, while tumor from animals treated with IL-12 and anti-Mig/anti-IP-10 had significantly reduced perforin expression. In this experiment, the reduction in perforin mRNA from animals receiving Ab to Mig alone is also evident.

Both IP-10 and Mig have been shown to inhibit angiogenesis in vivo and in vitro (38–41). Furthermore, IL-12 has been reported to exhibit antiangiogenic activity, and this has been attributed to IL-12-dependent expression of IP-10 (42, 43). To test the possibility that our Abs were inhibiting IL-12-mediated antitumor function by blocking the inhibition of angiogenesis, we assessed the relative intratumoral density of endothelial cells based upon immunoreactivity with a mAb against CD31, a marker highly specific for vascular endothelium. The density of CD31-positive cells present in the tumor was not different between experimental groups (data not shown). Tumors from IL-12-treated mice exhibited significant necrosis, and examination of endothelial cell density was restricted to nonnecrotic areas of the tumor; the distribution and density of CD31 staining were, however, equivalent in all fields examined regardless of treatment condition. Because tumor tissue was rapidly destroyed in T cell-dependent fashion following the initiation of IL-12 treatment, this result may not reflect the angiostatic potential of IL-12 or IP-10 and Mig.

Discussion

The goal of the present study was to test the importance of the chemokines IP-10 and Mig in IL-12-mediated regression of RENCA tumor growth. Although IL-12 was originally identified

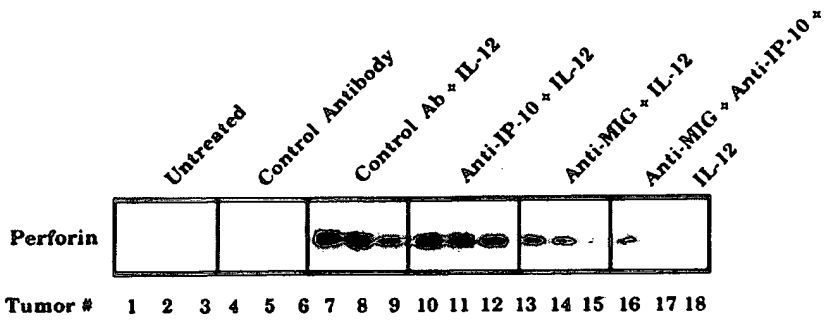

FIGURE 5. Abs to IP-10 and Mig reduce perforin mRNA levels in IL-12-treated RENCA tumors. Tumors were obtained from animals treated with IL-12 with or without control or anti-chemokine Abs as indicated and were used to prepare total RNA. RNA samples from individual tumors was used for semiquantitative RT-PCR detection of perforin mRNA as described in *Materials and Methods*. PCR products were separated on agarose gels, blotted onto nylon membrane, and hybridized with a radiolabeled cDNA corresponding to perforin mRNA. Similar results were obtained in two separate experiments.

as a stimulus of NK cells, it has since has been characterized as an important cytokine in many physiologic and pathophysiologic settings (8, 14, 44–46). IL-12-stimulated antitumor function is dependent upon the induction of IFN-γ and the presence of both $CD4^+$ and $CD8^+$ T cells (7, 9, 10). The observation that IL-12 treatment induces high levels of IFN-γ in tumor-bearing nude mice without marked antitumor effects indicates that IFN-γ is necessary, but not sufficient, for IL-12-mediated antitumor function (7, 9, 10). We hypothesize that the remarkable antitumor efficacy of IL-12 derives from its ability both to enhance the T cell-mediated immune response to the tumor and to promote the infiltration of the tumor by activated effector T cells. Our results indicate that this latter objective is achieved via the IFN-γ-mediated production of the non-ELR-containing CXC chemokines, IP-10 and Mig, and is supported by the following observations. 1) Rabbit Abs to IP-10 and Mig, when provided in combination, reduce the antitumor activity of IL-12 against established RENCA tumors growing s.c. 2) The anti-chemokine Ab treatment results in a marked reduction in the infiltration of tumors by $CD4^+$ and $CD8^+$ T cells and reduced expression of mRNA encoding the cytotoxic T cell effector molecule perforin. 3) There was no detectable change in the tissue density of endothelial cells within tumors receiving any of the experimental treatments.

While the effect of Ab treatment on antitumor function is not complete, the results clearly indicate that both chemokine gene products are functionally important components of the IL-12 antitumor mechanism. Since both Mig and IP-10 bind CXCR3 and mediate T cell chemotaxis (23), it is not surprising that both Abs should be required to achieve neutralization of IL-12-mediated T cell infiltration and tumor growth inhibition. Although statistically significant effects were only observed when Abs to both Mig and IP-10 were administered, anti-Mig Ab alone appeared to produce a reduction in the action of IL-12 in several animals. In this regard Mig has also been shown to exhibit higher potency than IP-10 in T cell chemotaxis (22, 23).

The results presented here suggest that the effect of anti-chemokine Abs on IL-12-driven tumor regression is a direct consequence of their ability to block chemokine-mediated recruitment of activated T cells to the site. Such a scenario is consistent with an early report showing that IP-10 expression by tumor cells could promote a strong T cell-dependent antitumor effect (47). Both IP-10 and Mig have been shown to exhibit other nonchemotaxis-related activities that may be relevant to the antitumor effects of IL-12. Specifically, both chemokines have been reported to exhibit potent antiangiogenic activity in vitro and in vivo (38–41). Interestingly, CXC chemokines that possess an ELR amino acid motif immediately preceding the CXC motif have been demonstrated to be angiogenic agents, while those that do not have the ELR sequence are angiogenesis inhibitors (41). Indeed, the balance of expression of ELR^+ and ELR^- CXC chemokines within a tumor has been proposed as an important determinant of progressive tumor growth and metastasis (41, 48). This hypothesis is supported by the finding that IP-10 expression by human lung tumors in SCID mice is associated with reduced tumor growth potential, while neutralization of IP-10 enhances growth (49). In our studies the density of endothelial cells within tumor tissue did not change in the presence of IL-12 treatment (and was not influenced by Abs to IP-10 or Mig). This result should not, however, be interpreted to mean that IL-12 did not produce an angiostatic effect in RENCA tumors. Because RENCA tumors are rapidly destroyed in immunocompetent mice treated with IL-12, the angiogenesis inhibitory action of IL-12 may be masked by its potent effect on the development of antitumor T cells. Thus, these experiments do not allow a direct determination of the antiangiogenic activity of IP-10 and Mig. In addition to effects on neovascularization, both IP-10 and Mig have also been reported to cause focal tumor necrosis when injected intratumorally or when expressed by tumor cells (50, 51). As discussed above with regard to angiogenesis inhibition, we cannot determine whether IP-10 and/or Mig are responsible for enhanced tumor necrosis because of the dominant role of T cell activity in this model.

There have been numerous reports attesting to the ability of CC and CXC chemokines to promote antitumor activity when expressed as transgenes by experimental tumors (39, 52–58). While there are examples where chemokine expression alone appears to be sufficient to promote an efficacious antitumor response, chemokines may function best in cooperation with other cytokine agents. For example, tumor cells transduced to express lymphotactin, a chemokine with specificity for T cells, grew normally when injected alone, but were destroyed rapidly in mice cotreated with IL-2 (59). The results of the present study support the concept of cooperativity between chemokines and other cytokines in antitumor strategies. IL-12 is able to promote chemokine expression through the enhanced expression of IFN-γ; this may not be sufficient, however, and IL-12 also promotes expansion and activation of tumor-specific T lymphocytes. The IFN-γ-induced chemokines may cooperate by recruiting such cells to the tumor site. One consequence of increased T cell infiltration would be additional IFN-γ production and further enhancement of chemokine synthesis. It is also likely that the nonchemotactic functions of Mig and IP-10, such as inhibition of angiogenesis, can act cooperatively with the chemotactic functions to promote more efficacious antitumor function.

References

1. Sayers, T. J., T. A. Wiltrout, K. McCormick, C. Husted, and R. H. Wiltrout. 1990. Antitumor effects of α-interferon and γ-interferon on a murine renal cancer (Renca) in vitro and in vivo. *Cancer Res. 50:5414.*
2. Brunda, M. J., and R. B. Wright. 1986. Differential antiproliferative effects of combinations of recombinant interferons α and γ on two murine tumor cell lines. *Int. J. Cancer 37:287.*

3. Brunda, M. J., V. Sulich, and D. Bellatoni. 1987. The anti-tumor effect of recombinant interferon α or γ is influenced by tumor location. *Int. J. Cancer 40: 807.*
4. Mule, J. J., J. C. Yang, R. Lafreniere, S. Shu, and S. A. Rosenberg. 1987. Identification of cellular mechanisms operational in vivo during the regression of established pulmonary metastases by systemic administration of high-dose recombinant interleukin-2. *J. Immunol. 139:285.*
5. Kedar, E. and E. Klein. 1992. Cancer immunotherapy: are the results discouraging? Can they be improved? *Adv. Cancer Res. 59:245.*
6. Tannenbaum, C. S., N. Wicker, D. Armstrong, R. Tubbs, J. Finke, R. M. Bukowski, and T. A. Hamilton. 1996. Cytokine and chemokine expression in tumors of mice receiving systemic therapy with IL-12. *J. Immunol. 156:693.*
7. Brunda, M. J., L. Luistro, R. R. Warrier, R. B. Wright, B. R. Hubbard, M. Murphy, S. F. Wolf, and M. K. Gately. 1993. Antitumor and antimetastatic activity of interleukin 12 against murine tumors. *J. Exp. Med. 178:1223.*
8. Brunda, M. J. 1994. Interleukin-12. *J. Leukocyte Biol. 55:280.*
9. Brunda, M. J., and M. K. Gately. 1994. Antitumor activity of interleukin-12. *Clin. Immunol. Immunopathol. 71:253.*
10. Nastala, C. L., H. D. Edington, T. G. McKinney, H. Tahara, M. A. Nalesnik, M. J. Brunda, M. K. Gately, S. F. Wolf, R. D. Schreiber, W. J. Storkus, and M. T. Lotze. 1994. Recombinant interleukin-12 (IL-12) administration induces tumor regression in association with interferon-γ production. *J. Immunol. 153:1697.*
11. Brunda, M. J., L. Luistro, J. A. Hendrzak, M. Fountoulakis, G. Garotta, and M. K. Gately. 1995. Role of interferon-γ in mediating the antitumor efficacy of interleukin-12. *J. Immunother. 17:71.*
12. Brunda, M. J., L. Luistro, L. Rumennik, R. B. Wright, M. Dvorozniak, A. Aglione, J. M. Wigginton, R. H. Wiltrout, J. A. Hendrzak, and A. V. Palleroni. 1996. Antitumor activity of interleukin 12 in preclinical models. *Cancer Chemother. Pharmacol. 38(Suppl.):S16.*
13. Trinchieri, G. 1993. Interleukin-12 and its role in the generation of Th1 cells. *Immunol. Today 14:335.*
14. Trinchieri, G., and P. Scott. 1994. The role of interleukin 12 in the immune response, disease and therapy. *Immunol. Today 15:460.*
15. Manetti, R., P. Parronchi, M. G. Giudizi, M.-P. Piccinni, E. Maggi, G. Trinchieri, and S. Romagnani. 1993. Natural killer cell stimulatory factor (interleukin 12 [IL-12]) induces T helper type 1 (Th1)-specific immune response and inhibits the development of IL-4-producing Th cells. *J. Exp. Med. 177:1199.*
16. Kobayashi, M., L. Fitz, M. Ryan, R. M. Hewick, S. C. Clark, S. Chan, F. Loudon, F. Sherman, B. Perussia, and G. Trinchieri. 1989. Identification and purification of natural killer cell stimulatory factor (NKSF), a cytokine with multiple biological effects on human lymphocytes. *J. Exp. Med. 170:827.*
17. Trinchieri, G. 1995. Interleukin-12: a proinflammatory cytokine with immunoregulatory functions that bridge innate resistance and antigen-specific adaptive immunity. *Annu. Rev. Immunol. 13:251.*
18. Clark-Lewis, I., B. Dewald, M. Loetscher, B. Moser, and M. Baggiolini. 1994. Structural requirements for interleukin-8 function identified by design of analogs and CXC chemokine hybrids. *J. Biol. Chem. 269:16075.*
19. Baggiolini, M., P. Loetscher, and B. Moser. 1995. Interleukin-8 and the chemokine family. *Int. J. Immunopharmacol. 17:103.*
20. Clark-Lewis, I., K.-S. Kim, K. Rajarathnam, J.-H. Gong, B. Dewald, B. Moser, M. Baggiolini, and B. D. Sykes. 1995. Structure-activity relationships of chemokines. *J. Leukocyte Biol. 57:703.*
21. Farber, J. M. 1990. A macrophage mRNA selectively induced by gamma-interferon encodes a member of the platelet factor 4 family of cytokines. *Proc. Natl. Acad. Sci. USA 87:5238.*
22. Liao, F., R. L. Rabin, J. R. Yannelli, L. G. Koniaris, P. Vanguri, and J. M. Farber. 1995. Human Mig chemokine: biochemical and functional characterization. *J. Exp. Med. 182:1301.*
23. Loetscher, M., B. Gerber, P. Loetscher, S. A. Jones, L. Piali, I. Clark-Lewis, M. Baggiolini, and B. Moser. 1996. Chemokine receptor specific for IP10 and Mig: structure, function and expression in activated T lymphocytes. *J. Exp. Med. 184:963.*
24. Meltzer, M. S. 1976. Tumoricidal response in vitro of peritoneal macrophages from conventionally housed and germ-free nude mice. *Cell. Immunol. 22:176.*
25. Sonouchi, K., T. A. Hamilton, C. S. Tannenbaum, R. R. Tubbs, R. Bukowski, and J. H. Finke. 1994. Chemokine gene expression in the murine renal cell carcinoma, RENCA, following treatment in vivo with interferon-α and interleukin-2. *Am. J. Pathol. 4:747.*
26. Laemmli, U. K. 1970. Cleavage of structural proteins during the assembly of the head of bacteriophage T4. *Nature 227:680.*
27. Sheibani, K., and R. R. Tubbs. 1984. Enzyme immunohistochemistry: technical aspects. *Semin. Diag. Pathol. 1:235.*
28. Chirgwin, J. M., R. J. Pryzbyla, R. J. MacDonald, and W. J. Rutter. 1979. Isolation of biologically active RNA from sources enriched in ribonuclease. *Biochemistry 18:5295.*
29. Sambrook, J., E. F. Fritsch, and T. Maniatis. 1989. *Molecular Cloning: A Laboratory Manual.* Cold Spring Harbor Laboratory, Cold Spring Harbor.
30. Hamilton, T. A., N. Bredon, Y. Ohmori, and C. S. Tannenbaum. 1989. IFN-γ and IFN-β independently stimulate the expression of lipopolysaccharide-inducible genes in murine peritoneal macrophages. *J. Immunol. 142:2325.*
31. Tannenbaum, C. S., T. J. Koerner, M. M. Jansen, and T. A. Hamilton. 1988. Characterization of lipopolysaccharide-induced macrophage gene expression. *J. Immunol. 140:3640.*
32. Alexander, J. P., S. Kudoh, K. A. Melsop, T. A. Hamilton, M. G. Edinger, R. R. Tubbs, D. Sica, L. Tauson, E. Klein, R. M. Bukowski, and J. H. Finke. 1993. T cells infiltrating renal cell carcinoma display a poor proliferative response even though they can produce IL-2 and express IL-2 receptors. *Cancer Res. 53:1380.*
33. Taub, D. D., A. R. Lloyd, K. Conlon, J. M. Wang, J. R. Ortaldo, A. Harada, K. Matsushima, D. J. Kelvin, and J. J. Oppenheim. 1993. Recombinant human interferon-inducible protein 10 is a chemoattractant for human monocytes and T lymphocytes and promotes T cell adhesion to endothelial cells. *J. Exp. Med. 177:1809.*
34. Podack, E. R., H. Hengartner, and M. G. Lichtenheld. 1991. A central role of perforin in cytolysis? *Annu. Rev. Immunol. 9:129.*
35. Cesano, A., S. Visonneau, S. C. Clark, and D. Santoli. 1993. Cellular and molecular mechanisms of activation of MHC nonrestricted cytotoxic cells by IL-12. *J. Immunol. 151:2943.*
36. Salcedo, T. W., L. Azzoni, S. F. Wolf, and B. Perussia. 1993. Modulation of perforin and granzyme messenger RNA expression in human natural killer cells. *J. Immunol. 151:2511.*
37. Lowin, B., F. Beermann, A. Schmidt, and J. Tschopp. 1994. A null mutation in the perforin gene impairs cytolytic T-lymphocyte and natural killer cell mediated cytotoxicity. *Proc. Natl. Acad. Sci. USA 91:11571.*
38. Angiolillo, A. L., C. Sgadari, D. D. Taub, F. Liao, J. M. Farber, S. Maheshwari, H. K. Kleinman, G. H. Reaman, and G. Tosato. 1995. Human interferon inducible protein IP-10 is a potent inhibitor of angiogenesis in vivo. *J. Exp. Med. 182:155.*
39. Luster, A. D., S. M. Greenberg, and P. Leder. 1995. The IP-10 chemokine binds to a specific cell surface heparan sulfate site shared with platelet factor 4 and inhibits endothelial cell proliferation. *J. Exp. Med. 182:219.*
40. Farber, J. M. 1997. Mig and IP-10: CXC chemokines that target lymphocytes. *J. Leukocyte Biol. 61:246.*
41. Strieter, R. M., P. J. Polverini, S. L. Kunkel, D. A. Arenberg, M. D. Burdick, J. Kasper, J. Dzuiba, J. Van Damme, A. Walz, and D. Marriott. 1995. The functional role of the ELR motif in CXC chemokine-mediated angiogenesis. *J. Biol. Chem. 270:27348.*
42. Voest, E. E., B. M. Kenyon, M. S. O'Reilly, G. Truitt, R. J. D'Amato, and J. Folkman. 1995. Inhibition of angiogenesis in vivo by IL-12. *J. Natl. Cancer Inst. 87:581.*
43. Sgadari, C., A. L. Angiolillo, and G. Tosato. 1996. Inhibition of angiogenesis by interleukin-12 is mediated by the interferon-inducible protein 10. *Blood 87:3877.*
44. Ozmen, L., M. Pericin, J. Hakimi, R. A. Chizzonite, M. Wysocka, G. Trinchieri, M. Gately, and G. Garotta. 1994. Interleukin 12, interferon-γ, and tumor necrosis factor α are the key cytokines of the generalized Shwartzman reaction. *J. Exp. Med. 180:907.*
45. Orange, J. S., T. P. Salazar-Mather, S. M. Opal, R. L. Spencer, A. H. Miller, B. S. McEwen, and C. A. Biron. 1995. Mechanism of interleukin 12-mediated toxicities during experimental viral infections: role of tumor necrosis factor and glucocorticoids. *J. Exp. Med. 181:901.*
46. Hendrzak, J. A., and M. J. Brunda. 1995. Interleukin-12: biologic activity, therapeutic utility, and role in disease. *Lab. Invest. 72:619.*
47. Luster, A. D., and P. Leder. 1993. IP-10, A C-X-C-chemokine, elicits a potent thymus-dependent antitumor response in vivo. *J. Exp. Med. 178:1057.*
48. Strieter, R. M., P. J. Polverini, D. A. Arenberg, A. Walz, G. Opdenakker, J. Van Damme, and S. L. Kunkel. 1995. Role of C-X-C chemokines as regulators of angiogenesis in lung cancer. *J. Leukocyte Biol. 57:752.*
49. Arenberg, D. A., S. L. Kunkel, P. J. Polverini, S. B. Morris, M. D. Burdick, M. C. Glass, D. T. Taub, M. D. Iannettoni, T. J. Whyte, and R. M. Strieter. 1996. Interferon-γ-inducible protein 10 (IP-10) is an angiostatic factor that inhibits human non-small cell lung cancer (NSCLC) tumorigenesis and spontaneous metastases. *J. Exp. Med. 184:981.*
50. Sgadari, C., A. Angiolillo, B. W. Cherney, S. E. Pike, J. M. Farber, L. G. Koniaris, P. Vanguri, P. R. Burd, N. Sheik, G. Gupta, J. Teruya-Feldstein, and G. Tosato. 1996. Interferon inducible protein 10 identified as a mediator of tumor necrosis in vivo. *Proc. Natl. Acad. Sci. USA 93:13791.*
51. Sgadari, C., J. M. Farber, A. L. Angiolillo, F. Liao, J. Teruya-Feldstein, P. R. Burd, L. Yao, G. Gupta, C. Kanegane, and G. Tosato. 1997. Mig, the monokine induced by interferon-γ, promotes tumor necrosis in vivo. *Blood 89:2635.*
52. Huang, S., R. K. Singh, K. Xie, M. Gutman, K. K. Berry, C. D. Bucana, I. J. Fidler, and M. Bar-Eli. 1994. Expression of the *JE/MCP-1* gene suppresses metastatic potential in murine colon carcinoma cells. *Cancer Immunol. Immunother. 39:231.*
53. Huang, S., K. Xie, R. K. Singh, M. Gutman, and M. Bar-Eli. 1995. Suppression of tumor growth and metastasis of murine renal adenocarcinoma by syngeneic fibroblasts genetically engineered to secrete the JE/MCP-1 cytokine. *J. Interferon Cytokine Res. 15:655.*
54. Manome, Y., P. Y. Wen, A. Hershowitz, T. Tanaka, B. J. Rollins, D. W. Kufe, and H. A. Fine. 1995. Monocyte chemoattractant protein-1 (MCP-1) gene transduction: an effective tumor vaccine strategy for non-intracranial tumors. *Cancer Immunol. Immunother. 41:227.*
55. Rothenberg, M. E., A. D. Luster, and P. Leder. 1995. Murine eotaxin: an eosinophil chemoattractant inducible in endothelial cells and in interleukin 4-induced tumor suppression. *Proc. Natl. Acad. Sci. USA 92:8960.*
56. Laning, J., H. Kawasaki, E. Tanaka, Y. Luo, and M. Dorf. 1994. Inhibition of in vivo tumor growth by the β chemokine TCA3. *J. Immunol. 153:4625.*
57. Rollins, B., and M. E. Sunday. 1991. Suppression of tumor formation in vivo by expression of the JE gene in malignant cells. *Mol. Cell. Biol. 11:3125.*
58. Mule, J. J., M. Custer, B. Averbook, J. C. Yang, J. S. Weber, D. V. Goeddel, S. A. Rosenberg, and T. J. Schall. 1996. RANTES secretion by gene modified tumor cells results in loss of tumorigenicity in vivo: role of immune cell subpopulations. *Hum. Gene Ther. 7:1545.*
59. Dilloo, D., K. Bacon, W. Holden, W. Zhong, W. Burdach, A. Zlotnik, and M. Brenner. 1996. Combined chemokine and cytokine gene transfer enhances anti-tumor immunity. *Nat. Med. 2:1090.*

EXHIBIT L

Immunity, Vol. 15, 837–846, November, 2001, Copyright ©2001 by Cell Press

A Novel TNF Receptor Family Member Binds TWEAK and Is Implicated in Angiogenesis

Steven R. Wiley[1,4], Linda Cassiano[1], Timothy Lofton[1], Terry Davis-Smith[1], Jeffrey A. Winkles[2], Volkhard Lindner[3], Hua Liu[1], Thomas O. Daniel[1], Craig A. Smith[1], and William C. Fanslow[1]
[1]Immunex Corporation
51 University Street
Seattle, Washington 98101
[2]Department of Vascular Biology
Holland Laboratory
American Red Cross
Rockville, Maryland 20855
[3]Center for Molecular Medicine
Maine Medical Center Research Institute
Scarborough, Maine 04106

Summary

TWEAK is a member of the TNF ligand family that induces angiogenesis in vivo. We report cloning of a receptor for TWEAK (TweakR) from a human umbilical vein endothelial cell (HUVEC) library. The mature form of TweakR has only one hundred and two amino acids and six cysteine residues in its extracellular region. Five different assays demonstrate TWEAK-TweakR binding, and the interaction affinity constant (Kd) is within a physiologically relevant range of 2.3 ± 0.1 nM. The TweakR cytoplasmic domain binds TRAFs 1, 2, and 3. Cross-linking of TweakR induces HUVEC growth, and mRNA levels are upregulated in vitro by a variety of agents and in vivo following arterial injury. Soluble TweakR inhibits endothelial cell migration in vitro and corneal angiogenesis in vivo.

Introduction

TWEAK is a member of the TNF family of cytokines that was first described as a weak inducer of apoptosis in transformed cell lines (Chicheportiche et al., 1997). TWEAK induces IL-8, IL-6, and ICAM-I expression in cultured human astrocytes (Saas et al., 2000), and cultured monocytes have been shown to respond to IFN-γ by inducing surface expression of TWEAK (Nakayama et al., 2000). TWEAK mRNA expression is also downregulated in murine models of inflammation (Chicheportiche et al., 2000). In addition, TWEAK induces proliferation of human smooth muscle and endothelial cells in vitro, and acts as a potent inducer of angiogenesis in a rat cornea pocket angiogenesis assay (Lynch et al., 1999). Given the involvement of TWEAK in inflammation models and its expression pattern on monocytes it is important to identify the receptor for TWEAK in order to better elucidate its role in the immune as well as angiogenic systems.

It was reported previously that TWEAK binds to DR3, a member of the TNF receptor family that contains a death domain in its cytoplasmic tail and can induce apoptosis (Marsters et al., 1998). We have been unable to reproduce these results by using similar techniques. In addition, TWEAK-DR3 interaction could not be confirmed using slide binding assays performed either by overexpressing TWEAK in transfected cells and probing with DR3-IgG-Fc fusion protein, or by overexpressing DR3 in transfected cells and probing with TWEAK (data not shown). In agreement with these findings, recently published studies indicate that TWEAK does not bind DR3 and that a receptor specific for TWEAK must exist (Schneider et al., 1999; Kaptein et al., 2000).

In this paper we report the identification of a member of the TNF receptor family, TweakR, which binds to TWEAK with high affinity. Members of the TNF receptor family can be identified by a distinctive set of cysteine-rich repeat regions in the extracellular domain (reviewed in Locksley et al., 2001). Most receptors have three to four of these regions, although some, such as the receptors for TRAIL/Apo2L and TACI have only two. One known member of the TNF receptor family, BCMA, has been described that has only one such region (Madry et al., 1998). TweakR also has just one cysteine-rich region in the extracellular domain, and with a total amino acid count of 102 (after signal peptide cleavage), it is the smallest TNF receptor family member so far described.

While this manuscript was in preparation, Feng et al. (2000) reported the cloning, chromosomal location, and expression properties of a human gene named Fn14. The Fn14 and TweakR nucleotide sequences have 100% identity. The Fn14 gene was first identified using a differential display approach to search for growth factor-inducible genes in murine NIH 3T3 fibroblasts, and Fn14 itself was shown to be a plasma membrane-anchored protein (Meighan-Mantha et al., 1999). However, due to the degree of amino acid sequence divergence from other TNF receptor family members, Fn14 was not classified as a member of the TNF receptor family. Here we demonstrate that this relatively small molecule is a fully functional member of the TNF receptor family able to transduce a signal to its host cell, and implicate TweakR in a variety of vascular cellular responses both in vitro and in vivo.

Results

Expression Cloning of TweakR from HUVECs

An expression cloning panning approach was used to identify a TWEAK binding receptor expressed in HUVEC. Magnetic beads were coated with the C-terminal receptor binding domain of TWEAK and used for two rounds of panning of COS cells transfected with a HUVEC cDNA expression library. The resulting enriched pool was further broken down by slide binding (Goodwin et al., 1993), in order to identify a single clone encoding the TWEAK binding activity. Sequence analysis of the recovered clone predicted TweakR to be a type-I transmembrane protein with a single extracellular cysteine-rich region comprising six cysteine residues in its extracellular do-

[4]Correspondence: wileys@immunex.com

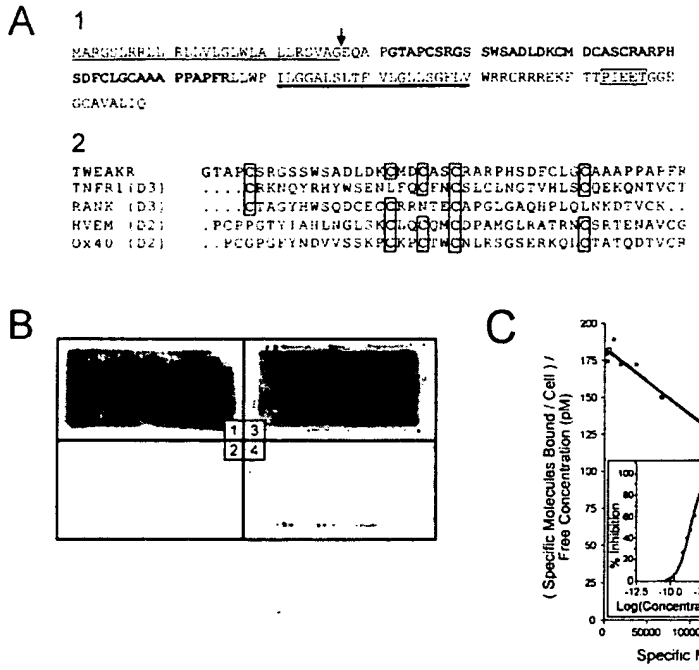

Figure 1. Features and Homology of Predicted TweakR Primary Amino Acid Sequence

(A1) Predicted primary amino acid sequence of TweakR showing major features. The leader sequence in underlined. The arrow indicates the predicted site of cleavage of the leader sequence. The region of TNF family receptor homology is shown in bold. The predicted transmembrane region is doubly underlined. The putative TRAF binding motif in the cytoplasmic domain is boxed.

(A2) Alignment of TweakR to selected cysteine-rich domains of other members of the TNF receptor family. The family member and cysteine-rich domain number are indicated on the left. Boxes emphasize aligned cysteines.

(B) Slide binding showing qualitative interaction of TweakR with TWEAK. Shown is an autoradiographic image of Cos cells transfected with TweakR versus control vector and probed with TWEAK-LZ and ^{125}I-labeled M15 antileucine zipper antibody (1 and 2, respectively), or CV1-EBNA cells transfected with human full-length TWEAK versus control vector and detected with TweakR-Fc and ^{125}I-labeled goat antimouse IgG antibody (3 and 4, respectively).

(C) CV-1 cells transfected with human full-length TWEAK were mixed at a 1:30 ratio with Raji cells and incubated with various concentrations of ^{125}I-labeled TweakR-Fc as described in the Experimental Procedures. Shown is a Scatchard representation of specific binding. (Inset) Plot of competitive inhibition of unlabeled verses ^{125}I-labeled TweakR-Fc.

main (Figure 1, A1). An alignment of the cysteine-rich extracellular region with the cysteine-rich region of other TNF receptor family members revealed a weakly conserved pattern of extracellular cysteines (Figure 1, A2). The predicted twenty-eight amino acid cytoplasmic domain contains a region, which bears resemblance to known binding sites for TRAF family signaling molecules (see below). Aside from the cysteine pattern, and the putative TRAF binding site, there is virtually no sequence conservation between TweakR and other TNF receptor family members. TWEAK-TweakR interaction was qualitatively confirmed by slide-binding assays conducted by either transfecting the isolated TweakR cDNA clone into cells and detecting with TWEAK-LZ and ^{125}I-labeled antileucine zipper antibody, or conversely by transfecting a full length TWEAK cDNA clone into cells and detecting by TweakR-Fc and ^{125}I-goat antihuman IgG antibody (Figure 1B).

TWEAK Ligand-Receptor Affinity

Given the unusually small size of TweakR, and the lack of strong similarity to other TNF family receptors, it was necessary to determine the affinity of its interaction with TWEAK. The intrinsic affinity between TWEAK ligand and receptor was estimated by measuring the equilibrium binding constant between TweakR-Fc and recombinant full-length surface ligand transiently expressed on CV1/EBNA cells. Direct binding of ^{125}I-TweakR-Fc to surface ligand, plotted in Scatchard format (Figure 1C), gave an affinity constant of 2.3 ■ 0.1 nM. Consistent with this value, competitive inhibition assays with unlabeled TweakR-Fc gave a K(I) of 2.5 ■ 0.1 nM (Figure 1C, inset). Confirmation that TweakR is largely responsible for TWEAK binding to native cells was demonstrated by the ability of a monoclonal antibody against TweakR to significantly inhibit binding of TWEAK to endothelial cells as measured by flow cytometry (data not shown). Together these experiments represent five independent experimental approaches demonstrating a TWEAK-TweakR interaction.

The TweakR Cytoplasmic Domain Binds TRAF1, 2, and 3

Many TNF receptor family members have been shown to bind members of the TRAF family of signal transduction molecules. This, combined with the observation that

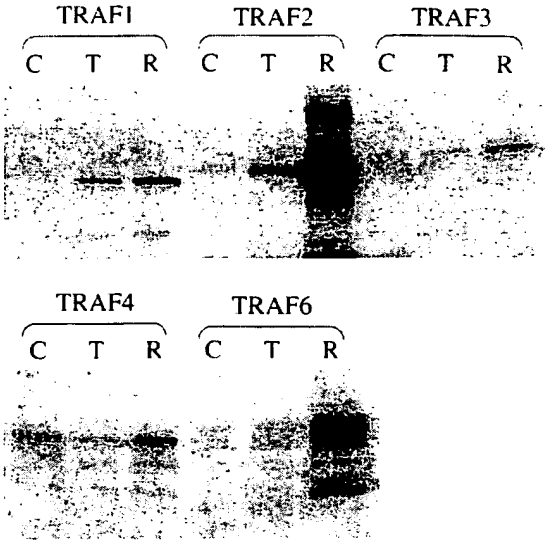

Figure 2. Qualitative Binding of TRAFs to the TweakR Cytoplasmic Domain

Indicated TRAF molecules were ^{35}S-labeled by coupled in vitro transcription/translation and incubated with GST beads (C), GST-TweakR cytoplasmic domain fusion beads (T), or GST-RANK cytoplasmic domain fusion beads (R). Beads were washed and the bound TRAF molecules were resolved by SDS-PAGE and visualized by autoradiography.

the TweakR cytoplasmic domain contains a region that resembles TRAF binding motifs found in many TNF family receptors, led us to qualitatively test the ability of this region to bind to various members of the TRAF family. The 28 amino acid TWEAK cytoplasmic domain was fused to glutathione S-transferase (GST) and then bound to glutathione-Sepharose beads. Control beads bound with GST lacking the TweakR cytoplasmic domain were used to determine background levels of binding. Beads bound with the cytoplasmic domain of the TNF receptor family member RANK fused to GST were used as a positive control. This RANK-GST fusion construct is a high affinity TRAF binder that contains two sites for TRAF interaction and binds to TRAF1, 2, 3, 5, and 6 (Galibert et al., 1998). The beads were incubated with in vitro translated ^{35}S-labeled TRAF proteins. The results show that under the conditions used TRAF1 and TRAF2 can interact with the TWEAK cytoplasmic region GST coated beads above background levels (Figure 2). TRAF3 binding is weaker, but still above background levels. TRAF4 and TRAF6 showed no binding to the TweakR cytoplasmic domain above background levels. TRAF5 did not express well in our in vitro system, and therefore the binding of this protein to the TweakR cytoplamic tail could not be evaluated.

Cross-Linking of TweakR Transmits a Proliferative Signal to HUVEC

Although TweakR binds to TWEAK with an affinity that is consistent with other TNF ligand-receptor interactions, these data do not demonstrate that TweakR functions as a receptor, which can transduce a signal into the host cell. For example, it is formally possible that TweakR actually inhibits rather than promotes TWEAK signaling. In order to investigate whether or not the molecule resulting from the panning experiment was a functional receptor, a construct was made that fuses a synthetic Flag octapeptide epitope onto the N-terminal extracellular domain of TweakR (Flag-TweakR). The resulting protein was expressed by transient transfection in HUVEC and incubated with cross-linked antiFlag monoclonal antibody. Cross-linking the receptor in this manner avoids background from the endogenous TweakR expressed by HUVEC. Proliferation was measured by BrdU incorporation into DNA. Lipid mediated transfection of HUVEC with Flag-TweakR resulted in expression of recombinant Flag-TweakR on the cell surface by 36 hr posttransfection. The Flag-TweakR was expressed at a high level by 9% of the transfected HUVEC used in these experiments, with a mean fluorescence intensity (MFI) of 99 compared to the MFI of the vector only HUVECs of 4.5. The results are expressed as the fold increase in the number of BrdU positive cells (BrDU mAb-FITC positive cells) under each culture condition over the number of negative-control FITC positive cells. In vitro culture of Flag-TweakR expressing HUVEC with the complex of M2 antiFlag and goat antimouse IgG increased BrdU incorporation 3-fold over the level of BrdU incorporation observed by culturing Flag-TweakR expressing cells with goat antimouse IgG alone (Figure 3). Culture of Flag-TweakR expressing HUVEC with the complex of M2 antiFlag and goat antimouse IgG increased BrdU incorporation 6-fold over the level of BrdU incorporation observed by culturing vector alone-transfected HUVEC with the cross-linking complex. Incubation with the cross-linking complex did not alter BrdU incorporation in vector alone-transfected HUVEC. The 2× increase in BrdU incorporation between cells expressing Flag-TweakR relative to control cells in the absence of cross-linking is likely because of a low level of spontaneous signaling due to overexpresson of the receptor. These data provide direct evidence that despite its small size, TweakR is capable of initiating a proliferative signal in human endothelial cells.

Regulation of TweakR mRNA Expression in Vascular SMC

Previous studies have demonstrated that growth factor stimulation of quiescent murine or human fibroblasts promotes a transient increase in TweakR (Fn14) gene expression (Meighan-Mantha et al., 1999; Feng et al., 2000). In consideration of the ability of TWEAK to stimulate proliferation of endothelial and smooth muscle cells (Lynch et al., 1999), we investigated whether TweakR gene activation also occurred in mitogen-stimulated vascular cells. First, rat aortic SMC were serum-starved and then treated with FGF-2 for various lengths of time. RNA was isolated and TweakR mRNA levels were examined by Northern blot hybridization. A single TweakR transcript of ~1.2 kb in size was detected in SMC. TweakR mRNA expression was transiently induced following FGF-2 addition, with maximal levels detected at 2 hr post-stimulation (Figure 4A). Second, we treated serum-starved SMC for 4 hr with various agents (e.g., phorbol ester, polypeptide growth factors, peptide

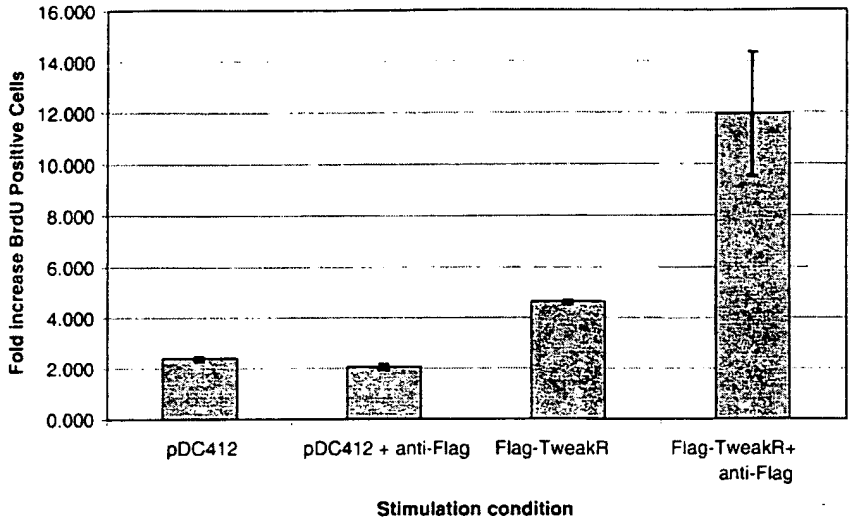

Figure 3. BrdU Incorporation into HUVECs Transfected with Either Empty Vector (pDC412) or a Flag Epitope-Tagged TweakR

Triplicate cultures of cells transfected as indicated were incubated in media containing goat-antimouse IgG in either the presence or absence of M2 antiFlag mAb. The results are expressed as the mean fold increase ± SEM in BrdU positive cells compared to control for each culture condition.

hormones), and then performed Northern blot analysis to determine whether TweakR gene expression could be induced by multiple, distinct, growth promoters. TweakR mRNA levels were significantly elevated above unstimulated levels following PMA, FBS, PDGF-BB, EGF, FGF-2, or Ang II treatment of rat SMC (Figure 4B). In comparison, TGF-β1, IGF-1, or α-thrombin treatment had only a slight stimulatory effect. These results indicate that TweakR is a growth factor-regulated gene in vascular SMC.

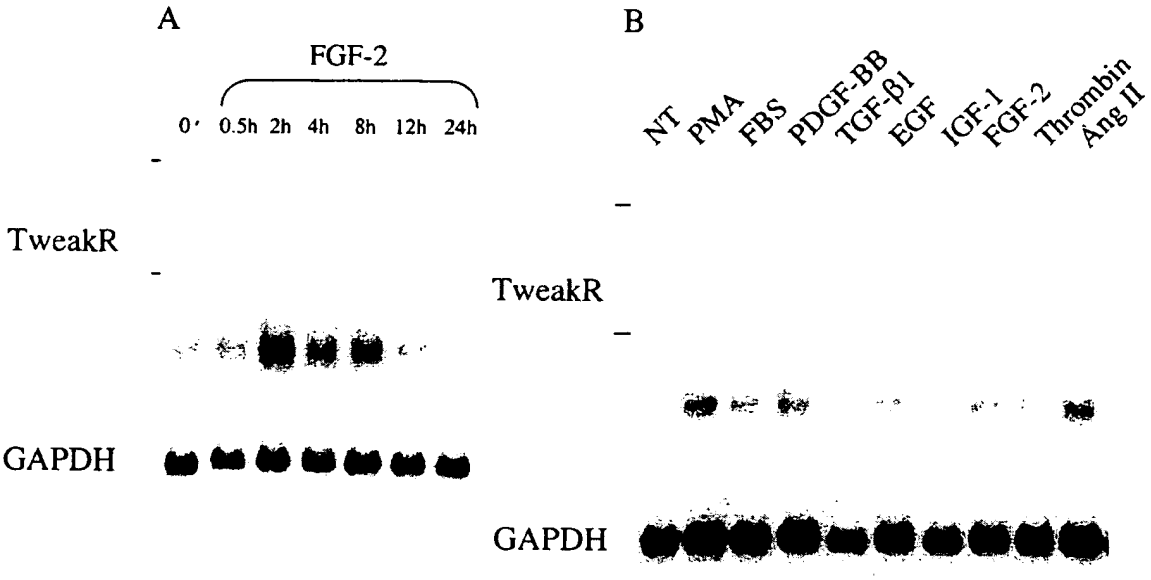

Figure 4. Regulation of TweakR mRNA Expression in Rat Aortic SMC

(A) Serum starved cells were either left untreated (0') or treated with FGF-2 for the indicated time periods. RNA was isolated, and equivalent amounts of each sample were analyzed by Northern blot hybridization using the two cDNA probes indicated. The positions of 28S and 18S rRNA are noted on the left with tick marks.

(B) Serum starved cells were either left untreated (NT, no treatment) or treated with phorbol myristate acetate (PMA), fetal bovine serum (FBS), PDGF-BB, TGF-β1, EGF, IGF-1, FGF-2, α-thrombin, or angiotensin II (Ang II) for 4 hr. RNA was isolated, and equivalent amounts of each sample analyzed by Northern blot hybridization.

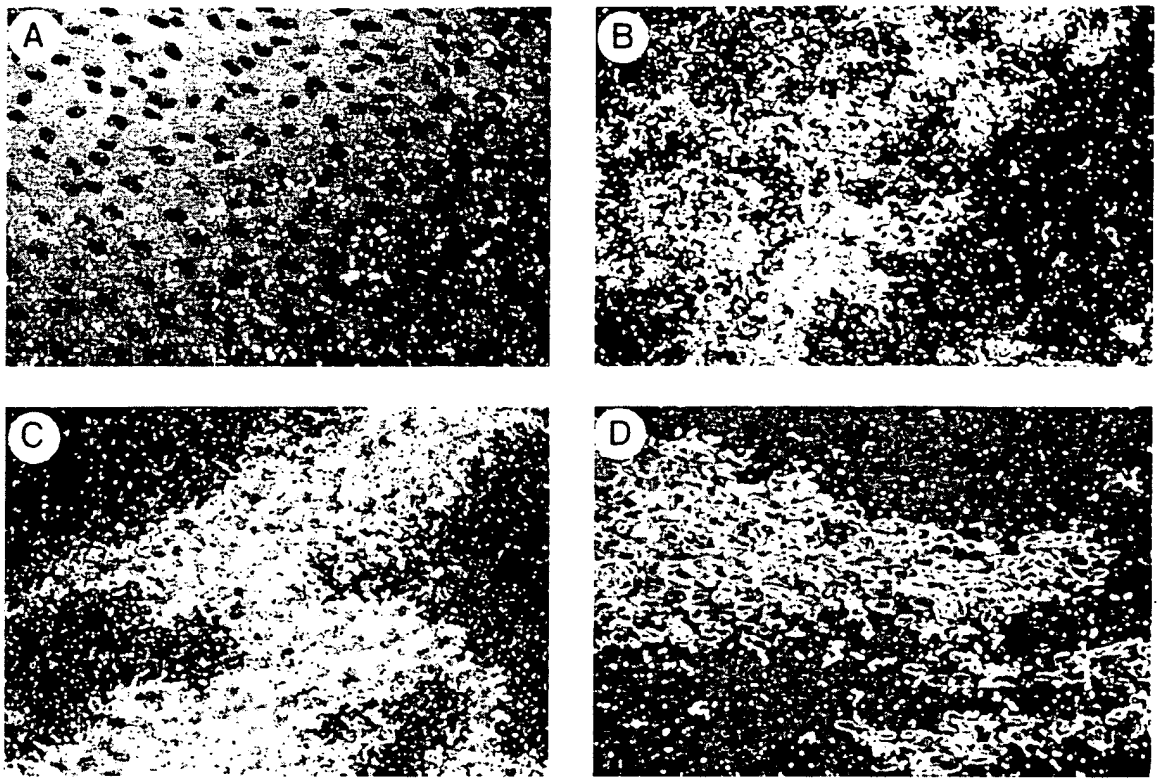

Figure 5. Photomicrographs of En Face Preparations of Rat Aortae Examined for TweakR Expression by In Situ Hybridization with ^{35}S-UTP Labeled Antisense and Sense Probes

(A) The uninjured aorta showed low levels of TweakR expression in the endothelium.

(B) Proliferating and migrating endothelium at the wound edge 8 days after aortic injury revealed upregulated expression of TweakR. The still denuded area is located on the right.

(C) Strong expression of TweakR mRNA was seen in proliferating SMC forming the neointima at 8 days following balloon injury.

(D) Hybridization with the sense probe showed very little background hybridization in SMC 8 days after injury. Hematoxylin was used for staining nuclei, and all specimens were viewed under dark field illumination at 200■ original magnification.

TweakR mRNA Expression in Injured Rat Arteries

A common clinical situation that involves proliferation of both smooth muscle and endothelial cells results from vessel damage induced by balloon angioplasty. Therefore, we examined TweakR mRNA expression following balloon catheter denudation of rat carotid arteries. In situ hybridization of en face preparations using ^{35}S-labeled riboprobes allowed us to compare TweakR mRNA expression levels in quiescent vs. proliferating EC, and also to examine TweakR mRNA expression in SMC accumulating on the luminal surface after injury. We found that endothelium from uninjured arteries expressed low levels of TweakR mRNA (Figure 5A); however, significantly higher levels of expression were detected in proliferating EC at the wound edge (Figure 5B). In addition, high levels of TweakR mRNA expression were found in proliferating, intimal SMC at 8 days after injury (Figure 5C). All en face preparations probed with a ^{35}S-labeled TweakR sense riboprobe as a control revealed low levels of hybridization (Figure 5D). These results indicate that TweakR mRNA expression is upregulated in proliferating EC and SMC in vivo.

TweakR-Fc Inhibits Migration of HRMECs In Vitro

Angiogenesis is a multi-step process that requires not only proliferation, but also morphological alterations and migration of vascular cells. Therefore, the effect of blocking TweakR signaling on endothelial cell migration was tested by use of an in vitro planar endothelial cell migration (wound closure) assay (Daniel et al., 1999). In this assay, migration of primary human renal microvascular endothelial cells (HRMEC) is measured by the rate of closure of a circular wound in a cultured cell monolayer. The rate of wound closure is linear, and is dynamically regulated by agents that stimulate and inhibit angiogenesis in vivo. By fusing the extracellular portion of TweakR to the human IgG1-Fc domain (TweakR-Fc), a soluble inhibitor of TweakR signaling was created. Two stimuli were used to increase the rate of closure of the HRMEC: PMA or EGF (Figure 6A and 6B). TweakR-Fc inhibited PMA-stimulated endothelial cell migration in a dose responsive manner, reducing the rate of migration to near basal levels at 1.5 μg/ml. Neither huIgG-Fc nor TweakR-Fc added alone inhibited basal (uninduced) migration (Figure 6A). EGF-induced HRMEC migration was

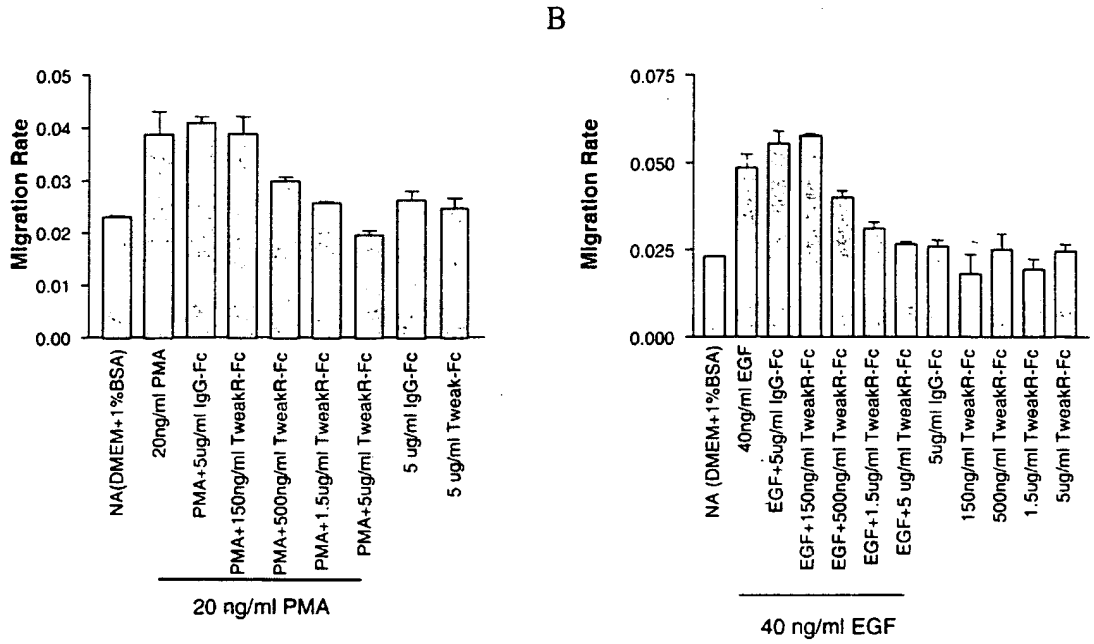

Figure 6. Human TweakR-Fc Inhibits PMA- or EGF-Stimulated Endothelial Cell Migration In Vitro

(A) At the time of wound initiation, basal media was supplemented with PMA, PMA ■ hulgG-Fc, PMA ■ titrated TweakR-Fc, hulgG-Fc alone, or huTweakR-Fc alone at the concentrations indicated. After 12 hr of incubation the means of the residual wound areas, expressed as fractions of the original wound, were converted into migration rate (expressed as the percentage of the original wound area covered per hour). The results expressed in the columns are the mean migration rate for each condition (triplicate cultures) at 12 hr ■ SEM (error bars).

(B) At the time of wound initiation, basal media was supplemented with EGF, EGF ■ hulgG-Fc, EGF ■ titrated TweakR-Fc, hulgG-Fc alone, or TweakR-Fc alone at the concentrations indicated. The experiment was performed and analyzed as described in (A).

similarly inhibited by TweakR-Fc, reducing the rate of migration to unstimulated levels at 5 μg/ml (Figure 6B). These results indicate that endogenous TWEAK regulates endothelial cell wound closure rate in this assay.

TweakR-Fc Inhibits FGF-2-Stimulated Corneal Angiogenesis In Vivo

In order to test the relevance of signaling by TweakR in vivo, TweakR-Fc was tested for its ability to inhibit FGF-2-induced angiogenesis in a mouse cornea pocket assay (Figure 7). In this assay, agents to be tested for angiogenic or antiangiogenic activity are immobilized in a slow release form in a hydron pellet, which is implanted into micropockets created in the corneal epithelium of anesthetized mice. Quantitation is measured by photography using a slit-lamp microscope followed by analysis with image processing software. Vascularization is measured as the area, density, and extent of vessel growth from the vascularized corneal limbus into the normally avascular cornea. The results show that local administration of TweakR-Fc (100 pmol) inhibited FGF-2-stimulated corneal angiogenesis (Figure 7A), reducing the vascular area to 50% of that induced by FGF-2 alone or FGF-2 plus control-IgG-Fc (Figure 7B). In addition to reducing vascular area, local administration of TweakR-Fc significantly inhibited FGF-2-stimulated induced vessel density (imaged on hemoglobin) by 70% compared to the vessel density in the presence of the control protein IgG-Fc. This demonstrates that TweakR signaling plays a role in certain types of angiogenesis in vivo.

Discussion

The results presented here describe the identification and initial functional characterization of a receptor for TWEAK in endothelial cells. The TweakR is a type-I transmembrane protein of 128 amino acids in length, making it the smallest of all known TNF receptor family members. It has only one cysteine-rich domain in the extracellular region, a feature shared with just one other known TNF receptor, BCMA (Madry et al., 1998). The short 28 amino acid putative cytoplasmic domain contains a sequence that is similar to TRAF binding motifs found in other TNF family receptors. However, these features are only clear in hindsight. Based on the primary amino acid sequence alone, it is very difficult to identify TweakR as a member of the TNF receptor family, or even as a receptor of any kind. An alignment of the cysteine-rich region of TweakR with those of other TNF receptor family members demonstrates the high degree of divergence from other family members (Figure 1, A2).

Despite this unusually small extracellular domain, and divergence in the cysteine-rich repeat region, the Ka of TWEAK-TweakR interactions ($4.2 \times 10^8\ M^{-1}$) is similar to the affinity of CD30 to its receptor (4.0×10^8) when measured the same way (Smith et al., 1993). Although

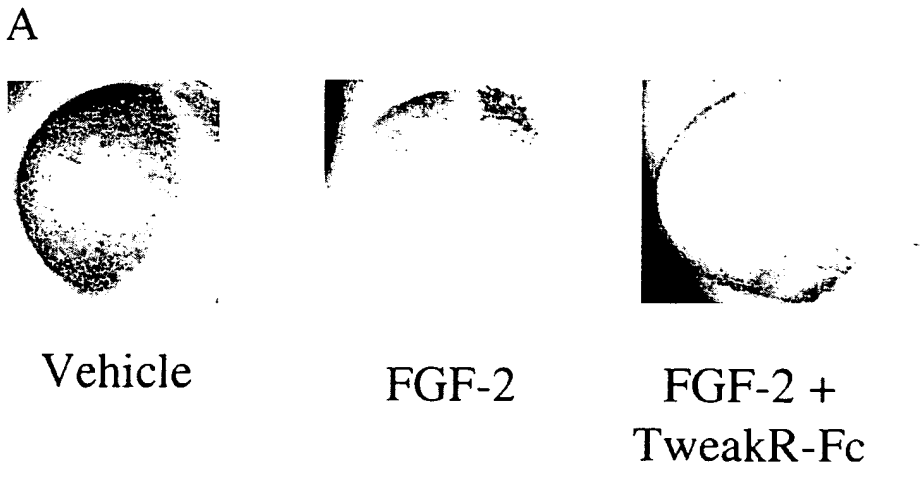

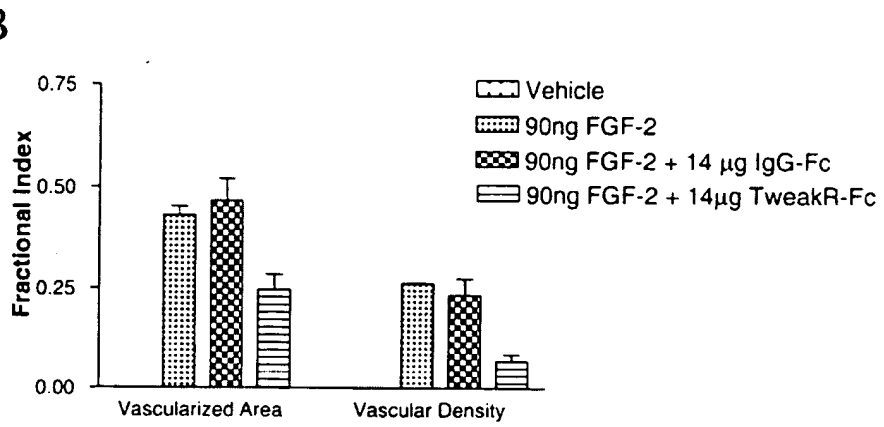

Figure 7. TweakR-Fc Treatment Reduces FGF-2-Stimulated Corneal Angiogenesis in the Mouse

(A) Representative photographs illustrating corneal vessel growth in vehicle only containing pellets as compared to localized administration of FGF-2 and concomitant administration of FGF-2 and TweakR-Fc.

(B) The results were quantified as described in Experimental Procedures. The fractional vascularized area of the cornea and the total vascular density within the corneal perimeter induced by FGF-2 in the presence of no inhibitor, hulgG or TweakR-Fc is shown (columns = mean, error bars = SEM). A significant decrease in new corneal vessels is observed with concomitant administration of FGF-2 and TweakR-Fc ($p = 0.0028$). Values for each experimental condition are obtained from a total of nine separate animals.

this affinity is approximately 20-fold less than that measured for TNF binding to TNF-R1, it is still in the physiological range for this family of ligand-receptor cognates. Also, the binding curve produced by the analyses is a monovalent curve, as opposed to the bivalent curve sometimes seen in similar analyses with other TNF family members. This indicates that only one type of binding site was detected, rather than a mixture of high and low affinity sites.

The 28 amino acid cytoplasmic domain of TweakR is also much smaller than many other receptors in the family. Nevertheless, the cytoplasmic region is capable of binding TRAF family members 1, 2, and 3 (Figure 2). Although this does not rule out other potential signaling pathways, one possible mechanism for TweakR signaling is through the TRAF family of adaptor proteins. After transfection into endothelial cells, full-length TweakR transduces a proliferative signal into the cell following receptor cross-linking (Figure 3). Cross-linking via an extracellular artificial epitope, rather than using the natural ligand, ensures that the increase in proliferation is due to signaling by TweakR, as opposed to some other hypothetical receptor for TWEAK. Therefore, despite its small cytoplasmic region, TweakR is a functioning receptor.

Northern blot analyses show that TweakR gene expression is rapidly upregulated in smooth muscle cells by a variety of agents and known growth factors (Figure 4). This leaves open the possibility that TweakR might be involved in a range of biological activities. One such activity is endothelial cell migration, which is a necessary component of angiogenesis. The rate of wound closure in a HRMEC monolayer is enhanced by multiple stimuli such as PMA and EGF. Blocking TweakR reduces

this enhanced rate of wound closure back to unstimulated levels (Figure 6). Presumably, this is due to inhibition of a TWEAK-TweakR autocrine loop. This possibility is supported by RT-PCR data indicating that these cells coexpress TWEAK and TweakR transcripts (data not shown). Failure of TweakR-Fc to inhibit the basal rate of closure suggests that induction of the TweakR pathway is a required component of this autocrine loop. The ability to neutralize this enhanced rate of closure is evidence that TweakR is a required part of the activation seen by PMA and EGF. Interestingly, the basal rate of wound closure is not significantly affected by TweakR-Fc, demonstrating that the basal response is not dependent on TweakR signaling.

We also found that FGF-2 angiogenic activity can be partially blocked by inhibition of TweakR signaling in vivo (Figure 7). Again, this implies that at least in part, a TWEAK-TweakR interaction mediates some of the FGF-2 effect. In particular, the effect of blocking TWEAK-TweakR signaling was more dramatic on vessel density than it was on overall vessel area.

TweakR mRNA expression is induced during tissue regeneration, both during repair of a denuded rat artery (Figure 5), and during liver regeneration (Feng et al., 2000). A pattern that seems to be emerging is that TweakR expression is upregulated in growing or regenerating tissues. Whether this expression is largely restricted to endothelial and smooth muscle cells is not clear. TweakR, for instance, is also present in fibroblast cells (Meighan-Mantha et al., 1999; Feng et al., 2000), and TWEAK can induce a signal in astrocytes (Saas et al., 2000). However, additional in situ hybridization data showing the cellular localization of TweakR expression in developing and regenerating tissues must be generated in order to help clarify the role of this molecule. Regardless of its presence in cell types not directly associated with vasculature, data presented here argue for a role for TweakR in vascular cell migration and angiogenesis.

Two other members of the TNF family have also previously been implicated in angiogenesis: TNF and Fas ligand (Pandey et al., 1995; Biancone et al., 1997). However, these effects are thought to be indirectly mediated by production of pro-angiogenic endothelial growth factors (Yoshizumi et al., 1992). In contrast, the proliferative effect of TWEAK on endothelial cell growth is not correlated with TWEAK-induced expression of known pro-angiogenic factors or their receptors (Lynch et al., 1999). This implies that the angiogenic effect of TWEAK in a cornea pocket angiogenesis assay is a direct effect rather than one mediated by better characterized angiogenic factors such as VEGF and FGF. However, the effects of some other angiogenic factors may be mediated in part by TWEAK-TweakR interactions. For example, both FGF-2 and EGF can upregulate TweakR expression in fibroblasts (Meighan-Mantha et al., 1999) and smooth muscle cells (Figure 4). We have shown that blocking TweakR signaling inhibits both EGF-stimulated endothelial cell wound closure (Figure 6B) and FGF-2-induced cornea angiogenesis (Figure 7).

In summary, TweakR, despite its small size, is a fully functional receptor for TWEAK, capable of both binding TWEAK at a reasonable affinity and of transducing a proliferative signal to endothelial cells. A variety of data, both in vitro and in vivo, supports the hypothesis that the TWEAK-TweakR system plays a role in endothelial cell growth and migration. This system may be important for both the biological activity of the TWEAK ligand itself, as well as for the biological activity observed with other more thoroughly characterized proangiogenic molecules.

Experimental Procedures

Cell Culture

Adult rat (Sprague-Dawley) thoracic aorta SMC were kindly provided by M. Majesky, Baylor College of Medicine, Houston, Texas. The cells were cultured at 37°C in a 1:1 mixture of Dulbecco's modified Eagle's medium and Ham's F-12 medium (Mediatech) supplemented with 5% fetal bovine serum (FBS; Hyclone Laboratories), 100 U/ml penicillin, 100 μg/ml streptomycin, and 0.25 μg/ml amphotericin B (JRH Biosciences). SMC cultures were fed every 48 hr and expanded by trypsin-EDTA (JRH Biosciences) treatment and subculturing at a 1:5 split ratio. Cells were incubated for ≈72 hr in cell culture medium containing 0.5% FBS to obtain a relatively quiescent SMC population. Serum-starved cells were then either left untreated or treated with one of the following: 10 ng/ml human recombinant FGF-2 (Bachem), 10 ng/ml human recombinant PDGF-BB (Genzyme), 2 ng/ml human recombinant TGF-β1 (R&D Systems), 10 ng/ml human recombinant IGF-1 (Bachem), 10% FBS, 20 ng/ml phorbol myristate acetate (PMA; Sigma), 10 ng/ml EGF (Genzyme), 10^{-8} M α-thrombin (Sigma), or 10^{-6} M angiotensin II (Ang II; Bachem). Primary human renal microvascular endothelial cells, HRMEC, were isolated, cultured, and used at the third passage after thawing as described (Martin et al., 1997). All other cell lines were cultured to a density of 2–5 × 10^5 cells per ml in RPMI medium supplemented with 10% fetal bovine serum, 100 μg/ml streptomycin, and 100 μg/ml penicillin.

Plasmid Construction and Expression

pDC412-LZ-TWEAK, the soluble form of human TWEAK, was constructed with a modified leucine zipper (LZ) on the N terminus preceded by the growth hormone leader. The construct was made essentially like the previously described soluble LZ-CD40 ligand (Fanslow et al., 1994) in the mammalian expression vector pDC412, a derivative of pDC409 (Wiley et al., 1995) that reverses the order of the BglII and NotI sites in the multiple cloning vector. Flag-TweakR was created by fusing the leader sequence of the murine Ig κ-chain (amino acids 1–21) to a Flag synthetic epitope, and abutting to the N-terminal end of the mature TweakR (amino acids 35–129), which was then placed in the pDC412 vector. TweakR-Fc was produced by placing amino acids (1–79) of TweakR into the SalI-BglII site of the pDC412-Fc vector (Smith et al., 1993). Expression and purification of the TweakR-Fc protein was performed essentially as described (Goodwin et al., 1993).

Expression Cloning of TweakR cDNA

pDC409-LZ-TWEAK conditioned supernatants were produced by transient transfection into CV1-EBNA cells. These supernatants were incubated with magnetic beads coated with polyclonal goat antimouse antibody (Ambion) that had previously been incubated with a mouse monoclonal antibody against the leucine zipper (M15, 5 μg/ml). Control beads were produced by mixing the M15 coated beads with supernatants from cells transfected with empty vector. A monolayer of COS cells, grown in a T175 flask, was transfected with 15 μg of DNA from a HUVEC cDNA expression library (Edge Biosystems). The complexity of the DNA pools was ≈100,000. After 2 days these cells were lifted from the flask by nonenzymatic means (Cell Dissociation Solution; Sigma) and incubated in 1.5 ml of binding media (Goodwin et al., 1993) plus 5% nonfat dried milk for 3 hr at 4°C on a rotator wheel. Cells were precleared by adding 1 μg of control beads and rotated at 4°C for an additional 45 min, after which bead-bound cells were removed with a magnet. Preclearing was repeated 2 to 3 times before 1 μg of the TWEAK-coated beads was added to the cells, which were then rotated 30 min at 4°C. Cells binding the TWEAK beads were separated by use of a magnet and

washed four times in PBS. Plasmid DNA was extracted from these cells by lysing in 0.1% SDS and used to transform the *Escherichia coli* strain DH101B. Colonies were grown 16 hr on ampicillin selective media. Transformants were pooled and used as a source of plasmid DNA pools for the next round of panning. After two rounds of panning, the positive clones were picked from the resulting pool using a slide binding protocol. Slide binding was performed as described (Goodwin et al., 1993), with the exception that TweakR positive slides were detected by incubation with pDC412-LZ-Tweak conditioned supernatants followed by incubation with ^{125}I-labeled M15 antileucine zipper.

TRAF Binding

TRAF binding to cytoplasmic domain GST fusion proteins was performed as described (Galibert et al., 1998) except that the ^{35}S-labeled TRAFs were produced using a coupled in vitro transcription and translation system (TNT Labeling Kit, Promega Corp., Madison, Wisconsin).

Receptor-Ligand Binding Assays

Equilibrium binding isotherms between ^{125}I-TweakR-Fc and surface TWEAK ligand were determined by standard methods (Smith et al., 1993). Briefly, CV1/EBNA cells transfected with full-length human TWEAK ligand were diluted 30-fold into Raji cells (TWEAK-negative), and the suspension (1.7×10^7 total cells/ml) incubated with serially diluted ^{125}I-TweakR-Fc (4.4×10^{15} cpm/mmole) in a total volume of 150 μl for 2 hr at 4°C. Duplicate aliquots of suspension were sampled, free and bound ^{125}I-TweakR-Fc determined, and the data plotted in Scatchard format. Competitive inhibition assays were performed similarly (Smith et al., 1996) with 0.1 nM ^{125}I-TweakR-Fc incubated with cells and increasing concentrations of unlabeled inhibitor (TweakR-Fc). Data were fitted to a single site competitive inhibition equation (Smith et al., 1993).

RNA Isolation and Northern Blot Hybridization

Total RNA was isolated from cultured SMC using RNA Stat-60 (Tel-Test) according to the manufacturer's instructions. Northern blot hybridization analysis was performed as described (Meighan-Mantha et al., 1999). The cDNA hybridization probes were mouse TweakR/Fn14, ~1.0 kb EcoRI/XhoI fragment of pBluescript/mFn14, and human GAPDH, ~0.8 kb PstI/XbaI fragment of pHcGAP (American Type Culture Collection).

Arterial Injury Model and In Situ Hybridization

Carotid arteries from anesthetized male Sprague-Dawley rats were denuded with a balloon catheter and perfusion fixed as described (Silverman et al., 1999). In situ hybridization was performed on en face preparations of vessel segments as described (Silverman et al., 1999). A pBluescript/Fn14 plasmid containing the murine Fn14 cDNA sequence without the 3' untranslated region and poly(A) tail was constructed using standard techniques. This plasmid was linearized with SmaI, transcribed with T7 polymerase to make the antisense probe or linearized with ApaI, blunt ended with T4 DNA polymerase 1, and then transcribed with T3 polymerase to make the sense probe. Vessel segments were treated with proteinase K (1 μg/ml) for 15 min at 37°C, prehybridized for 2 hr at 55°C in 0.3 M NaCl, 20 mM Tris-HCl (pH 7.5), 5mM EDTA, 1X Denhardt's solution, 10% dithiothreitol, and 50% formamide, and incubated with the appropriate [^{35}S]UTP-labeled riboprobe for 16 hr at 55°C. After washing, the slides were coated with autoradiographic emulsion (Kodak, NTB2), exposed for 2 weeks, and then developed. All specimens were examined under dark-field illumination after nuclear counterstaining with hematoxylin. Images were photographed and digitized.

BrdU Incorporation in Transfected HUVECs

Proliferating human umbilical vein endothelial cells (HUVEC) obtained from BioWhittaker-Clonetics (Walkersville, Maryland) were grown in EGM-2 media (Clonetics) and then subjected to lipid-mediated DNA transfection. HUVECs were plated overnight at 3×10^5 per well in six-well plates, in 2.0 ml of EGM-2 medium per culture. The following day, transfection solutions were prepared using polystyrene tubes. PerFect Lipid #7 (Invitrogen, Carlsbad, California) was added to serum free endothelial basal media (EBM; Clonetics) at 30 μg per 0.5 ml for each transfection and then incubated at room temperature for 30 min. The transfection DNA was added to separate tubes in serum free EBM at 5 μg per 0.5 ml for each transfection. The lipid and DNA solutions were then combined to make 1.0 ml of solution per transfection, which produced a solution with a lipid-to-DNA ratio of six to one (30 μg lipid to 5 μg DNA). The solution was then incubated for 15 min at room temperature.

Cell culture media was aspirated from all wells containing HUVEC for transfection. Then 1.0 ml of the appropriate transfection solution was added to culture wells and an additional 1.5 ml of serum free EBM was added. The transfection then proceeded at 37°C for 6 hr at 5% CO_2. Upon completion of incubation, the transfection solution was aspirated, and two washes were performed using 2.0 ml of pyrogen free PBS per wash. EGM-2 media was added back at 2.0 ml per well, and cells were incubated for 36–40 hr. Small samples of transfected cells were taken to determine the level of Flag-TWEAK expression by flow cytometry using M2 antiflag as a detection reagent.

The remaining HUVEC were used for proliferation assays in triplicate culture for each stimulation condition tested. First, anti-Flag M2 at 20 μg/ml per well of culture media was cross-linked with a goat anti-mouse IgG (Southern Biotechnology Associates, Birmingham, Alabama) at 40 μg/ml. This complex was preincubated for 15 min at room temperature and then added to culture (cross-linked M2). The culture medium was aspirated, the wells were washed once with pyrogen free PBS, and EBM plus 0.05% FBS was added back at 2.0 ml per well. The goat antimouse IgG alone or cross-linked M2 was then added to culture wells, and the assay was incubated for 3 days at 37°C and 5% CO_2. One day before harvest, BrdU (BrdU Flow Kit; BD Pharmingen, San Diego, California) at 10 μM final concentration was added to the cultures according to the manufacturer's instructions. Cells were incubated an additional 24 hr before trypsinization for assessment of BrdU incorporation. BrdU incorporation was measured by flow cytometry using a FITC-conjugated antiBrdU antibody supplied with the kit. BrdU mAb staining was compared to control staining and binding results analyzed using a FACScan (Becton Dickinson). In our hands, transfection efficiencies for Flag-TweakR using Lipid 7 averaged 8%. Flow cytometric BrdU incorporation results were evaluated by intensity of antiBrdU mAb binding and the percentage of the cells that bound antiBrdU mAb.

Planar Endothelial Migration Assay

Replicate circular lesions or "wounds" of 600–800 micron diameter were generated in confluent HRMEC monolayers using a silicon tipped drill press. At the time of wounding, the medium (DMEM + 1% BSA) was supplemented with 20 ng/ml PMA (phorbol 12-myristate 13-acetate), 4 ng/ml EGF, and 0.150–5 μg/ml TweakR-Fc, or a combination of 40 ng/ml EGF and 0.150 to 5 μg/ml TweakR-Fc. As a control for TweakR-Fc, some cells were treated with 5 μg/ml IgG-Fc. The residual wound area was measured as a function of time (0–12 hr) using microscope and image analysis software (Bioquant, Nashville, Tennessee). The relative migration rate was calculated for each agent and combination of agents by linear regression of residual wound area plotted over time.

Corneal Pocket Assay

Hydron pellets (Kenyon et al., 1996) incorporated sucralfate with FGF-2 (90 ng/pellet), FGF-2 and IgG-Fc (14 μg/pellet, control), or FGF-2 and TweakR-Fc (14 μg). The pellets were surgically implanted into corneal stromal micropockets created by microdissection 1 mm medial to the lateral corneal limbus of 6- to 8-week-old male C57BL6 mice. At the peak of neovascular response to FGF-2 (5 d), the corneas were photographed, using a Zeiss slit lamp, at an incipient angle of 35–50° from the polar axis in the meridian containing the pellet. Images were digitized and processed by subtractive color filters (Adobe Photoshop 4.0) to delineate established microvessels by hemoglobin content. Image analysis software (Bioquant) was used to calculate the fraction of the corneal image that was vascularized, the vessel density within the vascularized area, and the vessel density within the total cornea as described (Daniel et al., 1999). Statistical analysis (non-paired T test) was performed using GraphPad Prism software 3.0 (GraphPad Software, Inc., San Diego, California).

Acknowledgments

The authors thank W. Din for providing the pDC412-LZ-TWEAK construct, R. Goodwin and D. Williams for critical reading of this manuscript, G. Carlton for graphics assistance, and A. Aumell for editorial assistance. We thank Bill Dougall and Mark Tometsko for providing the TRAF constructs and the RANK-GST fusion construct. We also thank D. Hsu and K. Peifley for excellent technical assistance. This work was supported in part by National Institutes of Health Grant HL-39727 (to J.A.W.).

Received May 10, 2001; revised September 26, 2001.

References

Biancone, L., Martino, A.D., Orlandi, V., Conaldi, P.G., Toniolo, A., and Camussi, G. (1997). Development of inflammatory angiogenesis by local stimulation of Fas in vivo. J. Exp. Med. *186*, 147–152.

Chicheportiche, Y., Bourdon, P.R., Xu, H., Hsu, Y.M., Scott, H., Hession, C., Garcia, I., and Browning, J.L. (1997). TWEAK, a new secreted ligand in the tumor necrosis factor family that weakly induces apoptosis. J. Biol. Chem. *272*, 32401–32410.

Chicheportiche, Y., Fossati-Jimack, L., Moll, S., Ibnou-Zekri, N., and Izui, S. (2000). Down-regulated expression of TWEAK mRNA in acute and chronic inflammatory pathologies. Biochem. Biophys. Res. Commun. *279*, 162–165.

Daniel, T.O., Liu, H., Morrow, J.D., Crews, B.C., and Marnett, L.J. (1999). Thromboxane A2 is a mediator of cyclooxygenase-2-dependent endothelial migration and angiogenesis. Cancer Res. *59*, 4574–4577.

Fanslow, W.C., Srinivasan, S., Paxton, R., Gibson, M.G., Spriggs, M.K., and Armitage, R.J. (1994). Structural characteristics of CD40 ligand that determine biological function. Semin. Immunol. *6*, 267–278.

Feng, S.L., Guo, Y., Factor, V.M., Thorgeirsson, S.S., Bell, D.W., Testa, J.R., Peifley, K.A., and Winkles, J.A. (2000). The Fn14 immediate-early response gene is induced during liver regeneration and highly expressed in both human and murine hepatocellular carcinomas. Am. J. Pathol. *156*, 1253–1261.

Galibert, L., Tometsko, M.E., Anderson, D.M., Cosman, D., and Dougall, W.C. (1998). The involvement of multiple tumor necrosis factor receptor (TNFR)-associated factors in the signaling mechanisms of receptor activator of NF-kappaB, a member of the TNFR superfamily. J. Biol. Chem. *273*, 34120–34127.

Goodwin, R.G., Alderson, M.R., Smith, C.A., Armitage, R.J., VandenBos, T., Jerzy, R., Tough, T.W., Schoenborn, M.A., Davis-Smith, T., Hennen, K., et al., (1993). Molecular and biological characterization of a ligand for CD27 defines a new family of cytokines with homology to tumor necrosis factor. Cell *73*, 447–456.

Kaptein, A., Jansen, M., Dilaver, G., Kitson, J., Dash, L., Wang, E., Owen, M.J., Bodmer, J., Tschopp, J., and Farrow, S.N. (2000). Studies on the interaction between TWEAK and the death receptor WSL-1/TRAMP (DR3). FEBS Lett. *485*, 135–141.

Kenyon, B.M., Voest, E.E., Chen, C.C., Flynn, E., Folkman, J., and D'Amato, R.J. (1996). A model of angiogenesis in the mouse cornea. Investig. Ophthalmol. Vis. Sci. *37*, 1625–1632.

Locksley, R.M., Killeen, N., and Lenardo, M.J. (2001). The TNF and TNF receptor superfamilies: integrating mammalian biology. Cell *104*, 487–501.

Lynch, C.N., Wang, Y.C., Lund, J.K., Chen, Y.W., Leal, J.A., and Wiley, S.R. (1999). TWEAK induces angiogenesis and proliferation of endothelial cells. J. Biol. Chem. *274*, 8455–8459.

Madry, C., Laabi, Y., Callebaut, I., Roussel, J., Hatzoglou, A., Le Coniat, M., Mornon, J.P., Berger, R., and Tsapis, A. (1998). The characterization of murine BCMA gene defines it as a new member of the tumor necrosis factor receptor superfamily. Int. Immunol. *10*, 1693–1702.

Marsters, S.A., Sheridan, J.P., Pitti, R.M., Brush, J., Goddard, A., and Ashkenazi, A. (1998). Identification of a ligand for the death-domain-containing receptor Apo3. Curr. Biol. *8*, 525–528.

Martin, M., Schoecklmann, H., Foster, G., Barley-Maloney, L., McKanna, J., and Daniel, T.O. (1997). Identification of a subpopulation of human renal microvascular endothelial cells with capacity to form capillary-like cord and tube structures. In Vitro Cell Dev. Biol. Anim. *33*, 261–269.

Meighan-Mantha, R.L., Hsu, D.K., Guo, Y., Brown, S.A., Feng, S.L., Peifley, K.A., Alberts, G.F., Copeland, N.G., Gilbert, D.J., Jenkins, N.A., et al. (1999). The mitogen-inducible Fn14 gene encodes a type I transmembrane protein that modulates fibroblast adhesion and migration. J. Biol. Chem. *274*, 33166–33176.

Nakayama, M., Kayagaki, N., Yamaguchi, N., Okumura, K., and Yagita, H. (2000). Involvement of TWEAK in interferon gamma-stimulated monocyte cytotoxicity. J. Exp. Med. *192*, 1373–1380.

Pandey, A., Shao, H., Marks, R.M., Polverini, P.J., and Dixit, V.M. (1995). Role of B61, the ligand for the Eck receptor tyrosine kinase, in TNF-alpha-induced angiogenesis. Science *268*, 567–569.

Saas, P., Boucraut, J., Walker, P.R., Quiquerez, A.L., Billot, M., Desplat-Jego, S., Chicheportiche, Y., and Dietrich, P.Y. (2000). TWEAK stimulation of astrocytes and the proinflammatory consequences. Glia *32*, 102–107.

Schneider, P., Schwenzer, R., Haas, E., Muhlenbeck, F., Schubert, G., Scheurich, P., Tschopp, J., and Wajant, H. (1999). TWEAK can induce cell death via endogenous TNF and TNF receptor 1. Eur. J. Immunol. *29*, 1785–1792.

Silverman, E.S., Khachigian, L.M., Santiago, F.S., Williams, A.J., Lindner, V., and Collins, T. (1999). Vascular smooth muscle cells express the transcriptional corepressor NAB2 in response to injury. Am. J. Pathol. *155*, 1311–1317.

Smith, C.A., Gruss, H.J., Davis, T., Anderson, D., Farrah, T., Baker, E., Sutherland, G.R., Brannan, C.I., Copeland, N.G., Jenkins, N.A., et al. (1993). CD30 antigen, a marker for Hodgkin's lymphoma, is a receptor whose ligand defines an emerging family of cytokines with homology to TNF. Cell *73*, 1349–1360.

Smith, C.A., Hu, F.Q., Smith, T.D., Richards, C.L., Smolak, P., Goodwin, R.G., and Pickup, D.J. (1996). Cowpox virus genome encodes a second soluble homologue of cellular TNF receptors, distinct from CrmB, that binds TNF but not LTα. Virology *223*, 132–147.

Wiley, S.R., Schooley, K., Smolak, P.J., Din, W.S., Huang, C.P., Nicholl, J.K., Sutherland, G.R., Smith, T.D., Rauch, C., Smith, C.A., et al., (1995). Identification and characterization of a new member of the TNF family that induces apoptosis. Immunity *3*, 673–682.

Yoshizumi, M., Kourembanas, S., Temizer, D.H., Cambria, R.P., Quertermous, T., and Lee, M.E. (1992). Tumor necrosis factor increases transcription of the heparin-binding epidermal growth factor-like growth factor gene in vascular endothelial cells. J. Biol. Chem. *267*, 9467–9469.